Real-Time Simulations Laboratory
RTS@UNSW

AUSTRALIAN RESEARCH FOR POWER SYSTEM TRANSITION

Topic 9 – DER and Stability

Stage 4 Final Report

20/05/2025

This document and the information provided within are based on the work conducted during Stage 4 of the Australian Research for Power System Transition (AR-PST), May 2024 – April 2025.

Contributors to this work include:

The University of New South Wales (UNSW Sydney)

- *Awais Ahmad, Research Associate, School of Electrical Engineering and Telecommunications*
- *Georgios Konstantinou, Associate Professor, School of Electrical Engineering and Telecommunications*
- *John Fletcher, Professor, School of Electrical Engineering and Telecommunications*

University of Wollongong (UoW)

- *Obaidur Rahman, Associate Research Fellow, Australian Power Quality Research Centre*
- *Sean Elphick, Research Coordinator, Australian Power Quality Research Centre*
- *Duane Robinson, Associate Professor, Australian Power Quality Research Centre*

Australian Energy Market Operator (AEMO)

- *Jenny Riesz: Manager, Operational DER Management*
- *Pat Graham: Principal Engineer, Operational DER Management*
- *Taru Veijalainen: Principal Engineer, DER Technical Integration*
- *Daena Ho: Senior Engineer, Operational DER Management*

CSIRO

- *Thomas Brinsmead, Senior Research Scientist*
- *Julio Braslavsky, Senior Principal Research Scientist*

CONTACT:
Dr. Awais Ahmad,
Research Associate,
School of Electrical Engineering and Telecommunications, UNSW Sydney
awais.ahmad@unsw.edu.au

Acknowledgments

The research presented in this report is funded by CSIRO as a part of CSIRO's contribution to the initiatives of the Australian Research in Power Systems Transition (AR-PST) and is carried out with the support of subject matter experts from both AEMO and CSIRO. This research supports Australia's transition to a stable, secure and affordable power system and contributes to critical research identified by the AR-PST required to accelerate the decarbonisation of our electricity grid. More details can be found at Australian Research in Power Systems Transition (AR-PST) - CSIRO

Executive Summary

The electricity distribution landscape is undergoing profound transformation through the continuous growth of distributed inverter-based resources (DIBR), the evolution of load profiles toward inverter-based demand (IBD), and the emergence of low short-circuit ratio, low-inertia connections at points of common coupling (PCC), a direct consequence of weakening transmission networks. Together, these concurrent changes create significant challenges to the operation of future power systems as they challenge all aspects of a stable and secure electricity network. The particular concern is Distributed Inverter-Based Systems (DIBS), which encompass both DIBRs and IBDs, as their operation in weak grid environments require specialised consideration. Significant knowledge gaps persist even within existing network configurations despite the urgent need for accurate modelling and representation of these systems. These modelling deficiencies hinder our ability to predict system behaviour and develop effective mitigation strategies for maintaining grid reliability during this critical transition period.

Stage 4 of Topic 9, **"DER and Stability,"** focused on analysing the interactions and behaviour of DIBRs under weak grid conditions, along with the performance of Distributed Energy Resources (DERs), Energy Storage Systems (ESS), and modern loads. The goal was to equip system operators with the insights needed to maintain and enhance power system security in today's evolving operational landscape. The work of Stage 4 provides robust, accurate data on DIBR responses to power system transients, derived from rigorous bench testing and experimental methodologies. The findings directly contribute to the refinement of composite load models used by AEMO and, by extension, other distribution network operators, ensuring more accurate and effective power system management.

The motivation behind Stage 4 initiatives has been the continuous growth of DER, ESS, and modern loads, along with the need to address untested aspects of the existing DER fleet: specifically, inverters interactions, response to grid disturbances under weak grid conditions and Electric Vehicles (EV) testing. These activities contribute significantly to the lack of comprehensive experimental data for critical systems, such as EV chargers (in Grid-to-Vehicle (G2V) and Vehicle-to-Grid (V2G) modes), DIBRs interactions and ESS, which continue to limit the accuracy of current models. The enhancement of composite load modelling and the development of more sophisticated load models designed to accurately represent the responses of DERs, including during grid disturbances, are crucial for capturing the dynamic behaviour of the modern power system. By improving these models, we can better predict the behaviour of the distribution system as it integrates a growing number of DER and modern electronic loads, supporting more effective planning and operational strategies.

This report summarises UNSW's and UoW's findings on DER responses and interactions, and EV testing, predominantly during power system disturbances. The results collected also provide input to the ongoing load modelling activities of AEMO. The activities detailed in this report were undertaken as part of three broad tasks proposed in the Stage 4 RfQ, summarised below:

- **Task 1: Multi-Inverter interaction:** Experimental bench-testing of DER and ESS interactions in response to power system transients expanding the previous testing of Battery ESS (BESS), Hybrid ESS (HESS), EV charging infrastructure, and various modern inverter-driven loads in stage 3. These devices introduce complex dynamic interactions between the grid and converters, necessitating a comprehensive study. Also investigating stability concerns arising from the integration of multiple converters within the same or adjacent grid nodes, a scenario that is becoming increasingly common in future power systems.

- **Task 2: Distributed Inverter-Based Systems in Weak Grids:** Update the testing setup to accommodate testing of DERs under weak grid conditions. The research focused on understanding the impact of weak grid conditions, particularly under scenarios of low inertia and voltage instability, on the behaviour of DIPS, especially given that the available experimental data remains insufficient. Additionally, it involved updating the existing models, which previously did not have such data, to incorporate all the new testing outcomes.
- **Task 3: Electric Vehicle testing:** This task involved executing the testing procedure for EVs with different chargers to accurately capture the aggregate behaviour and dynamic performance of EV chargers (as a subset of DIPS) during power system disturbances in both charging and Vehicle-to-Grid (V2G) modes.

Key Findings on Inverter Interactions

1. **Increased System Vulnerability Due to Configuration Complexity:** The extension of the testing platform from single to multiple inverters (i.e., two-inverter and three-inverter configurations) at the same point of common coupling (PCC), increased significantly the complexity of interactions. Testing in three-inverter setups exhibited more pronounced vulnerabilities that may appear in the distribution system, including the simultaneous disconnection of all units even under during moderate disturbances.

2. **Cross-Manufacturer Compatibility Issues:** Deployments featuring inverters from different manufacturers consistently demonstrated a decline in performance compared to their operation as a standalone system, for either inverter. Inverters that maintained grid connections during individual testing unexpectedly disconnected when operating in parallel with units from other manufacturers.

3. **Persistent Individual Inverter Vulnerabilities:** Some inverters, notably Inverter 48, showed consistent vulnerabilities in both two and three-inverter configurations. These units disconnected at Voltage Phase Angle Jump (VPAJ) values as low as 30° in parallel arrangements, despite maintaining connections during standalone testing. Such outcomes point towards a lack of robustness for single inverter testing especially when considering real-world conditions.

4. **Cascading System Failures:** A critical escalation of vulnerabilities was observed in three-inverter configurations, where the simultaneous disconnection of all units occurred during moderate VPAJ disturbances. This created a potential risk for widespread cascading outages in larger deployments.

5. **Enhanced Resilience in Same-Manufacturer Deployments:** Three-inverter arrangements from the same manufacturer showed marked stability improvements, especially when hybrid operational modes were utilised. The connection of three inverters from the same OEM at the same PCC allowed for successful ride-through of disturbances, including those that had previously caused disconnection during standalone tests or in configurations where inverters from different OEMs where tested.

The authors note that testing multiple parallel converter configurations significantly increases the number of possible combinations and required tests. Therefore, the above conclusions are based on consistent behaviours observed in the tests completed during Stage 4.

Key Findings on Weak Grid Testing

1. **Inverter stability is highly sensitive to additional impedance at the PCC:** Even minor increases in line inductance (e.g., from 3mH to 4mH) resulted in disconnections, highlighting the crucial influence of weak grid conditions on inverter behaviour.

2. **Power Level Critically Affects Stability:** Inverters consistently performed worse at full power compared to half power under weak grid conditions, with multiple units (44, 48, 49, 30, 31) demonstrating superior disturbance ride-through at 50% output, indicating that the operational power level is one of the key factors in inverter resilience.

3. **Duration Sensitivity Emerges as New Vulnerability:** Beyond magnitude-based criteria, some inverters exhibited time-dependent sensitivity. For instance, Inverter 35 managed a 1.2 p.u. voltage swell for 80 ms but disconnected when the same swell persisted for 220 ms.

4. **Disturbance response varies non-linearly among inverters:** Some inverters disconnected during minor voltage sags or frequency steps under weak grid conditions, while others demonstrated strong ride-through capabilities especially at lower impedances or power levels.

5. **Only a few inverters showed high impedance tolerance:** Inverters such as 31, 30, and 36 maintained grid synchronisation even at 10mH inductance, but still exhibited a compromised response to long-duration disturbances.

6. **Parallel operation reduces overall system stability:** Inverters that performed well individually under weak grid conditions exhibited disconnections or power curtailments, which further degraded the performance in parallel inverter operation.

7. **Compliance with AS 4777.2:2020 may not guarantee similar performance in weaker grids:** All inverters meet the standard requirements under strong grid assumptions, but many fail to meet those expectations under weak grid conditions, suggesting a need to extend standards to cover low-SCR environments.

The authors note that distribution networks typically have lower X/R ratios than transmission networks. In this study, additional impedance was introduced at the PCC to provide a preliminary demonstration of weaker grid conditions. However, more extensive testing, considering specific feeder types and overhead/cable arrangements, is recommended in future work.

Key Findings on EV Chargers and EVs

1. **EV Charger response under voltage sags:** Extensive experimental testing was carried out on four different EVs to analyse the responses of EV chargers, particularly their disconnection and reconnection behaviour, when subjected to voltage sag disturbances of varying depths and durations. The results indicate different responses to voltage sags of EVs when being charged using identical chargers. Key observations include:
2. **The model of the EV matters:** Disconnection and reconnection response to voltage sag disturbances varies across EV models. Some EVs exhibited abrupt reconnection, while others demonstrated slower reconnection response with varying ramp up characteristics.
3. **Sensitivity to Sag depth and Charger Types:** The EVs were found to be more sensitive to sag depth when charged using the Level 2 charger as opposed to the Level 1, specifically most EVs disconnected for the Level 2 charger at less extreme sag depths (0.6-0.7 pu). Most EVs exhibited a momentary power surge, at both Level 1 and Level 2 charging, during voltage sag ride-through.
4. **Fault duration sensitivity:** Some EVs were more likely to ride through 120-ms sags than 80-ms ones, indicating timing sensitivity in their operations. This further necessitates additional testing to determine if this trend holds true for all EVs.
5. **Other responses:** Irregular disconnection and reconnection behaviour appeared during extended charging periods, potentially due to thermal effects on internal components.

The authors again note the limited number of EVs tested in Stage 4 and recommend a more comprehensive testing platform or program, given the anticipated growth in EV penetration and the introduction of new models across all Australian networks.

Updates on Dynamic Performance Modelling

1. To date, a total of eight EVs have been evaluated for response to voltage sag disturbances. These responses have been generalised to identify key parameters for generic EV load models.
2. EV modelling parameters include overshoot during ride-through and charging disconnection events, disconnection time, reconnection time, and reconnection behaviour. However, for the purpose of stability analysis, the present stage primarily focuses on disconnection and reconnection characteristics, as overshoots are momentary and have limited impact.
3. The generalised EV responses obtained from experimental testing are proposed for inclusion in the aggregated EV load model developed in MATLAB Simulink. Each EV response type will contribute to the overall model according to assigned fractional weights, representing their prevalence in the EV population. This approach is inspired by the methodology proposed by EPRI, which introduced an aggregated EV model comprising four representative EV response types based on preliminary data [1].

Updates on Field Load Measurements

- **Site 1 – EV Fast Charging Station:** Over a three-month monitoring period, only one voltage sag event was recorded. While no charging disconnection was observed, current waveforms exhibited noticeable distortion during the sag, indicating a transient impact on the charging infrastructure.
- **Site 2 – Commercial Supermarket Area:** A total of 14 voltage sag events were captured, primarily affecting HVAC and refrigeration equipment. Nearly all events resulted in a drop in active power demand post-disturbance (indicating that some equipment disconnected), along with a brief overshoot in power consumption when the sag occurred, suggesting dynamic load responses from motor-driven appliances.
- **Site 3 – Industrial area with cold rolling, metal/paint coating, and finishing facilities:** Five sag events were detected, displaying system behaviour similar to that of Site 2. Load disconnection and transient power overshoots were consistently observed, even for moderate sag depths, reflecting the sensitivity of industrial motor drives to voltage

Progress Against the Roadmap

The Stage 4 research on "DER and Stability" demonstrates strong strategic alignment with the Research Roadmap for Topic 9, advancing critical priorities while adapting to the rapidly evolving power systems landscape. As the energy transition accelerates and new challenges emerge, this research has expanded beyond the original scope to address urgent grid stability concerns identified through ongoing investigation. The alignment spans five key areas:

Model Development and Comprehensive Testing: Work completed under Stage 4 directly addresses roadmap priorities by helping develop models that capture the complex dynamic behaviour of DERs under challenging grid conditions, particularly in weak grid environments. Through extensive bench testing and real-world data analysis, the research enhances the understanding of load-DER interactions and help improve tools essential for accurate system planning. This comprehensive approach has revealed the gaps in existing models and established new benchmarks for DER performance assessment under varying grid strength conditions.

Inverter Performance Analysis: A major focus of both the Roadmap and Stage 4 research is understanding inverter behaviour during grid disturbances, particularly under weak grid conditions where traditional assumptions no longer apply. The research has uncovered significant variations in inverter performance that were previously unrecognized or undocumented, demonstrating that current compliance with standards does not guarantee adequate performance under emerging grid conditions. Stage 4 research provides crucial insights into system security implications as inverter-based resources increasingly replace traditional synchronous generation.

Electric Vehicle Integration: Recognising EVs as both a transformative opportunity and a complex challenge for grid management, Stage 4 research has incorporated aggregated EV modelling. This work addresses the roadmap's emphasis on understanding how large-scale EV adoption will interact with existing DER deployment, providing empirical data on impacts and developing frameworks for managing EV-grid integration in distributed energy environments.

Multi-Inverter Interactions and Weak Grid Vulnerability: Stage 4 research has provided valuable insights into parallel inverter operations at the PCC, revealing previously unknown interaction effects that cannot be predicted from individual inverter performance. The comprehensive weak grid testing established impedance tolerance thresholds and identified stability boundaries that fundamentally challenge existing planning assumptions. These findings directly support the roadmap's emphasis on developing robust testing methodologies to ensure grid stability in high-DER scenarios.

Standards Evolution and Regulatory Framework: Both the Roadmap and Stage 4 activities acknowledge that existing standards are not adequate for the emerging grid paradigm. Forward-looking revisions should be considered to ensure the system remains resilient to future stability challenges. The results of the research and testing undertaken provide empirical evidence that demonstrate critical gaps in current compliance requirements, particularly regarding weak grid performance. This work establishes the foundation for next-generation standards that can adequately address DER behaviour under realistic future grid conditions, ensuring that regulatory frameworks evolve in step with technological deployment.

Stage 4 research has advanced beyond the original Roadmap objectives, uncovering key insights and addressing emerging gaps along the way. Its findings lay a strong foundation for future grid planning, the evolution of equipment standards, and the development of operational strategies, supporting a

reliable and resilient power system as the sector moves confidently toward a distributed, renewable energy future.

Future Directions

The insights gained from Stage 4 research have fundamentally transformed our understanding of inverter-based resource (IBR) behaviour under weak grid conditions, revealing critical knowledge gaps that require urgent attention. The identification of significant inconsistencies in IBR performance during grid disturbances has highlighted serious vulnerabilities in current planning assumptions. Meanwhile, load representation and modelling advancements have equipped us with essential tools for navigating the energy transition. These findings provide a compelling foundation for the next phase of research, which will be crucial for the success of power system transformation. As the power system undergoes an unprecedented transformation, characterized by the displacement of traditional generation by inverter-based resources and the evolution of load profiles driven by electrification, maintaining grid stability has become increasingly complex. The rise of weak grid conditions as a predominant operational characteristic necessitates a fundamental shift in research focus toward understanding and managing high IBR penetrations under challenging network environments. This evolution calls for more sophisticated approaches beyond traditional testing methodologies to address the intricate interactions occurring within modern distribution networks.

Future research should prioritise comprehensive testing and modelling of DERs across a wide range of challenging operational scenarios. This includes systematically exploring dynamic responses to intricate, multi-dimensional grid disturbances that more accurately reflect real-world conditions rather than relying on simplified test cases. The investigation should extend beyond traditional inverter testing to include advanced storage solutions, bidirectional electric vehicle (EV) charging infrastructure, and hybrid systems integrating multiple technologies at shared connection points. It is essential to critically emphasise validating and enhancing composite load models that treat IBRs, energy storage systems, and electric vehicles as active participants in the grid rather than passive loads.

An in-depth investigation of steady-state and reconnection performance under weak grid conditions is crucial for defining future grid reliability. This research should encompass large-scale inverter installations and their collective impact on grid stability, establishing performance benchmarks reflecting modern grid operations' realities. Developing network models and load profiles representative of Australian conditions will be vital for validating these findings and ensuring their relevance to local circumstances. It will also identify critical thresholds at which system behaviour shifts from stable to unstable operation. Furthermore, integrating machine learning algorithms with extensive testing datasets will facilitate automated parameter optimisation and model refinement at an unprecedented scale, enabling researchers to uncover patterns and relationships that manual analysis might miss.

Strengthened partnerships with original equipment manufacturers OEMs of the Australian market will ensure that research models reflect the latest technological advancements and firmware capabilities. This collaboration will bridge the laboratory testing and field deployment, guaranteeing that research outcomes translate directly into practical solutions for grid management. Establishing and maintaining comprehensive open data repositories represents a transformative approach to research collaboration, yielding high-resolution testing data and enabling distributed research teams to contribute effectively to model development and validation. The outcomes will include enhanced standards for integrating IBRs, improved grid planning methodologies, and operational strategies that ensure reliability under high levels of renewable penetration. The research will position Australia at the forefront of power system transformation, delivering both the technical solutions and the knowledge infrastructure essential for a successful energy transition, setting new benchmarks for international research, and addressing the unique challenges and opportunities of the Australian electricity system.

Contents

Tables

Figures

1. Introduction and Project Overview

Australia's electricity supply networks are experiencing unprecedented transformation through the rapid proliferation of Distributed Energy Resources (DER), with a significant portion being minimally regulated and insufficiently monitored. These systems now contribute substantial generation capacity during peak demand periods, fundamentally altering traditional power flow dynamics. This accelerating transition creates formidable challenges for system operators, particularly Independent System Operators (ISOs) and Transmission System Operators (TSOs), who must maintain power system security amid increasingly unpredictable generation patterns and reduced system visibility. The technical complexity of integrating these diverse resources while preserving grid stability represents one of the most pressing challenges in Australia's energy transition [1].

Integrating DER grid-friendly is vital for Australia's energy sector, ensuring affordability and reliability while enabling continued DER deployment without overly conservative grid operation. Using accurate DER models enables system operators to maintain security and stability through targeted measures rather than over-investing in unnecessary mitigation equipment. Enhanced modelling and a deeper understanding of DER responses significantly increase network hosting capacity while simplifying integration. However, operating networks with high DER penetration becomes particularly challenging during grid disturbances, as demonstrated by the South Australian islanding incident in November 2022 [1] which required a forecasted contingency management of 255 MW of predominantly distributed PV and the February 2024[2] In Victorian storm disruptions [2], approximately 2,293 MW of distributed PV (comparable to the 2,690 MW output from Loy Yang A & B) required curtailment to protect system stability. The widespread adoption of inverter-based resources (IBRs) such as solar PV and wind generation and the integration of distributed energy resources (DERs) define the ever-evolving energy landscape. A critical consequence for large-scale power systems is the shift from centralised synchronous generation (SG) toward IBRs, resulting in a significant reduction of system strength (Figure 2.1 These emerging weaker grids exhibit diminished resilience to disturbances, manifesting as voltage and frequency oscillations and severe instabilities following system disturbances [3]. The challenges for stable power system operation is primarily from low short-circuit ratios (SCRs), as IBRs cannot match the fault current capabilities of traditional SGs and substantially reduced system inertia, even when accounting for synthetic inertia provided by grid-forming

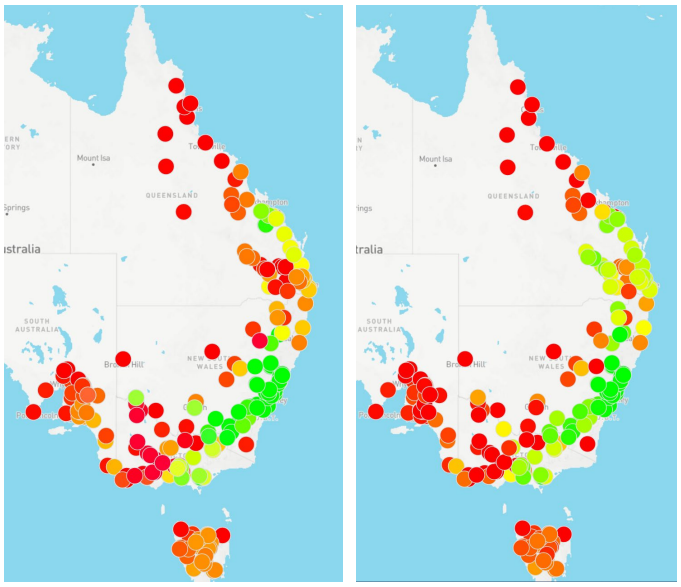

Figure 2.1. AEMO forecasts substantial reduction in system strength (green: strong grid, red: weak grid) in the next couple of decades throughout the NEM (left: 2020-21, right: 2034-45).

[1] A maximum DER contingency of 255 MW (predominantly due to distributed PV systems) was forecasted for the 17th of November 2022 which led AEMO to direct "scheduled generation, curtailment of non-scheduled wind generation, and/or an instruction to maintain DPV generation below a secure DPV generation threshold."

[2] Approximately 2,293MW of DPV were connected in Victoria at 1305 hrs on 13 February 2024, just prior to the incident. As a comparison, Loy Yang A & B combined output at the same time was 2,690MW.

converters [4]. The technical complexities are further compounded by changing power flow dynamics, reduced system visibility, and increasingly unpredictable generation patterns. Addressing these complex challenges necessitates sophisticated solutions spanning grid design, advanced control architectures, and forward-thinking regulatory frameworks to maintain power quality and reliability standards.

While substantial research on weak grids has focused on transmission-level impacts of reduced system strength [5] a prevailing assumption has been that distributed IBRs (DIBRs) only encounter weak grid conditions in isolated, remote networks. However, many areas in distribution networks now experience increased sensitivity to voltage and frequency disturbances, which challenge the stable operation of DIBRs. The excess of DIBRs, combined with changing load compositions and evolving network characteristics, has created vulnerability zones even within previously robust distribution systems. Addressing these emerging challenges is crucial for developing effective stability enhancement strategies across the entire power system. The essential first step in this process involves methodically replicating, evaluating, and comprehensively understanding DIBR responses to weak grid disturbances through rigorous laboratory testing and field observations. Developing accurate, validated models for DIBRs serves as the critical bridge between experimental findings and practical field solutions, enabling system operators to predict behaviour, identify vulnerabilities, and implement targeted measures to maintain grid stability as the energy transition accelerates.

Weak grid challenges significantly amplify existing issues in networks with high DIBR penetration [6], where millions of distributed photovoltaic inverters must now coordinate with an expanding fleet of inverter-based demand (IBD) including EV chargers, DC supplies, variable speed drives, and bidirectional systems like battery energy storage systems (BESS). This complex interaction landscape creates unprecedented operational challenges at the distribution level. Comprehensively evaluating responses of EV charging infrastructure and analysing interactions between DIBRs and IBDs has become crucial for developing accurate aggregate load models. These models are essential for understanding and addressing emerging distribution network instabilities.

Precise load modelling is critical for Network Service Providers (NSPs) and system operators to assess system performance, identify stability concerns, and design effective control strategies [7], [8], particularly as distributed energy resources (DERs) including electric vehicles (EVs) increasingly transform electricity networks. These modern loads exhibit complex dynamic behaviour when subjected to faults and transient disturbances [9][10], challenging the adequacy of traditional models. In Australia, the load modelling approach used by AEMO relies on polynomial ZIP models, last calibrated in 1999, which are now insufficient for accurately capturing the dynamic nature of modern loads.

Internationally, the WECC has introduced the CMPLDW (Composite Load Model with DERs), which incorporates various load types, including motors, static and electronic loads, and DERs [11]. The CMPLDW is recommended by The North American Electric Reliability Corporation (NERC) for dynamic power system studies [12]. However, the implementation of this model presents practical challenges, as it requires up to 133 input parameters to accurately reflect the characteristics of the composite load. These parameters are typically derived from a combination of fault event data provided by NSPs and laboratory-based testing of consumer appliances. Despite its comprehensiveness, the CMPLDW lacks detailed modelling of EV charging loads. These loads involve advanced controllers, communications, and protection mechanisms, making them fundamentally different from the generic electronic loads currently represented.

To address the lack of an EV load model, EPRI has proposed an aggregated EV charging model based on response to four representative sag types. While this is a step forward, the responses were simplified due to limited empirical data, particularly regarding varying sag depths and durations. Existing studies

have examined EV charger performance under PQ disturbances such as sags and swells [10]-[13], but often excluded EV-side behaviour and did not fully explore EV supply equipment (EVSE)-EV system interactions. Recent experimental works [14]-[16] evaluated complete systems and identified sensitivity to rate-of-change-of-frequency (RoCoF) but did not conclusively demonstrate sensitivity to voltage sag conditions.

Systematic testing of DIBS and motor-driven loads in distribution systems [17] delivers multiple benefits: it enables significantly enhanced network hosting capacity through improved modelling accuracy, prevents unnecessary capital expenditure on redundant network equipment, and eliminates overly conservative operational constraints [18]. These testing programs provide the empirical foundation for developing sophisticated models and analytical tools that directly inform essential standards revisions while establishing performance requirements for next-generation inverters. As distribution networks evolve rapidly, this evidence-based approach becomes increasingly critical for maintaining system stability while maximising renewable energy integration.

1.1. Scope of Work - UNSW

Simulation-based and model-driven methodologies are indispensable for developing dynamic load models in evolving power systems. However, these approaches frequently fall short in capturing the intricate complexities of real-world conditions, particularly when modelling distributed energy resources such as photovoltaic systems, battery energy storage systems (BESS), hybrid energy storage systems (HESS), electric vehicles, and intelligent load management systems. The interactions between these diverse technologies, especially in weak grid conditions with low short-circuit ratios and reduced system inertia, create emergent behaviours that theoretical models often fail to predict accurately. While computational simulations provide valuable theoretical insights into DER performance and grid integration challenges, rigorous laboratory bench-testing and systematic experimental evaluation are essential for validating these findings. This empirical verification process ensures model accuracy and reliability, bridging the critical gap between theoretical predictions and actual field performance. As Australia's electricity networks continue transitioning toward higher DER penetration rates, this evidence-based approach becomes increasingly vital for maintaining system security while maximizing renewable energy integration without unnecessarily conservative operational constraints.

Previous testing and analysis of DIBRs in Stage 3 focused primarily on grid reconnection behaviours and identifying critical vulnerability points during grid disturbances. However, this has revealed a significant knowledge gap regarding inverter responses to large-scale system events, particularly during low-probability, high-impact scenarios where photovoltaic generation exceeds the minimum loading requirements of large synchronous generators operating in parallel. This emerging concern represents a critical blind spot in our understanding of system dynamics during extreme events. Currently, substantial research gaps persist in evaluating the complex interactions between different DIBS located within the same network, which can create emergent behaviours that are not predictable through individual component analysis. Furthermore, no experimental data characterises DIBR responses under weak grid conditions, severely hampers their accurate representation in aggregate load models. This data gap becomes increasingly problematic as distribution networks experience diminishing system strength due to the ongoing transition from centralised synchronous generation and DIBRs interactions.

These interaction studies are essential for understanding collective system impacts and must incorporate sophisticated probabilistic formulations of aggregate models that capture the stochastic nature of these interactions. The growing complexity of distribution networks, characterised by diverse DIBS technologies with varying control algorithms and response characteristics, necessitates a comprehensive approach to enhance load composite model accuracy.

Work Package 1 (WP1) of Stage 4 was undertaken exclusively by UNSW to address these concerns, described below in detail.

1.1.1. Work Package 1

This work package comprehensively evaluated inverter performance when multiple units share a common PCC. Also, this investigation analysed the dynamic response characteristics of various inverter technologies under weak grid conditions, focusing on their behaviour during different power system disturbances, including voltage sags, swells, phase jumps and frequency deviations.

Multi-inverters Interaction Testing: Focused on inverter interaction testing to provide comprehensive experimental bench-testing of inverters available in the Australian market. This testing emphasised multi-inverters' interactions from similar and different OEMs under various grid disturbances, including time and frequency domain responses and representations. Taking the next step on the work completed in Stage 3 for Topic 9. Integrating multiple converters within the same or adjacent grid nodes is an increasingly common scenario in future power systems and amplifies the coupling effect between converters, leading to novel stability concerns. This task considers these diverse interactions to facilitate thorough testing and resolution of the emerging stability issues, utilising existing hardware.

Weak Grid Condition Testing: Focused on bench testing of hardware, which is the most critical element in deciphering the intricacies of control algorithms and operation in weak grids in real-time, as it is the main method of offering substantial validation for phenomena observed in simulations and then translated into models. The testing included energising the DIBS, confirming proper synchronisation and facilitating a comprehensive understanding of system behaviour under weak grid conditions. Bench testing enables a detailed examination of DIBS performance in steady-state and transient conditions while recording the system response in real-time. These experiments were instrumental in deriving key learnings about the system's dynamics and operational resilience in weak grid scenarios.

1.2. Scope of Work - UOW

With the ever-changing composition of loads in modern power networks, it is paramount to that these changes be incorporated into power system models. This allows NSPs to identify and predict potential power reduction and system stability issues. It also supports studies that validate the interaction between DER and flexible loads, aids research in improving system operability during fault events, and contributes to industry-wide information sharing concerning systemic risks.

The work conducted by UOW comprises of three core tasks aimed at improving the understanding and representation of dynamic load behaviour within the electrical power system. These tasks were

- Conducting experimental evaluation of EV charger performance when subject to controlled voltage sag conditions to observe and analyse their dynamic response;
- Developing detailed EV charging load models that can accurately reflect transient behaviours; and
- Performing field measurements at commercial and industrial sites to capture real-world charging patterns.

This multi-faceted approach supports the integration of EV loads into network planning and stability assessments with greater precision.

1.2.1. Work on EV Testing

Regarding EV testing, a series of laboratory experiments were conducted to examine the response of various EV models subjected to voltage sag disturbances while connected to identical chargers. This phase involved testing four different EVs, namely GWM Ora, Hyundai Kona, Tesla Model Y, and Peugeot E-Partner. The analysis focussed on identifying behavioural patterns under varying sag depths and durations, with particular attention paid to disconnection trends and their differences across vehicle models. These insights will help determine key parameters for accurate EV load modelling and provide implications for network stability. The overarching objective of this work was to enhance understanding of EV behaviour during power disturbances and inform future research on integrating EVs into power systems. Future investigations could explore Vehicle-to-Grid (V2G) functionalities, recently introduced in some EV models, when subject to power system disturbances.

1.2.2. Work on EV Modelling

This work modelled the behaviour of EV loads in response to voltage sags, focussing on the disconnection patterns observed under different charging conditions. The data collected from various EV and charger combinations, including Level 1 and Level 2 Chargers A and B, provided insights into how the EVs responded to voltage sags of varying depths and durations. By analysing these results, a model that accurately represents the response of the EV load to voltage sags was developed, which will be useful for understanding the impact of voltage disturbances on grid stability. The findings will contribute to the design of more resilient charging infrastructure and improved EV load modelling in power systems.

For EV dynamic modelling, data collected from laboratory experiments across Stages 2 to 4 was used to generalise typical EV responses to voltage sag disturbances. The behaviours of eight EVs were analysed for sags with retained voltage magnitudes of 0.8, 0.5, and 0.2 pu, shallow, moderate, and severe scenarios. Key parameters considered for this generalisation included critical sag depth threshold, power overshoot during ride-through and disconnection events, disconnection duration, reconnection duration, and the shape of the reconnection response. However, at this stage, power overshoot was not the primary focus of the modelling effort and will be assessed in more detail as part of the future work. Based on the generalised responses, both the critical sag depths and their corresponding fractional weights in the aggregated model were determined to support the development of the EV dynamic model. While the proposed model draws on the EPRI aggregated framework, it enhances accuracy by incorporating empirically derived generalised behaviours, thereby improving its suitability for dynamic load analysis.

1.2.3. Work on Field Measurements

This work involved field measurements conducted at three representative sites to support the development and validation of dynamic load models under voltage sag conditions. The selected sites were as follows:

- Site 1: EV DC fast-charging station to examine the real-world response of electric vehicle loads
- Site 2: A commercial shopping centre with significant HVAC and refrigeration equipment to support motor load modelling
- Site 3: An industrial facility featuring cold rolling and metal coating processes, where motor drives and general distribution dominate the load profile.

Power quality monitoring equipment was installed at each location to record three-phase voltage and current waveforms. Over an extended observation period, voltage sag events were identified, recorded,

and analysed to capture characteristic load behaviours such as disconnection, reconnection, and recovery dynamics. These field measurements play a critical role in validating and refining the load models developed through laboratory experiments, ensuring their applicability under practical disturbance scenarios.

2. Parallel Inverters Bench-Testing

Testing of DER inverters - whether for standards compliance, performance evaluation, or inclusion on the CEC-approved product list - typically assumes a single grid-connected converter operating at the PCC. These tests capture the response of individual converters under complex grid scenarios but do not account for interactions between multiple converters operating in proximity. This assumption may have been valid during earlier deployment phases, when households primarily installed PV systems in passive networks. However, the addition of BESS and EV charging infrastructure means multiple converters at the same PCC are becoming increasingly common.

Interactions between converters result in different behaviours between single and parallel inverter configurations. Differences in response times between OEMs, measurement accuracy, and synchronisation algorithms make modelling and analysis more complex, introducing risks such as current mismatches and frequency oscillations. Stability becomes particularly challenging with parallel inverters, as disturbances in one unit can propagate to others—unlike single inverters, which are more easily analysed and managed.

Stage 4 includes experimental bench testing of parallel inverters compliant with AS 4777.2:2020. This testing provides insight into potential DER interactions at the same PCC and examines the dynamic response of inverters from both similar and different OEMs during network disturbances. The results will inform the development of a load model that more accurately represents dynamic operation in modern distribution networks.

Each inverter pair underwent identical testing to compare behaviour under individual and parallel operation. Testing has been completed for 21 pairs, including DER, BESS, and HESS units. The inverters were subjected to various disturbances to evaluate how they implement and respond to the Australian standard, enabling compliance and performance assessment. This approach helps identify regulatory gaps and technical limitations in the current standard.

As in previous stages, all inverters tested in Stage 4 of the AR-PST have been anonymised to ensure impartiality and avoid potential consequences for specific OEMs. The following sections present detailed results for all tested inverters. While the tests may differ from those in AS 4777.2:2020 [24] they provide valuable insight. By assessing how new inverters adapt to the standard and evaluating their performance, the testing helps identify potential gaps requiring further investigation.

2.1. Inverter Pairs

The experimental setup used a parallel configuration with two inverters directly interconnected at the PCC. Figure 3.1 provides schematics of the parallel inverters' interaction between the pair of inverters under controlled grid disturbance conditions. This schematic illustrates how both inverters share electrical connection points while maintaining independent control systems. It creates the necessary conditions to evaluate both individual responses and the emergent behaviours resulting from their combined operation during standardised grid stability testing procedures.

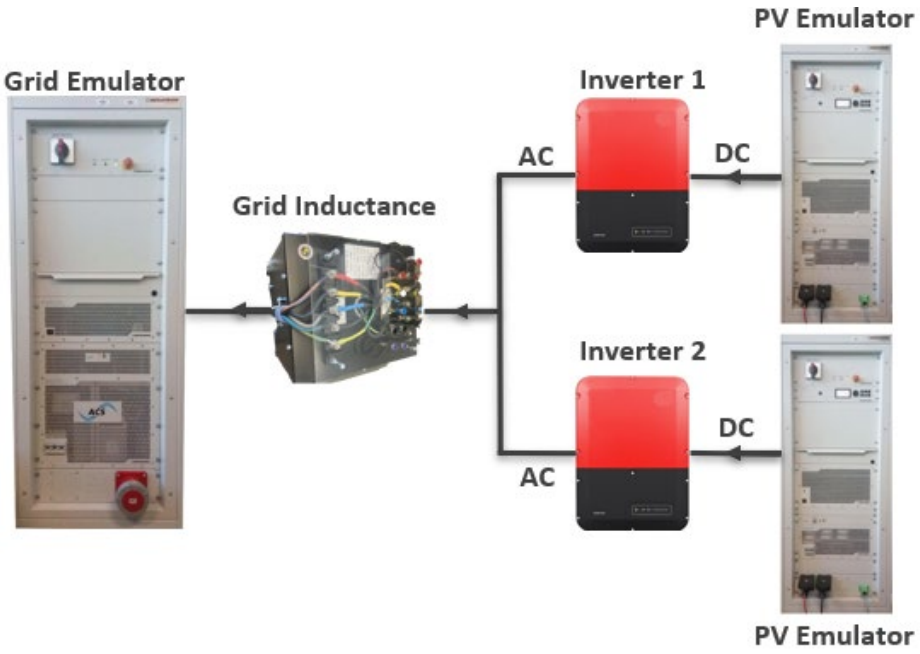

Figure 3.1. Simplified diagram of the experimental setup for parallel inverter testing.

2.1.1. Inverters 44 and 51

This study of parallel inverter interactions involved inverters from the same manufacturer but of different models (44 and 51). This configuration allowed us to compare the standalone performance of each inverter against its behaviour when operating in parallel at a shared PCC. When subjected to a 60° Voltage Phase Angle Jump (VPAJ) disturbance generated by the grid emulator, Inverter 51 successfully maintained grid connection (ride-through) when tested individually. However, it displayed unexpected power curtailment behaviour when connected in parallel with Inverter 44. Inverter 44 disconnected from the grid during the disturbance in both standalone and parallel configurations, maintaining its characteristic response as illustrated in Figure 3.2. These findings demonstrate that parallel operation can significantly alter inverter fault response characteristics, even among devices from the same manufacturer.

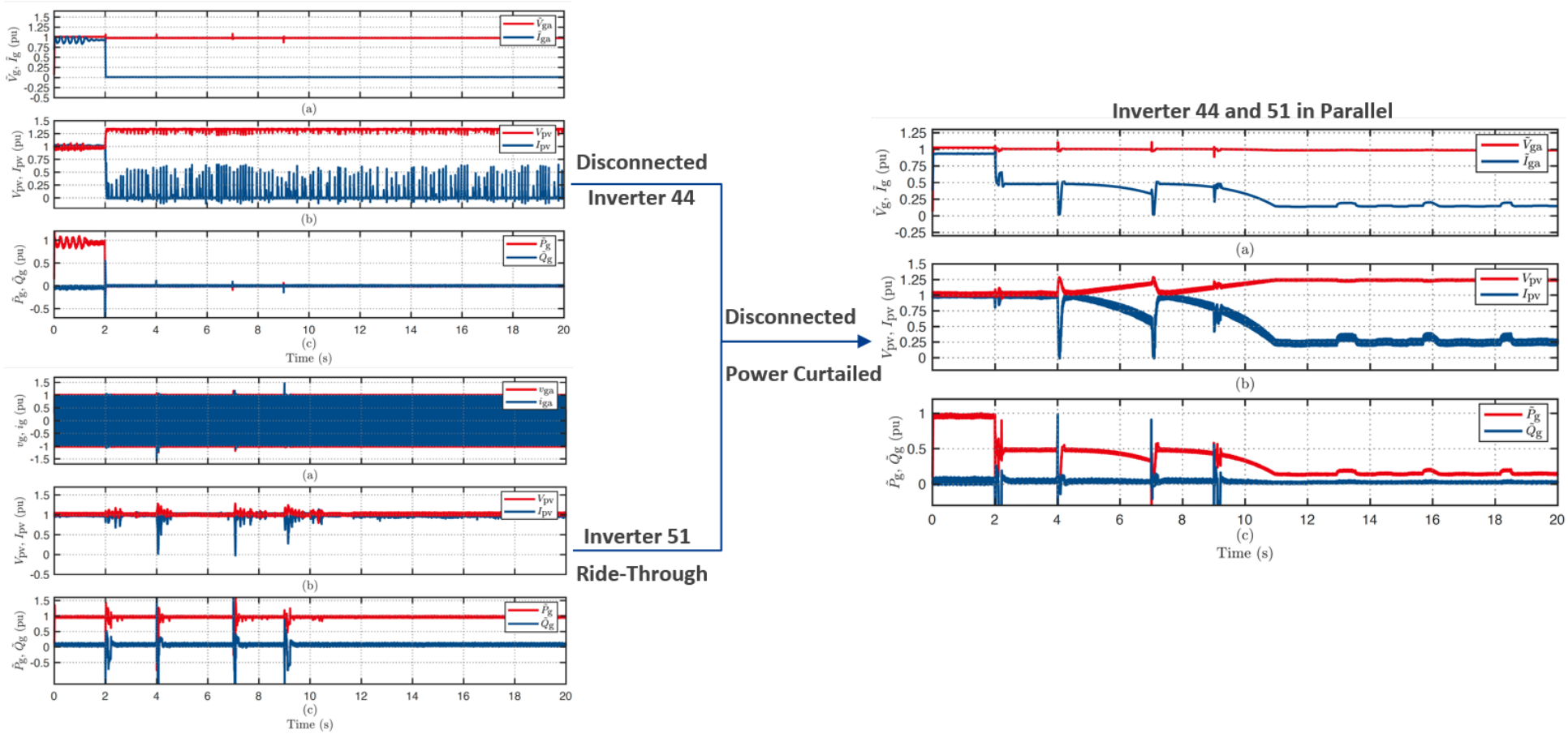

Figure 3.2. Response of Inverters to 60° VPAJ grid disturbance: individual vs parallel configuration.

2.1.2. Inverters 44 and 49

This investigation examined parallel inverter configurations using devices from different manufacturers to assess how performance in shared PCC arrangements compares to standalone operation. When subjected to a 45° VPAJ disturbance generated by the grid emulator, Inverter 49 exhibited unexpected disconnection behaviour, specifically when operating in parallel with Inverter 44, the response was not observed during its standalone testing. This finding is particularly significant as Australian standards mandate that inverters should maintain grid connection (ride through) during VPAJ disturbances of up to 60°. In contrast, Inverter 44 demonstrated consistent behaviour across both testing configurations, disconnecting from the grid during the 45° VPAJ disturbance, whether operating alone or in parallel, as clearly documented in Figure 3.3.

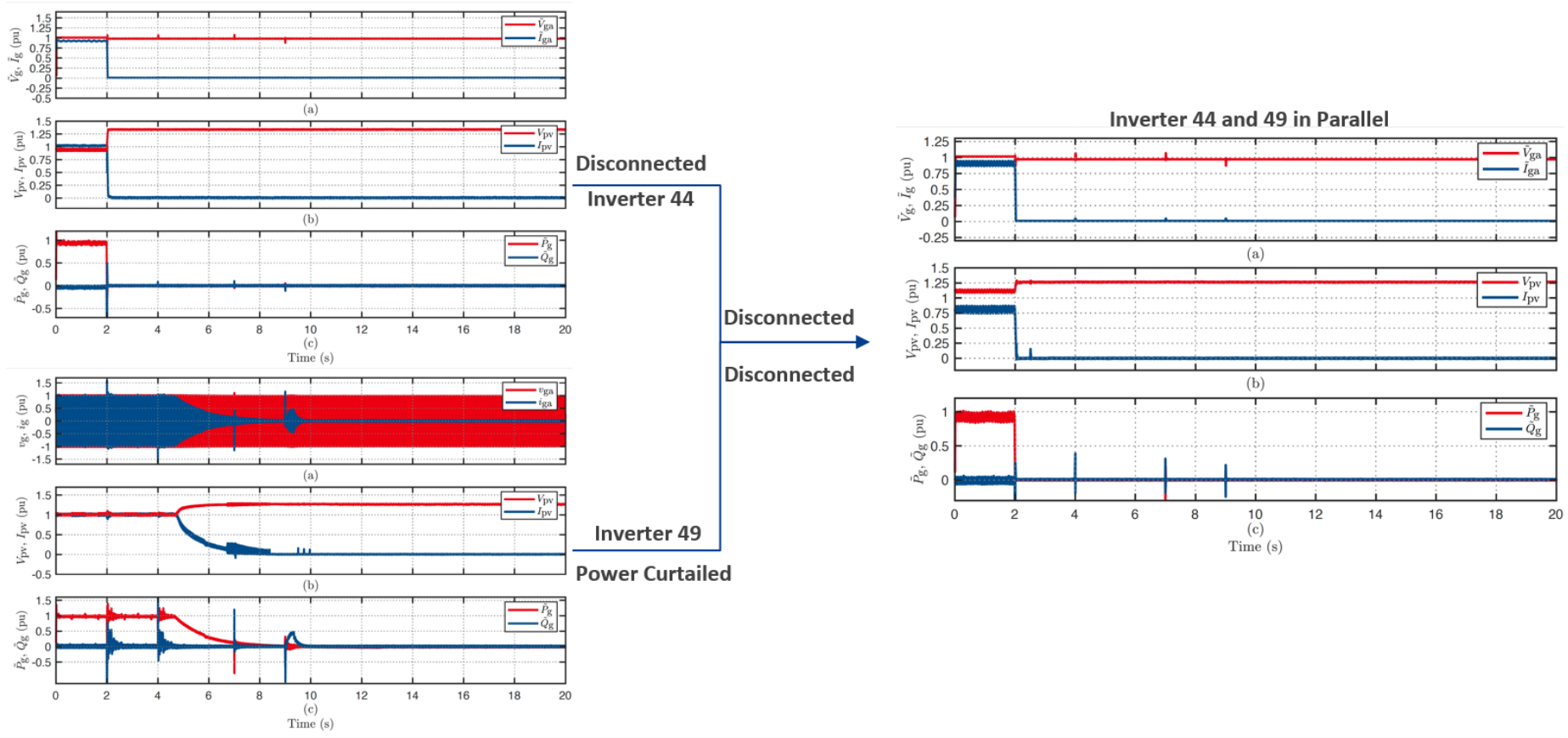

Figure 3.3. Response of Inverters to 45° VPAJ grid disturbance: individual vs parallel configuration.

2.1.3. Inverters 44 and 47

Inverters 44 and 47, identical units from the same manufacturer and model, were connected in parallel and subjected to a 15° VPAJ; inverter 47 exhibited power curtailment when operating in this parallel configuration, as shown in Figure 3.4. This response is particularly significant since both inverters successfully maintained grid connection during individual testing, and Australian standards mandate inverter ride-through capability for VPAJ disturbances up to 60°. The divergent responses between identical inverters reveal how devices' internal inductance can significantly alter performance characteristics in parallel configurations. Furthermore, Inverter 44 demonstrated power curtailment in response to a voltage swell of 1.15 p.u. for 120 ms, as shown in the Figure A1.1.

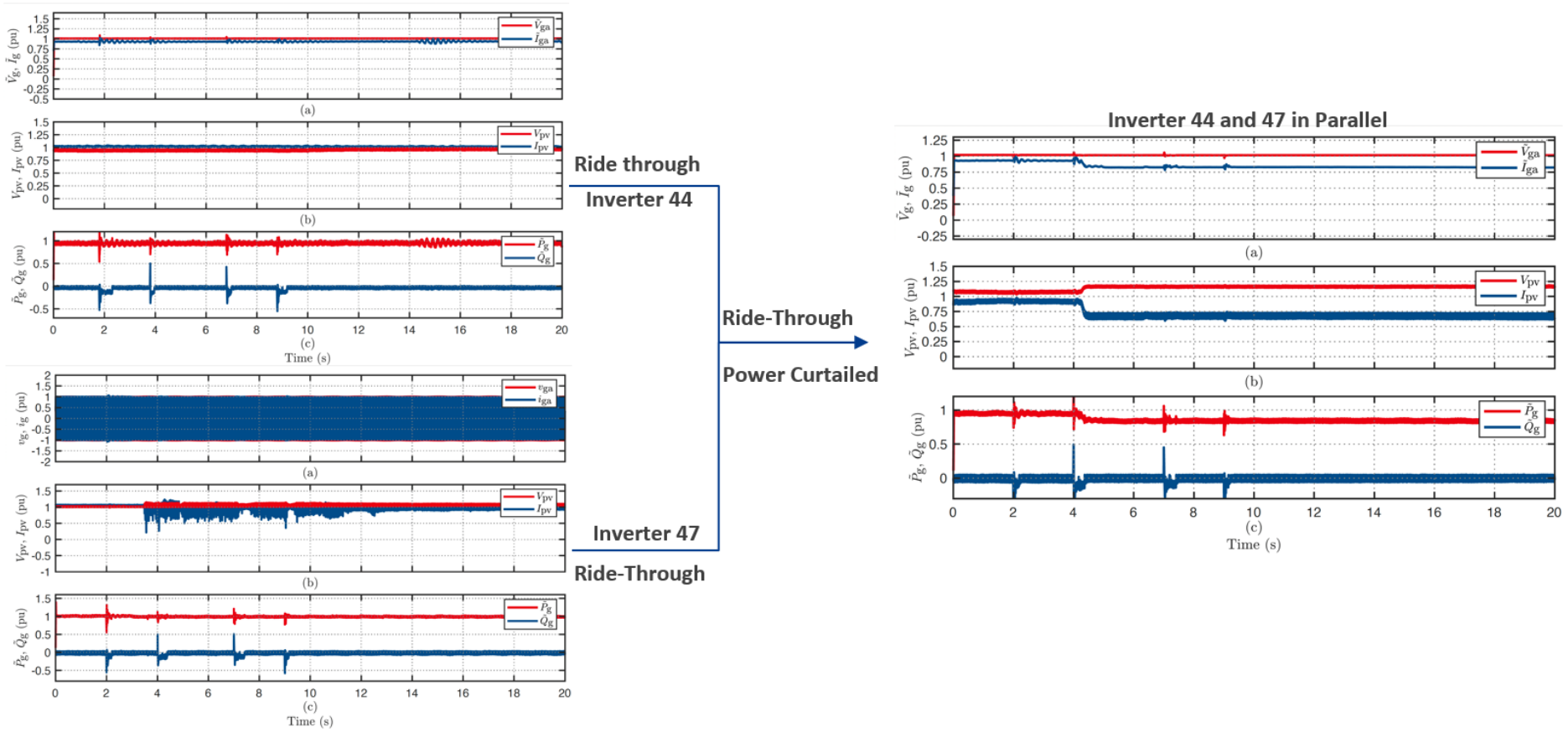

Figure 3.4. Response of Inverters to 15° VPAJ grid disturbance: individual vs parallel configuration.

2.1.4. Inverters 42 and 49

When Inverters 42 and 49 from different manufacturers were connected in parallel and subjected to a 45° VPAJ, significant behavioural differences between the two inverters were observed. Inverter 49 demonstrated critical performance degradation when tested alone, curtailing the output power and now completely disconnecting from the grid, as shown in Figure 3.5. Inverter 42 maintained a grid connection throughout the disturbance without any detectable changes in output characteristics. The response of both inverters to voltage sag of 0.8 p.u for 80 ms is presented in Figure A1.2. These findings have important implications for multi-vendor microgrid deployments, suggesting that parallel operation may introduce unexpected interaction patterns that are not predictable from standalone performance testing.

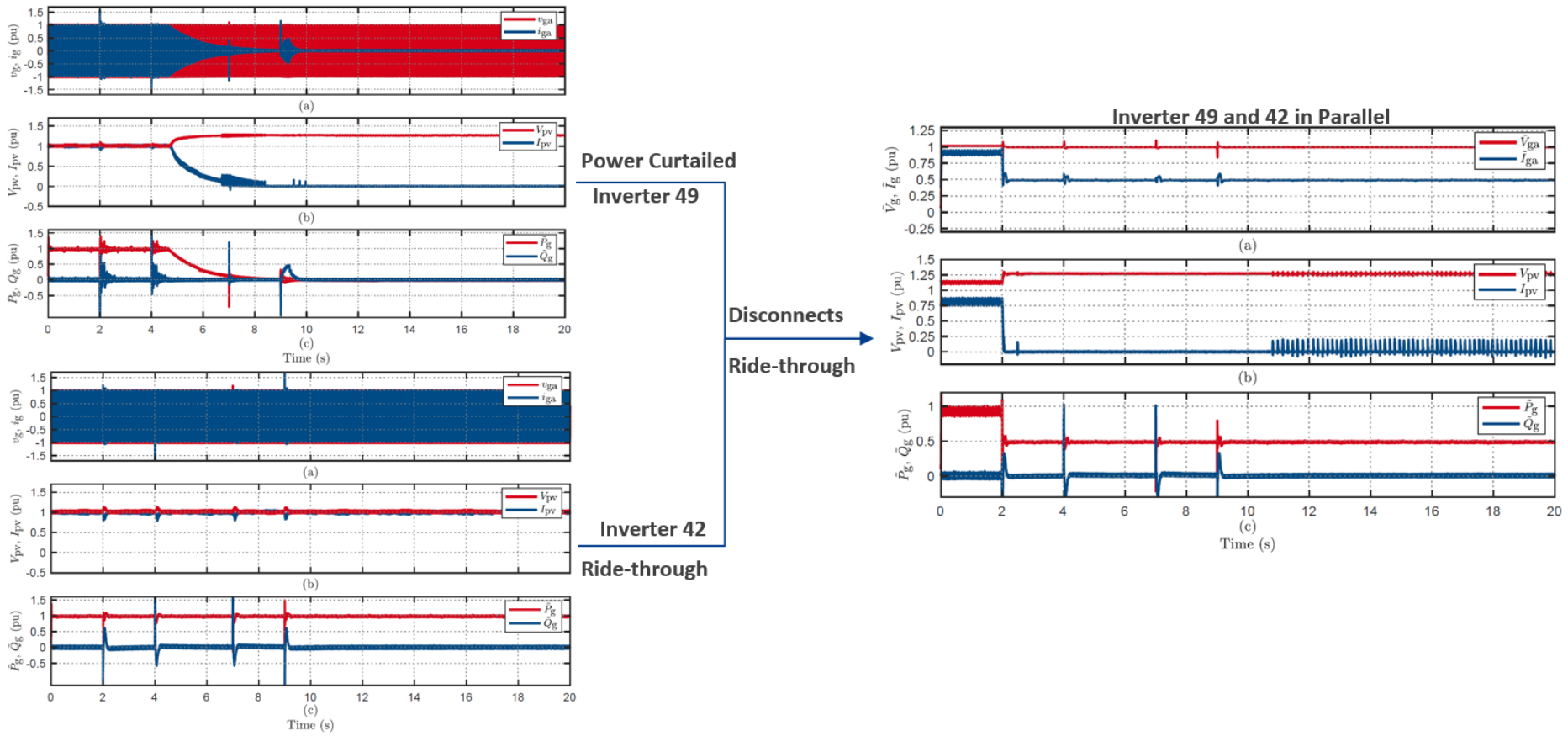

Figure 3.5. Response of Inverters to 45° VPAJ grid disturbance: individual vs parallel configuration.

2.1.5. Inverters 48 and 49

Parallel testing of inverters 48 and 49 from different OEMs revealed critical interaction effects that significantly compromised grid stability responses. When subjected to VPAJ disturbances, both inverters exhibited substantially degraded performance compared to their standalone behaviour. Inverter 48 demonstrated heightened sensitivity in the parallel configuration, disconnecting from the grid at VPAJ values of 30° and above (see Figure A1.3). Similarly, Inverter 49 began disconnecting at VPAJ values of 45° and above (see Figure 3.6). This represents a marked deterioration from their standalone performance, where both units successfully maintained grid connection through power curtailment or complete ride-through, as illustrated in Figure 2.5.

The parallel configuration also affected the response to voltage disturbances. Inverter 48 disconnected when exposed to voltage sags of 0.6 p.u. and below, lasting 80ms as shown in Figure A1.5. Meanwhile, Inverter 49 maintained connection during standalone testing and began power curtailment when subjected to a 0.7 p.u. voltage sag for 220ms while operating in parallel with Inverter 48, as shown in Figure A1.4.

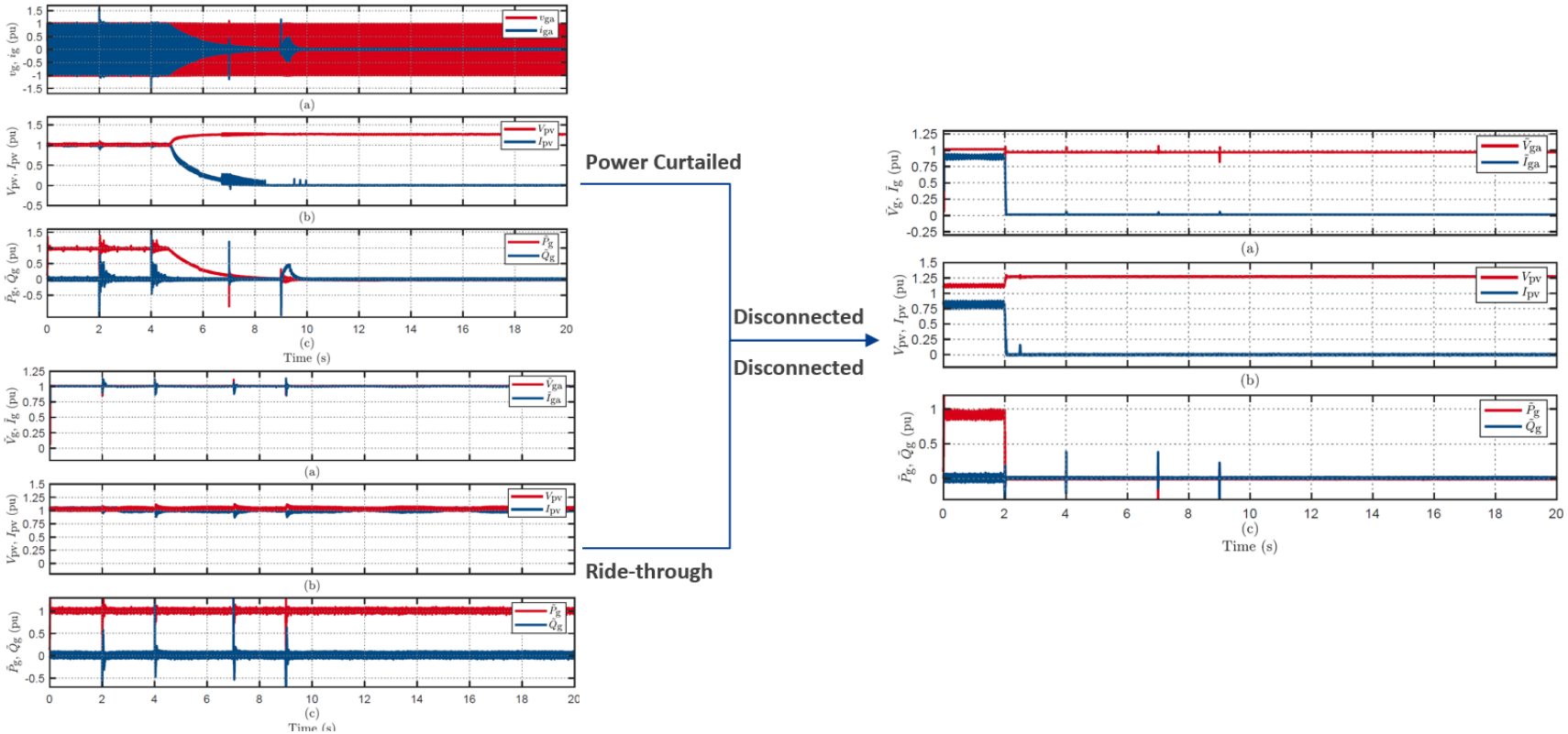

Figure 3.6. Response of Inverters to 45° VPAJ grid disturbance: individual vs parallel configuration.

2.1.6. Inverters 47 and 48

A comprehensive evaluation of Inverters 47 and 48 from different OEMs revealed significant performance degradation when operating in parallel compared to their standalone capabilities. The most pronounced effects were observed in the Inverter 48 response to grid disturbances. When subjected to VPAJ disturbances in the parallel configuration, Inverter 48 exhibited increased sensitivity, disconnecting from the grid at VPAJ values as low as 30°, well below the threshold, and maintaining connection during standalone testing, see Figure 3.7. This compromised performance also extended to voltage disturbances, with Inverter 48 disconnecting when exposed to a 180V sag lasting 0.9 seconds, as shown in Figure A1.7. In contrast, Inverter 47 maintained consistent performance across standalone and parallel testing scenarios.

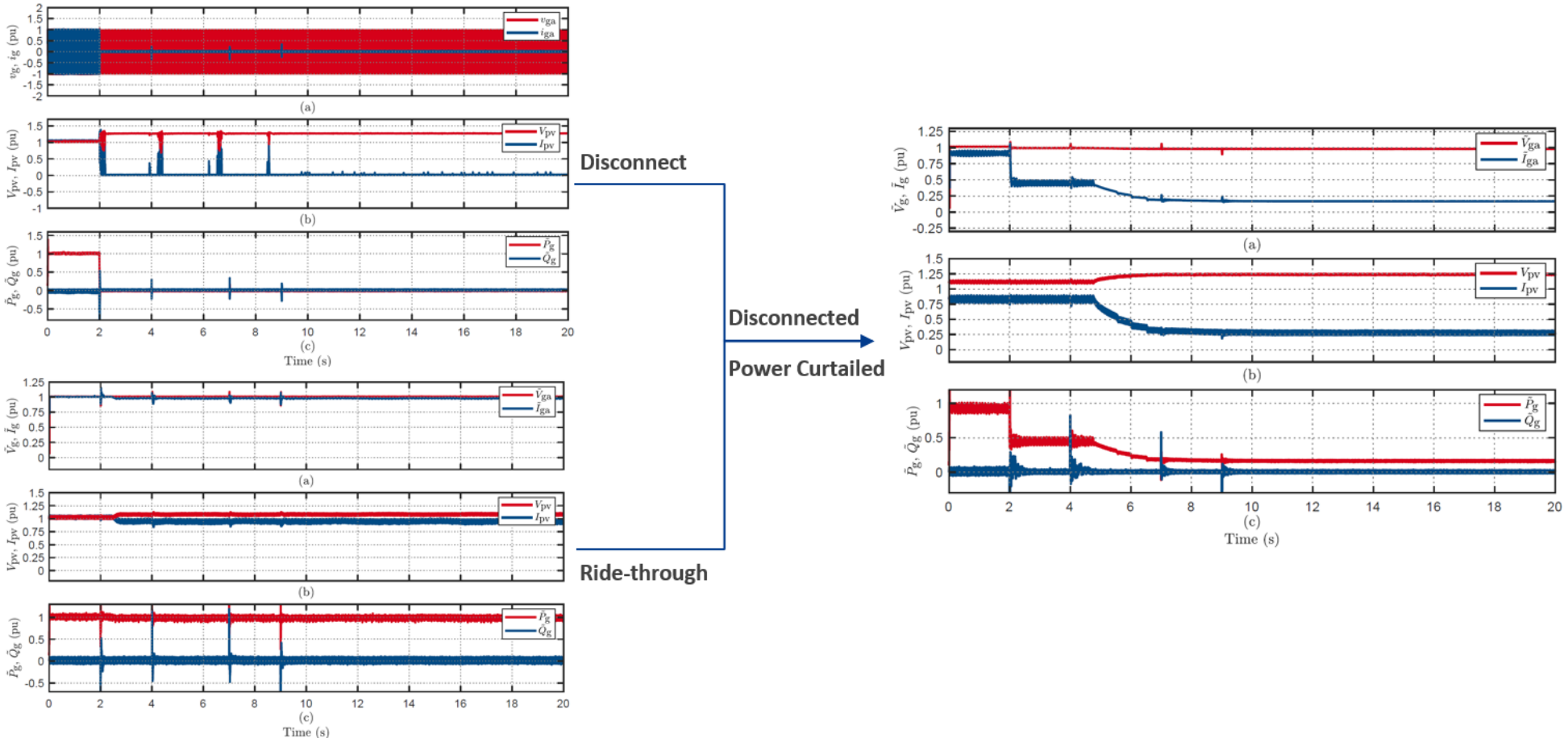

Figure 3.7. Response of Inverters to 30° VPAJ grid disturbance: individual vs parallel configuration.

2.1.7. Inverters 48 and 51

Evaluation of inverters 48 and 51 sourced from different OEMs revealed significant operational vulnerabilities when deployed in parallel configurations. Most notably, when subjected to a 60° VPAJ, both inverters disconnected from the grid, as shown in Figure 3.8. This synchronized disconnection represents a critical system vulnerability, as it could potentially trigger cascading outages in larger deployment scenarios. Furthermore, Inverter 48 exhibited sensitivity to voltage fluctuations in the parallel configuration, disconnecting from the grid when exposed to a voltage sag of 0.7 p.u. for 220ms, as illustrated in Figure A1.9. This response threshold indicates significant degradation compared to typical standalone performance parameters for inverters in this class.

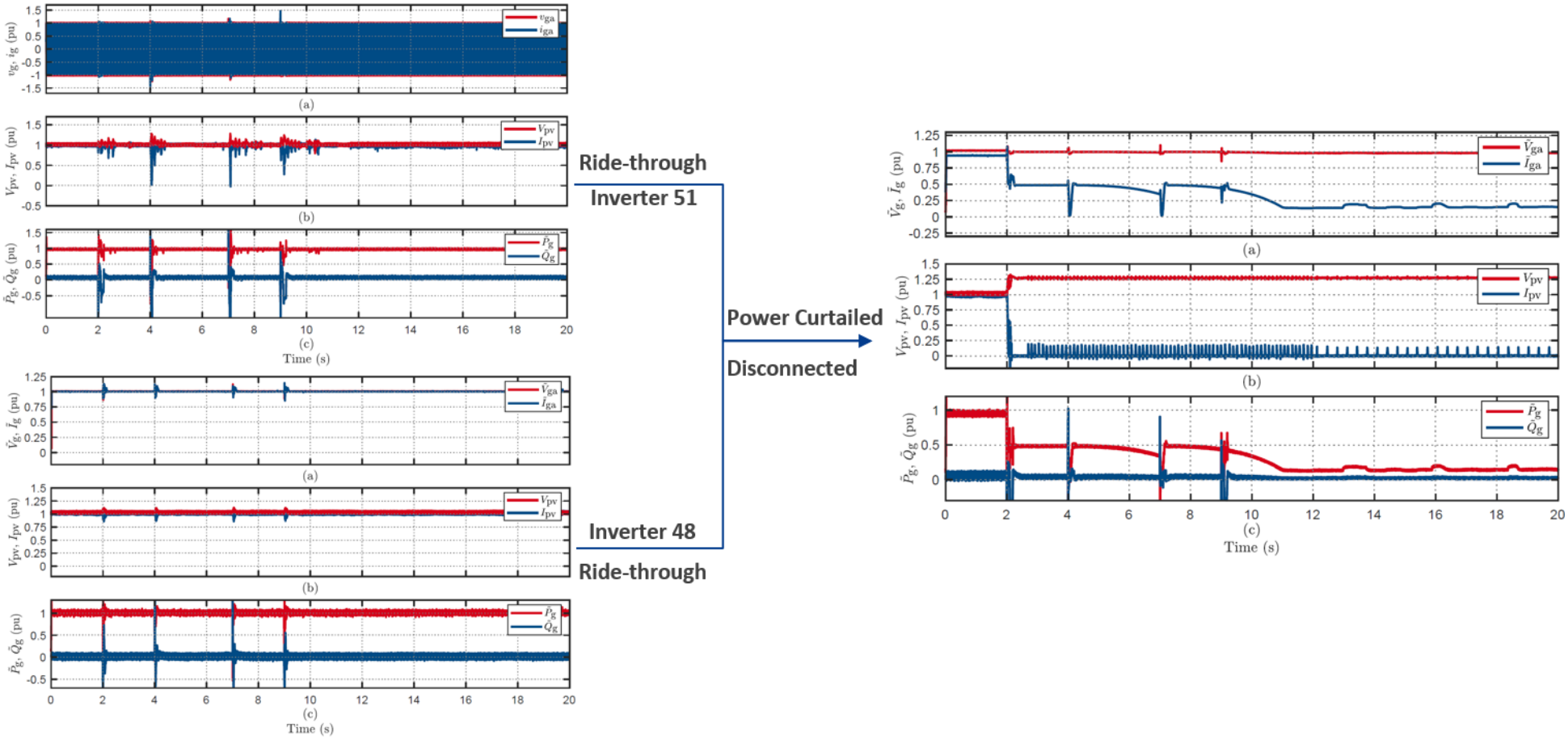

Figure 3.8. Response of Inverters to 60° VPAJ grid disturbance: individual vs parallel configuration.

2.1.8. Inverters 54 and 48

The comprehensive analysis of inverters 54 and 48 from different OEMs revealed complex patterns with both detrimental and beneficial effects when operating in parallel configurations. Inverter 48 demonstrated significant operational vulnerabilities across multiple disturbance types. When subjected to VPAJ of 30°, inverter 48 is disconnected from the grid while operating in parallel with Inverter 54, as shown in Figure 3.9. Similar disconnection behaviour was observed during voltage sag disturbances, with inverter 48 separating from the grid when exposed to 180V for 0.9 seconds (Figure A1.10) and a more severe sag of 0.5 p.u lasting 80ms (Figure A1.11).

It is worth noting a positive interaction effect was observed during voltage sag conditions. When exposed to a prolonged voltage sag of 50V for 9 seconds, the parallel configuration allowed both inverters to ride through the disturbance effectively Figure A1.12. This represented a significant improvement for inverter 54, which had previously disconnected during standalone testing when faced with the same disturbance.

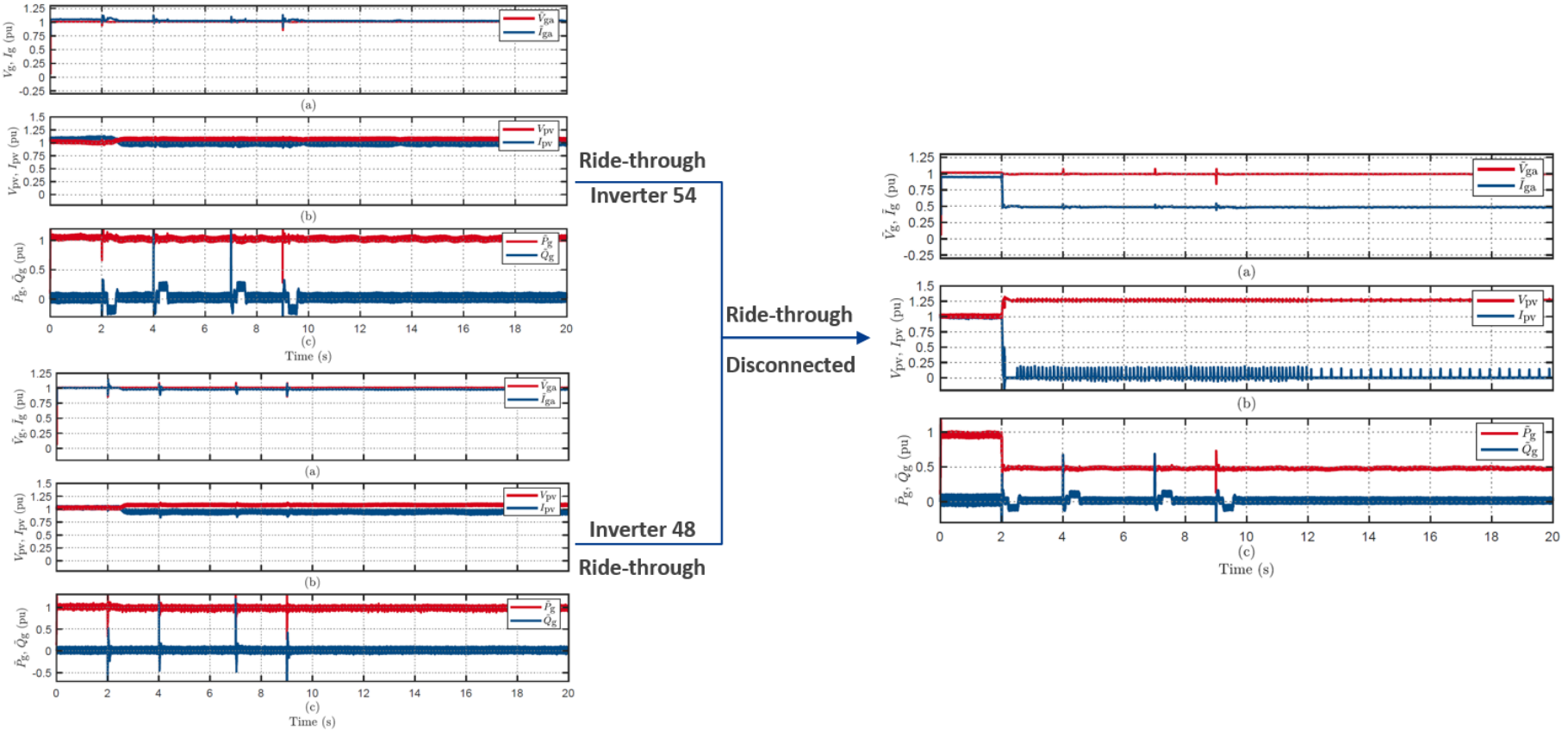

Figure 3.9. Response of Inverters to 30° VPAJ grid disturbance: individual vs parallel configuration.

2.1.9. Inverters 49 and 54

Comprehensive analysis of inverters 49 and 54 by different OEMs revealed a change in response characteristics when transitioning from standalone to parallel operation. When tested independently, inverter 49 demonstrated power curtailment in response to a voltage sag of 0.8 p.u. lasting 220ms. The inverter maintained the pre-fault power level when tested in parallel with inverter 54, as shown in Figure 3.10. Similarly, Inverter 54 rode through the voltage swell of 1.15 p.u for 220ms when tested in parallel with Inverter 51, but curtailed the output power when tested alone, as shown in Figure A1.13. Most significantly, parallel configuration testing revealed enhanced system resilience in this case.

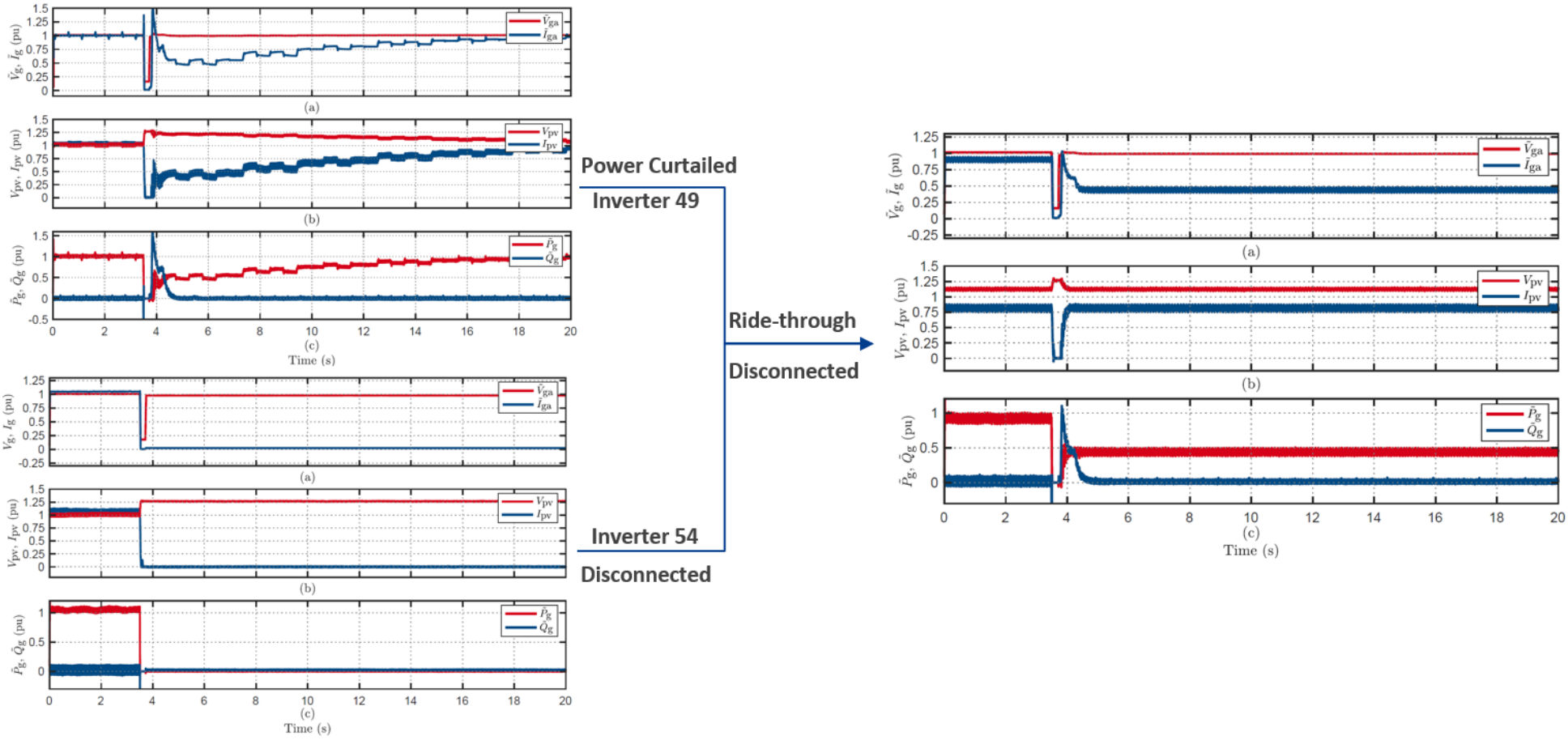

Figure 3.10. Response of Inverters to voltage swell of 30V : individual vs parallel configuration.

2.1.10. Inverters 47 and 54

A comprehensive analysis of inverters 47 and 54, which belong to the same OEM but are different models, revealed improvements in disturbance response when transitioning from standalone to parallel operation. When subjected to a 45° VPAJ during individual testing, inverter 54 presented power curtailment behaviour; however, this same inverter maintained full pre-disturbance output power levels when operating in parallel with Inverter 47, as shown in Figure 3.11.

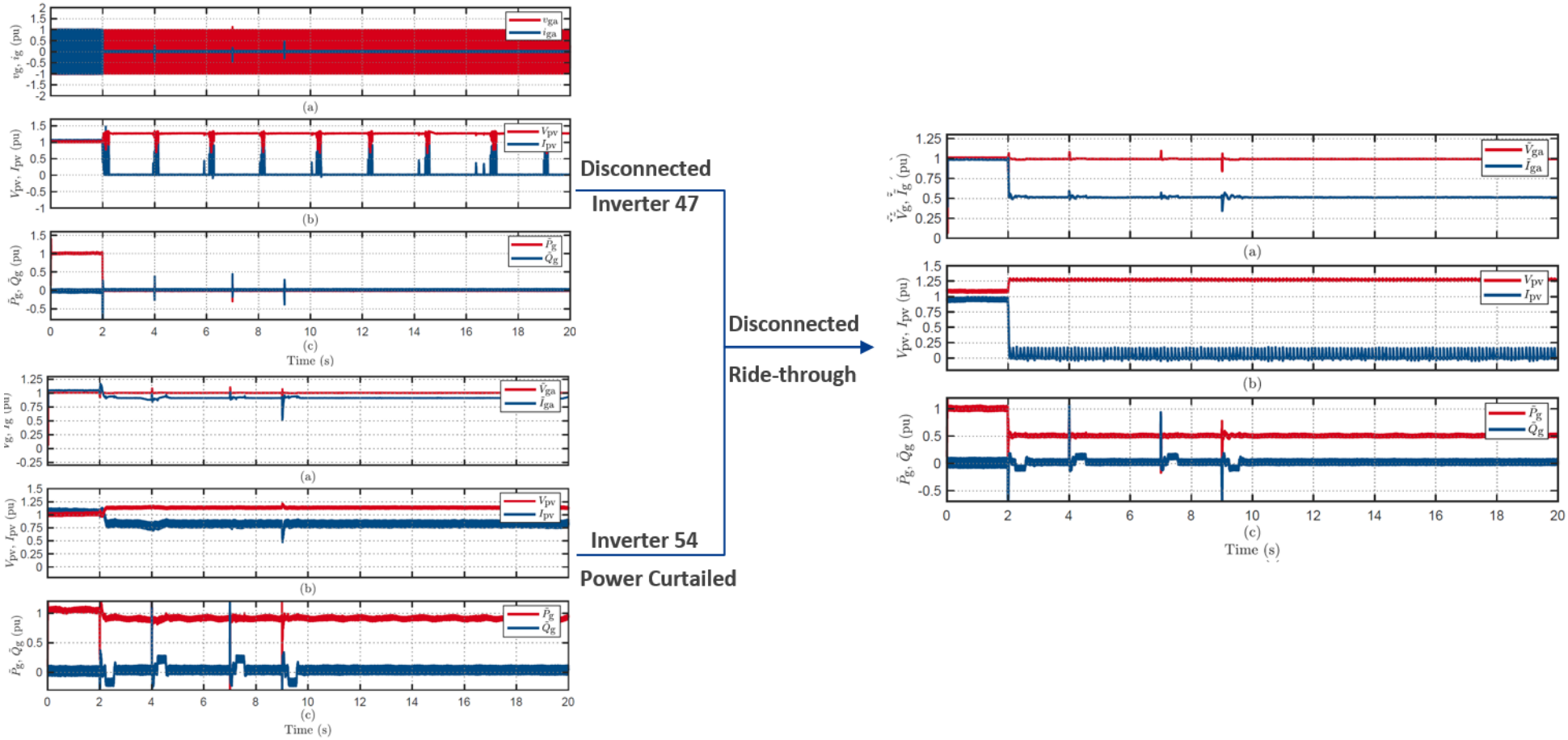

Figure 3.11. Response of Inverters to 45° VPAJ grid disturbance: individual vs parallel configuration.

2.1.11. Inverters 38 and 54

A comprehensive analysis of inverters 38 and 54 from different manufacturers revealed performance deterioration when operating in parallel configurations compared to standalone operations. When subjected to a voltage sag disturbance of 0.8 p.u for 220ms, Inverter 38 successfully maintained full output power with complete ride-through capability during individual testing. However, this same inverter exhibited compromised performance when operating in parallel with Inverter 54, implementing unnecessary power curtailment, as shown in Figure 3.12. This adverse interaction effect between dissimilar inverters highlights critical compatibility concerns in mixed-manufacturer deployments, suggesting that parallel configurations can potentially undermine the certified capabilities of otherwise robust grid-support functionality.

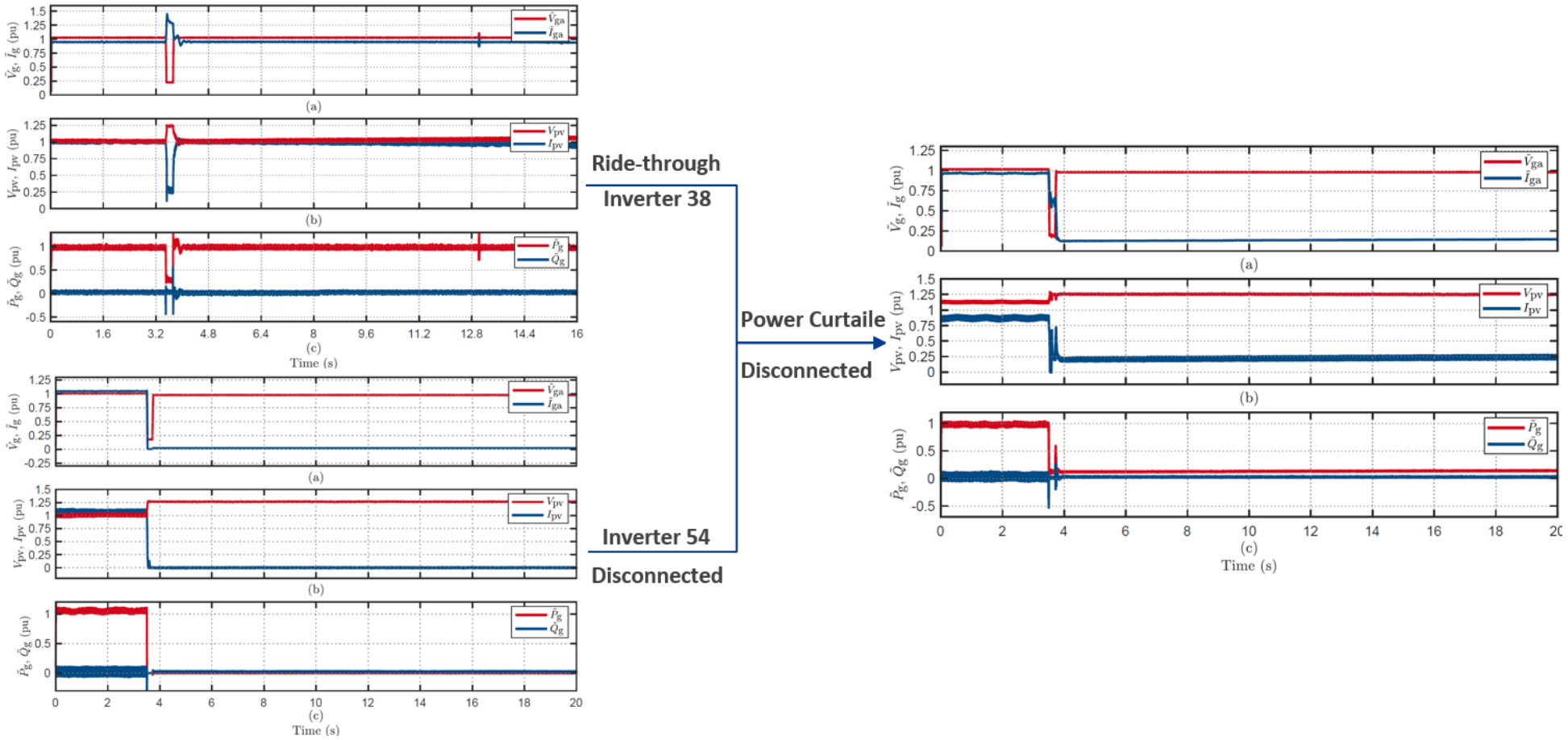

Figure 3.12. Response of Inverters to 45° VPAJ grid disturbance: individual vs parallel configuration.

2.1.12. Inverters 47(H) and 48

Inverters 48 and 47 from different manufacturers revealed significant performance deterioration when operating in parallel configurations compared to their standalone capabilities. When subjected to a modest VPAJ of 30°, Inverter 48 maintained grid connection with full output power during individual testing but exhibited severely compromised performance when paired with Inverter 47, completely disconnecting from the grid as shown in Figure 3.13. This degradation pattern extended to Inverter 47 as well, which successfully rode through voltage swells of 1.175 p.u for 220ms during standalone testing, but implemented unnecessary power curtailment when operating in parallel with Inverter 48 see Figure A1.14. These findings demonstrate how inter-manufacturer compatibility issues can create bidirectional adverse effects that substantially compromise the grid support capabilities.

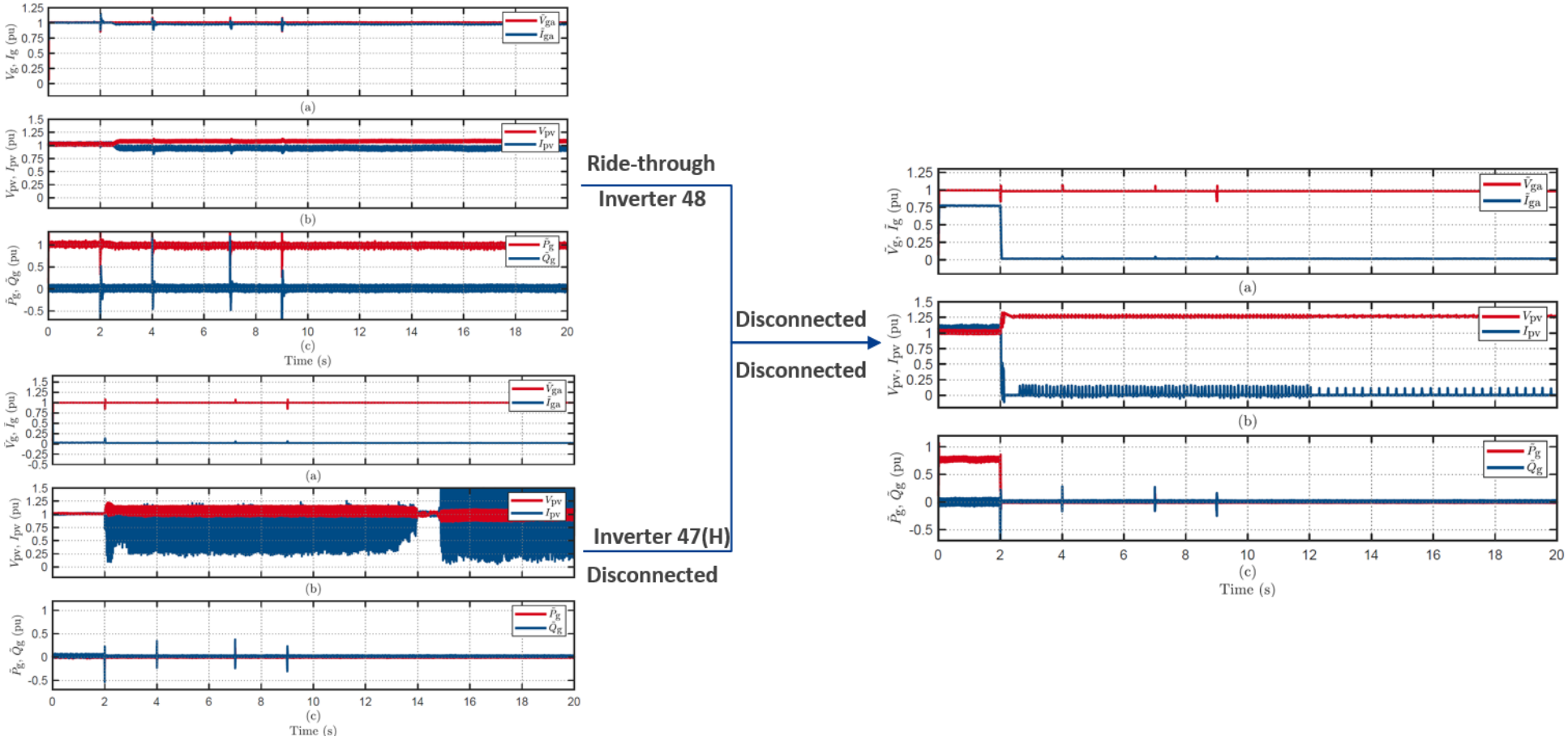

Figure 3.13. Response of Inverters to 30° VPAJ grid disturbance: individual vs parallel configuration.

2.1.13. Inverters 47(H) and 49

Analysis of inverters 47 and 49 from different manufacturers revealed complex interaction effects when operating in parallel configurations, with deterioration and performance enhancement compared to standalone operation. When subjected to a 45° VPAJ, inverter 49 exhibited critical performance degradation, completely disconnecting from the grid during parallel operation. This was a significant deterioration from its standalone behaviour, where it successfully maintained grid connection through power curtailment, as shown in Figure 3.14. Conversely, inverter 47 demonstrated markedly improved resilience in the parallel configuration, successfully riding through a severe voltage swell of 1.2 p.u for 800ms while operating alongside inverter 49, despite having disconnected when facing this identical disturbance during individual testing, as shown in Figure A1.15.

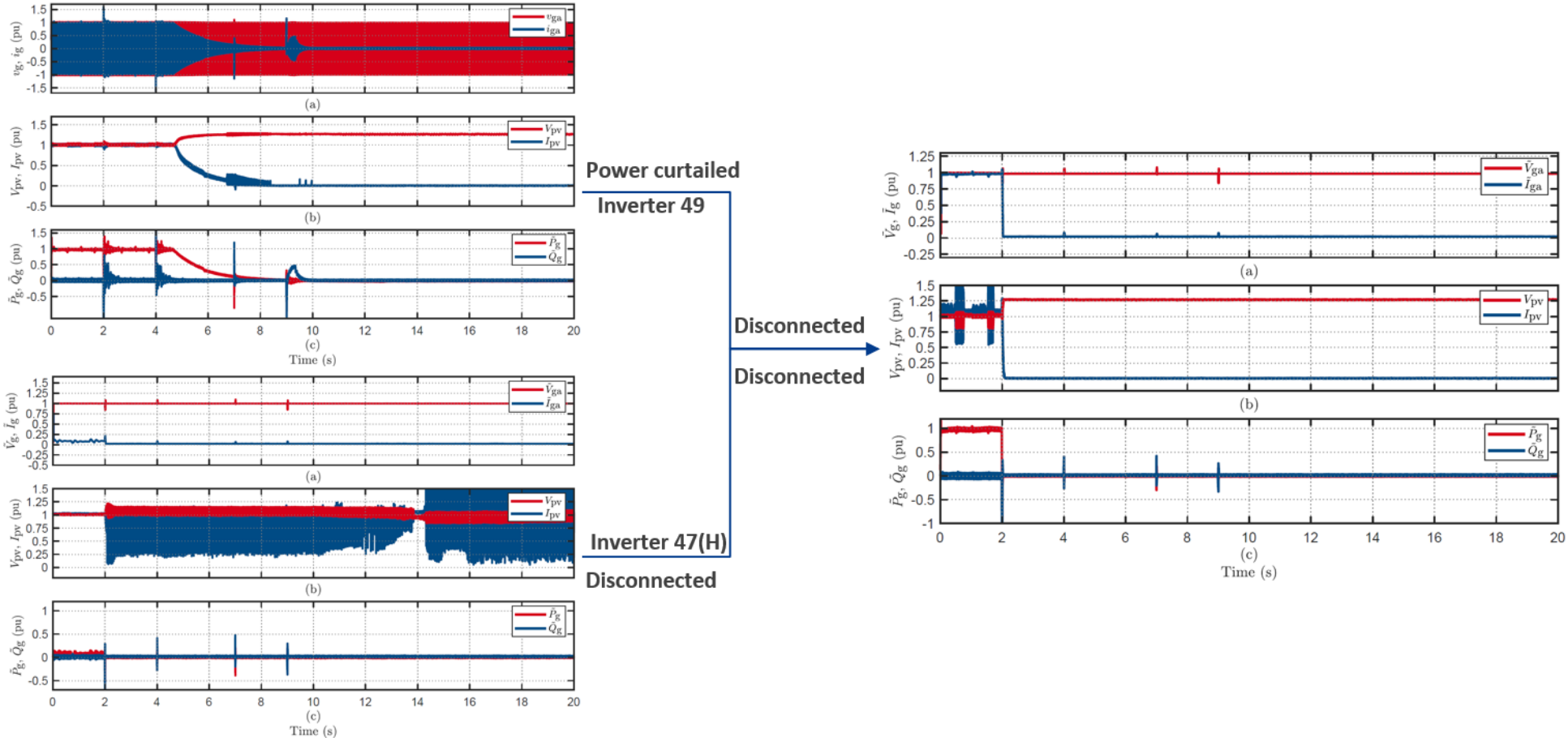

Figure 3.14. Response of Inverters to 45° VPAJ grid disturbance: individual vs parallel configuration.

2.2. Triple Inverter Testing

A three-inverter parallel configuration was used to expand the experimental framework, interconnecting three inverters at a shared Point of Common Coupling (PCC). This setup, shown in Figure 3.15, was implemented to extend the investigation beyond two-inverter interactions and observe cumulative effects unique to multi-inverter systems. The schematic illustrates how all three inverters share the PCC while operating with independent control architectures, allowing analysis of grid stabilisation behaviours not evident in simpler configurations. This setup was used to examine how disturbance responses propagate through larger inverter groups, potentially leading to cascading stability impacts or damping effects that only arise with three or more units.

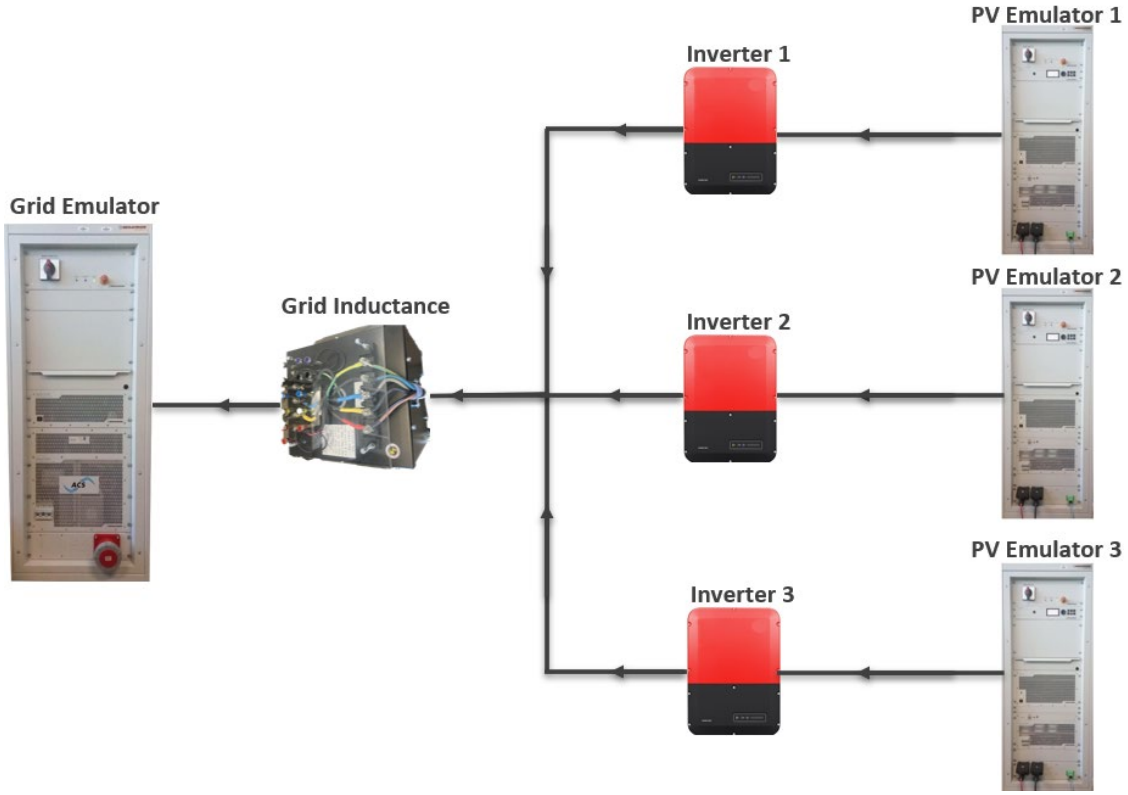

Figure 3.15. Simplified diagram of the experimental setup for parallel inverter testing of three inverters.

2.2.1. Inverters 42, 48 and 52

The analysis of three parallel inverters (42, 48, and 52), each by different OEMs, revealed the pronounced vulnerability of specific units within the multi-inverter configuration. Inverter 48 demonstrated significant performance degradation across multiple disturbance types, emerging as the most susceptible component in this complex system arrangement.

When subjected to a VPAJ of 30°, the inverter 48 was disconnected from the grid while both inverters 54 and 42 maintained stable operation. The comparative waveforms in Figure 3.16 display individual and combined results, clearly illustrating the inverter 48's disconnection following the VPAJ disturbance. Similarly, the inverter 48 disconnects when exposed to a voltage sag of 0.6 p.u for 80ms, as shown in Figure A2.1, while the other inverters remain connected. These findings highlight how inverters can create asymmetric stability profiles in multi-vendor deployments, potentially compromising overall system resilience during grid disturbances.

2.2.2. Inverters 42, 47 and 48

The analysis of three parallel inverters (42, 47, and 48) from different OEMs presented stability challenges emerging specifically within multi-inverter configurations. Notably, inverters 42 and 48 exhibited degradation in their response when subjected to VPAJ disturbances in this three-inverter arrangement. When exposed to a 60° VPAJ, both inverters 42 and 48 disconnected from the grid, a critical deviation from their standalone testing, where both units successfully maintained grid connection through the identical disturbance. Figure 3.17 displays individual and combined results, illustrating the inverter 42 and 48 disconnections following the VPAJ disturbance.

Voltage disturbance testing revealed additional interaction-induced performance variations. Inverter 42 presented power curtailment behaviour when exposed to a voltage swell of 30V, as shown in Figure 3.17, while the other inverters presented the same behaviour when tested individually. Inverter 47 disconnected from the grid when subjected to a voltage swell of 1.2 p.u for 220ms while operating in this three-inverter arrangement, as shown in Figure A2.2.

2.2.3. Inverters 48, 49 and 52

Inverters 48, 49, and 52 from different OEMs exhibited vulnerabilities when operated in a parallel configuration, with all units demonstrating significantly degraded performance compared to their individual capabilities. Most notably, when subjected to a moderate 45° VPAJ, all three inverters disconnected from the grid simultaneously. This behaviour deviated from their individual testing results, where they successfully maintained grid connection during identical disturbances through either complete ride-through or power curtailment, as illustrated in Figure 3.18. Furthermore, Inverter 52 displayed a modified response to voltage disturbances in this configuration by power curtailment when exposed to a voltage sag of 80V lasting 0.9s. These findings underscore how interactions among multiple inverters can fundamentally compromise the grid support capabilities of otherwise compliant units.

2.2.4. Inverters 47, 48 and 49

The analysis of inverters 47, 48, and 49, two from the same OEM and one from a different OEM, revealed complex asymmetric interaction patterns in a three-inverter parallel configuration. This setup exhibited performance degradation in certain units, alongside unexpected improvements in resilience for others. When subjected to a 45° VPAJ, inverters 48 and 49 simultaneously disconnected from the grid, contrasting with their standalone performance, where they had maintained connection through similar disturbances via ride-through and power curtailment, as illustrated in Figure 3.19. Notably, this configuration demonstrated enhanced voltage disturbance resilience in inverters 47 and 48, allowing them to successfully ride through voltage swell conditions that had previously triggered protective responses during individual testing.

2.2.5. Inverters 46, 47(H) and 54

The analysis of inverters 46 47, and 54, which belong to the same OEM, demonstrated improved performance when operating in a parallel configuration with three inverters. Notably, inverter 47 showed enhanced resilience to voltage disturbances in this setup. When exposed to a 40V voltage swell lasting 0.9 seconds, this inverter successfully maintained its grid connection through a power curtailment response. This represents a significant improvement compared to its standalone performance, where similar disturbance conditions resulted in complete disconnection, as illustrated in Figure 3.20. The enhanced performance can be directly attributed to the inverter 47 hybrid operational mode, which was effectively engaged within the multi-inverter configuration.

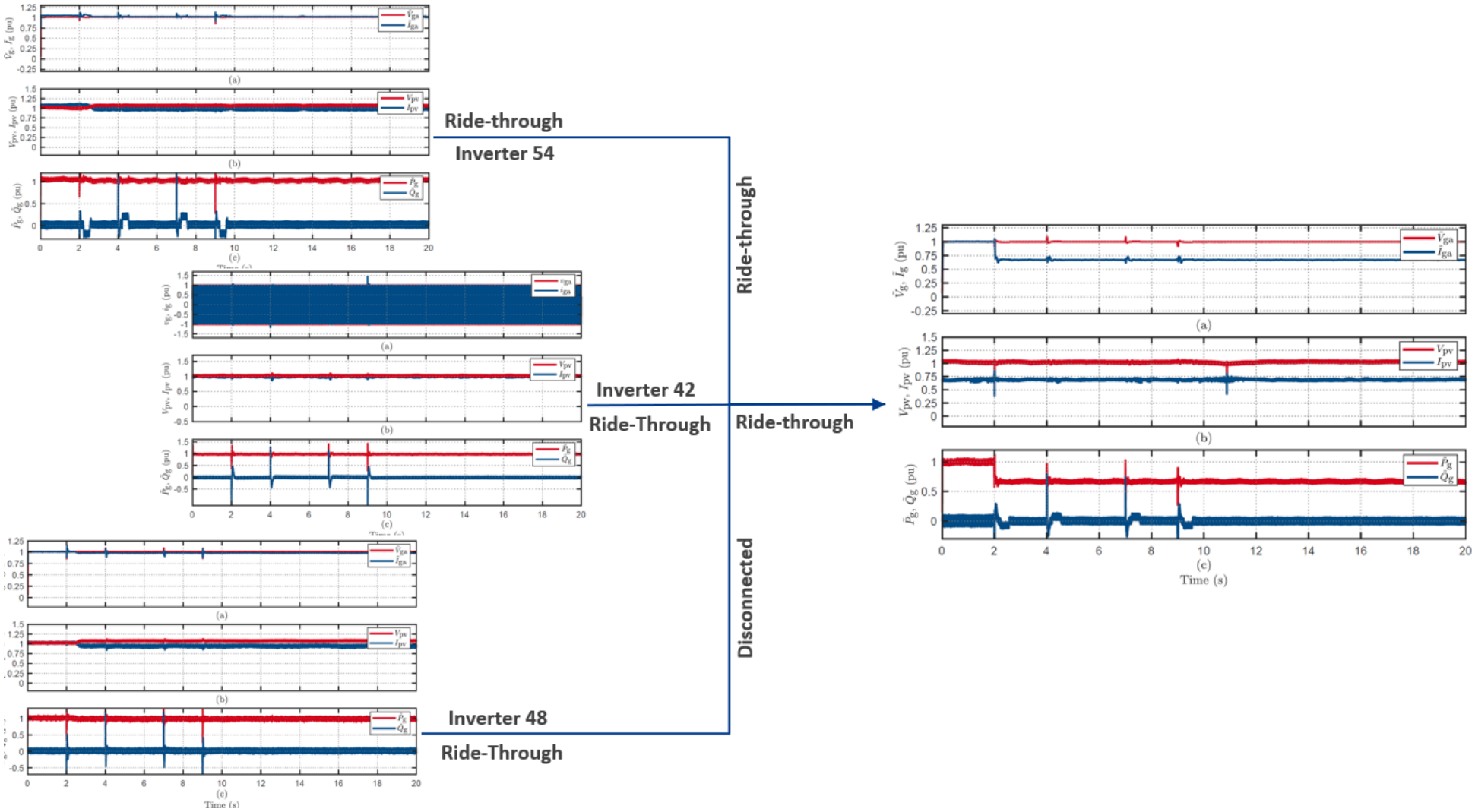

Figure 3.16. Response of Inverters to 30° VPAJ grid disturbance: individual vs parallel configuration.

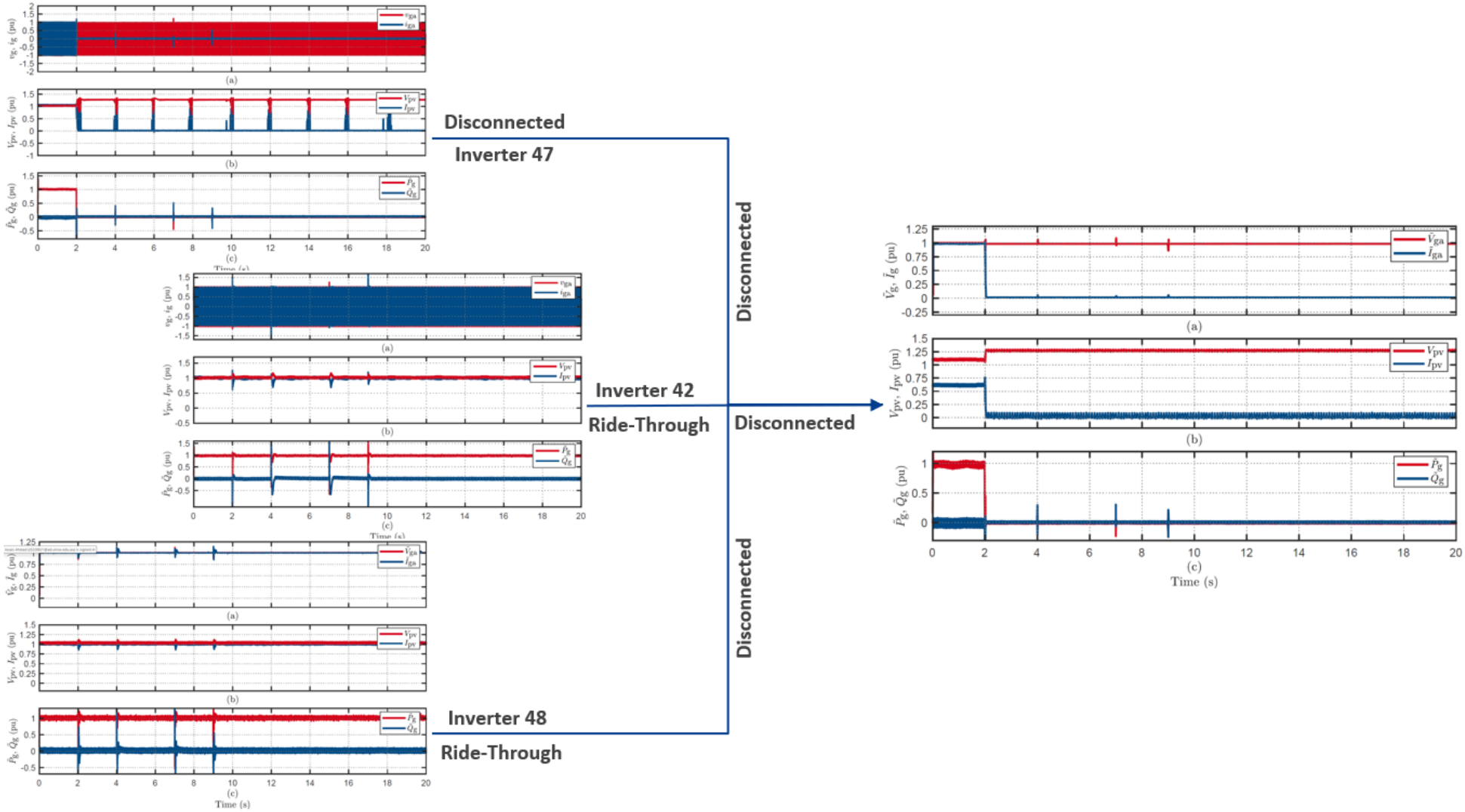

Figure 3.17. Response of Inverters to 60° VPAJ grid disturbance: individual vs parallel configuration.

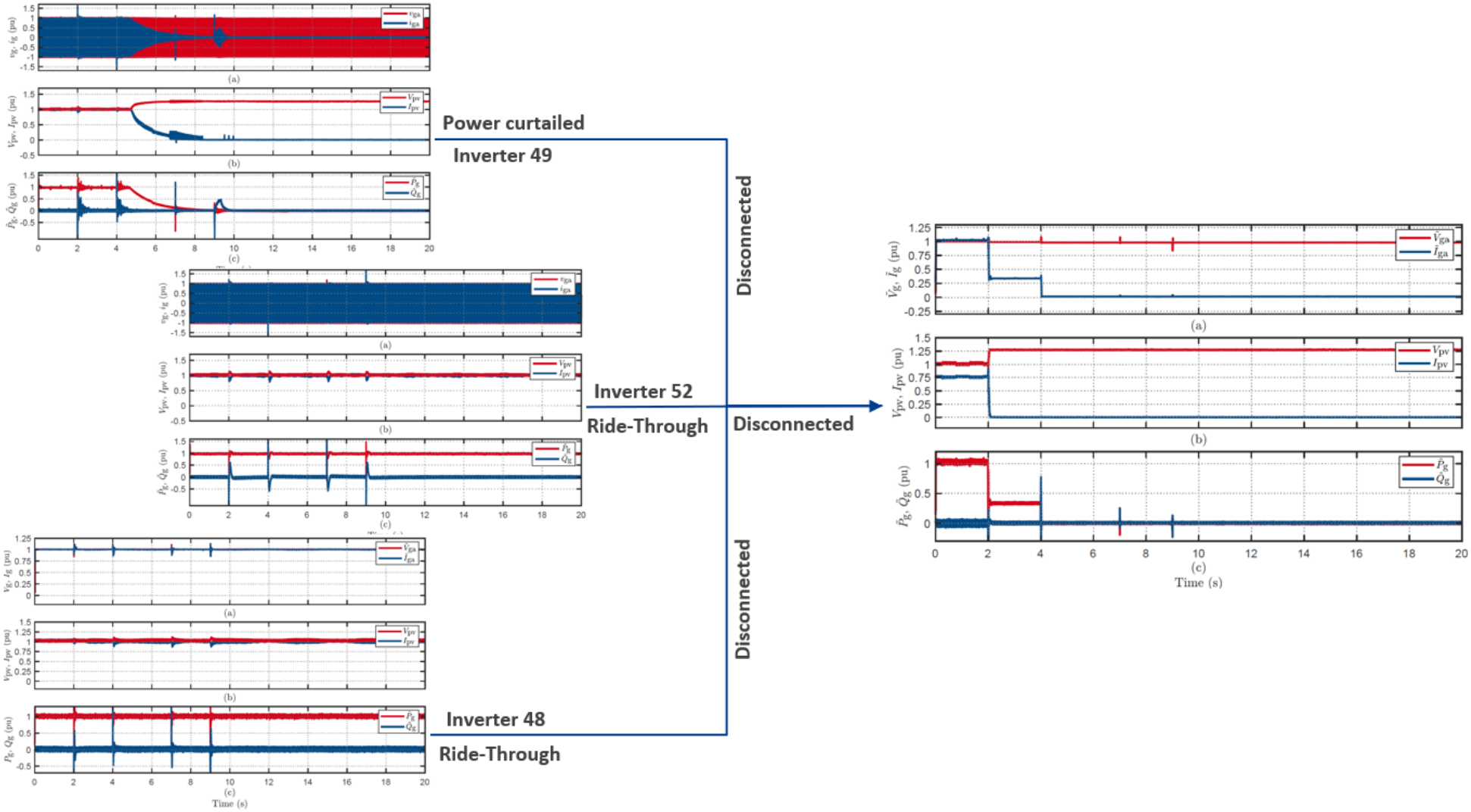

Figure 3.18. Response of Inverters to 45° VPAJ grid disturbance: individual vs parallel configuration.

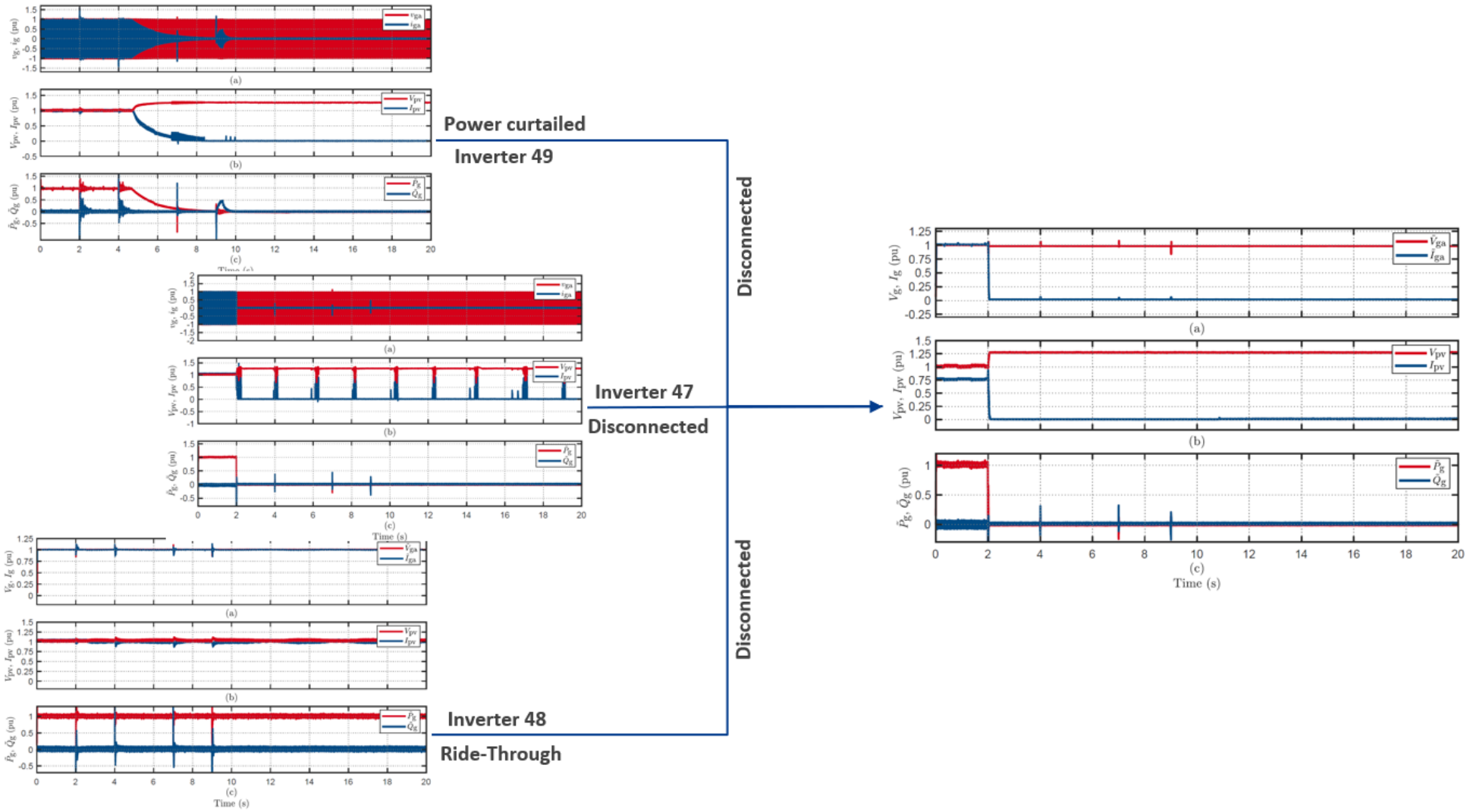

Figure 3.19. Response of Inverters to 45° VPAJ grid disturbance: individual vs parallel configuration.

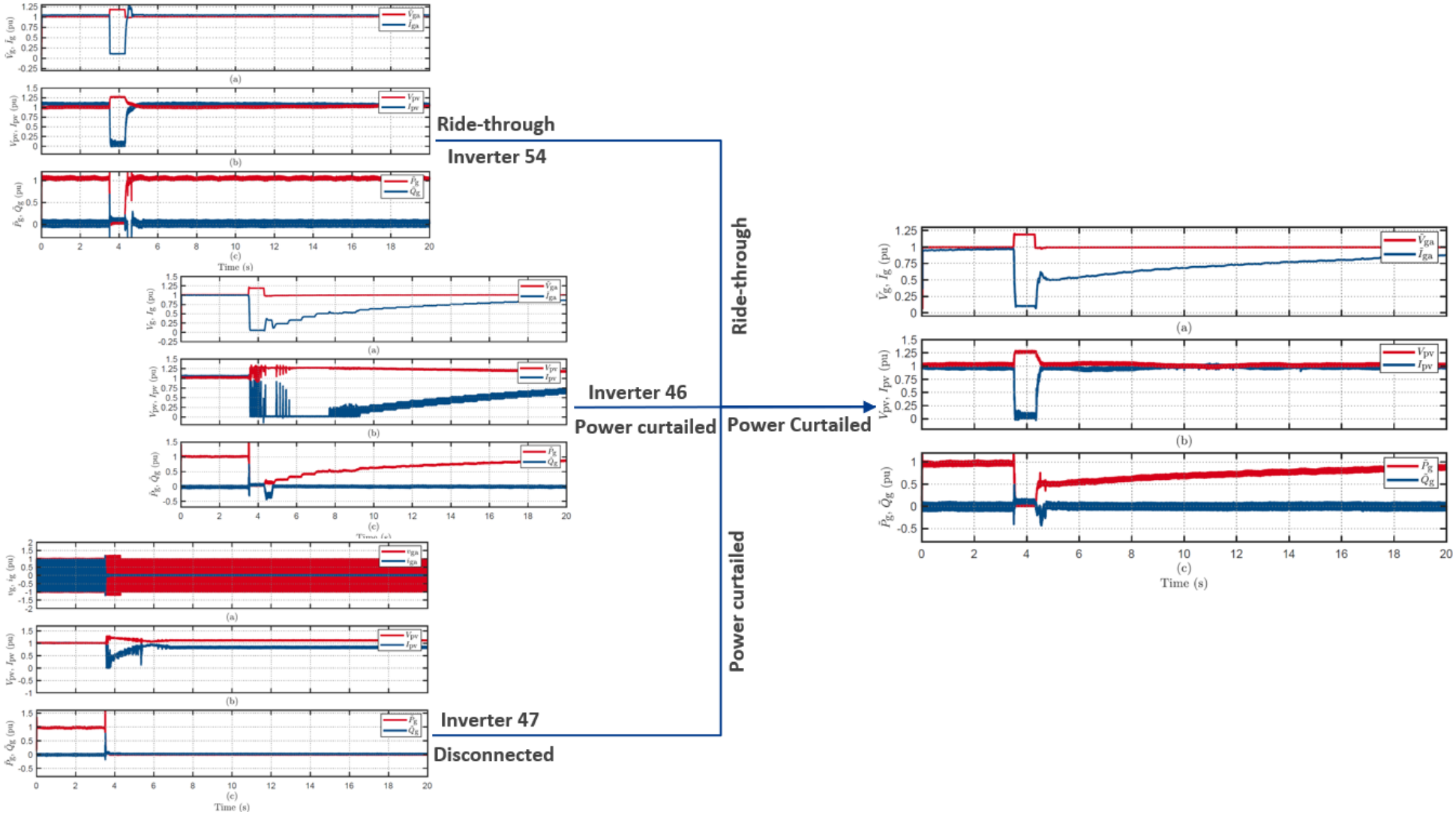

Figure 3.20. Response of Inverters to voltage swell of 40V for 0.9s grid disturbance: individual vs parallel configuration.

2.3. Conclusion

Testing of parallel inverter configurations revealed increasingly complex interaction effects as systems progressed from two to three inverters. In two-inverter setups, fifteen pairings across different manufacturers showed that parallel operation can significantly affect inverter behaviour. In several cross-manufacturer cases, inverters that remained connected during standalone testing disconnected when operated in parallel. Inverters 48 and 49 were notably sensitive, showing consistent disconnection under VPAJ and voltage sag disturbances when paired with other units.

Three-inverter configurations showed further stability issues, particularly in mixed-OEM setups. The combination of Inverters 48, 49, and 52 disconnected simultaneously under a 45° VPAJ, despite all units remaining connected during individual testing. This contrasts with the two-inverter tests, where typically only one unit disconnected. The increased sensitivity in three-inverter setups highlights the potential for cascading failures not visible in simpler configurations. Inverter 48 remained the most consistently vulnerable, disconnecting at VPAJ values as low as 30° in parallel setups while remaining connected in standalone operation—suggesting inherent limitations in its design for coordinated deployment.

Some parallel configurations showed improved performance. In two-inverter setups, Inverters 47 and 54 (same manufacturer, different models) demonstrated enhanced ride-through, with Inverter 54 maintaining full output at 45° VPAJ. In three-inverter tests, combinations of Inverters 46, 47 and 54 (same manufacturer) also showed improved stability. Inverter 47, operating in hybrid mode, successfully rode through events that triggered disconnection during standalone testing. These results show that interaction effects increase non-linearly with additional inverters. While two-inverter configurations revealed bilateral interactions, three-inverter setups exposed broader system-level instabilities and, in some cases, beneficial damping effects. Critically, standalone inverter testing does not adequately predict behaviour in parallel configurations—especially with mixed manufacturers. The findings highlight the need for detailed evaluation of multi-inverter interactions, as aggregated operation alters the response characteristics of individual units and introduces additional modelling and operational complexity.

Testing with three inverters revealed greater system-wide vulnerabilities, particularly in mixed-manufacturer configurations. The setup involving Inverters 48, 49, and 52 (from different OEMs) experienced cascading instability, with all three disconnecting simultaneously under a 45° VPAJ. Each inverter had remained connected during standalone testing. This synchronous disconnection marked a clear escalation compared to two-inverter tests, where typically only one unit disconnected under similar conditions. The three-inverter arrangement also showed broader stability degradation under VPAJ disturbances that were handled during individual tests. Inverter 48 consistently demonstrated the highest sensitivity, disconnecting at VPAJ values as low as 30° in both two- and three-inverter configurations, despite stable standalone performance. This pattern suggests that some inverter designs may not be well suited for parallel operation.

Despite the general trend of performance degradation, certain parallel configurations showed improved stability. For example, the pairing of Inverters 47 and 54 (same manufacturer, different models) maintained performance during a 45° VPAJ, with Inverter 54 sustaining full output. Similar benefits were seen in the three-inverter setup with Inverters, 46, 47 and 54, where Inverter 47 operated in hybrid mode, remained connected through disturbances that caused disconnection in standalone tests.

These results show that interaction effects increase non-linearly with system size. Two-inverter setups revealed interactions between the converters, while three-inverter configurations introduced broader

system-level effects that included both unstable cases as well as improved ride-through performance in some same-manufacturer groupings. Importantly, standalone testing is insufficient to guarantee stable performance in parallel configurations, especially with mixed OEMs. The findings highlight a key challenge: as more inverters are interconnected, sensitivity to grid disturbances increases, complicating both modelling and coordination. Parallel configurations can change inverter behaviour, reinforcing the need for testing approaches that account for multi-inverter dynamics and interaction effects.

2.3.1. Summary of Results

Table 3.1.Summary of 14 pairs of two inverters in parallel compared with individual inverter responses

Parallel				Individual	
Sr.	Inverter Pairs	Test	Behaviour	Inverter	Behaviour
1	44 & 51	VPAJ 60°	DC, PC	51	RT
2	44 & 49	VPAJ 45°	DC, DC	49	PC
3	44 & 47	VPAJ 15°	PC, PC	47	RT
		Swell 1.175p.u for 120ms	PC, RT	44	RT
4	42 & 49	Sag of 0.8p.u for 80ms	RT, RT	49	PC
		VPAJ 45°	DC, RT	49	PC
5	48 & 49	VPAJ 30°	PC, DC	48	RT
		VPAJ 45°	DC, DC	49, 48	PC, RT
		VPAJ 60°	DC, DC	49, 48	PC, RT
		Sag of 0.7p.u for 220ms	PC, DC	49, 48	RT, RT
		Sag of 0.7p.u for 80ms	PC, DC	49, 48	RT, RT
		Sag of 0.6p.u for 80ms	RT, DC	48	RT
6	47 & 48	VPAJ 30°	PC, DC	48	RT
		VPAJ 45°	DC, DC	48	RT
		Sag to 50 V for 0.9s	DC, DC	48	RT
		Swell 1.175p.u for 220ms	RT, RT	47	PC
7	48 & 41	VPAJ 30°	PC, DC	51	RT
		VPAJ 60°	PC, DC	48	RT
		Sag 0.7p.u for 220ms	RT, DC	48	RT
8	48 & 54	VPAJ 30°	RT, DC	48	RT
		Sag to 50 V for 0.9s	DC, DC	48	RT
		Sag to 170 V for 9s	PC, PC	54	DC
		Sag of 0.5p.u for 80ms	RT, DC	48	RT
9	49 & 54	Swell to 260V	PC, PC	54	RT
		Swell 1.175p.u for 220ms	RT, RT	49	PC
10	42 & 54	Sag of 0.8p.u for 220ms	RT, DC	54	RT
11	47 & 54	VPAJ 30°	DC, RT	54	PC
		VPAJ 45°	DC, RT	54	PC
		Sag of 0.8p.u for 80ms	DC, DC	54	RT
12	38 & 54	Sag of 0.8p.u for 220ms	RT, DC	38	PC
13	47(H) & 49	Swell 230 to 270 for 0.9s	PC, PC	47	DC
		VPAJ 45°	DC, DC	49	PC
		Swell 1.2p.u for 800ms	DC, RT	47	DC
14	47(H) & 48	Swell 230 to 270 for 0.9s	PC, PC	47	DC
		VPAJ 30°	DC, DC	48	RT
		VPAJ 45°	DC, DC	48	RT
		VPAJ 60°	DC, DC	48	RT
		Swell 1.175p.u for 220ms	RT, PC	47	RT

		Swell 1.2p.u for 800ms	DC, PC	47	DC

Legend: RT: Ride-through, PC: Power Curtailment, DC: Disconnection

Table 3.2. Summary of 6 pairs of three inverters in parallel compared with individual inverter responses.

Parallel				Individual	
Sr.	Inverter Pairs	Test	Behaviour	Inverter	Behaviour
1	54, 46 & 47	VPAJ 30°	RT, DC, DC	54	PC
2	54, 46 & 47(H)	Swell 230V to 270V for 0.9s	PC, PC, RT	47	DC
		Swell 1.175p.u for 220ms	RT, RT, PC	46	PC
		Swell 1.25p.u for 800ms	RT, PC, PC	46, 47	PC, DC
3	49, 52 & 48	Sag to 160 V for 9s	PC, RT, PC	52	PC
		VPAJ 15°	PC, RT, RT	48	RT
		VPAJ 30°	PC, RT, DC	52, 48	RT
		VPAJ 45°	DC, DC, DC	49, 52, 48	PC, RT, RT
		VPAJ 60°	DC, DC, DC	49, 52, 48	DC, RT, RT
4	47, 42 & 48	Swell 230V to 260V	PC, RT, PC	42	PC
		VPAJ 30°	DC, RT, DC	48	RT
		VPAJ 45°	DC, RT, DC	48	RT
		VPAJ 60°	DC, DC, DC	52, 48	RT, RT
		VPAJ 90°	DC, DC, DC	52, 48	RT, RT
		Swell 1.2p.u for 220ms	RT, RT, DC	47	PC
5	54, 42 & 48	Sag to 50V for 0.9s	DC, DC, RT	52	RT
		VPAJ 30°	RT, RT, DC	48	RT
		VPAJ 45°	PC, RT, DC	48	RT
		VPAJ 60°	PC, RT, DC	48	RT
		VPAJ 90°	PC, RT, DC	48	RT
		Sag of 0.7p.u for 80ms	RT, RT, DC	48	RT
		Sag of 0.6p.u for 80ms	RT, RT, DC	48	RT
6	49, 47 & 48	VPAJ 15°	PC, PC, RT	47	RT
		VPAJ 30°	PC, DC, DC	48	RT
		VPAJ 45°	DC, DC, DC	49, 48	PC, RT
		VPAJ 60°	DC, DC, DC	48	RT
		VPAJ 90°	DC, DC, DC	48	RT
		Sag of 0.3p.u for 220ms	RT, DC, RT	49	PC
		Swell 1.2p.u for 800ms	DC, PC, RT	48	DC
		Swell 1.2p.u for 80ms	DC, RT, RT	48	DC
		Swell 1.175p.u for 220ms	RT, RT, RT	47	PC

Legends: RT: Ride-through, PC: Power Curtailment, DC: Disconnection

3. Weak Grid Testing

Typical testing of DER inverters assumes a relatively strong network at the PCC; again, this is a valid assumption for networks with limited DER penetration and sufficient amounts of synchronous generation and the associated inertia and grid strength provided by synchronous generators. However, as IBRs displace synchronous generation, a significant knowledge gap has emerged due to a lack of comprehensive experimental data on DER performance under weak grid conditions. This gap fundamentally limits the ability to develop accurate aggregate models for distribution networks in an evolving power system. Experimental investigations on DER performance during steady-state and transient conditions and real-time system response monitoring provide a crucial understanding of decentralised energy systems' dynamics and operational resilience.

Weak grid condition for DER testing in the experimental setup is created by introducing additional line inductance between the inverter and the grid emulator (see Figure 4.1), corresponding to an increase of the equivalent Thevenin impedance from the infinite bus to the PCC. Each inverter was tested with varying inductance values to determine the threshold at which their performance deviates from their behaviour in strong grid conditions during both steady-state and grid disturbances. This approach allows for a detailed understanding of the impact of grid strength on inverter stability and response characteristics. Preliminary findings [3] reveal several issues under weak-grid conditions. All tested inverters exhibited undesirable responses to voltage disturbances, with one also demonstrating poor performance during frequency disturbances. Performance is also affected by operating power levels, highlighting a dependency on the inverters' operational power.

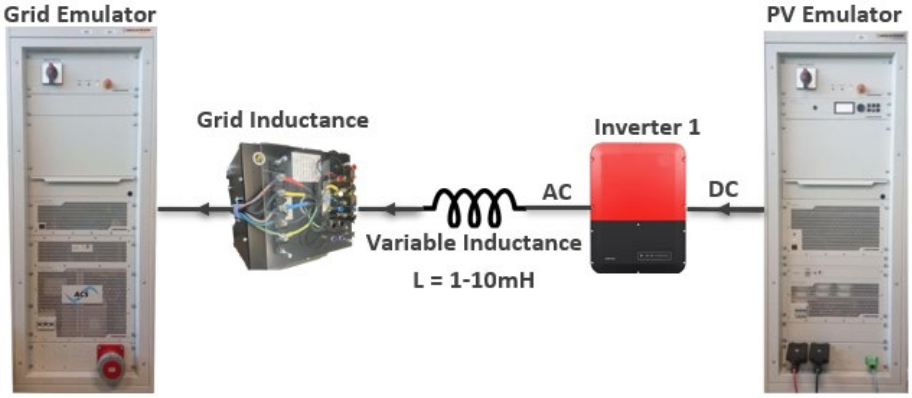

Figure 4.1. Experimental setup schematics for weak grid testing of inverters.

A comprehensive assessment of PV and HESS inverters under weak grid conditions has been conducted on the inverters following AS 4777.2:2020 standard [23]. The SCR of the system is calculated based on the line inductance and the operating power level of the inverter. The evaluation methodology was structured systematically, beginning with an in-depth characterisation of steady-state performance to establish baseline operational parameters. Building on this foundation, the system was methodically subjected to a series of complex grid disturbances to evaluate its dynamic response capabilities, stability characteristics, and adherence to regulatory requirements under challenging network conditions. The following section presents the results of the bench testing for these inverters.

[3] A higher current variable inductor was designed and ordered for the purposes of weak grid condition testing and was delivered to the lab at the end of December. Tests with the new inductors started in Q1, 2025.

3.1. Inverter 46

During weak grid testing, the inverter was connected through a 5mH line inductance and initially followed standard startup procedures. However, upon approaching maximum power output, the inverter exhibited recurring behaviour, triggering unexpected disconnections followed by automatic reconnections with the ramp-rate outlined in AS 4777.2:2020[23]. Figure 4.2 illustrates the cyclic disconnection pattern at maximum power levels. When the line inductance was reduced to 4mH (See Figure 4.3) similar instability persisted, though with marginally extended connection duration compared to the 5mH configuration. Notably, when the line inductance was further reduced to 3mH, the inverter demonstrated complete stability, successfully achieving and maintaining maximum power output without interruption, as shown in Figure 4.4. This behaviour indicates a clear correlation between grid impedance thresholds and inverter stability, with a critical transition point occurring between 3mH and 4mH line inductance values.

The introduction of 3mH line inductance significantly changed the inverter's response to voltage and frequency disturbances when compared to configurations with no line inductance. During a 30V voltage swell disturbance, the inverter completely disconnected from the grid, while under zero-inductance conditions, it maintained its connection, as illustrated in Figure A3.1 and Figure A3.2, respectively. This pattern of altered response characteristics is also seen in step frequency disturbances. In a test involving a 1.95Hz step frequency disturbance, the inverter demonstrated a similar connection-dependent behaviour, disconnecting when line inductance was present but curtailing output power without it, as shown in Figure A3.3 and Figure A3.4. These findings underscore the critical role that network impedance plays in influencing inverter stability thresholds across various disturbances.

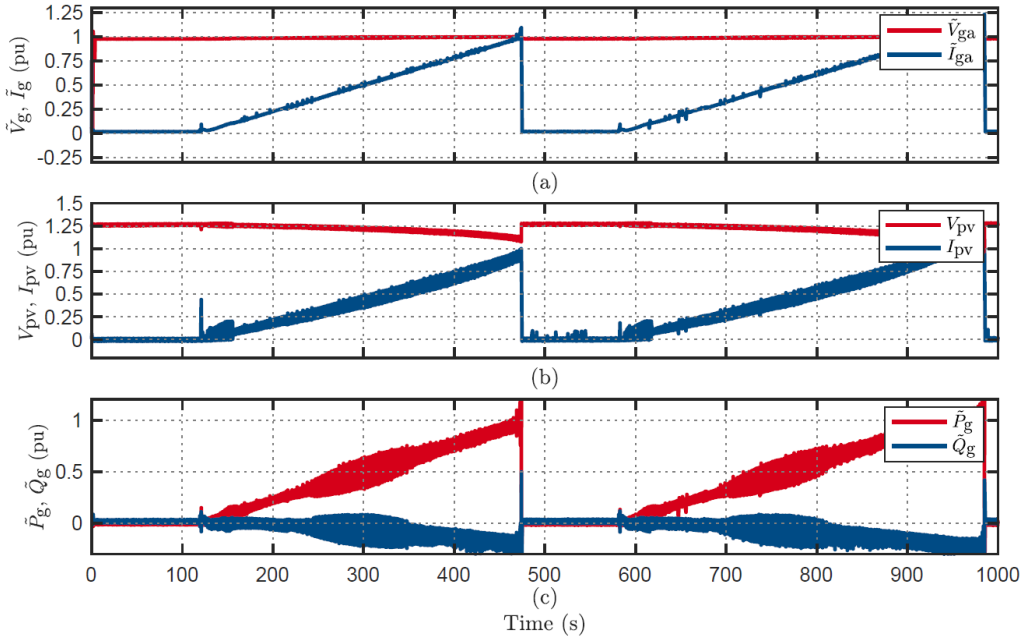

Figure 4.2. Inverter steady state response with 5mH (SCR 6.7) line inductance shows disconnection at maximum power.

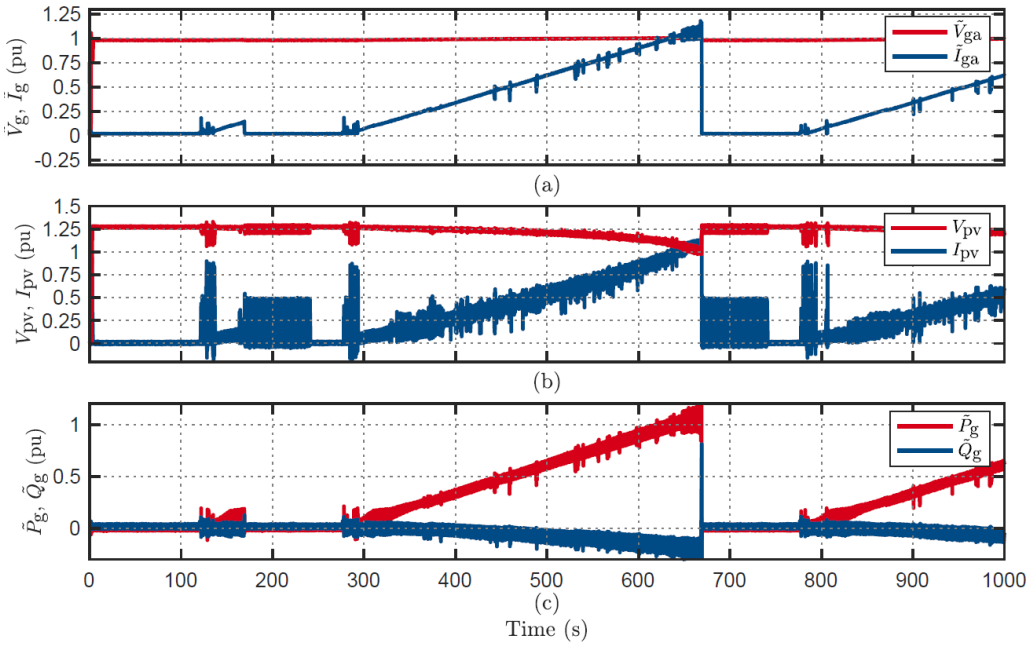

Figure 4.3. Inverter steady state response with 4mH (SCR 8.4) line inductance shows disconnection at maximum power.

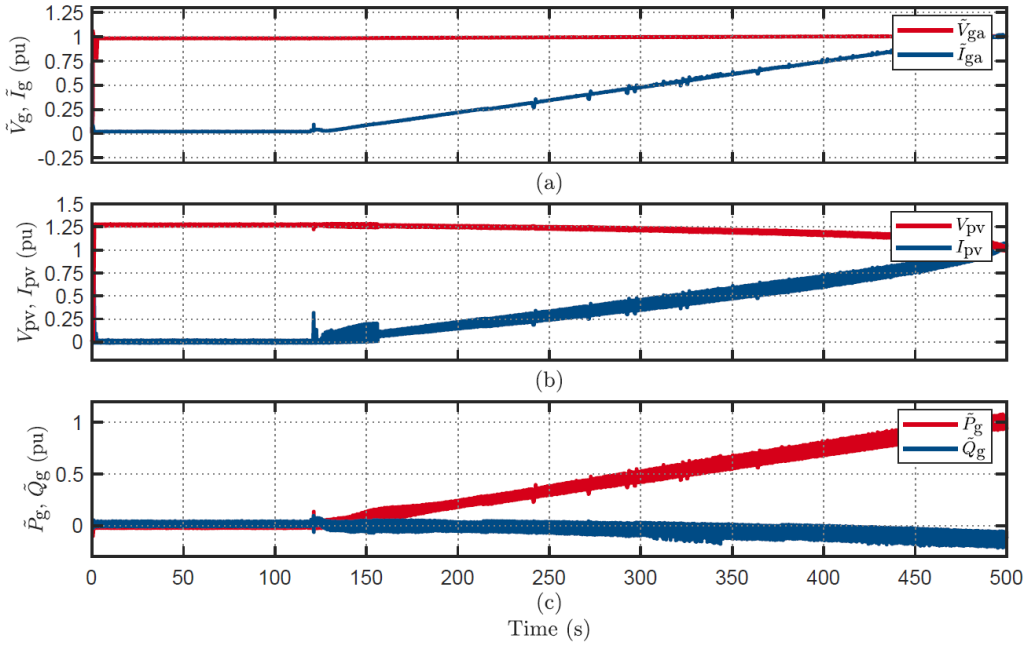

Figure 4.4. Inverter steady state response with 3mH (SCR 11.2) line inductance shows stable operation at maximum power.

3.2. Inverter 44

The inverter was initially connected with a line inductance of 4mH to assess the startup procedure, systematically reducing the value until stability was attained. At 4mH line inductance, the inverter displayed connection instability during startup, struggling to establish a sustainable grid interface and showcasing a cyclic pattern of disconnection and automatic reconnection attempts when approaching maximum power output, as illustrated in Figure A3.5. A reduction to 3mH yielded only marginal improvements, with the inverter managing to maintain connection for longer durations, yet still exhibiting periodic instability, as depicted in Figure A3.6. The breakthrough occurred at 2mH line inductance, where

the inverter demonstrated stable operation, successfully reaching and maintaining maximum power output without interruptions or connection anomalies, as shown in Figure A3.7.

Furthermore, the 2mH line inductance configuration revealed substantial changes to the inverter's disturbance response characteristics. During a 15° VPAJ test while operating at full power, the inverter disconnected from the grid, contrasting sharply with its behavior in two reference conditions: 1) at half power with 2mH inductance, where it successfully rode-through the disturbance as outlined in AS4777.2:2020, and 2) at full power with zero-line inductance, where it maintained a stable grid connection. These comparative responses are shown in Figure 4.5, Figure 4.6, and Figure 4.7, underscoring the intricate interrelationship between operating power, network impedance, and disturbance resilience.

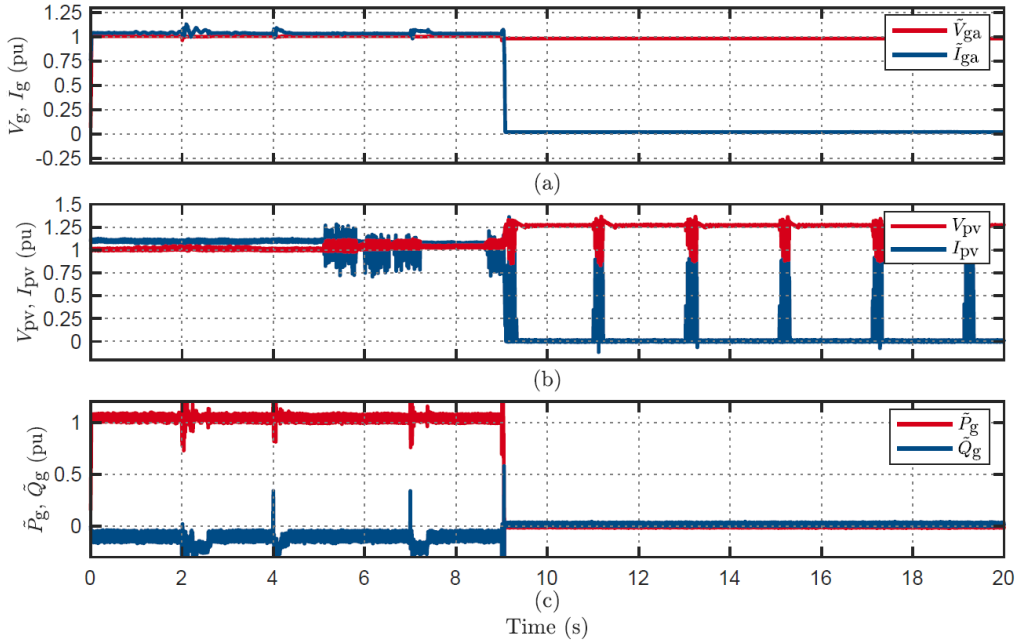

Figure 4.5. Inverter disconnection response to 15° VPAJ with line inductance of 2mH (SCR 16.8) (Full power).

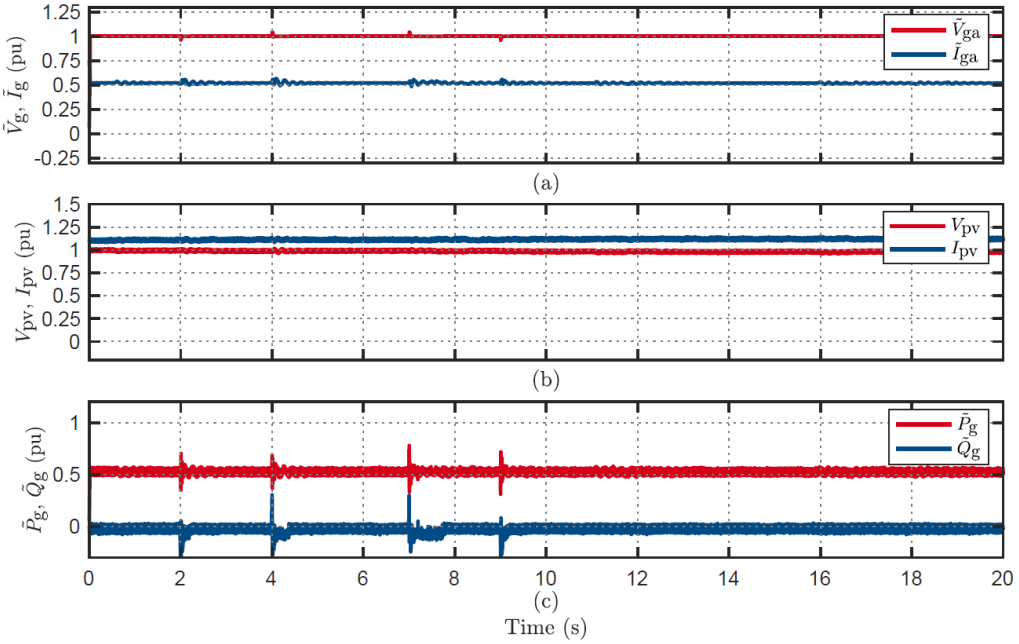

Figure 4.6. Inverter ride-through response to 15° VPAJ with line inductance of 2mH (SCR 16.8) (Half power).

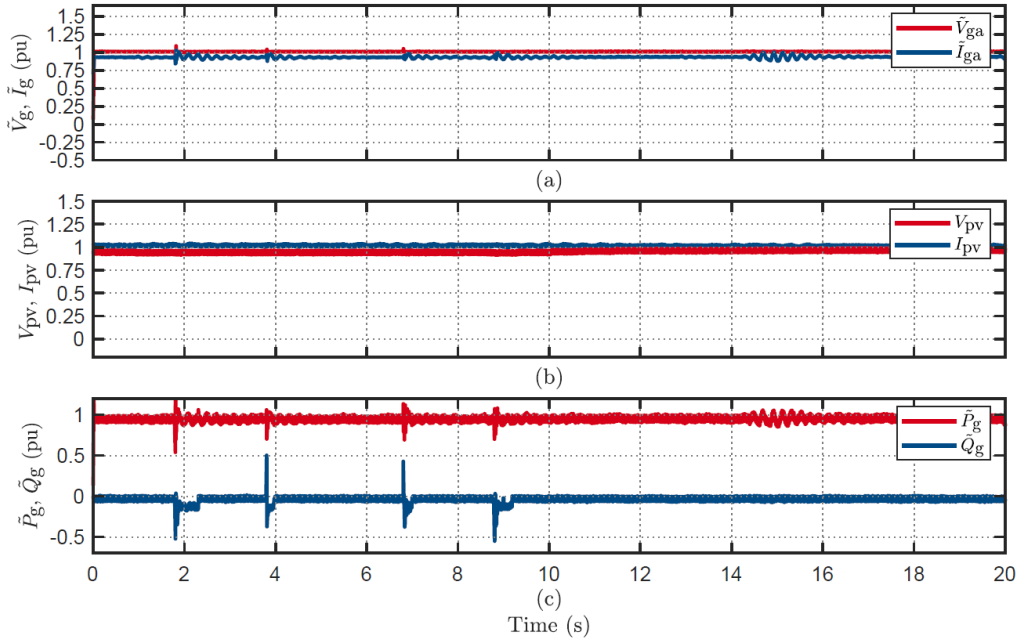

Figure 4.7. Inverter ride-through response to 15° VPAJ without line inductance (full power).

3.3. Inverter 52

A systematic evaluation of the inverter's grid integration capabilities under varying network impedance conditions revealed a critical stability threshold at 4mH line inductance. When subjected to line inductance values exceeding 4mH, the inverter consistently struggled to establish and maintain stable synchronisation with the grid during startup sequences, despite multiple attempts at initialisation. This operational limitation is illustrated in **Figure 4.8,** which depicts the characteristic disconnection pattern observed in these high-impedance startup scenarios. These findings outline a boundary for this specific inverter model, offering vital guidance for field deployment in weak grid environments where higher line inductance values may be present.

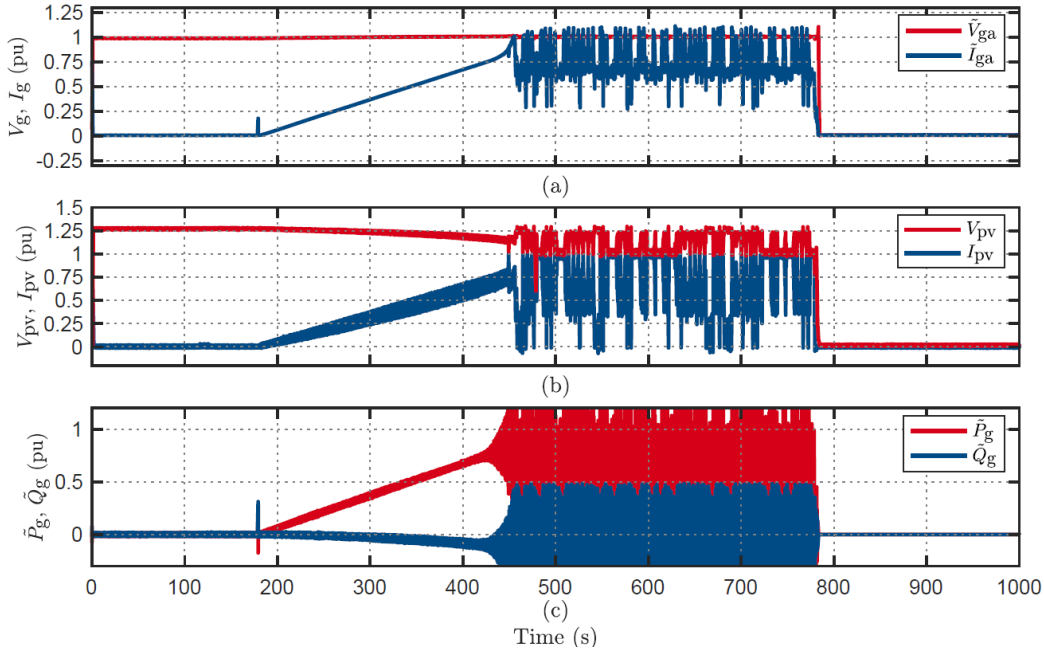

Figure 4.8. Inverter steady state response with 5mH (SCR 6.7) line inductance shows disconnection at maximum power.

3.4. Inverter 48

This inverter displayed tolerance to high line impedance conditions, maintaining a stable grid connection even at line inductance significantly higher than those at which inverters tested before failed during testing. Notably, it successfully maintained grid synchronisation at a high line impedance level of 10mH while operating at half power, and sustained connection at 9mH under full-power conditions. Despite this impedance resilience, the inverter demonstrated nuanced response characteristics to grid disturbances that varied considerably depending on both the operating power and line inductance values. A particular example is during voltage sag testing, where the inverter effectively rode through a 0.3 p.u. sag for 220ms while operating at half power with 9mH line inductance. However, it disconnected when subjected to the same disturbance at full power under identical impedance conditions, as illustrated in Figure 4.9 and Figure 4.10, respectively.

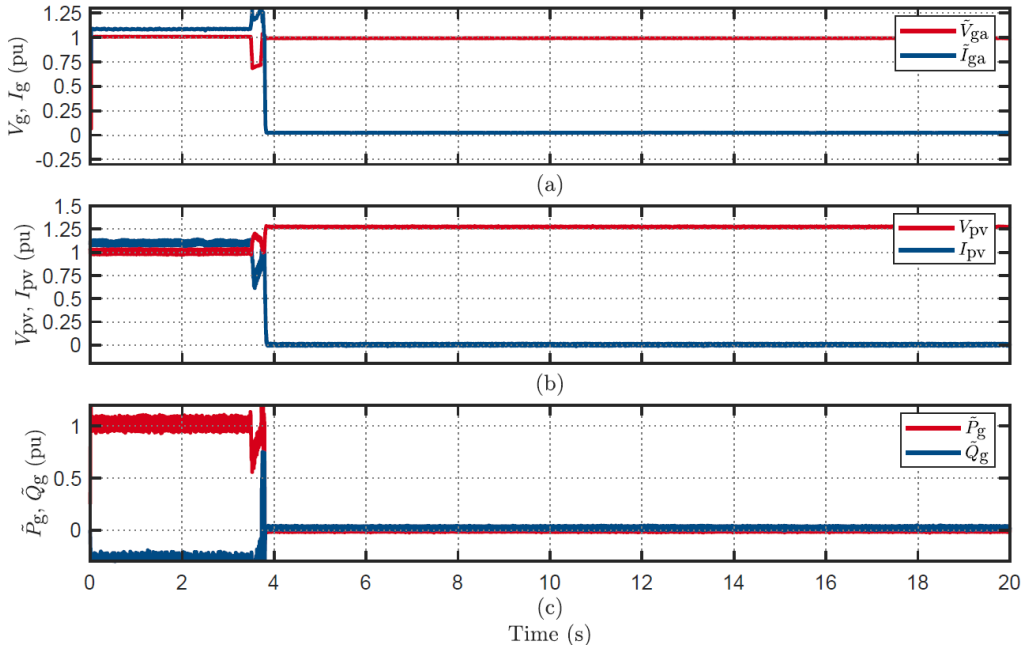

Figure 4.9. Inverter disconnection response to a voltage sag of 0.3p.u for 220ms with line inductance of 10mH (SCR 3.36) (full power).

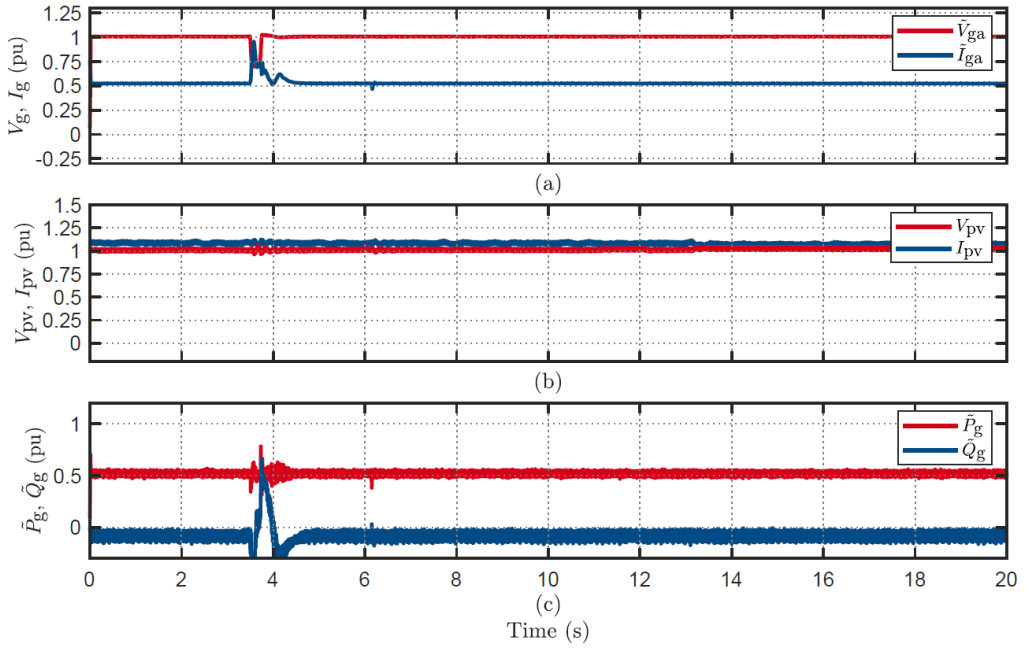

Figure 4.10. Inverter ride-through response to a voltage sag of 0.3p.u for 220ms with line inductance of 10mH (SCR 3.36) (Half power).

A comprehensive summary of the inverter's response across the impedance spectrum is presented in Table 4.1, specifically addressing conditions where behaviour deviated from baseline zero-impedance testing. The data reveals a clear correlation between reduced line inductance and enhanced disturbance resilience. The table also highlights how the inverter's response varies between full and half operational power of the inverter. This can be observed in the voltage sag response, where the transition from 7 mH to 6 mH line inductance, the inverter began successfully riding through 70 V voltage sags that previously caused disconnection, as illustrated in Figure A3.8 and Figure A3.9These findings demonstrate how variations in network impedance can fundamentally alter inverter stability thresholds, which has significant implications for inverter integration in weak network environments.

Table 4.1: Summary of the inverter 48 test results with different line inductances.

Inverter 48				
Test	**9mH (SCR 3.7)**		**8mH (SCR 4.2)**	
	Behavior (FP)	Behavior (HP)	Behavior (FP)	Behavior (HP)
Startup	Ride-Through	--	--	--
230 to 160 for 9s	Disconnected	Disconnected	Disconnected	--
VPAJ 30°	Disconnected	Disconnected	Disconnected	--
VPAJ 45°	Disconnected	Disconnected	Disconnected	--
VPAJ 60°	Disconnected	Disconnected	--	--
Sag of 0.8p.u for 220ms	Disconnected	Disconnected	--	--
Sag of 0.7p.u for 220ms	Disconnected	Disconnected	--	--
Sag of 0.6p.u for 220ms	Disconnected	Disconnected	--	--
Sag of 0.5p.u for 220ms	Disconnected	Disconnected	Disconnected	--
Sag of 0.4p.u for 220ms	Disconnected	Disconnected	Disconnected	--
Sag of 0.3p.u for 220ms	Disconnected	Ride-Through	Ride-Through	--
Sag of 0.2p.u for 220ms	Ride-Through	Ride-Through	--	--
Test	**7mH (SCR 4.8)**		**6mH (SCR 5.6)**	
	Behavior (FP)	Behavior (HP)	Behavior (FP)	Behavior (HP)
230 to 160 for 9s	Disconnected	--	Power Curtailed	--
VPAJ 30°	Disconnected	--	Ride-Through	--
Sag of 0.5p.u for 220ms	Disconnected	--	Disconnected	--
Sag of 0.4p.u for 220ms	Disconnected	--	Ride-Through	--
Sag of 0.3p.u for 220ms	Ride-Through	--	--	
Test	**5mH (SCR 6.7)**		**4mH (SCR 8.4)**	
	Behavior (FP)	Behavior (HP)	Behavior (FP)	Behavior (HP)
230 to 160 for 9s	Power Curtailed	--	Power Curtailed	--
Sag of 0.5p.u for 220ms	Disconnected	--	Disconnected	Ride-Through
Sag of 0.4p.u for 220ms	Ride-Through	--	Ride-Through	--
Test	**3mH (SCR 11.2)**		**2mH (SCR 16.8)**	
	Behavior (FP)	Behavior (HP)	Behavior (FP)	Behavior (HP)
230 to 160 for 9s	Power Curtailed	--	--	--
Sag of 0.6p.u for 220ms	Disconnected	--	Disconnected	--
Sag of 0.5p.u for 220ms	Ride-Through	--	Ride-Through	--
Sag of 0.4p.u for 220ms	Ride-Through	--	Ride-Through	--

3.5. Inverter 54

Inverter 54 demonstrated sensitivity to network impedance conditions, revealing an operational threshold at 3mH line inductance. Although the inverter successfully established and maintained grid connection at this impedance level, its ability to withstand disturbances was significantly compromised, leading to disconnection even under minimal grid disturbances that are typically considered manageable. Notably, the inverter disconnected when subjected to VPAJ disturbances of 15° and a modest 0.3p.u voltage sag, indicating fundamental stability limitations in higher-impedance network

environments. However, when the line inductance was decreased from 3mH to 2mH, there was a marked improvement in disturbance resilience across multiple test categories. This change is clearly illustrated in Figure 4.11, which depicts the inverter's disconnection response during a 15° VPAJ event with 3mH line inductance, in contrast to Figure 4.12, which showcases the power curtailment performance of the inverter during the same disturbance with the impedance reduced to 2mH.

Table 4.2 presents a detailed analysis of the inverter's performance across both impedances, incorporating coloured highlights to underscore the distinct behavioural transitions observed at various inductance values. The tabulated results indicate stability characteristics for both the 3mH and 2mH configurations, with the latter demonstrating effective ride-through capabilities across multiple disturbance categories that had previously resulted in disconnection.

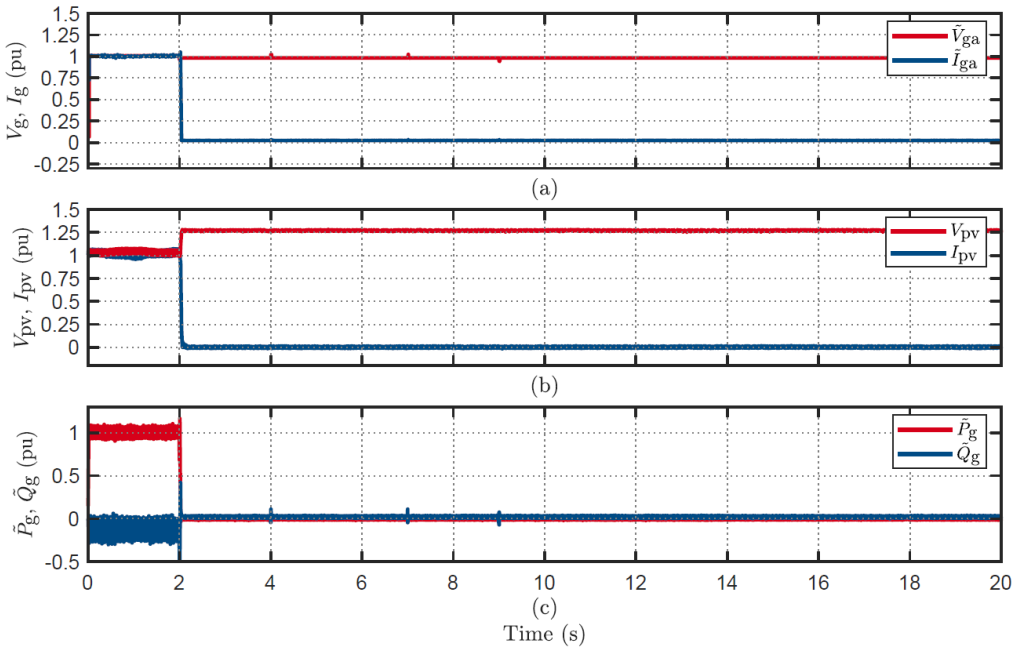

Figure 4.11. Inverter disconnection response to VPAJ of 15° with line inductance of 3mH (SCR 11.2).

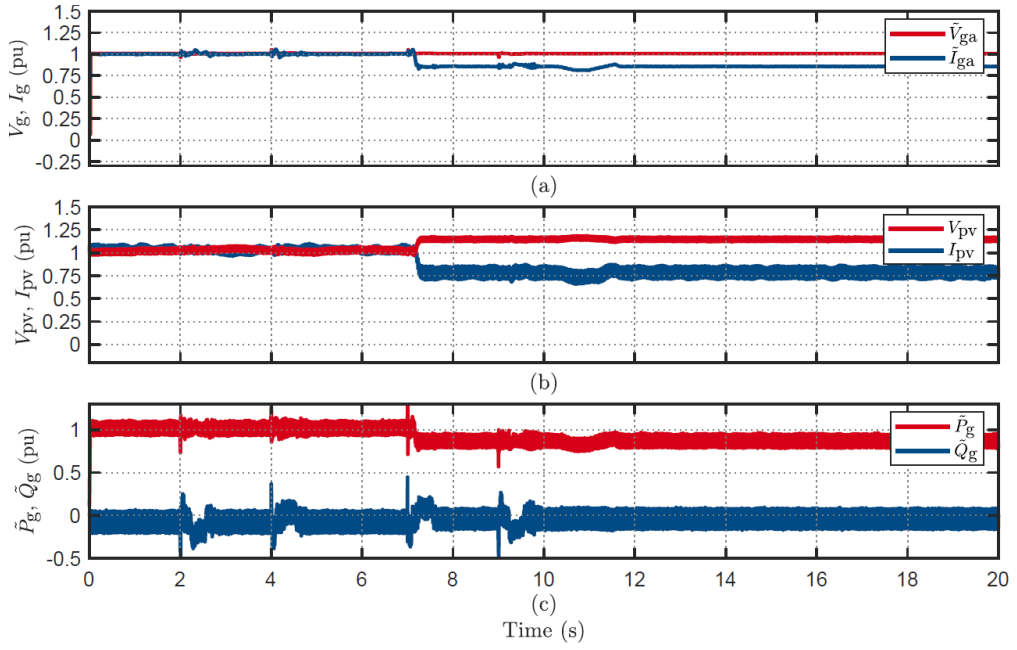

Figure 4.12. Inverter power curtailment response to VPAJ of 15° with line inductance of 2mH (SCR 16.8).

Table 4.2: Summary of the inverter 54 test results with different line inductances.

Inverter 54				
Test	3mH (SCR 11.2)		2mH (SCR 16.8)	
	Behavior (FP)	Behavior (HP)	Behavior (FP)	Behavior (HP)
Startup	Ride-Through	--	Ride-Through	--
VPAJ 15°	Disconnected	--	Ride-Through	--
VPAJ 30°	Disconnected	--	Ride-Through	--
VPAJ 45°	Disconnected	--	Ride-Through	--
VPAJ 60°	--	--	Disconnected	--
Sag of 0.7p.u for 220ms	Disconnected	--	Ride-Through	--
Sag of 0.6p.u for 220ms	Disconnected	--	Ride-Through	--
Sag of 0.5p.u for 220ms	Disconnected	--	Ride-Through	--
Sag of 0.4p.u for 220ms	Disconnected	--	Ride-Through	--
Sag of 0.3p.u for 220ms	Ride-Through	--	--	--
Swell of 1.2p.u for 220ms	Disconnected	--	Ride-Through	--
Swell of 1.175p.u for 220ms	Disconnected	--	Ride-Through	--
Swell of 1.15p.u for 220ms	Disconnected	--	Ride-Through	--
Swell of 1.15p.u for 80ms	Ride-Through	--	--	--
Swell of 1.125p.u for 220ms	Ride-Through	--	--	--

3.6. Inverter 49

Inverter 49 exhibited sensitivity to network impedance conditions, revealing an operational threshold at a line inductance of 3mH. While the inverter maintained a grid connection at this impedance level, its ability to resist disturbances was compromised, leading to disconnections even during minor voltage sags. Figure A3.10 illustrates the output current oscillations experienced during startup with a 4mH line inductance, which resulted in unstable power injection. In contrast, a 3mH impedance facilitated stable grid synchronisation as seen in Figure A3.11. The inverter demonstrated enhanced performance at reduced power levels (50% versus 100%) and with lower line inductance values. This operational divergence is clearly shown in the comparative responses to identical disturbances: a 0.7 p.u voltage sag lasting 80ms caused complete disconnection at full power (Figure 4.13), whereas the same disturbance at half power led to temporary power curtailment without loss of grid connection (Figure 4.14).

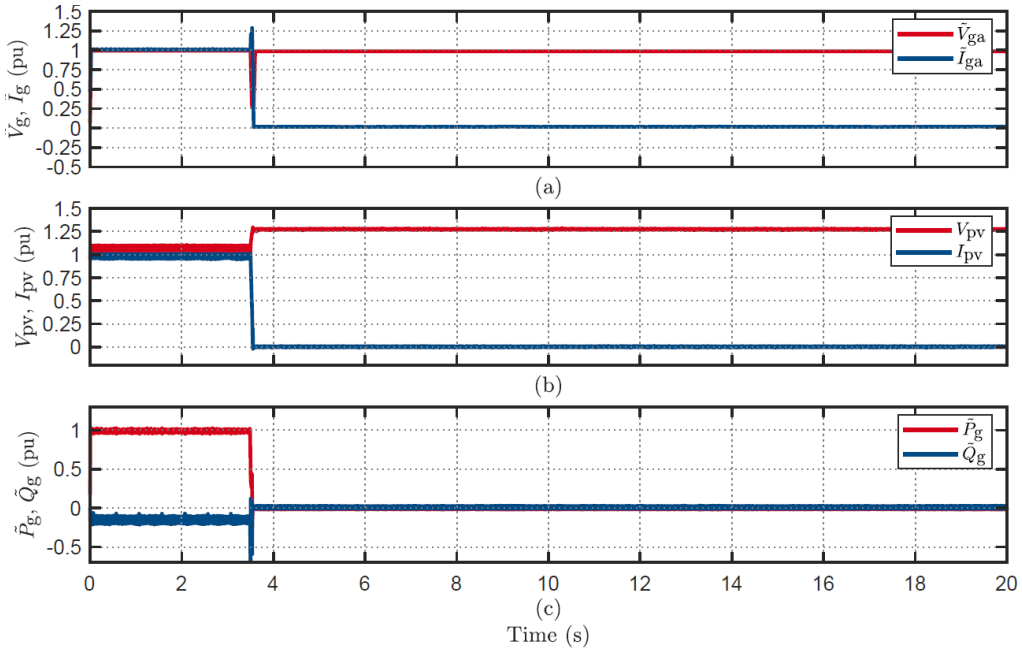

Figure 4.13. Inverter disconnection response to a voltage sag of 0.7p.u for 80ms with line inductance of 3mH (SCR 7.4) (full power).

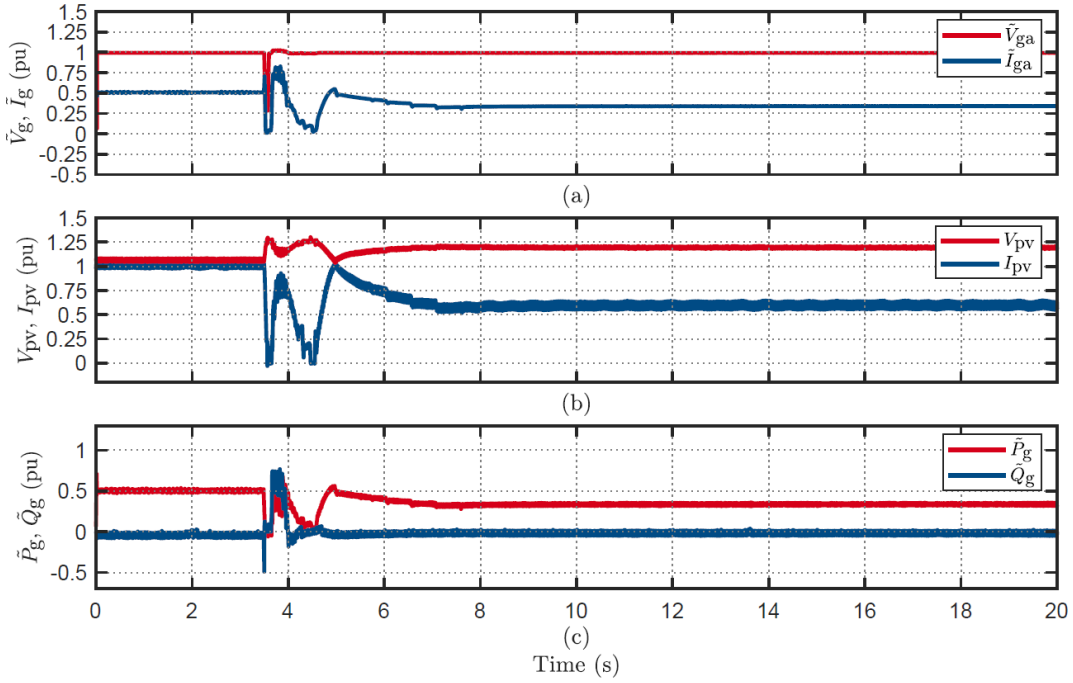

Figure 4.14. Inverter disconnection response to a voltage sag of 0.7p.u for 80ms with line inductance of 3mH (SCR 7.4) (half power).

Table 4.3 provides a detailed analysis of the inverter's performance across various impedance configurations and power levels, utilising colour-coded highlighting to underscore distinct behavioural shifts. The data demonstrates enhanced stability characteristics at 2mH inductance, which facilitated successful ride-through of multiple disturbances that caused disconnection at higher impedance values.

Table 4.3: Summary of the inverter 49 test results with different line inductances.

Inverter 49				
Test	3mH (SCR 7.4)		2mH (SCR 11.2)	
	Behavior (FP)	Behavior (HP)	Behavior (FP)	Behavior (HP)
Startup	Ride-Through		Ride-Through	
230 to 270 for 0.9s	Disconnected	--	Power Curtailed	--
VPAJ 45°	Disconnected	--	Disconnected	--
Sag of 0.8p.u for 80ms	Disconnected	Disconnected	Disconnected	--
Sag of 0.7p.u for 80ms	Disconnected	Power Curtailed	Disconnected	Power Curtailed
Sag of 0.6p.u for 80ms	Disconnected	--	Ride-Through	--
Sag of 0.5p.u for 80ms	Disconnected	--	--	--
Sag of 0.4p.u for 80ms	Disconnected	--	--	--
Sag of 0.3p.u for 80ms	Power Curtailed	--	--	--
Swell 1.175p.u for 220ms	Disconnected	Power Curtailed	Power Curtailed	--

3.7. Inverter 40

This inverter demonstrated outstanding tolerance to high network impedance conditions, successfully maintaining a stable grid connection even at line inductance values that far exceeded those at which many previously tested inverters failed. It achieved reliable grid synchronisation at 9mH line inductance while operating at full power, establishing itself as one of the most impedance-resilient inverter in the testing cohort. However, despite this impedance tolerance, the inverter exhibited poor response characteristics to grid disturbances, which varied significantly depending on operating power and line inductance values. A notable example occurred during a minor 15° VPAJ disturbance: the inverter was able to ride-through while operating at half power with 9mH line inductance, but it disconnected when subjected to the same disturbance at full power under identical impedance conditions. Interestingly,

when the line inductance was reduced to 8mH, the inverter regained the ability to withstand the same disturbance at full power, as illustrated in Figure 4.15, Figure 4.16, and Figure 4.17.

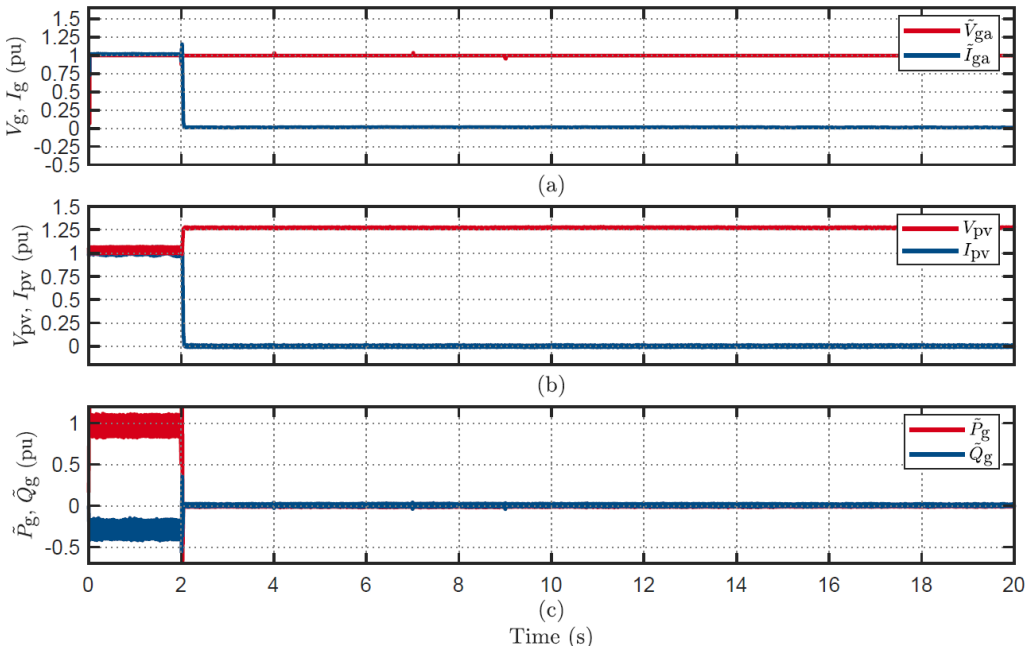

Figure 4.15. Inverter disconnection response to a VPAJ 15° with line inductance of 9mH (SCR 3.7) (full power).

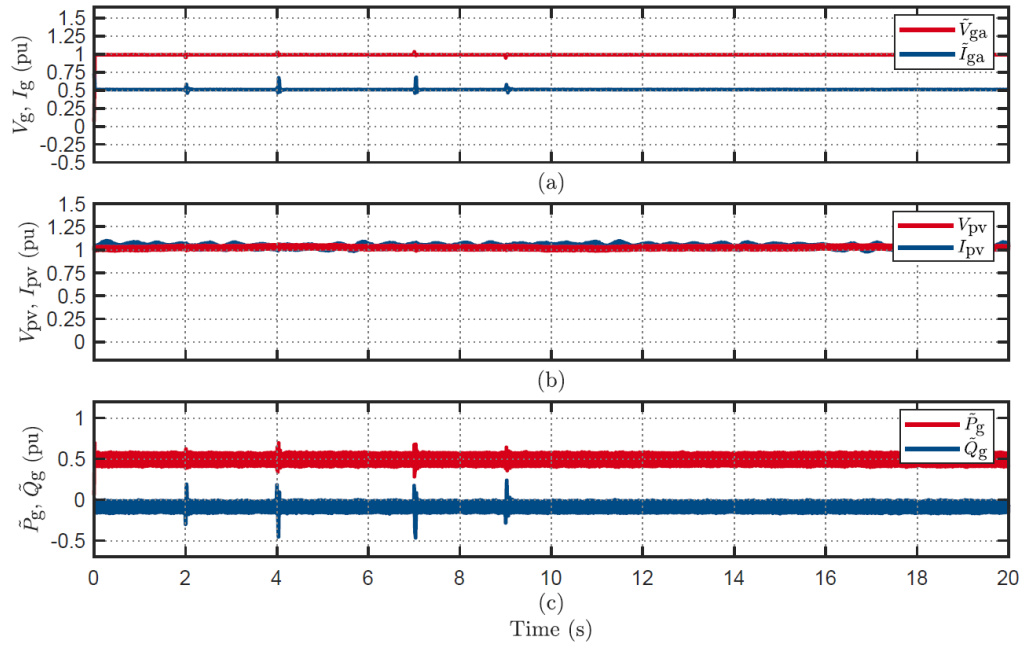

Figure 4.16. Inverter ride-through response to a VPAJ 15° with line inductance of 9mH (SCR 3.7) (half power).

Table 4.4 presents a detailed analysis of the inverter's performance across various impedance values, emphasising specific conditions where the behaviour deviated from the baseline zero-impedance testing. The data indicates a clear correlation between reduced line inductance and enhanced disturbance resilience, while also revealing notable variations in response between full and half-power operations. This trend is particularly pronounced in the voltage swell response, especially as the transition from 5mh to 4mh represents a critical threshold. This change enabled the inverter to maintain operation during a 1.125 p.u voltage swell lasting 80 ms, which had previously caused disconnection at full power but allowed for continued connection at half power, as shown in Figure A3.12, Figure A3.13,

and Figure A3.14. These findings demonstrate how network impedance significantly influences inverter stability thresholds, carrying important implications for integration within weak grid environments.

Table 4.4: Summary of the inverter 40 test results with different line inductances.

Inverter 40				
Test	**9mH (SCR 3.7)**		**8mH (SCR 4.2)**	
	Behavior (FP)	Behavior (HP)	Behavior (FP)	Behavior (HP)
Startup	Ride-Through	--	Ride-Through	--
230 to 270 for 0.9s	Disconnected	--	Disconnected	--
VPAJ 15°	Disconnected	Ride-Through	Ride-Through	--
VPAJ 30°	Disconnected	Disconnected	Disconnected	--
Sag of 0.8p.u for 80ms	Disconnected	Power Curtailed	Disconnected	--
Sag of 0.7p.u for 80ms	Ride-Through	--	--	--
Swell 1.2p.u for 80ms	Disconnected	--	--	--
Swell 1.175p.u for 80ms	Disconnected	--	--	--
Swell 1.15p.u for 80ms	Disconnected	--	--	--
Swell 1.125p.u for 80ms	Disconnected	Disconnected	Disconnected	--
Swell 1.1p.u for 80ms	Ride-Through	--	--	--
Swell 1.1p.u for 220ms	Power Curtailed	Ride-Through	Ride-through	--
Test	**7mH (SCR 4.8)**		**6mH (SCR 5.6)**	
	Behavior (FP)	Behavior (HP)	Behavior (FP)	Behavior (HP)
230 to 270 for 0.9s	Disconnected	--	Disconnected	Disconnected
VPAJ 15°	Ride-Through	--		--
VPAJ 30°	Disconnected	--	Disconnected	Ride-through
Sag of 0.8p.u for 80ms	Disconnected	--	Ride-Through	--
Sag of 0.7p.u for 80ms	Ride-Through	--	--	--
Swell 1.125p.u for 80ms	Disconnected	--	Disconnected	Ride-Through
Swell 1.1p.u for 220ms	Ride-Through	--	Ride-through	--
Test	**5mH (SCR 6.7)**		**4mH (SCR 8.4)**	
	Behavior (FP)	Behavior (HP)	Behavior (FP)	Behavior (HP)
230 to 270 for 0.9s	Disconnected	Disconnected	Ride-Through	--
VPAJ 30°	Disconnected	Ride-Through	Power Curtailed	--
VPAJ 60°	--	--	Disconnected	Ride-Through
Sag of 0.8p.u for 800ms	Ride-Through	--	--	--
Swell 1.15p.u for 80ms	--	--	Disconnected	Disconnected
Swell 1.125p.u for 80ms	Disconnected	Ride-Through	Ride-Through	--
Test	**3mH (SCR 11.2)**		**2mH (SCR 16.8)**	
	Behavior (FP)	Behavior (HP)	Behavior (FP)	Behavior (HP)
VPAJ 60°	Disconnected	Ride-Through	Ride-Through	--
Swell 1.15p.u for 80ms	Disconnected	Ride-Through	Disconnected	Ride-Through

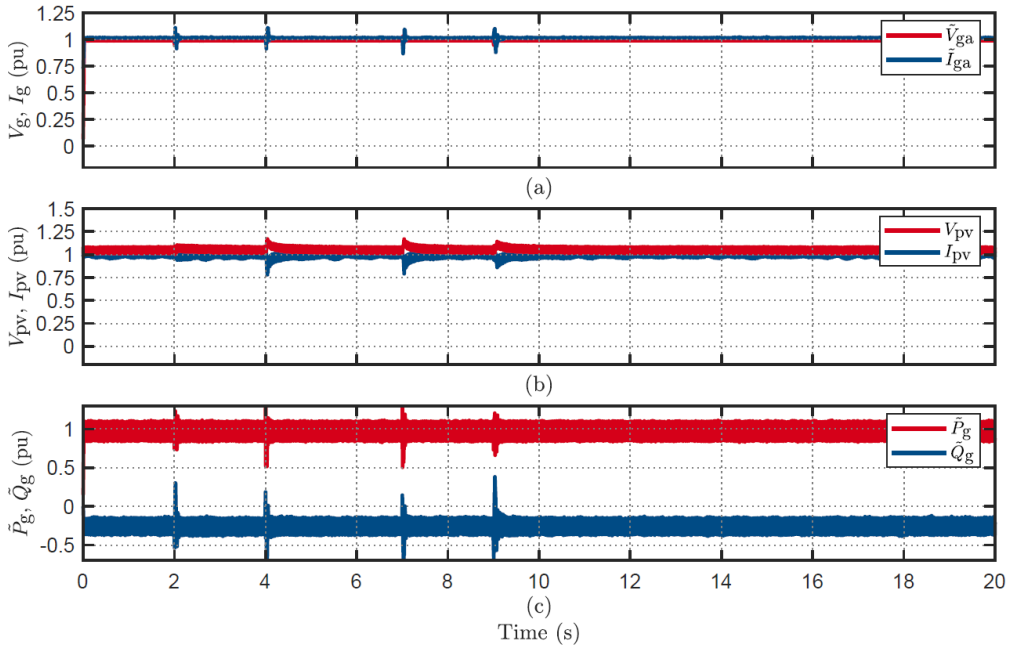

Figure 4.17. Inverter ride-through response to a VPAJ 15° with line inductance of 8mH (SCR 4.2) (full power).

3.8. Inverter 38

During weak grid testing, the inverter was connected via a 5mH line inductance and initially followed standard startup procedures. However, as it approached maximum power output, the inverter displayed persistent instability, resulting in cyclical disconnections followed by automatic reconnection attempts. Figure 4.18 illustrates this recurring disconnection pattern at a 0.75 p.u output power. When the line inductance was reduced to 4mH (as shown in Figure 4.19 similar instability persisted with slightly longer connection intervals compared to the 5mH configuration. Stability was achieved when the line inductance was further reduced to 3mH, at which point the inverter demonstrated complete stability, successfully reaching and maintaining maximum power output without interruption, as shown in Figure 4.20. This behaviour establishes a clear correlation with grid impedance thresholds. The 3mH line inductance notably modified the inverter's response to voltage disturbances compared to zero-inductance configurations.

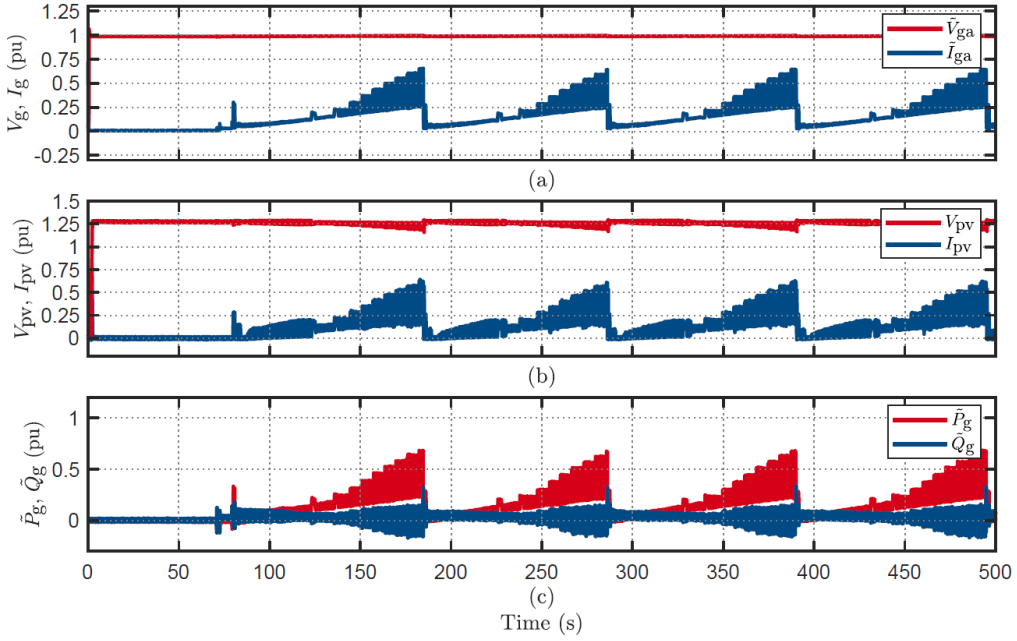

Figure 4.18. Inverter steady state response with 5mH (SCR 6.7) line inductance shows disconnection.

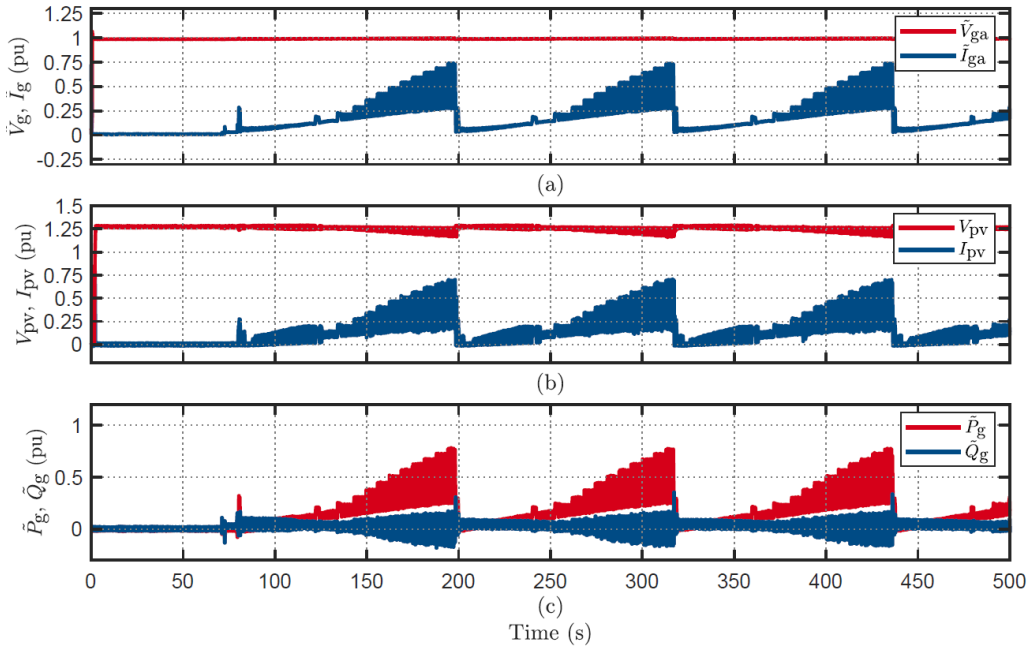

Figure 4.19. Inverter steady state response with 4mH (SCR 8.4) line inductance shows disconnection at 0.75 p.u.

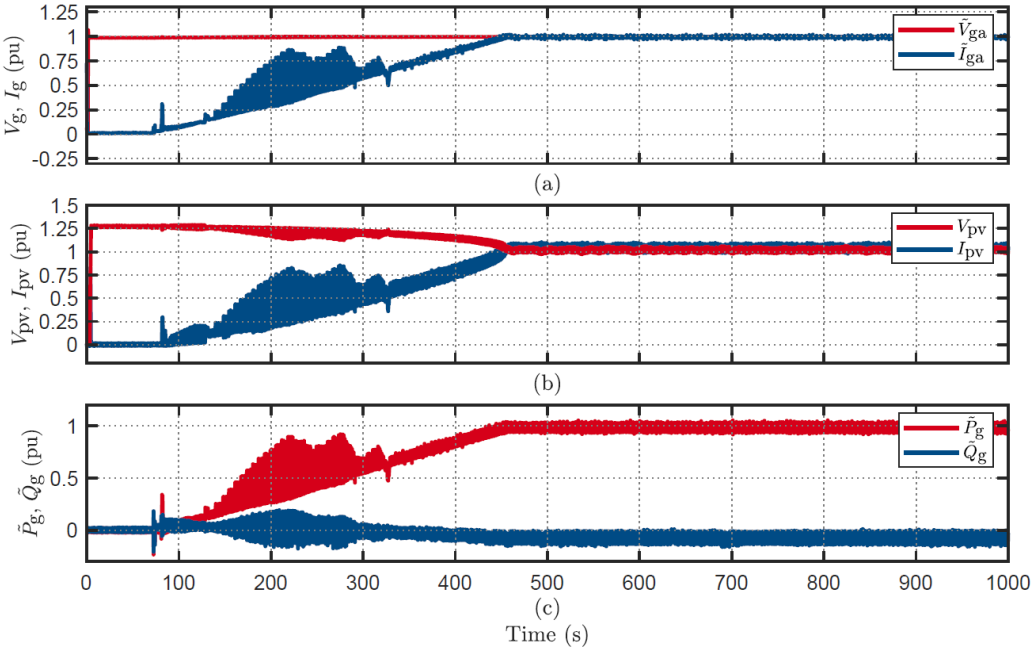

Figure 4.20. Inverter steady state response with 3mH (SCR 11.2) line inductance shows ride-through.

Table 4.5 provides a summary of the responses of inverter 38 to various voltage disturbances at different inductance levels, showing specific changes influenced by network impedance conditions.

Table 4.5: Summary of the inverter 38 test results with different line inductances.

Inverter 38				
3mH (SCR 11.2)			2mH (SCR 16.8)	
Test	Behavior (FP)	Behavior (HP)	Behavior (FP)	Behavior (HP)
230 to 160 for 9s	Disconnected	Disconnected	Disconnected	Disconnected
230 to 270 for 0.9s	Disconnected	Disconnected	Disconnected	Disconnected
Swell 1.2p.u for 800ms	Disconnected	Disconnected	Disconnected	Disconnected
Swell 1.2p.u for 220ms	Disconnected	Disconnected	Disconnected	Disconnected

3.9. Inverter 31

This inverter demonstrated tolerance to high network impedance conditions, successfully maintaining a stable grid connection even at line inductance values that significantly exceed those at which many previously tested units failed. It achieved reliable grid synchronisation at high impedance value of 10mH while operating at full power, marking it as the most impedance-resilient inverter in the test group. However, despite this impedance tolerance, the inverter displayed a compromised response to grid disturbances, with performance varying significantly depending on operating power and line inductance values. For instance, during a minor voltage sag of 0.4 p.u. lasting 80ms, the inverter managed to ride through the disturbance with an 8mH line inductance but disconnected when faced with the same disturbance at 9mH, as illustrated in Figure 4.21 and Figure 4.22, respectively. Furthermore, at 8mH line inductance, the inverter was unable to withstand a 0.6 p.u voltage sag of 80ms at full power, although it successfully maintained connection during the same disturbance when operating at half power, as shown in Figure A3.15 and Figure A3.16.

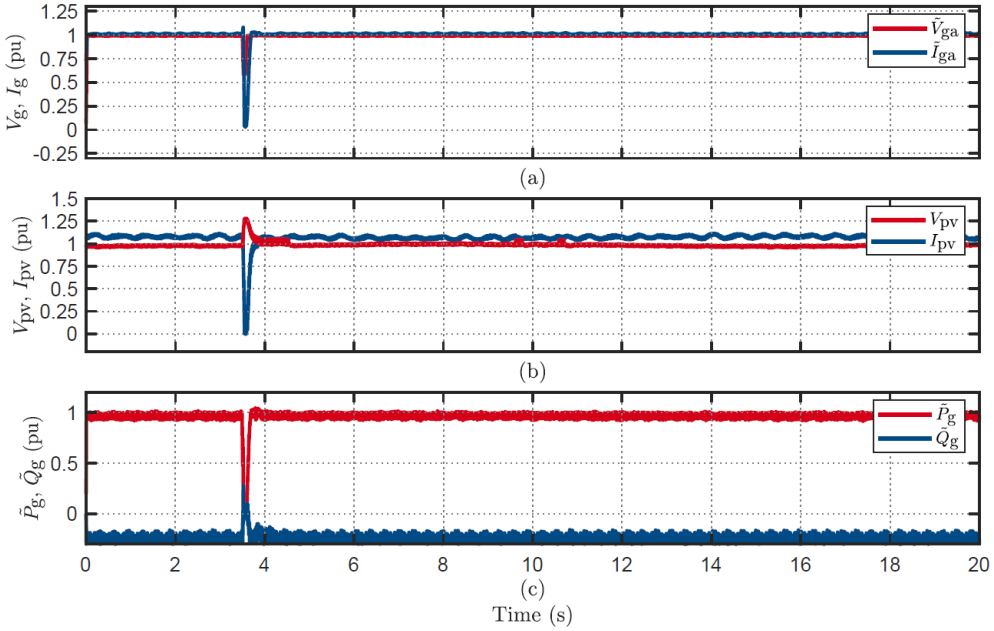

Figure 4.21. Inverter disconnection response to a voltage sag of 0.4p.u for 80ms with 8mH (SCR 4.2) line inductance.

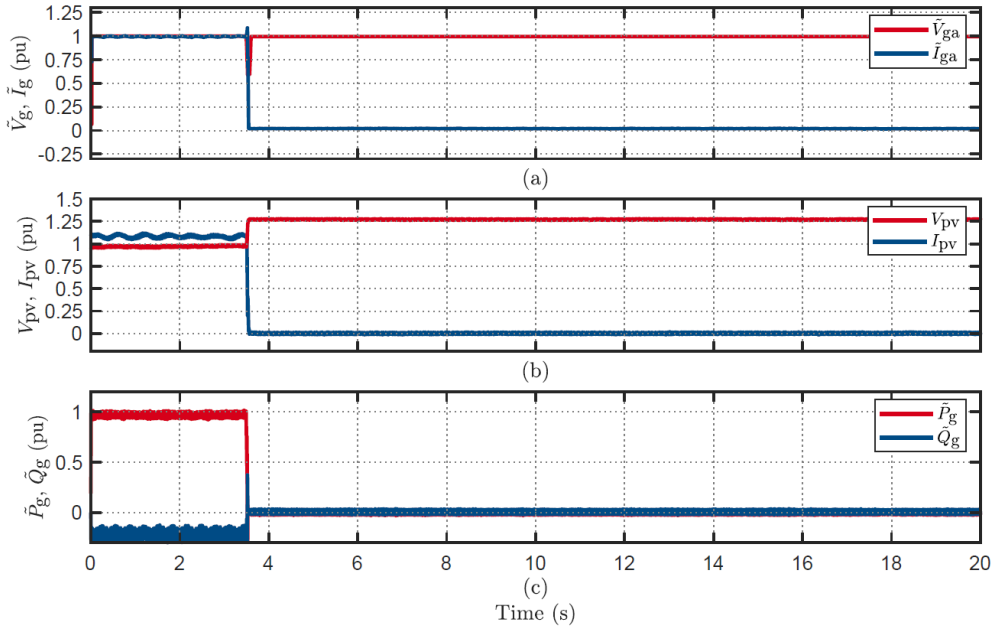

Figure 4.22. Inverter disconnection response to a voltage sag of 0.4p.u for 80ms with 9mH (SCR 3.7) line inductance.

Table 4.6 presents a comprehensive response of inverter across the impedance spectrum, highlighting specific conditions where the behaviour deviated from baseline zero-impedance testing. The data indicates a clear relationship between reduced line inductance and enhanced disturbance resilience, while also revealing significant variations in response between full and half-power operation. These findings highlight how network impedance fundamentally alters the stability thresholds of inverters, carrying important implications for their deployment in weak grid environments.

Table 4.6: Summary of the inverter 31 test results with different line inductances.

Inverter 31				
Test	**10mH (SCR 3.3)**		**9mH (SCR 3.7)**	
	Behavior (FP)	Behavior (HP)	Behavior (FP)	Behavior (HP)
230 to 50 for 0.9s	Disconnected	--	--	--
230 to 270 for 0.9s	Disconnected	--	--	--
VPAJ 45°	Disconnected	--	--	--
VPAJ 60°	Disconnected	Disconnected	Disconnected	Disconnected
Sag of 0.8p.u for 80ms	Disconnected	Disconnected	Disconnected	Disconnected
Sag of 0.7p.u for 80ms	Disconnected	Ride-Through	Disconnected	Ride-Through
Sag of 0.6p.u for 80ms	Disconnected	--	Disconnected	--
Sag of 0.5p.u for 80ms	Disconnected	--	Disconnected	--
Sag of 0.4p.u for 80ms	Disconnected	--	Disconnected	--
Sag of 0.3p.u for 80ms	Ride-Through	--	Ride-Through	--
Swell 1.2p.u for 80ms	Ride-Through	--	Ride-Through	--
Test	**8mH (SCR 4.2)**		**7mH (SCR 4.8)**	
	Behavior (FP)	Behavior (HP)	Behavior (FP)	Behavior (HP)
230 to 270 for 0.9s	--	--	Ride-Through	--
VPAJ 60°	Disconnected	Disconnected	Disconnected	Disconnected
Sag of 0.8p.u for 80ms	Disconnected	Disconnected	Disconnected	--
Sag of 0.7p.u for 80ms	Disconnected	Disconnected	Disconnected	Disconnected
Sag of 0.6p.u for 80ms	Disconnected	Ride-through	Disconnected	Ride-through
Sag of 0.5p.u for 80ms	Disconnected	--	Disconnected	--
Sag of 0.4p.u for 80ms	Ride-Through	--	Ride-through	--
Test	**6mH (SCR 5.6)**		**5mH (SCR 6.7)**	
	Behavior (FP)	Behavior (HP)	Behavior (FP)	Behavior (HP)
VPAJ 60°	Disconnected	Disconnected	Disconnected	Ride-Through
Sag of 0.8p.u for 80ms	Disconnected	--	Disconnected	Ride-Through
Sag of 0.7p.u for 80ms	Disconnected	--	Disconnected	--
Sag of 0.6p.u for 80ms	Disconnected	Ride-through	Disconnected	--
Sag of 0.5p.u for 80ms	Disconnected	--	Disconnected	--
Sag of 0.4p.u for 80ms	Ride-Through	--	Ride-through	--
Test	**4mH (SCR 8.4)**			
	Behavior (FP)	Behavior (HP)		
VPAJ 60°	Disconnected	Ride-Through		
Sag of 0.8p.u for 80ms	Ride-Through	--		

3.10. Inverter 35

This inverter demonstrated the weakest response to network impedance conditions among all tested units, failing to achieve reliable grid synchronisation even at the minimal impedance value of 2mH while operating at full power. Its exceptional sensitivity to line inductance positions it as the least impedance-resilient inverter within the entire test group. In addition to these fundamental impedance limitations, the inverter exhibited a severely compromised response to voltage disturbances, showing sensitivity to the duration of disturbances rather than their magnitude. This vulnerability is clearly illustrated by its reaction to voltage swells; during a 1.2 p.u swell lasting 80ms, the inverter maintained grid connection,

yet it disconnected when subjected to an identical magnitude swell lasting 220ms, as shown in Figure 4.23 and Figure 4.24, respectively. Table 4.7 reveals the inverter's behaviour, outlining critical thresholds across various disturbance categories that greatly limit its deployment suitability, restricting its application to only the most robust grid environments.

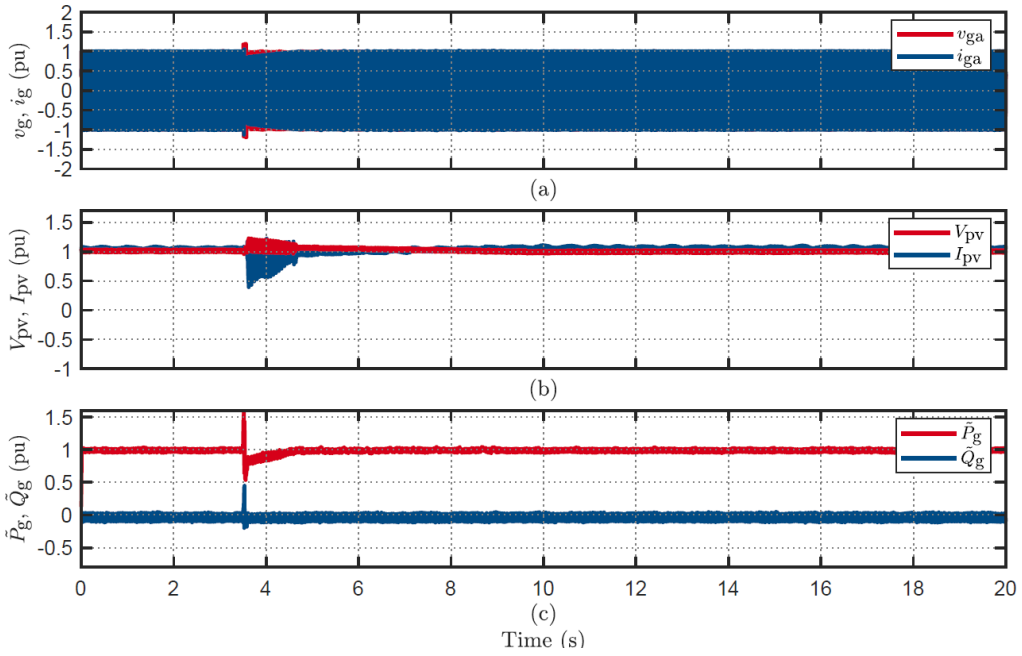

Figure 4.23. Inverter ride-through response to a voltage swell of 1.2p.u for 80ms with 1mH (SCR 33.6) line inductance.

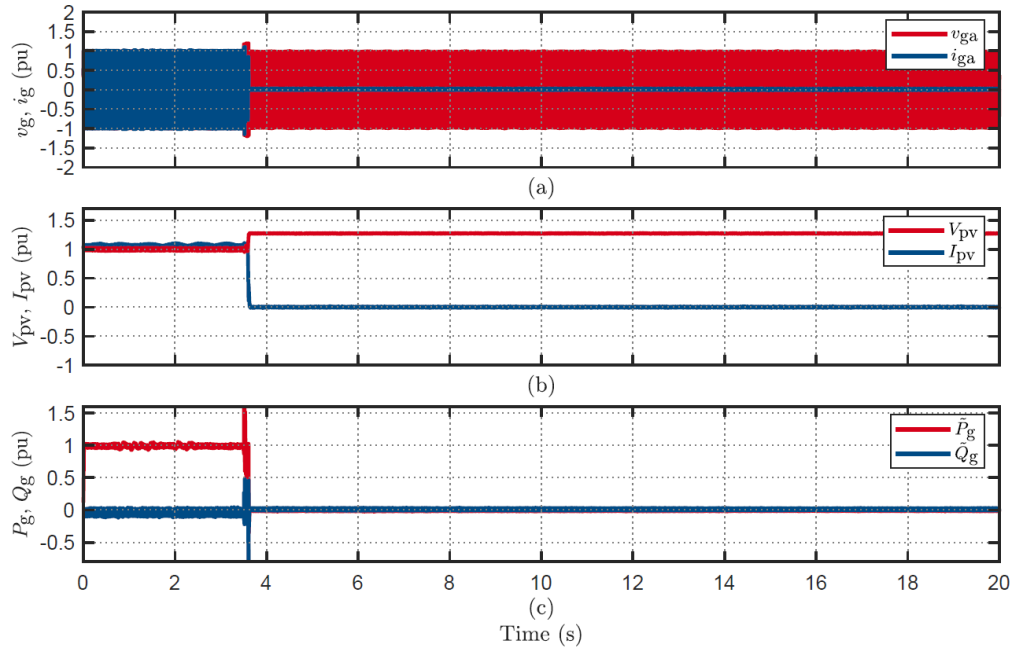

Figure 4.24. Inverter disconnection response to a voltage swell of 1.2p.u for 220ms with 1mH (SCR 33.6) line inductance.

Table 4.7: Summary of the inverter 35 test results with 1mH line inductance.

Inverter 35		
Test	1mH (SCR 33.6)	
	Behavior (FP)	Behavior (HP)
Startup	Ride-Through	--
230 to 50 for 0.9s	Power Curtailed	--
230 to 160 for 9s	Disconnected	Disconnected
230 to 270 for 0.9s	Disconnected	Disconnected
Sag of 0.8p.u for 80ms	Ride-Through	--
Sag of 0.8p.u for 220ms	Power Curtailed	--
Sag of 0.8p.u for 800ms	Power Curtailed	--
Swell of 1.2p.u for 80ms	Ride-Through	--
Swell of 1.2p.u for 120ms	Disconnected	Disconnected
Swell 1.175p.u for 120ms	Disconnected	Disconnected

3.11. Inverter 30

This inverter demonstrated tolerance to high network impedance conditions, successfully maintaining a stable grid connection even at line inductance values significantly higher than those at which many previously tested units failed. It achieved reliable grid synchronisation at high impedance value of 10mH while operating at full power, establishing itself as the most impedance-resilient inverter in the test cohort. However, despite this impedance tolerance, the inverter's response to grid disturbances was compromised, with performance varying significantly based on both operating power and line inductance values. A notable example occurred during a voltage sag of 0.7 p.u lasting 80ms: the inverter was able to ride-through this disturbance while operating at half power but disconnected when subjected to the same disturbance at full power, as demonstrated in Figure 4.25 and Figure 4.26, respectively. Moreover, at 9mH line inductance, the inverter maintained grid connection during a 0.7 p.u voltage sag lasting 80ms at full power, yet it failed to sustain the connection under identical conditions at full power with 10mH line inductance, as illustrated in Figure 4.27.

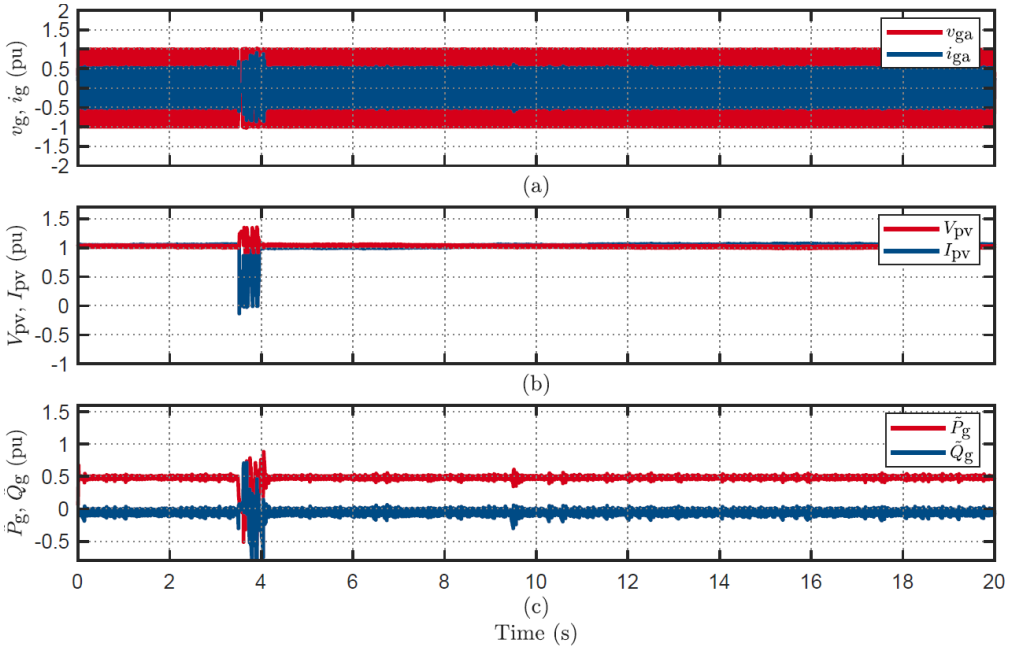

Figure 4.25. Inverter ride-through response to a voltage sag of 0.7p.u for 80ms with 10mH (SCR 3.3) line inductance (half power).

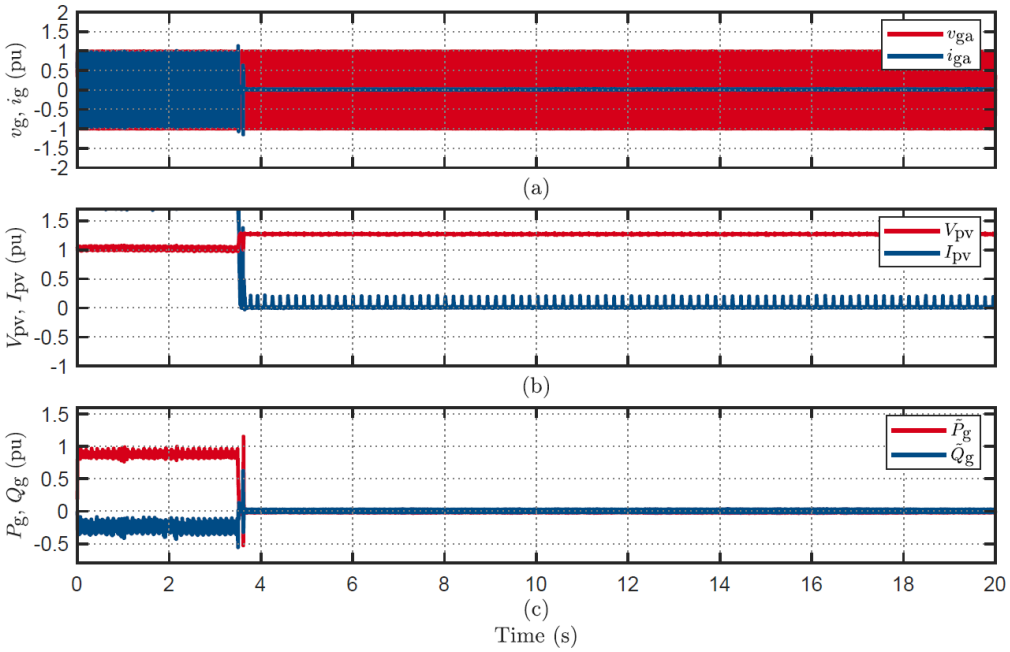

Figure 4.26. Inverter disconnection response to a voltage sag of 0.7p.u for 80ms with 10mH (SCR 3.3) line inductance (full power).

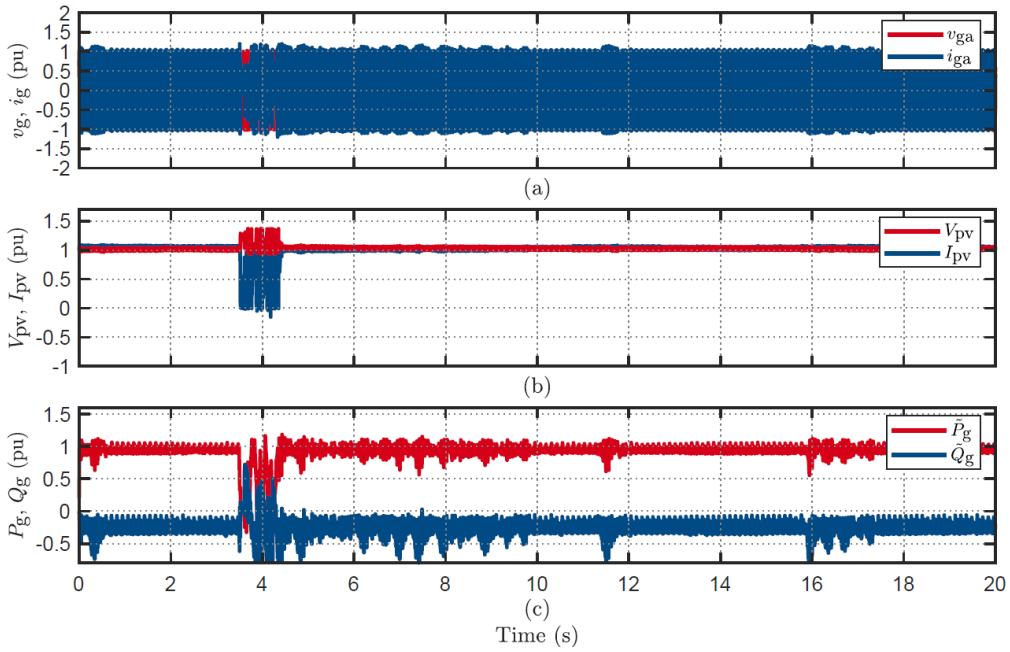

Figure 4.27. Inverter ride-through response to a voltage sag of 0.7p.u for 80ms with 9mH (SCR 3.7) line inductance (full power).

Table 4. provides a detailed analysis of the inverter's response across the impedance spectrum, highlighting specific conditions where its behaviour diverged from that observed during zero-impedance testing. The data reveals a clear correlation between decreasing line inductance and improved disturbance resilience, while also demonstrating significant variations in response between full and half-power operation. These findings emphasise how network impedance fundamentally alters the stability thresholds of the inverter.

Table 4.8: Summary of the inverter 30 test results with different line inductances.

Inverter 30				
Test	**10mH (SCR 3.3)**		**9mH (SCR 3.7)**	
	Behavior (FP)	Behavior (HP)	Behavior (FP)	Behavior (HP)
Startup	Ride-Through	--	--	--
230 to 50 for 0.9s	Disconnected	--	Disconnected	Disconnected
VPAJ 45°	Disconnected	Disconnected	Disconnected	Ride-through
Sag of 0.8p.u for 80ms	Disconnected	Disconnected	Disconnected	Disconnected
Sag of 0.7p.u for 80ms	Disconnected	Ride-Through	Ride-through	--
Sag of 0.6p.u for 80ms	Disconnected	--	--	--
Sag of 0.5p.u for 80ms	Disconnected	--	--	--
Sag of 0.4p.u for 80ms	Disconnected	--	--	--
Sag of 0.3p.u for 80ms	Disconnected	--	--	--
Sag of 0.2p.u for 80ms	Disconnected	--	--	--
Sag of 0.1p.u for 80ms	Ride-Through	--	--	--
Swell 1.2p.u for 80ms	Disconnected	--	Ride-through	--
Test	**8mH (SCR 4.2)**		**7mH (SCR 4.8)**	
	Behavior (FP)	Behavior (HP)	Behavior (FP)	Behavior (HP)
230 to 50 for 0.9s	Ride-Through	--	--	--
VPAJ 45°	Disconnected	Ride-Through	Ride-Through	--
VPAJ 60°	--	--	Disconnected	Ride-Through
Sag of 0.8p.u for 80ms	Ride-Through	--	--	--
Sag of 0.8p.u for 220ms	Disconnected	Ride-Through	Ride-Through	--
Swell 1.2p.u for 220ms	Disconnected	--	Ride-through	--
Test	**6mH (SCR 5.6)**		**5mH (SCR 6.7)**	
	Behavior (FP)	Behavior (HP)	Behavior (FP)	Behavior (HP)
VPAJ 60°	Disconnected	Ride-Through	Ride-Through	--

3.12. Inverter 36

This inverter exhibited tolerance to high network impedance conditions, effectively maintaining a stable grid connection even at line inductance values significantly higher than those at which many previously tested units failed. It achieved reliable grid synchronisation at an exceptionally high impedance value of 10mH while operating at full power, establishing itself as the most impedance-resilient inverter in the test group. However, despite this tolerance to high impedance values, the inverter exhibited a compromised response to grid disturbances, with its performance varying significantly depending on the line inductance values and the duration of the disturbances. This vulnerability is evident in its response to voltage swells: during a 1.2 p.u swell lasting 80ms, the inverter maintained its grid connection, but it disconnected when subjected to an identical magnitude swell extended to 220ms, as illustrated in Figure 4.28 and Figure 4.29, respectively.

Table 4.9 provides a detailed analysis of the inverter's response across the impedance spectrum, highlighting specific conditions where its behaviour deviated from baseline zero-impedance testing. The data reveals a clear correlation between decreasing line inductance and enhanced disturbance resilience. These findings emphasise how network impedance fundamentally alters the stability thresholds of inverters in grid-connected applications.

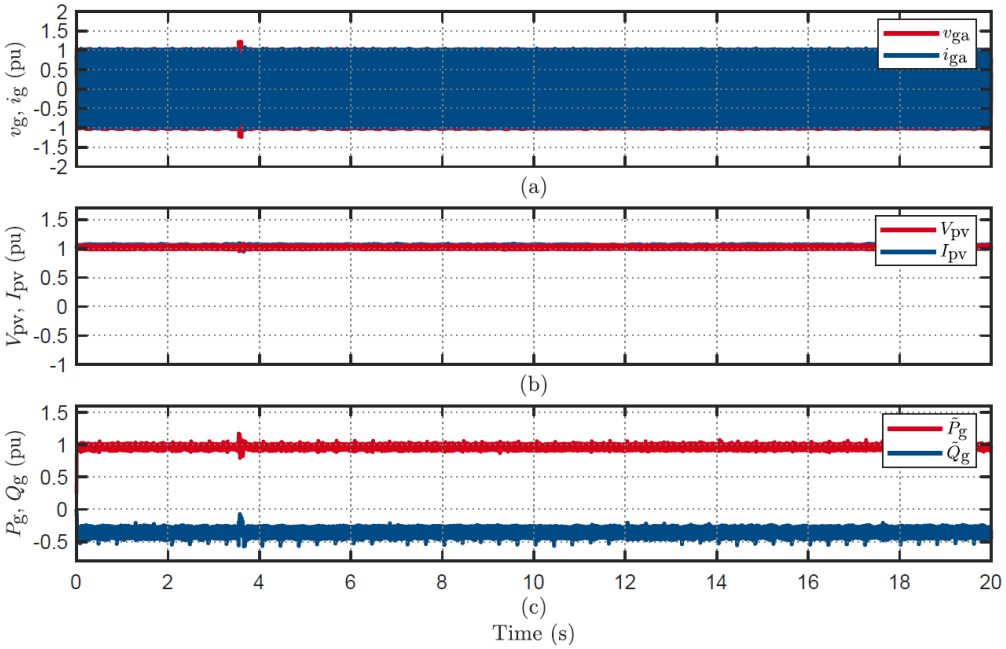

Figure 4.28. Inverter ride-through response to a voltage swell of 1.2p.u for 80ms with 10mH (SCR 3.3) line inductance.

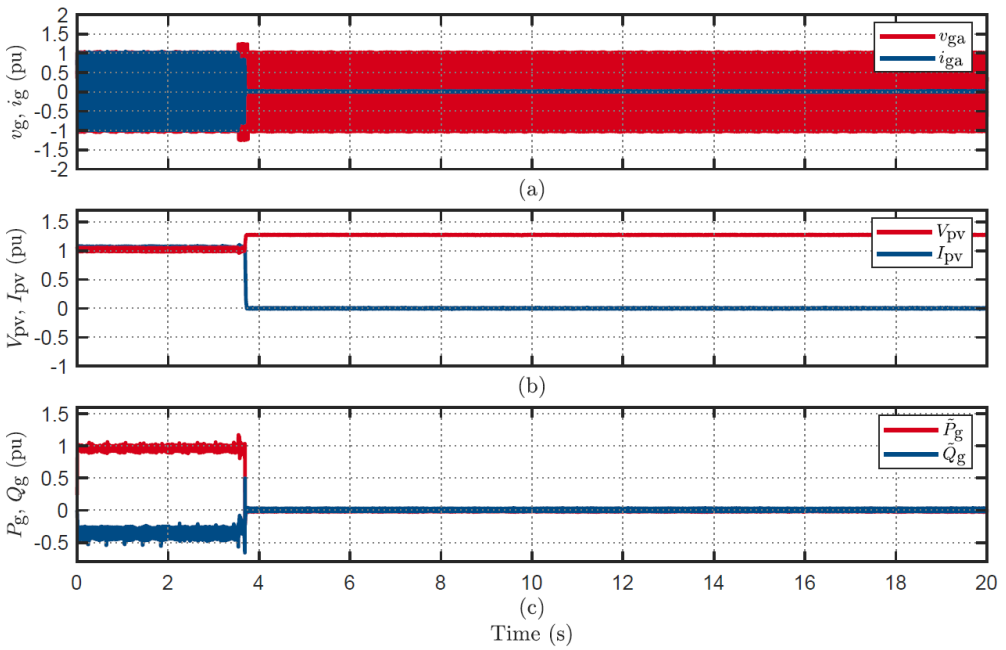

Figure 4.29. Inverter disconnection response to a voltage swell of 1.2p.u for 220ms with 10mH (SCR 3.3) line inductance.

Table 4.9: Summary of the inverter 36 test results with different line inductances.

Inverter 36				
Test	**10mH (SCR 3.3)**		**9mH (SCR 3.7)**	
	Behavior (FP)	Behavior (HP)	Behavior (FP)	Behavior (HP)
230 to 50 for 0.9s	Disconnected	Disconnected	Disconnected	Disconnected
230 to 160 for 9s	Disconnected	Disconnected	Disconnected	Disconnected
230 to 270 for 0.9s	Disconnected	Disconnected	Disconnected	Disconnected
Sag of 0.8p.u for 80ms	Ride-Through	--	--	--
Sag of 0.8p.u for 120ms	Disconnected	Disconnected	Disconnected	Disconnected
Sag of 0.8p.u for 220ms	Disconnected	Disconnected	--	--
Swell 1.2p.u for 80ms	Ride-Through	--	--	--
Swell 1.2p.u for 220ms	Disconnected	Disconnected	Disconnected	Disconnected
Test	**8mH (SCR 4.2)**		**7mH (SCR 4.8)**	
	Behavior (FP)	Behavior (HP)	Behavior (FP)	Behavior (HP)
230 to 50 for 0.9s	Disconnected	Disconnected	Disconnected	Disconnected
230 to 160 for 9s	Disconnected	Disconnected	Disconnected	Disconnected
230 to 270 for 0.9s	Disconnected	Disconnected	Disconnected	Disconnected
Sag of 0.8p.u for 120ms	Disconnected	Disconnected	Ride-Through	--
Swell 1.2p.u for 220ms	Disconnected	Disconnected	Disconnected	Disconnected
Test	**6mH (SCR 5.6)**		**5mH (SCR 6.7)**	
	Behavior (FP)	Behavior (HP)	Behavior (FP)	Behavior (HP)
230 to 50 for 0.9s	Disconnected	Disconnected	Disconnected	Disconnected
230 to 160 for 9s	Disconnected	Disconnected	Disconnected	Disconnected
230 to 270 for 0.9s	Disconnected	Disconnected	Disconnected	Disconnected
Sag of 0.8p.u for 220ms	Disconnected	Disconnected	Ride-Through	--
Swell 1.2p.u for 220ms	Disconnected	Disconnected	Disconnected	Disconnected
Test	**4mH (SCR 8.4)**		**3mH (SCR 11.3)**	
	Behavior (FP)	Behavior (HP)	Behavior (FP)	Behavior (HP)
230 to 50 for 0.9s	Ride-Through	Ride-Through	--	--
230 to 160 for 9s	Disconnected	Disconnected	Disconnected	Disconnected
230 to 270 for 0.9s	Disconnected	Disconnected	Disconnected	Disconnected
Sag of 0.8p.u for 220ms	Ride-Through	Ride-Through	--	--
Swell 1.2p.u for 220ms	Disconnected	Disconnected	Disconnected	Disconnected

3.13. Inverter 33

During weak grid testing, the inverter was connected through a 7mH line inductance and initially subjected to standard startup procedures. However, as it approached maximum power output, the inverter demonstrated persistent instability, resulting in cyclical disconnections followed by automatic reconnection attempts. Figure A3.17 illustrates this distinct disconnection pattern observed at maximum power levels. A significant improvement in operational stability was achieved when the line inductance was further decreased to 5mH, where the inverter exhibited complete stability, successfully attaining and maintaining maximum power output without interruption, as documented in Figure A3.18. This behaviour highlights a clear correlation between grid impedance thresholds and inverter stability, particularly marking a critical transition point between the 6mH and 5mH line inductance values.

Despite achieving stable operation at 5mH, the inverter's response to VPAJ and voltage swell disturbances was affected, with performance fluctuating considerably depending on the power output and line inductance values. A notable instance occurred during a voltage swell of 1.2 p.u lasting 220ms: the inverter disconnected while operating at full power but successfully maintained grid connection under the same disturbance at half power, as depicted in Figure 4.30, and Figure 4.31, respectively. Table 4.10 offers a detailed summary of the inverter's response to voltage swell and VPAJ disturbances across different line inductance values.

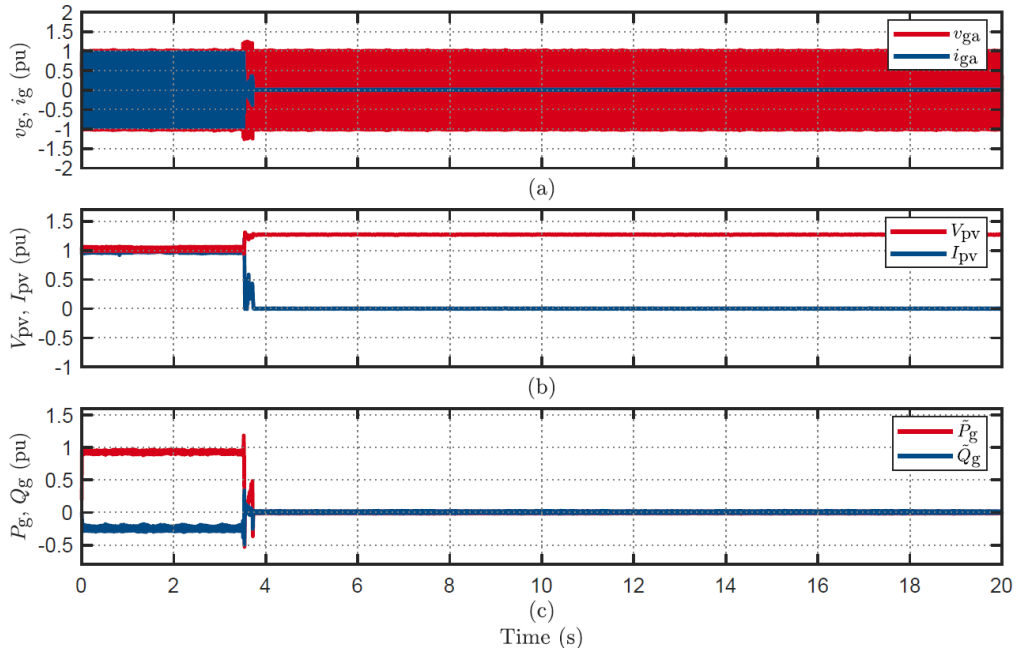

Figure 4.30. Inverter disconnection response to a voltage swell of 1.2p.u for 220ms with 5mH (SCR 4.2) line inductance (full power).

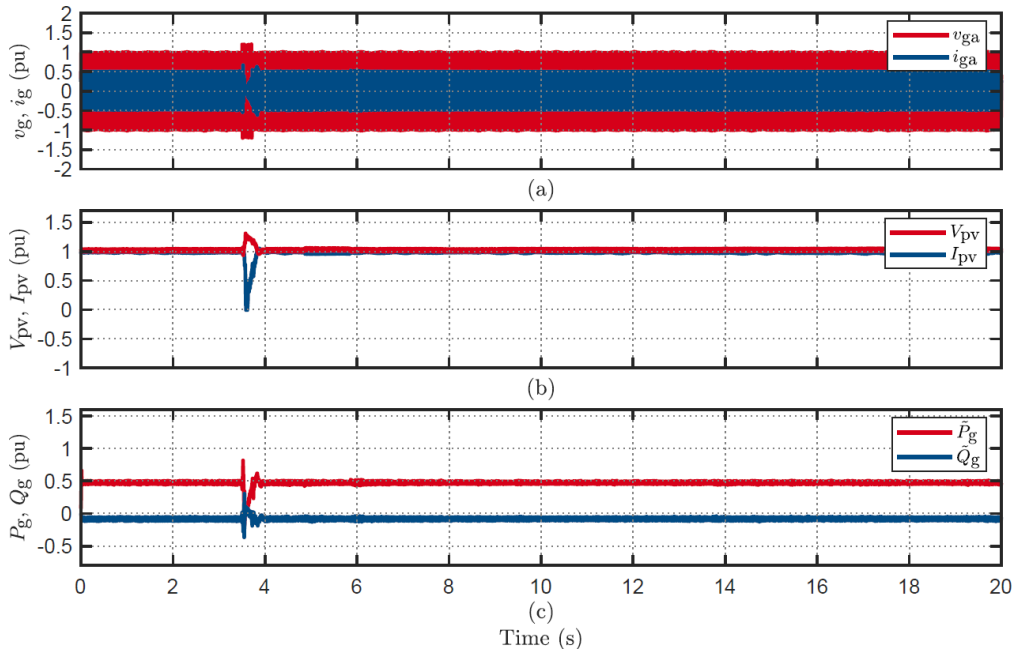

Figure 4.31. Inverter ride-through response to a voltage swell of 1.2p.u for 220ms with 5mH (SCR 4.2) line inductance (half power).

Table 4.10: Summary of the inverter 33 test results with different line inductances.

Inverter 33				
Test	**5mH (SCR 4.2)**		**4mH(SCR 5.2)**	
	Behavior (HP)	Behavior (FP)	Behavior (HP)	Behavior (FP)
VPAJ 60	Disconnected	Disconnected	Disconnected	Ride-Through
Swell 1.2p.u for 220ms	Disconnected	Ride-Through	Ride-Through	--
Test	**4mH (SCR 5.2)**		**3mH (SCR 7.0)**	
	Behavior (FP)	Behavior (HP)	Behavior (FP)	Behavior (HP)
VPAJ 60	Disconnected	Ride-Through	Ride-Through	--
Swell 1.2p.u for 800ms	Disconnected	Ride-Through	Ride-Through	--

3.14. Parallel Inverters in Weak Grid

Preliminary weak grid testing of parallel inverter configurations was conducted to systematically assess the combined effects of network impedance and multi-inverter interactions at shared connection points. This comprehensive investigation established critical benchmarks for comparing three distinct operational scenarios: inverters operating in parallel with line impedance, inverters operating in parallel without line impedance, and the performance of individual inverters under weak grid conditions. The comparative analysis unveiled previously unidentified interaction mechanisms that arise specifically at the intersection of network impedance and parallel operation, with implications that extend beyond the mere superposition of these two factors. By quantifying these complex interdependencies, the study offers vital insights for grid integration planning in distributed generation, particularly in network segments with higher impedance values.

3.14.1. Inverters 47 and 54

The parallel operation of Inverters 47 and 54 (same OEM) across varying line inductance values provided valuable insights when compared to their individual performance under weak grid conditions and in the absence of line impedance. Although both inverters demonstrated the capability to withstand 3mH line inductance individually and achieved maximum power output during standalone testing (as detailed in Sec 3.1.10, 4.5 and 4.1), their parallel configuration struggled to maintain stable operation when line inductance exceeded 2mH. This decline in impedance tolerance resulted in complicated interaction patterns during disturbance events. For instance, when subjected to a 15° VPAJ with 2mH line inductance, Inverter 47 disconnected, while Inverter 54 engaged in power curtailment. This contrasted sharply with their parallel performance without line impedance, where the same VPAJ led to power curtailment from Inverter 47 and complete ride-through from Inverter 54, as illustrated in Figure 4.32 and Figure 4.33, respectively.

Table 4.11 presents a comparative analysis of the responses of parallel inverters against individual performance across various grid disturbances, underscoring the distinct behavioural changes introduced by network impedance in multi-inverter configurations. These findings indicate that parallel operation significantly alters the impedance tolerance of otherwise robust individual units, which has critical implications for system design in weak grid environments.

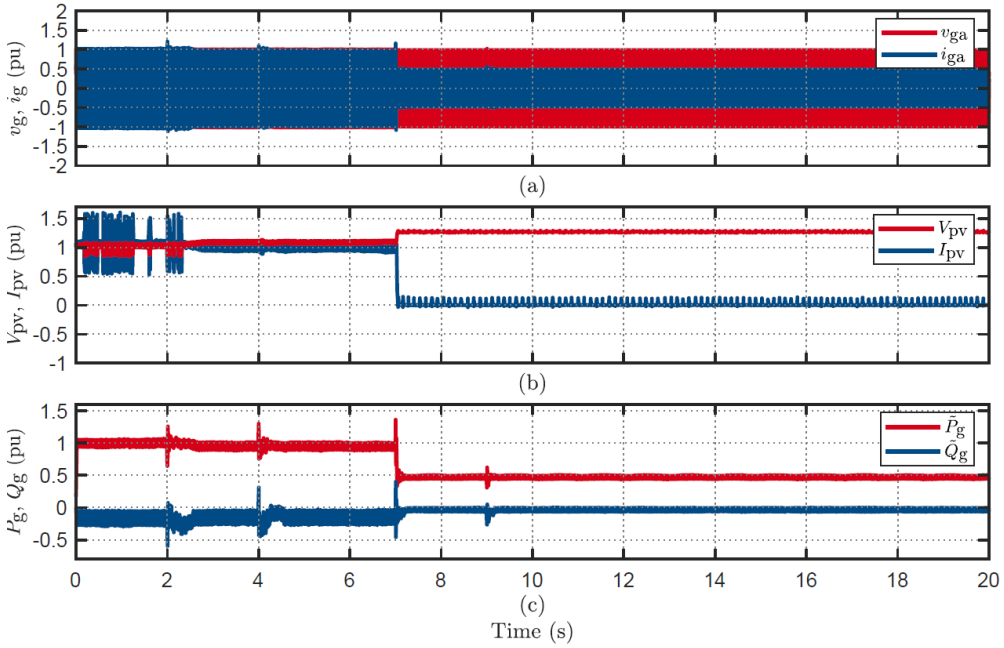

Figure 4.32. Parallel inverters (54: power curtailed, 47: disconnected) response to VPAJ 15° with 2mH (SCR 8.7) line inductance.

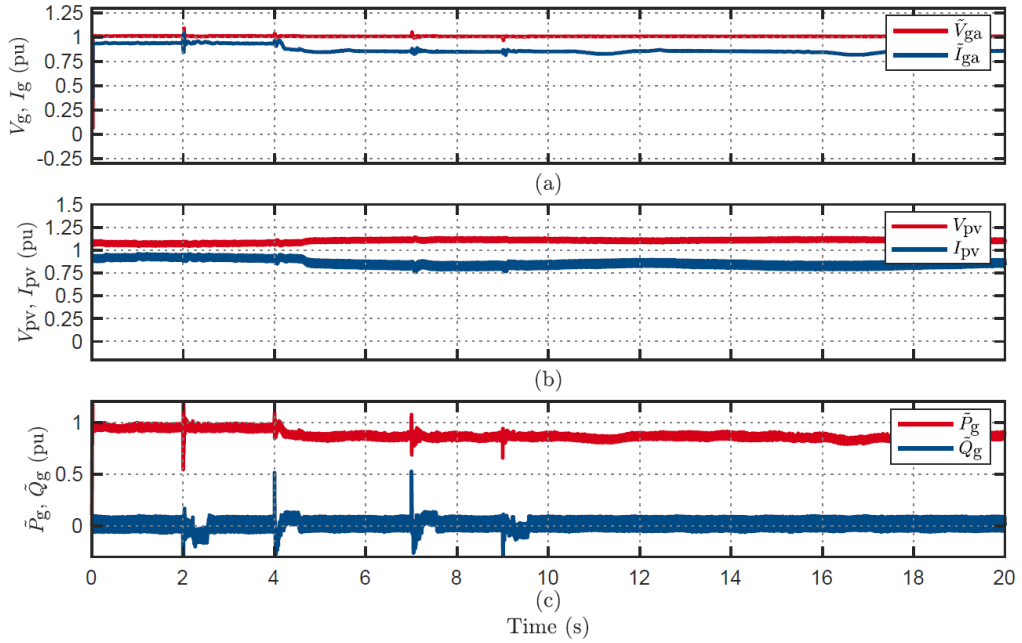

Figure 4.33. Parallel inverters (54: power curtailed, 47: ride-through) response to VPAJ 15° without line inductance.

Table 4.11: Summary of the parallel inverter 54 & 47 test results with different line inductances.

Inverter 54 & 47			
Test	**2mH (SCR 8.7)**		**1mH (SCR 17.5)**
	Parallel	Individual	Parallel
Startup	RT, RT	--	--
VPAJ 15°	PC, DC	RT, PC	PC, PC
VPAJ 30°	DC, DC	PC, DC	RT, DC
VPAJ 45°	--	PC, DC	RT, DC
VPAJ 60°	--	PC, DC	RT, DC
Sag of 0.7p.u for 220ms	DC, DC	RT, DC	RT, DC
Swell of 1.2p.u for 220ms	DC, PC	RT,PC	RT, RT
Swell of 1.2p.u for 800ms	DC, PC	RT,PC	RT, PC

Legends:

RT: Ride-through, PC: Power Curtailment, DC: Disconnection

3.14.2. Inverters 38 and 54

The parallel operation of Inverters 38 and 54 from different OEMs, across varying line inductance values, has yielded critical insights when analysed against their individual weak grid performance and parallel operation with no line impedance. Both inverters successfully withstood a 3mH line inductance during individual testing and achieved maximum power output during parallel testing under weak grid conditions (as detailed in Sec 3.1.11, 4.5 and 4.8). However, their response characteristics to disturbances were significantly affected by the presence of network impedance. When exposed to a 15° VPAJ with a 3mH line inductance, Inverter 54 disconnected, while Inverter 38 sustained its grid connection through effective ride-through behaviour contrasting with their parallel performance without line impedance, where the same VPAJ allowed both units to successfully ride-through the disturbance, as shown in Figure 4.34 and Figure 4.35, respectively. This divergent behaviour was further highlighted during voltage swell testing: a swell of 1.2 p.u lasting 220ms resulted in the simultaneous disconnection of both inverters when operating in parallel with 3mH line inductance. In contrast, both inverters managed to ride through the disturbance without impedance, see Figure A3.19 and Figure A3.20.

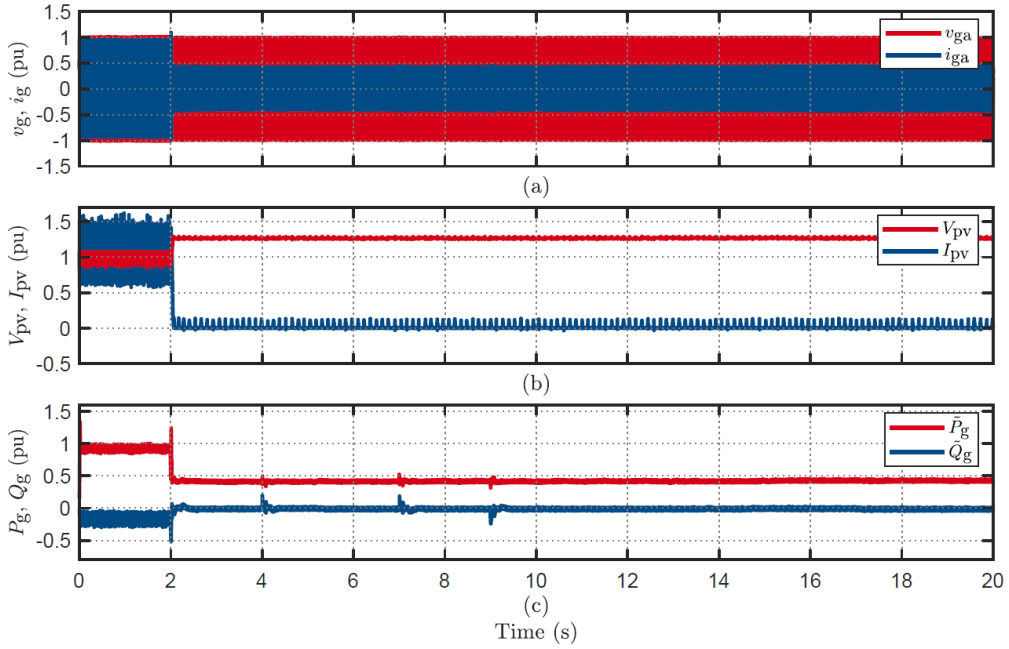

Figure 4.34. Parallel inverters (54: disconnected, 38: ride-through) response to VPAJ 15° with 3mH (SCR 5.8) line inductance.

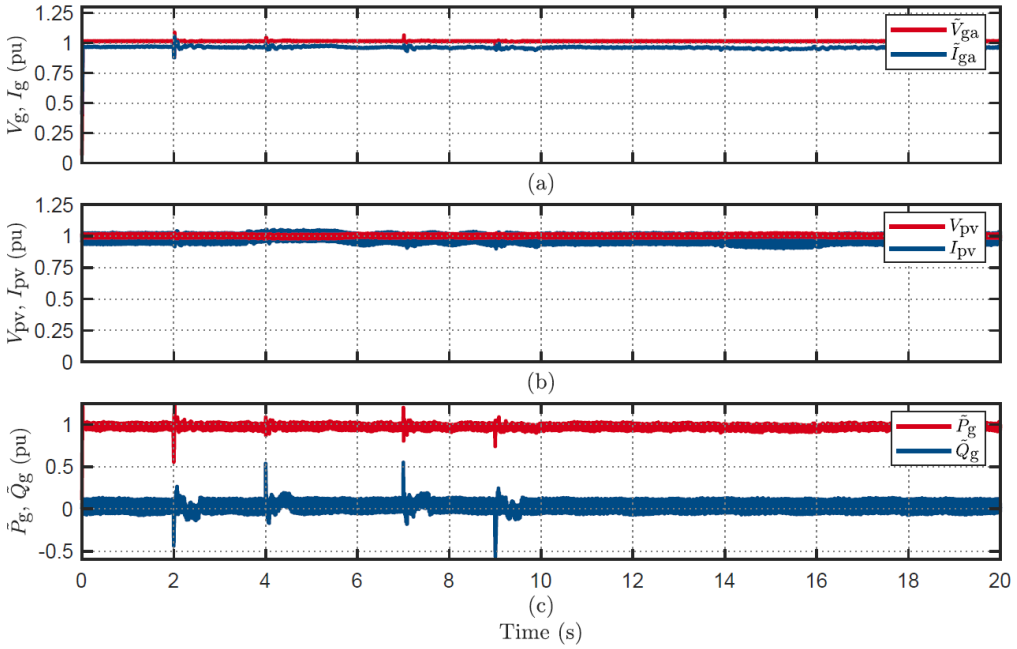

Figure 4.35. Parallel inverters (54: disconnected, 38: ride-through) response to VPAJ 15° without line inductance.

Table 4.12 provides a comprehensive comparative analysis of the parallel inverter responses versus their individual weak grid performance across multiple disturbance categories. It emphasises the significant behavioural modifications introduced by network impedance in multi-inverter configurations. These findings indicate that parallel operation can fundamentally compromise the impedance tolerance and stability characteristics of otherwise robust units, with serious implications for system reliability in weak grid deployment scenarios.

Table 4.12: Summary of the parallel inverter 54 & 38 test results with different line inductances.

Inverter 54 & 38			
Test	3mH (SCR 8.7)		
	Parallel	Individual 54	Individual 38
Startup	RT, RT	--	--
VPAJ 15°	DC, RT	DC	--
VPAJ 30°	DC, PC	DC	PC
VPAJ 45°	DC, PC	DC	PC
VPAJ 60°	DC, PC	--	PC
230V to 160V for 9s	DC, DC	--	DC
230V to 270V for 0.9s	RT, DC	RT	DC
Sag of 0.7p.u for 80ms	DC, PC	DC	--
Sag of 0.6p.u for 80ms	DC, PC	DC	--
Sag of 0.5p.u for 80ms	DC, PC	DC	--
Sag of 0.4p.u for 80ms	RT, PC	DC	--
Swell of 1.2p.u for 220ms	DC, DC	DC	DC

Legends:

RT: Ride-through, PC: Power Curtailment, DC: Disconnection

3.15. Conclusion

The comprehensive study underscores the essential paradigm shift required for the integration of IBRs within evolving power systems, especially under conditions of weak grid stability. This research identified significant operational vulnerabilities and a marked disparity in inverter resilience through a systematic evaluation of fifteen inverters with varying levels of network line impedance. Notably, despite full compliance with existing standards AS4777.2:2020, inverter performance exhibited considerable variability, with impedance levels ranging from 1mH to 10mH. These findings reveal a critical shortfall in current standards and planning practices, which do not adequately address the impact of reduced grid strength on inverter functionality. As impedance levels increased, many inverters demonstrated instability, manifesting in issues such as startup failures, cyclic disconnections, and compromised responses to voltage and frequency fluctuations. This variability highlights a significant knowledge gap and raises serious concerns regarding grid stability as the penetration of IBRs continues to grow.

The study uncovers a crucial and previously overlooked interaction between inverter performance, operating power levels, and grid strength. A consistent trend emerged throughout the tests: several inverters that operated reliably under weak grid conditions at half power experienced failures under identical circumstances when functioning at full power. This indicates that power-dependent stress factors, such as increased current injection and the challenges of maintaining phase synchronization, significantly increase in low-strength grids. Notably, inverter responses to disturbances were highly non-linear and device-specific; some units disconnected during minor voltage sags or frequency fluctuations, while others remained stable even under high impedance, often within narrow operational margins. These findings highlight a significant gap in existing standards, which typically do not consider the effects of power levels in performance assessments. The degradation of behaviour observed at full power, particularly when coupled with weak grid conditions, presents a compounded risk of instability and widespread disconnection during peak generation periods, exactly when grid support is most critical. This underscores the necessity to reconsider conventional approaches to inverter testing, sizing, and operational planning in future DER integration strategies.

The variability in inverter performance highlights the limitations of a one-size-fits-all approach in current grid codes and emphasises the necessity for inverter-specific modelling in network planning. Notably, certain models, such as inverters 31, 30, and 36, demonstrated exceptional tolerance to high impedance values, successfully maintaining synchronism at inductances of up to 10mH. However, even these highly resilient units displayed vulnerability to disturbances when grid strength was further reduced or when disturbance durations exceeded critical thresholds. On the other hand, inverters like 35 exhibited significant instability, struggling to operate reliably even under relatively low impedance conditions, indicating their unsuitability for deployment in weak grid scenarios. Furthermore, the study's exploration of parallel inverter configurations introduced additional complexity. While individual inverters may perform adequately on their own, their interactions in parallel configurations, especially in the presence of impedance, can lead to performance degradation, asymmetric behavior, and the emergence of previously unobserved instability modes. A summary of the tested inverters' findings is presented in Table 4.13.

The research highlights an urgent need for the power industry to move beyond the conventional strong grid model. It emphasises that grid strength should be prioritised alongside voltage regulation and thermal capacity in network planning processes. The significant performance variations observed indicate that future standards must incorporate mandatory protocols for testing weak grids, impedance tolerance ratings, and assessments of multi-unit interactions. Without these advancements, the industry faces the risk of deteriorating grid reliability as renewable energy penetration increases, potentially jeopardising the transition to sustainable energy technologies. Looking ahead, this study offers the essential evidence needed to drive comprehensive reforms in the testing, certification, planning, and operation of IBRS. The shift from synchronous generator-dominated grids to IBRs presents one of the most formidable technical challenge and this research underscores that achieving success necessitates

immediate action to establish new standards, testing protocols, and planning methodologies that explicitly consider weak grid scenarios.

3.15.1. Results Summary

Table 4.13: Summary of all inverters performance under weak grid conditions.

Inverter	Max Stable Inductance (Full Power)	Weaknesses	Strengths
46	3mH	Disconnected during voltage swell & frequency step with inductance	Clear threshold between 3–4mH
44	2mH	Disconnected during 15° VPAJ at full power	Stable at 2mH & half power
52	4mH	Startup failed above 4mH	Reliable below threshold
48	9mH	Disconnected during voltage sag at full power	Excellent impedance tolerance
54	2mH	Poor disturbance response at 3mH	Stable at 2mH
49	3mH	Disconnects even during minor sags at full power	Performs well at half power & 2mH
40	9mH	Poor disturbance response at full power	High impedance tolerance
38	3mH	Disconnected above 3mH	Stable at 3mH
31	10mH	Fails under small sags at high impedance	Best tolerance to impedance
35	<2mH	Unstable even at 2mH	Extremely weak performance
30	10mH	Poor disturbance response at full power	Best tolerance to impedance
36	10mH	Disconnects with prolonged disturbances	Best tolerance to impedance
33	5mH	Disconnection during voltage swell at full power	Stable at 5mH

4. Laboratory EV Performance Evaluation

This final report outlines the progress made by the University of Wollongong (UOW) for Topic 9 of Stage 4 of the AR-PST Load Testing project, focusing on equipment evaluation, dynamic performance modelling, and field measurements.

4.1. Introduction

This section of the report presents the findings from comprehensive testing conducted on four electric vehicles (EVs) using three different EV chargers, one operating at Level 1 and two at Level 2. These tests build upon initial investigations undertaken in Stage 2 of the AR-PST project, which concluded that EV charging behaviour remains largely unaffected by frequency and phase jump disturbances. As a result, the focus of subsequent stages, namely Stage 3 and Stage 4, was solely on the impacts of voltage sag events, which are more likely to cause disruptions in EV charging operations.

The detailed testing carried out in this phase offers critical insights into how modern EVs respond to voltage sags of varying depths and durations. By analysing the disconnection, reconnection, and power ramping behaviour across multiple EV models and charger configurations, this study contributes to a more nuanced understanding of EV load dynamics when subjected to power system disturbances. These insights are particularly valuable for Network Service Providers (NSPs) and system operators seeking to maintain grid stability in the face of increasing EV penetration.

Furthermore, the observed variability in EV responses suggests that present load modelling approaches may lack the granularity needed to accurately represent EV behaviour. This raises the potential need for the development or inclusion of a dedicated EV component within the AEMO Composite Load Model. Such an addition would enhance the ability of the model to capture the dynamic and heterogeneous nature of EV charging loads, particularly during power system faults or voltage disturbances, and support more reliable grid planning and operation strategies.

4.2. EV Testing Methodology

The primary objective of the tests conducted was to assess the response of charging EVs to voltage sag disturbances. Due to the high-power output of DC Level 3 chargers, which exceeds the capacity of the available e test equipment, the experiments were limited to Level 1 and Level 2 chargers. Furthermore, Level 1 and Level 2 chargers are commonly utilised in residential networks, whereas Level 3 chargers are predominantly found in commercial premises. Initially, the plan was to evaluate charger performance in a laboratory setting with a resistive load bank simulating the response of the charging EV. However, upon analysing the initial data, it was discovered that Level 1 and Level 2 chargers operate on AC power, and the conversion to DC power occurs within the vehicle, resulting in varied responses across different EVs. Consequently, actual EVS were used as the charger load as opposed to resistors.

The experimental setup used for the EV testing for the four EVs is depicted in Figure 5.1. For the purposes of anonymity, the exact models of the EVs have not been labelled and instead have been labelled EV1, EV2, EV3, and EV4. The EVs were chosen to include the most common EVs based on recent statistical data of EV sales in Australia. All the tested EVS were able to fully accept the Level 2 charging capacity of 7 kW. Throughout the tests, the State of Charge (SoC) of the vehicles was kept below 80% to ensure the consistency of the charging process.

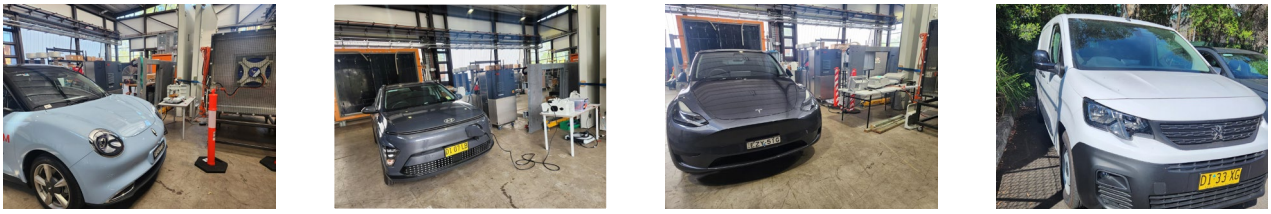

Figure 5.1. Experiment setup for four different EVs

Each EV was tested with three chargers: one Level 1 charger (referred to as Level 1 in this report) and two Level 2 chargers, hereafter denoted as Charger A and Charger B. Both Level 2 chargers were rated at 7.4 kW. This mix of equipment resulted in twelve combinations of EV/Charger configurations. Response for all charging scenarios was evaluated when subjected to voltage sags of durations of 80 ms and 120 ms, and depths ranging from 0.2 pu to 0.8 pu in 0.1 pu increments. This equates to a total of 96 individual tests.

4.3. Test Results

4.3.1. EV 1

4.3.1.1. Level 1 Charger

For EV1 under Level 1 charging, the vehicle drew approximately 1650 W of active power and 60 VAr of reactive power, resulting in a power factor (PF) close to unity. Throughout testing, EV1 successfully rode through all voltage sags except for a retained voltage of 0.2 pu for both the 80 ms and 120 ms duration scenarios. Figure 5.2 illustrates the ride-through response of EV during these disturbances. A consistent transient was observed immediately upon sag initiation. Regarding disconnection behaviour, as depicted in Figure 5.3, the charging process typically ceased for approximately 4 seconds following the sag. During the initial 2 seconds, active power dropped to 0 kW, indicating a complete disconnection. A small transient power was recorded during after the disconnection phase, likely caused by the closing of a relay in preparation for reconnection. Subsequently, charging resumed, with the active power rapidly returning to approximately 1500 W within 0.5 seconds and gradually ramping up to full power over the next 3.5 seconds.

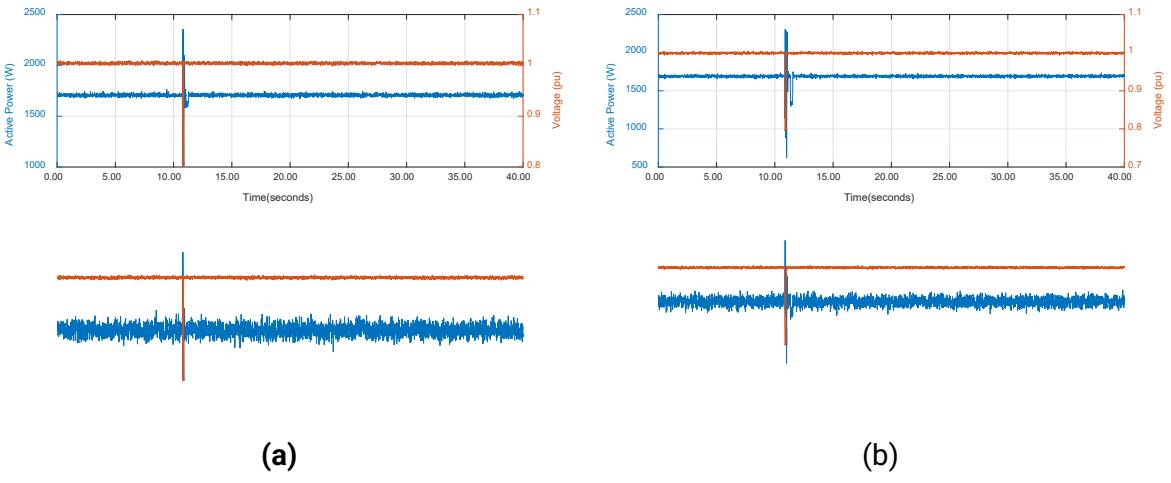

(a) (b)

Figure 5.2. Ride-through response of EV 1 with Level 1 Charger for (a) 0.8 pu-80 ms sag and (b) 0.8 pu-120 ms sag

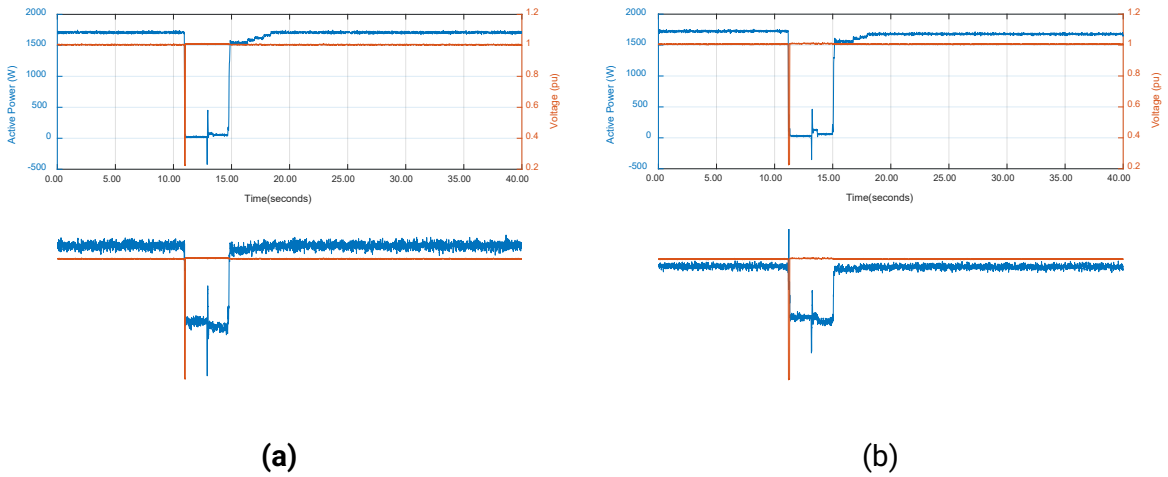

Figure 5.3. Disconnection response of EV1 with Level 1 Charger for (a) 0.2 pu-80 ms sag and(b) 0.2pu-120 ms sag

Table 5.1 summarises the response of EV1, while being charged with the Level 1 charger, when exposed to voltage sags. The cases in which EV disconnected are noted in red. This method of presentation will be maintained throughout the remainder of the report.

Table 5.1. Response of EV 1 with Level 1 Charger

Duration (ms)	Sag Voltage (pu)						
	0.8	0.7	0.6	0.5	0.4	0.3	0.2
80	Ride Through	Ride Through	Ride Through	Ride Through	Ride Through	Ride Through	Disconnect for 0.4s
120	Ride Through	Ride Through	Ride Through	Ride Through	Ride Through	Ride Through	Disconnect for 0.4s

4.3.1.2. Level 2 Charger A

For Level 2 charging, EV1 operated at 7400 W of active power and 410 VAr of reactive power. In contrast to Level 1 charging, which only disconnected at a retained voltage of 0.2 pu, disconnection was observed for the significantly less severe sag of 0.6 pu, suggesting that operation using the Level 2 charger is more sensitive to voltage sag disturbances. Similar to Level 1 operation, a transient was observed during the ride-through phase, with the active power momentarily peaking at approximately 9500 W. The disconnection behaviour was consistent across all applicable tests, with the disconnection and reconnection durations observed to be approximately 4 s and 6.5 s, respectively. However, for one sag test of 0.5 pu retained voltage and 120 ms duration, the disconnection time was prolonged to almost 7 s, as shown in Figure 5.4 (b). A minor transient, similar to that observed for the Level 1 charger scenario, was detected during the disconnection phase as shown in Figure 5.4. Upon reconnection, the power rapidly increased to approximately 6100 W in under 0.5 s before gradually ramping up to the rated power of 7400 W.

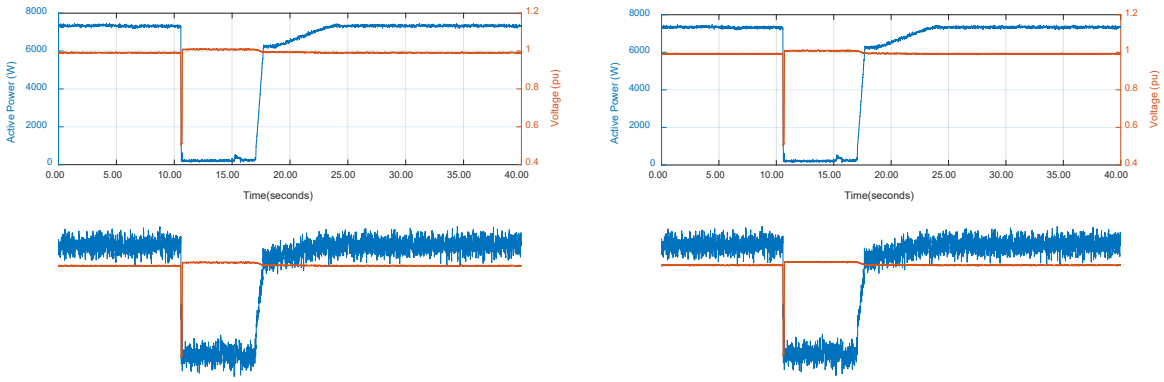

(a) (b)

Figure 5.4. Disconnection response of EV1 with Level 2 Charger A for (a) 0.5 pu-80 ms sag and (b) 0.5pu-120 ms sag

Table 5.2 summarises the response of EV2, while being charged using Level 2 charger A, when exposed to voltage sag conditions. Notably, the data recorded for a 0.5 pu–120 ms sag event is highlighted, as it resulted in a longer disconnection duration of 7 seconds, compared to the typical 4-second disconnection observed in other cases.

Table 5.2. Response of EV 1 with Level 2 Charger A

Duration (ms)	Sag Voltage (pu)						
	0.8	0.7	0.6	0.5	0.4	0.3	0.2
80	Ride Through	Ride Through	Disconnect for 4s	Disconnect for 4s	Disconnect for 4s	Disconnect for 4s	Disconnect for 4s
120	Ride Through	Ride Through	Disconnect for 4s	Disconnect for 4s	Disconnect for 4s	Disconnect for 4s	Disconnect for 4s

4.3.1.3. Level 2 Charger B

The response of EV1 when tested with Level 2 Charger B was identical to that observed with Level 2 Charger A. In all ten tests conducted with retained voltages ranging from 0.6 to 0.2 pu, the charging process was interrupted. Consistently, the disconnection duration was approximately 4 seconds across most cases. However, one exception was noted during the 0.6 pu–120 ms sag event, where the disconnection extended to nearly 7 seconds, as illustrated Figure 5.5(b) and highlighted in Table 5.3, which summarises all test results.

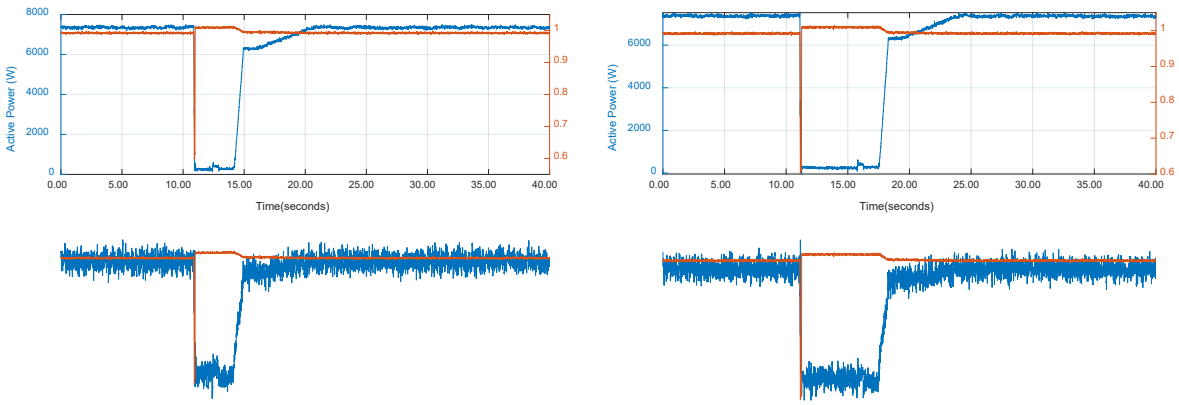

(a) (b)

Figure 5.5. Disconnection response of EV1 with Level 2 Charger B for (a) 0.6 pu-80 ms sag and (b) 0.6 pu-120 ms sag

Table 5.3. Response of EV 1 with Level 2 Charger B

Duration (ms)	Sag Voltage (pu)						
	0.8	0.7	0.6	0.5	0.4	0.3	0.2
80	Ride Through	Ride Through	Disconnect for 4s	Disconnect for 4s	Disconnect for 4s	Disconnect for 4s	Disconnect for 4s
120	Ride Through	Ride Through	Disconnect for 4s	Disconnect for 4s	Disconnect for 4s	Disconnect for 4s	Disconnect for 4s

4.3.2. EV 2

4.3.2.1. Level 1 Charger

Using Level 1 charging, EV2 drew 1400 W of active power and -260 VAr of reactive power, indicating a leading power factor characteristic. Unlike EV1, EV2 was unable to ride through voltage sags with retained voltage of 0.4 pu and 0.5 pu. However, during successful ride-through events, EV2 consistently exhibited a momentary power surge at the instant the sag was applied as illustrated in Figure 5.6.

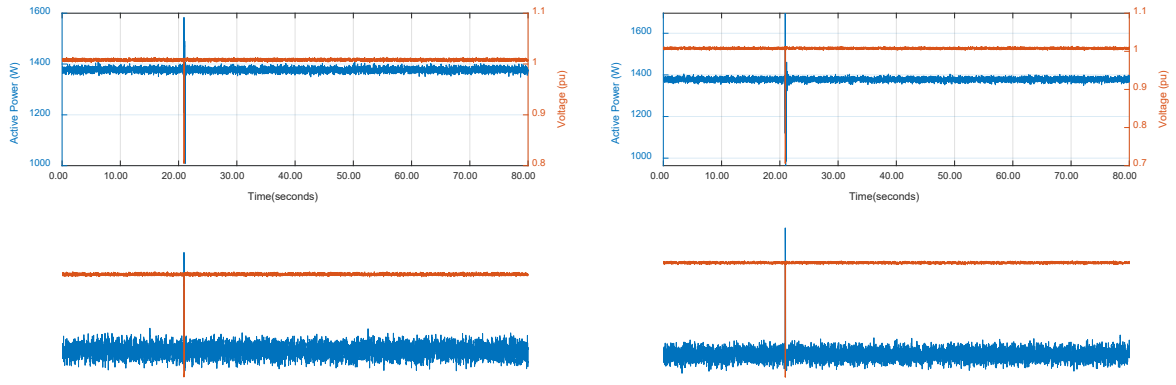

(a) (b)

Figure 5.6. Ride-through response of EV2 for (a) 0.8 pu-80 ms sag and (b) 0.7 pu-80 ms sag

Two distinct disconnection behaviours were observed for EV2. In most test cases, the charging process disconnected for approximately 10 seconds, after which it immediately resumed at full power, accompanied by a noticeable power overshoot as shown in Figure 5.7 (a) and (b). However, under the more severe sag condition of 0.2 pu for both 80 ms and 120 ms durations, a significantly shorter disconnection time of only 1.5 seconds was observed as shown in Figure 5.7 (c) and (d). This rapid reconnection is considered potentially grid-unfriendly, as discussed by the authors in [24], [25]. Notably, following a short disconnection period, the reactive power of EV2 did not return to its nominal charging value but instead decreased further to approximately -400 VAr, despite the active power being fully restored. Table 5.4 summarises the response of EV being charged at Level 1 when exposed to voltage sag conditions, with the unusually short disconnection at 0.2 pu highlighted.

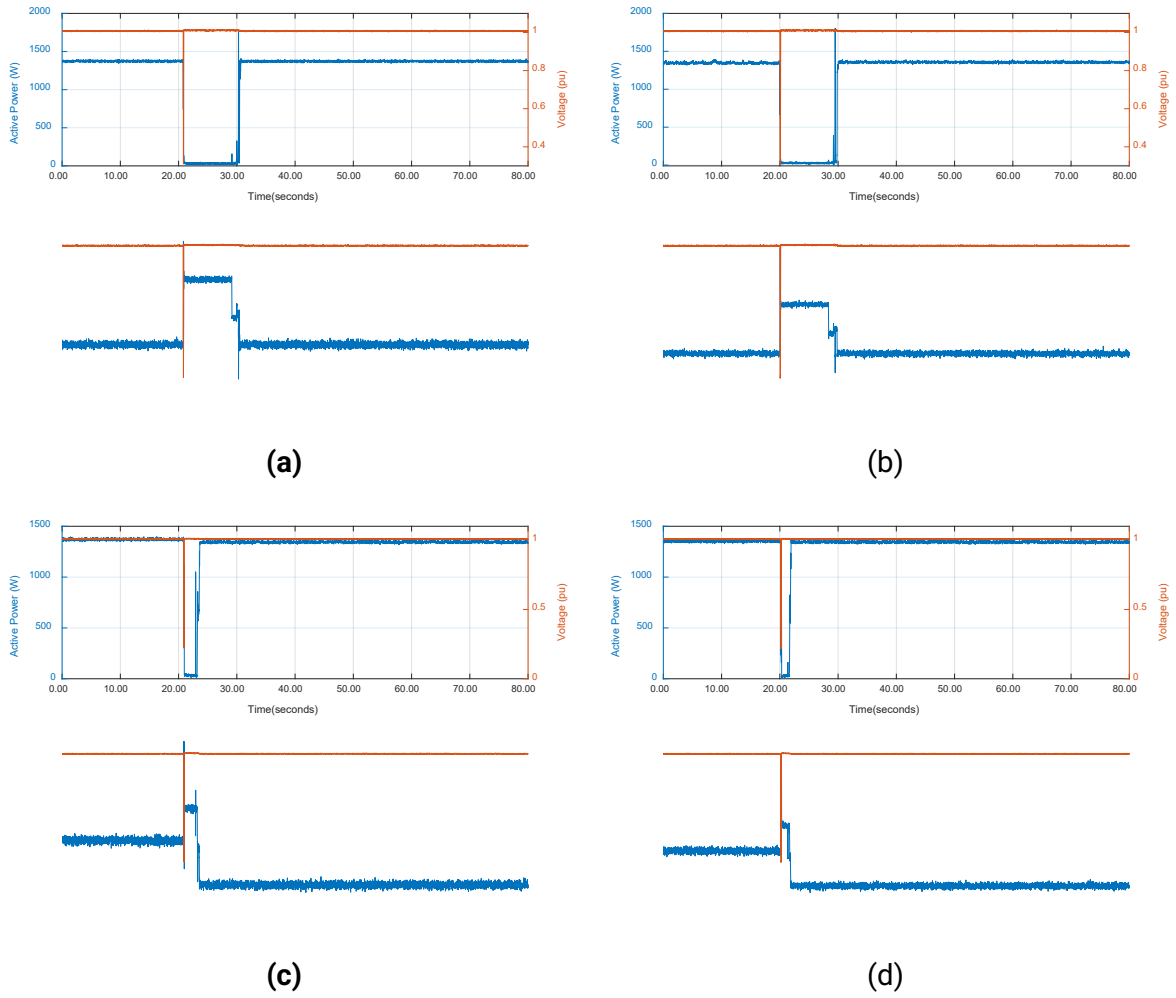

Figure 5.7. Disconnection response of EV1 with Level 1 Charger for (a) 0.3 pu-80 ms sag, (b) 0.3 pu-120 ms sag, (c) 0.2 pu-80 ms sag and (d) 0.2 pu-120 ms sag

Table 5.4. Response of EV 1 with Level 1 Charger

Duration (ms)	Sag Voltage (pu)						
	0.8	0.7	0.6	0.5	0.4	0.3	0.2
80	Ride Through	Ride Through	Ride Through	Ride Through	Disconnect for 10s	Disconnect for 10s	Disconnect for 1.5s
120	Ride Through	Ride Through	Ride Through	Disconnect for 10s	Disconnect for 10s	Disconnect for 10s	Disconnect for 1.5s

4.3.2.2. Level 2 Charger A

With Level 2 Charger A, EV2 drew 7400 W of active power and -300 VAr of reactive power. The vehicle was only able to ride through the voltage sag of 0.8 pu retained voltage. For retained voltages ranging from 0.2 pu to 0.7 pu, a disconnection in the charging process was observed with varying disconnection durations. Specifically, for sags under 80-ms within the 0.4–0.7 pu retained voltage range, the disconnection period was approximately 6 seconds, whereas for deeper sags of retained voltage of 0.2–0.3 pu, the interruption extended to between 25 and 33 seconds.

However, for 120-ms sags, the disconnection behaviour exhibited greater variability. Notably, extended disconnection durations of 36 s and 40 s were recorded for retained voltages of 0.5 pu and 0.2 pu, respectively. Conversely, at 0.7 pu and 0.6 pu, the disconnection period was approximately 6 s, while at 0.4 pu and 0.3 pu, it shortened to approximately 3 s. Figure 5.8 illustrates the three distinct disconnection

responses (very short, short, and long) corresponding to these cases and demonstrates that the charger is capable of resuming operation immediately after the disconnection, irrespective of its duration. Table 5.5 summarises the test results for EV2 with Charger A and highlights the cases in which the disconnection phase lasted considerably longer.

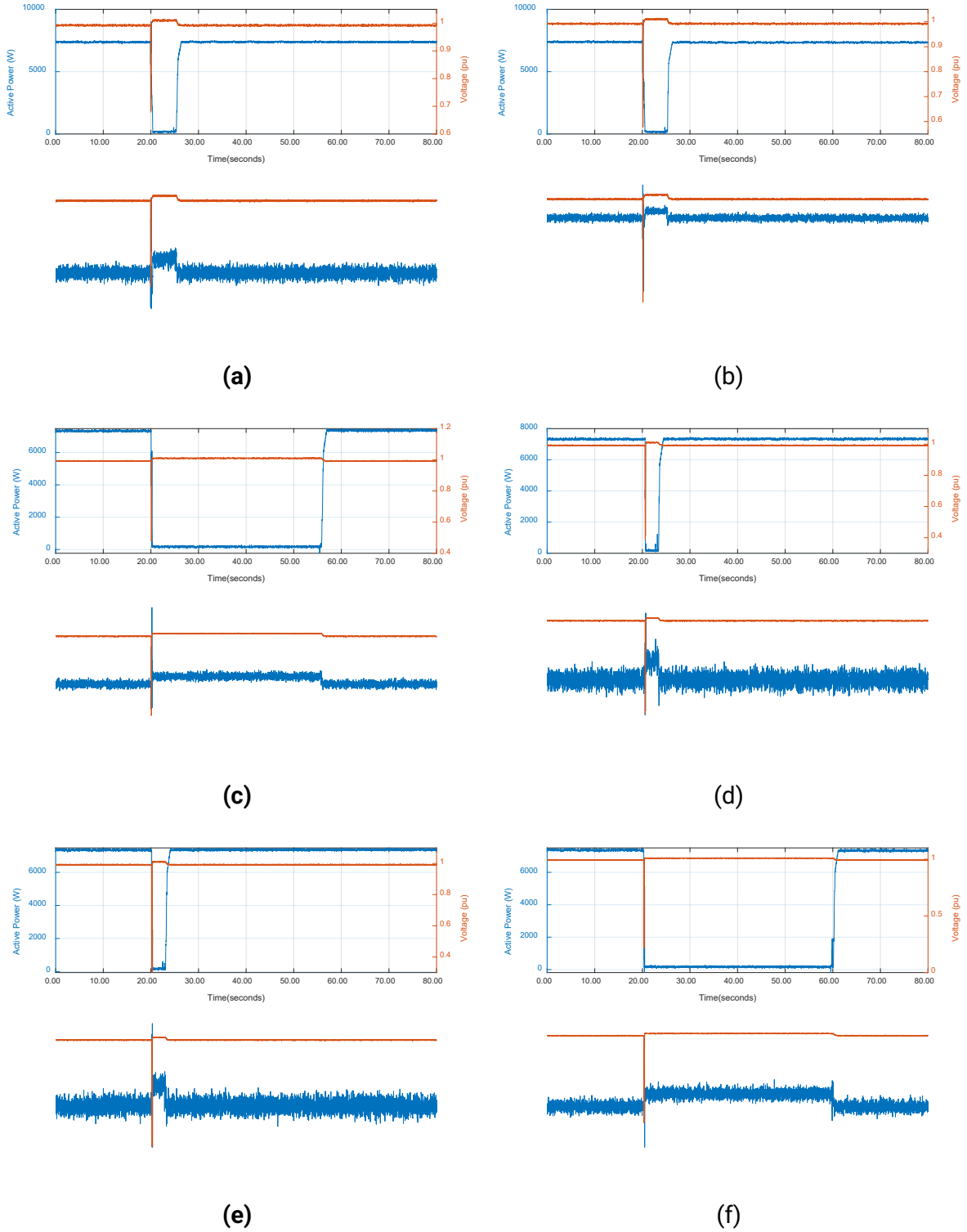

Figure 5.8. Disconnection response of EV2 with Level 2 Charger A for voltage sag duration of 120 ms at (a) 0.7 pu, (b) 0.6 pu, (c) 0.5 pu, (d) 0.4 pu, (e) 0.3 p and, (f) 0.2 pu

Table 5.5. Response of EV2 with Level 2 Charger A

Duration (ms)	Sag Voltage (pu)						
	0.8	0.7	0.6	0.5	0.4	0.3	0.2
80	Ride Through	Disconnect for 6s	Disconnect for 6s	Disconnect for 6s	Disconnect for 6s	Disconnect for 25s	Disconnect for 33s
120	Ride Through	Disconnect for 6s	Disconnect for 6s	Disconnect for 36s	Disconnect for 3s	Disconnect for 3s	Disconnect for 40s

4.3.2.3. Level 2 Charger B

EV2 was charged at the same power level using Charger B as for Charger A. Similar to performance for Level 2 Charger A, , the disconnection behaviour varied, and power surges were observed during the ride-through of the disturbances. For 80-ms sag durations, a prolonged disconnection lasting 40 seconds was recorded for 0.2 pu retained voltage. Otherwise, the disconnection duration was approximately 6 seconds. In contrast, for 120-ms sag events, no extensive disconnections were observed. However, at 0.3 pu and 0.2 pu retained voltage the disconnection durations were notably short, less than 3 seconds, as illustrated in Figure 5.9. Table 5.6 summarises the test results for EV2 with Charger A with the extended disconnection time scenario highlighted.

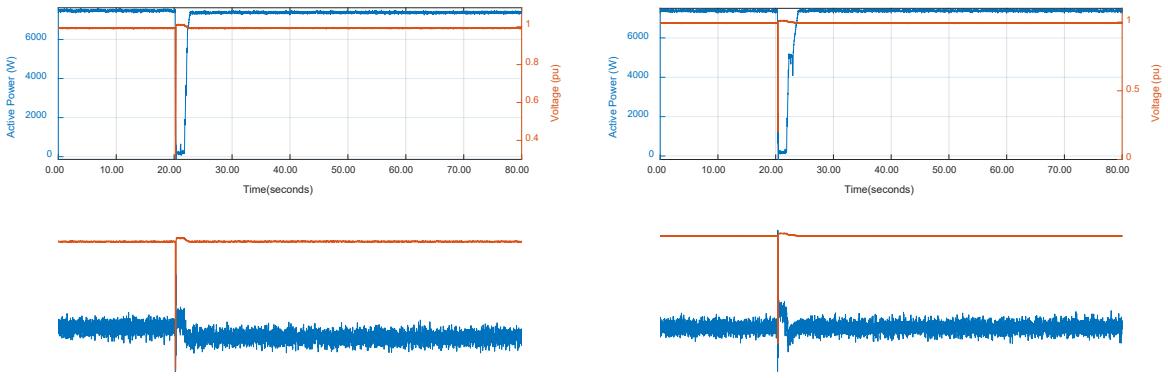

Figure 5.9. Disconnection response of EV2 with Charger B for (a) 0.3 pu-120 ms sag and (b) 0.2 pu-120 ms sag.

Table 5.6. Response of EV2 with Level 2 Charger B

Duration (ms)	Sag Voltage (pu)						
	0.8	0.7	0.6	0.5	0.4	0.3	0.2
80	Ride Through	Disconnect for 6s	Disconnect for 6s	Disconnect for 6s	Disconnect for 6s	Disconnect for 6s	Disconnect for 40a
120	Ride Through	Disconnect for 6s	Disconnect for 6s	Disconnect for 6s	Disconnect for 4s	Disconnect for <3s	Disconnect for <3s

4.3.3. EV 3

4.3.3.1. Level 1 Charger

Using the Level 1 charger, EV3 drew 2300 W of active power and close to 0 VAr of reactive power, indicating unity power factor operation. Throughout the tests, EV3 successfully rode through voltage sag disturbances ranging from 0.6 to 0.8 pu retained voltage for 80 ms duration, and from 0.4 to 0.8 pu retained voltage for 120 ms duration. During ride-through events, EV3 exhibited minimal or no power overshoot with momentary cessation, as shown in Figure 5.10. Regarding disconnection behaviour, performance remained consistent across all test conditions. In every instance where the charging

process was interrupted, the disconnection duration was nearly 10 seconds, followed by a ramp-up period of approximately 3 seconds to restore full power, as illustrated in Figure 5.11.

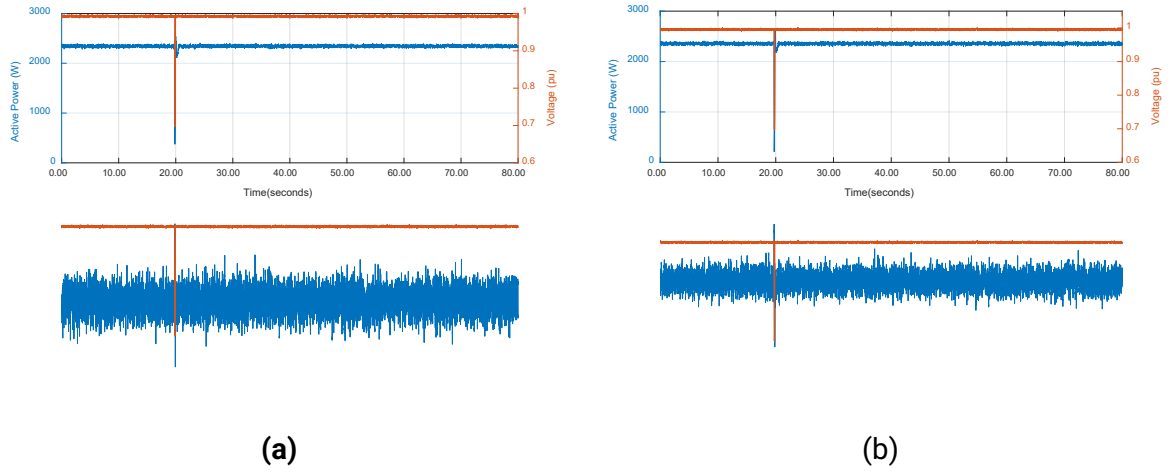

(a) (b)

Figure 5.10. Ride-through response of EV3 with Level 1 Charger for (a) 0.7 pu-80 ms sag and (b) 0.7 pu-120 ms sag

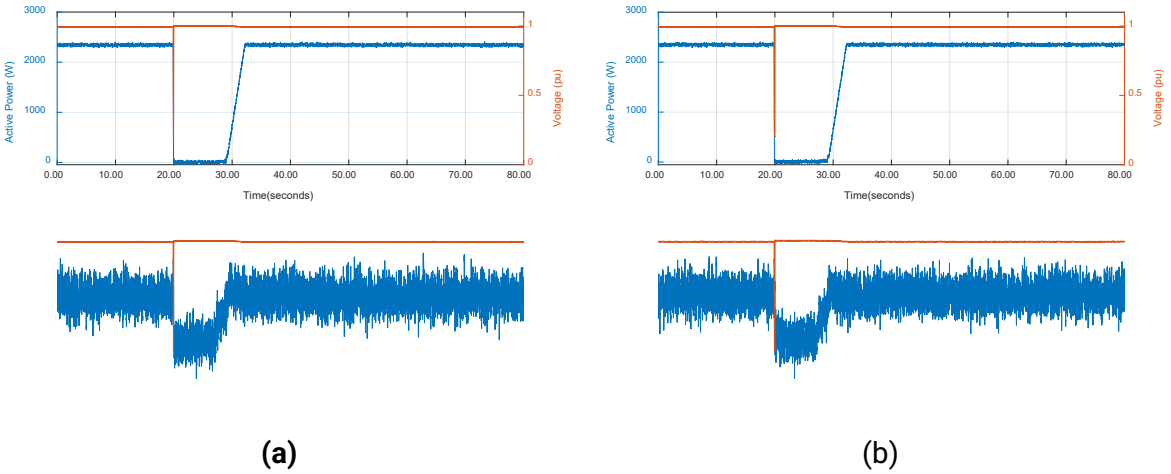

(a) (b)

Figure 5.11. Disconnection response of EV3 with Level 1 Charger for (a) 0.2 pu-80 ms sag and (b) 0.2 pu-120 ms sag

Table 5.7 summarises the test results for EV3 with the Level 1 charger. Overall, the vehicle demonstrated the ability to ride through deeper voltage sags at longer durations, suggesting a sensitivity to the sag time duration.

Table 5.7. Response of EV3 with Level 1 Charger

Duration (ms)	Sag Voltage (pu)						
	0.8	0.7	0.6	0.5	0.4	0.3	0.2
80	Ride Through	Ride Through	Ride Through	Disconnect for 10s	Disconnect for 10s	Disconnect for 10s	Disconnect for 10s
120	Ride Through	Ride Through	Ride Through	Ride Through	Ride Through	Disconnect for 10s	Disconnect for 10s

4.3.3.2. Level 2 Charger A

Similar to EV1 and EV2, EV3 also exhibited increased sensitivity to voltage sags when supplied using the Level 2 charger (7400 W). Under the 80-ms duration sag condition, the vehicle was only able to ride through at retained voltage of 0.8 pu, whereas for 120 ms, it successfully rides through sags with retained voltage of 0.6–0.8 pu. During the ride-through events, EV3 behaved similarly to its response with the Level 1 charger, showing limited power overshoot.

However, the disconnection response differed. Upon sag initiation, the vehicle immediately ceased charging, resulting in power consumption dropping to zero for approximately 10 s. The subsequent reconnection process lasted approximately 16 s and can be divided into three phases: in the first phase, power ramped up to half charging capacity (3700 W) within 5 s; the second phase involved a steady hold at this level for 6 s; and the third phase included a final increase to the full rated power (7400 W) within 5 s. This behaviour was consistently observed across all tests in which the EV disconnected. An example of disconnection response can be seen in Figure 5.12. The test results for EV3 with Level 2 Charger A is summarised in Table 5.8.

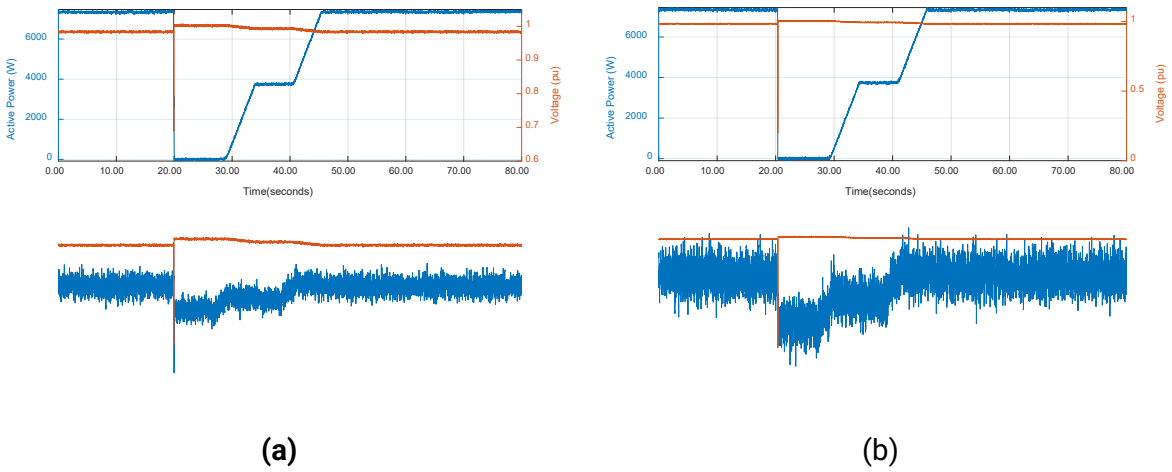

(a) (b)

Figure 5.12. Disconnection response of EV3 with Level 2 Charger B for (a) 0.7 pu-80 ms sag and (b) 0.2 pu-80 ms

Table 5.8. Response of EV3 with Level 2 Charger A

Duration (ms)	Sag Voltage (pu)						
	0.8	0.7	0.6	0.5	0.4	0.3	0.2
80	Ride Through	Disconnect for 10s	Disconnect for 10s	Disconnect for 10s	Disconnect for 10s	Disconnect for 10s	Disconnect for 10s
120	Ride Through	Ride Through	Ride Through	Disconnect for 10s	Disconnect for 10s	Disconnect for 10s	Disconnect for 10s

4.3.3.3. Level 2 Charger B

When charged with Charger B, EV3 operated at the same power level as for Level 2 Charger A and maintained a near-unity power factor. However, with Charger B, EV3 was only able to ride through voltage sags for 0.8 pu retained voltage for both 80 ms and 120 ms durations. In terms of disconnection and reconnection behaviour, inconsistencies were observed across the tests. In some instances, the disconnection response mirrored that recorded with Level 2 Charger A. However, several distinct responses were also identified and are outlined in Figure 5.13.

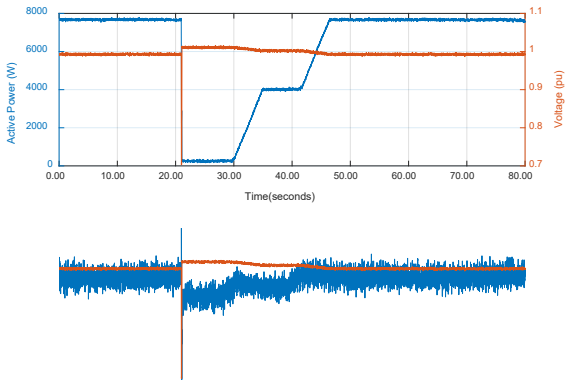
Active Power (W)
Voltage (pu)
Time(seconds)

(a)

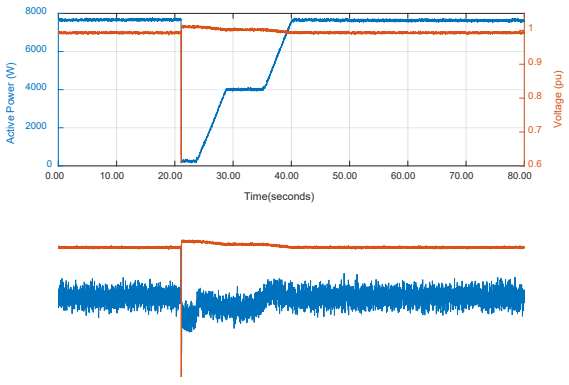
Active Power (W)
Voltage (pu)
Time(seconds)

(b)

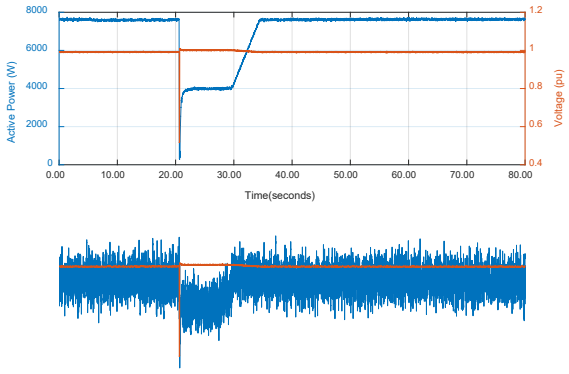
Active Power (W)
Voltage (pu)
Time(seconds)

(c)

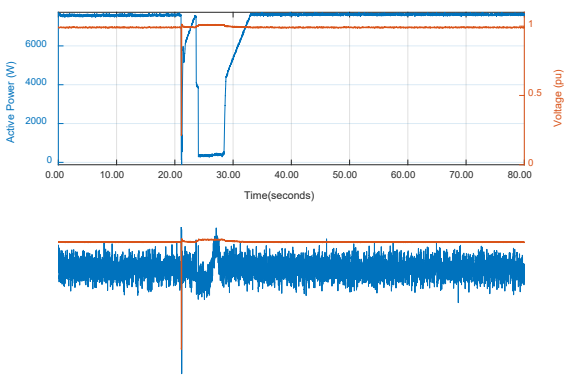
Active Power (W)
Voltage (pu)
Time(seconds)

(d)

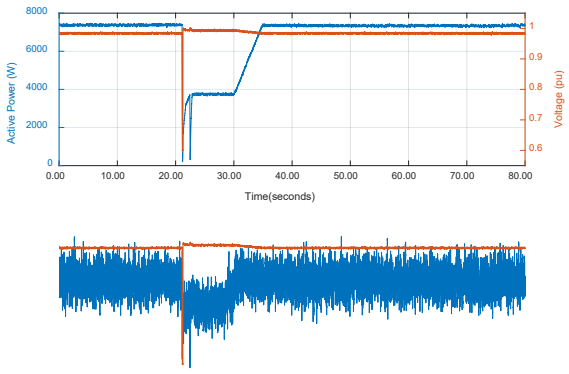
Active Power (W)
Voltage (pu)
Time(seconds)

(e)

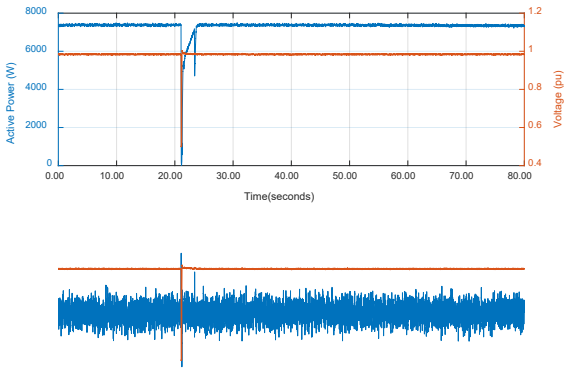
Active Power (W)
Voltage (pu)
Time(seconds)

(f)

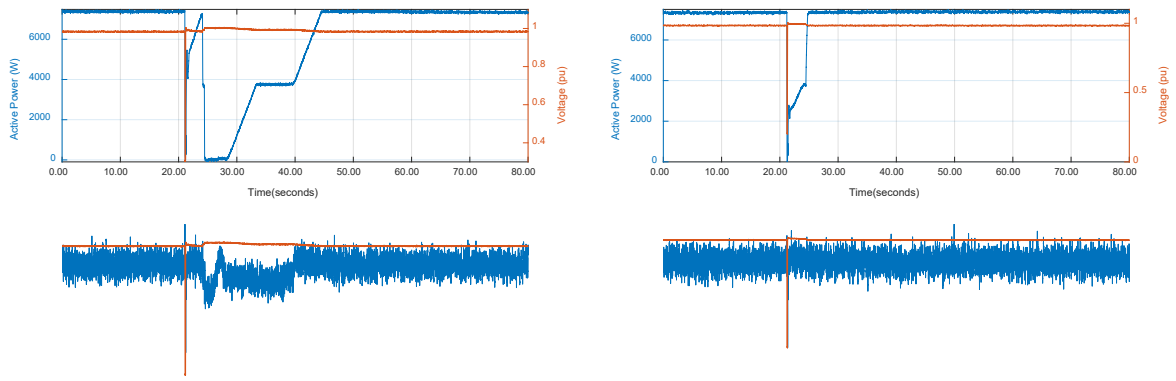

(g) (h)

Figure 5.13. Disconnection responses of EV3 with Charger B for (a) 0.7 pu-80 ms sag, (b) 0.6 pu-80 ms sag, (c) 0.5 pu-80 ms sag, (d) 0.2 pu- 80ms sag, (e) 0.6 pu-120 ms sag, (f) 0.5 pu-120 ms sag, (g) 0.3 pu-120 ms sag and (h) 0.2 pu-120 ms sag

Figure 5.13 (a) presents the reference response, characterised by a 10-s disconnection period followed by a multi-stage reconnection process: a 5-s ramp-up to half of the rated power, a 6-s stabilisation period, and a subsequent 5-s ramp-up to full power. In Figure 5.13 (b), the disconnection duration was reduced to approximately 3 s, while the reconnection behaviour remained consistent with the reference. Figure 5.13 (c) and (e) illustrate a different pattern, where the disconnection phase was replaced by a momentary cessation, followed by a sharp increase to half power, which was sustained for 10 s before full power restoration. In other cases, a brief cessation was followed by a rapid restoration to full rated power within 4 s. It is noted that these atypical behaviours were observed during the final series of tests, indicating that EV4 had undergone a prolonged charging period compared to earlier assessments. Table 5.9 summarises the test results for EV3 with Charger B.

Table 5.9. Response of EV3 with Level 2 Charger B

Duration (ms)	Sag Voltage (pu)						
	0.8	0.7	0.6	0.5	0.4	0.3	0.2
80	Ride Through	Disconnect for 10s	Disconnect for 10s	Disconnect (unusual)	Disconnect for 10s	Disconnect for 10s	Disconnect (unusual)
120	Ride Through	Disconnect for 10s	Disconnect (unusual)	Momentary cessation	Disconnect for 10s	Disconnect (unusual)	Momentary cessation

4.3.4. EV 4

4.3.4.1. Level 1

With Level 1 charging, EV4 drew 2100 W of active power and −100 VAr of reactive power. Notably, EV4 exhibited significant charging current ripple despite an undistorted supply voltage, which is may to suboptimal input filter capacitor sizing. This resulted in a high degree of fluctuation in power consumption. As shown in the test results, EV4 was unable to ride through voltage sags for 0.2 pu retained voltage and 80 ms duration and for sags with 0.2 to 0.3 pu retained voltage for 120 ms duration. During ride-through events, EV4 demonstrated pronounced power surges, with peak active power momentarily reaching up to 7000 W, as illustrated in Figure 5.14.

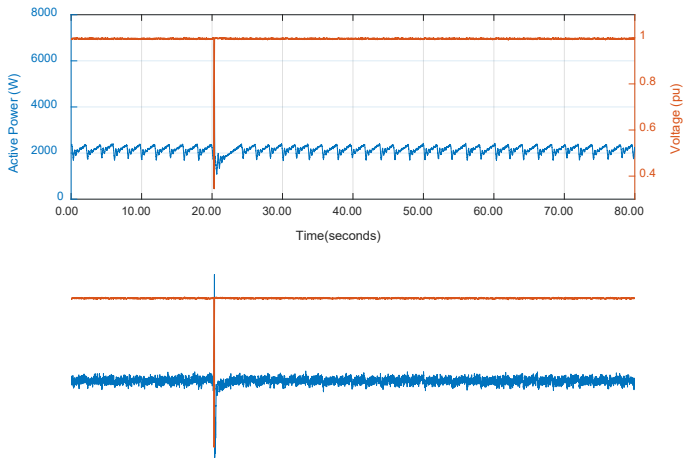

Figure 5.14. Ride-through response of EV4 with Level 1 Charger for 0.4 pu-80 ms sag

In terms of disconnection response, the charging process ceased for approximately 13 seconds and then resumed to full power within 8 seconds. As shown Figure 5.15, a transient event occurred near the 9-s mark during the disconnection phase, likely indicating a relay state change. The response of EV4 to voltage sag disturbances when charged at Level 1 is summarised in Table 5.10.

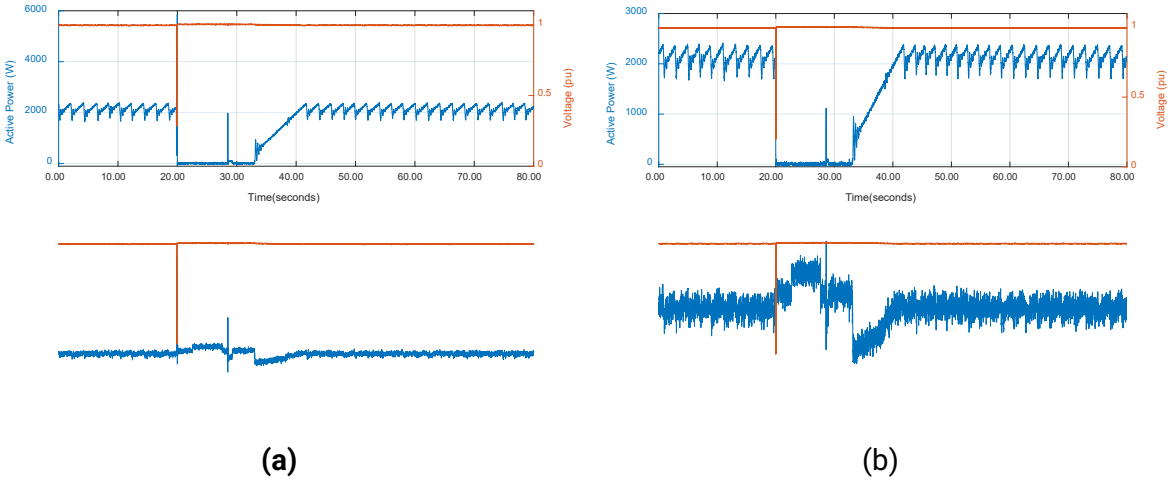

(a) (b)

Figure 5.15. Disconnection response of EV4 with Level 1 Charger for (a) 0.3 pu-120 ms sag and (b) 0.2 pu-120 ms sag

Table 5.10. Response of EV 4 with Level 1 Charger

Duration (ms)	Sag Voltage (pu)						
	0.8	0.7	0.6	0.5	0.4	0.3	0.2
80	Ride Through	Ride Through	Ride Through	Ride Through	Ride Through	Ride Through	Disconnect for 13s
120	Ride Through	Ride Through	Ride Through	Ride Through	Ride Through	Disconnect for 10s	Disconnect for 10s

4.3.4.2. Level 2 Charger A

Similar to the other vehicles, EV4 also disconnected for less extreme sag when supplied using the Level 2 Chargers, particularly for the retained voltage range of 0.2-0.7 pu. When riding through the sag disturbances, EV4 exhibited a significant power surge, reaching nearly 10,000 W, as shown in Figure 5.16. Disconnection behaviour was consistent across the tests. Examining Figure 5.17, the disconnection and reconnection times were recorded to be around 10 s and 30 s, respectively. Notably,

the reconnection phase followed a continuous, nearly linear slope throughout the 30 s. Similar to the Level 1 Charger results, a transient event was also witnessed during the disconnection phase, specifically at 5.5 s.

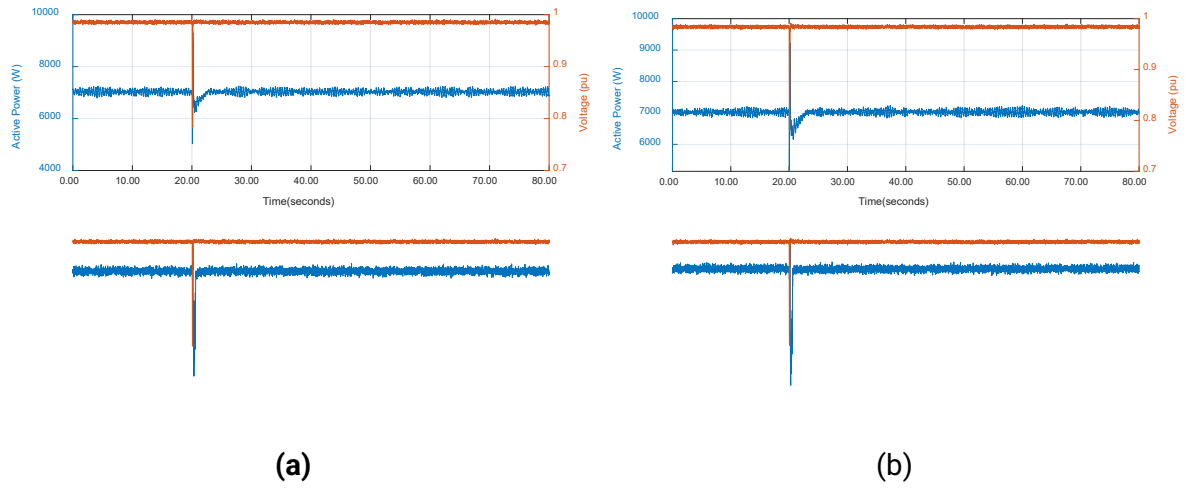

(a) (b)

Figure 5.16. Ride-through response of EV4 with Level 2 Charger B for (a) 0.8 pu-80 ms sag and (b) 0.8 pu-120 ms

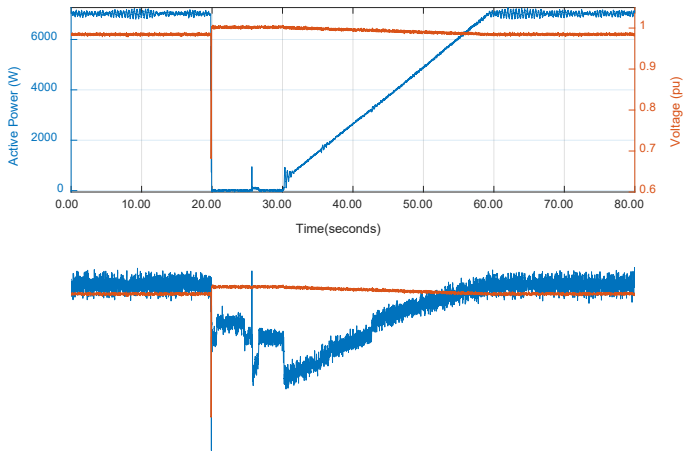

Figure 5.17. Disconnection response of EV4 with Level 2 Charger A for 0.7 pu-80 ms sag

Table 5.11. Response of EV 4 with Level 1 Charger A

Duration (ms)	Sag Voltage (pu)						
	0.8	0.7	0.6	0.5	0.4	0.3	0.2
80	Ride Through	Disconnect for 10-11s	Disconnect for 10-11s	Disconnect for 10-11s	Disconnect for 10-11s	Disconnect for 10-11s	Disconnect for 10-11s
120	Ride Through	Disconnect for 10-11s	Disconnect for 10-11s	Disconnect for 10-11s	Disconnect for 10-11s	Disconnect for 10-11s	Disconnect for 10-11s

4.3.4.3. Level 2 Charger B

When supplied using Level 2 Charger B, EV4 exhibited identical ride-through and disconnection behaviours to those observed with Level 2 Charger A, as presented in Figure 5.18 and Table 5.12.

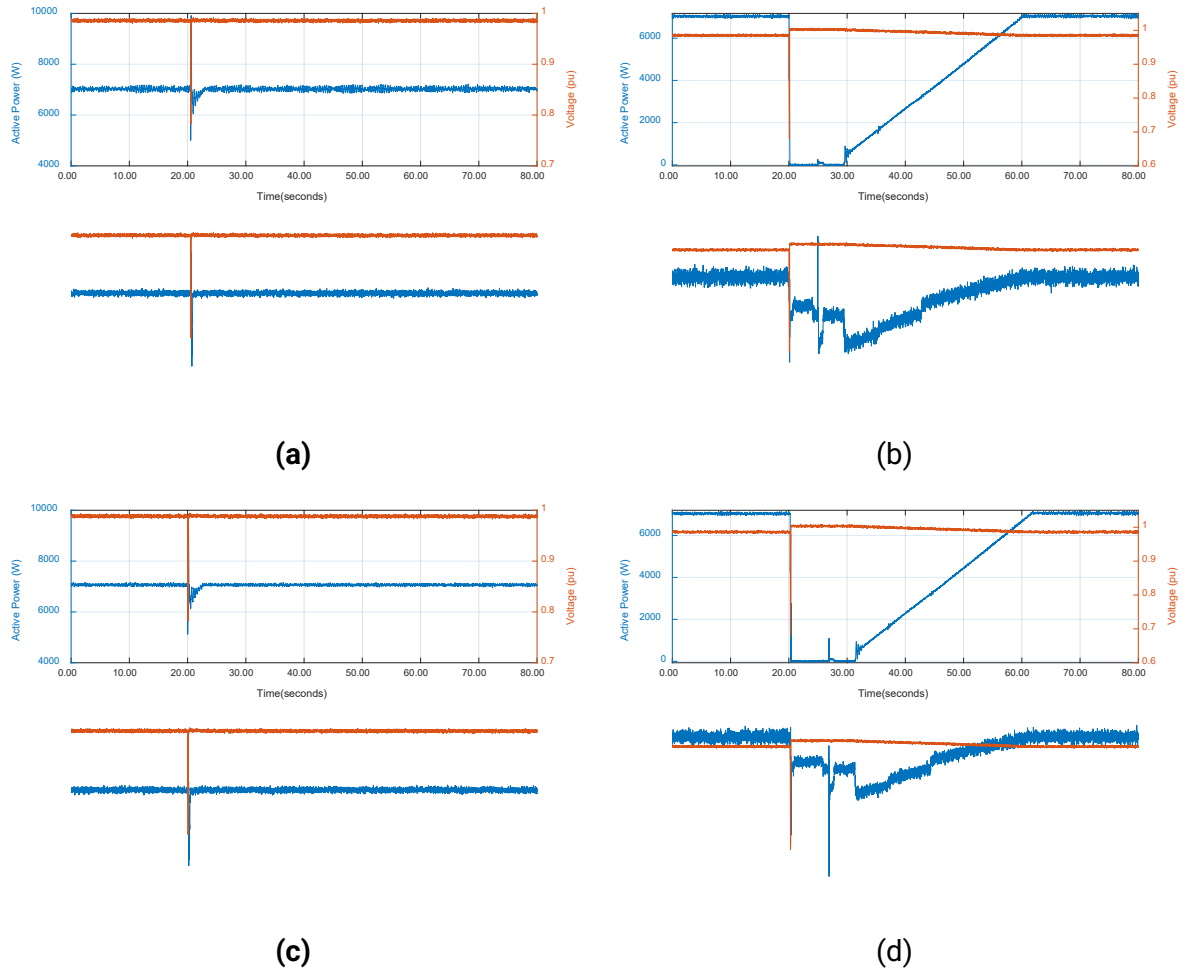

Figure 5.18. Response of EV4 with Level 2 Charger B for (a) 0.8 pu-80 ms sag, (b) 0.7 pu-80 ms sag, (c) 0.8 pu-120 ms sag and (d) 0.7 pu-120 ms sag

Table 5.12. Response of EV 4 with Level 1 Charger B

Duration (ms)	Sag Voltage (pu)						
	0.8	0.7	0.6	0.5	0.4	0.3	0.2
80	Ride Through	Disconnect for 10-11s	Disconnect for 10-11s	Disconnect for 10-11s	Disconnect for 10-11s	Disconnect for 10-11s	Disconnect for 10-11s
120	Ride Through	Disconnect for 10-11s	Disconnect for 10-11s	Disconnect for 10-11s	Disconnect for 10-11s	Disconnect for 10-11s	Disconnect for 10-11s

4.4. Summary and Next Steps

The EV test results can be summarised as follows:

- Disconnection and reconnection behaviour varied across the EVs, even when charged using identical chargers.
- Following disconnection, EV1 and EV2 demonstrated abrupt power restoration, whereas EV3 and EV4 ramped gradually to full power.
- For Level 2 charging, EVs typically disconnected at sag depths of 0.6–0.7 pu retained voltage. In contrast, for the Level 1 charger disconnection thresholds were less consistent and harder to determine.
- Level 2 charging is more sensitive to sag depth than Level 1 charging.
- The tested EVs are more likely to ride through 120-ms duration sags than 80-ms ones, indicating timing-sensitive operation of the installed relays. However, further testing is necessary to verify whether this trend is consistent across other EV.

Next steps should consider investigating vehicles with V2G capability enabled through bi-directional power converters, with a focus on the interaction and communication protocols between the EVSE and the EV under disturbed conditions.

5. EV Modelling

5.1. Introduction

The surge in popularity of EVs has sparked concerns regarding the necessary network adaptations required to accommodate a potential substantial increase in load. The current complex load model lacks an embedded EV load model, and the authors have identified only limited research related to modelling of the dynamic response of EV chargers in the presence of grid faults, with only a small number of references directly addressing this topic [1], [25][27]]. In [27], the authors propose an RMS EV model based on sag disturbances, tested using a power system laboratory simulator. However, this study only examines the Level 1 charger response of a single EV and focuses solely on sags, neglecting other types of disturbances. Reference [26] expands the test set to include responses from onboard Level 1 chargers of four EVs, analysing the frequency response of TasNetwork's Real-Time simulator model. However, the study does not cover the diverse responses of various EV OEMs in the Australian market, and it overlooks responses to different charging levels (Level 2). In [1], EPRI presents an aggregated model based on [25], developed from the sag response of six different EV chargers. However, this model has limitations, as it does not include other types of disturbances and does not incorporate the time variable aspect of disconnections at different sag depths.

5.1. Experimental Aggregated Response of EVs

To date, the EVs evaluated are the Nissan Leaf, BYD, Tesla Model 3, GWM Ora, Hyundai Kona, Tesla Model Y, and Peugeot E-Partner. These EVs are anonymously as referred to in this report as EV1 through EV7. The anonymisation of this section is different to the names used in the previous section of the report and includes results from Stage 3 testing. The response of these EVs to voltage sags has been evaluated using both Level 1 and Level 2 chargers to support the development of an aggregated EV response model. The aim is for the resulting model to serve as a functional block diagram that can be incorporated into the CMPLD framework. At this stage, the analysis focusses on active power responses, capturing the disconnection and reconnection behaviour during voltage sag disturbances. While sag tests covered a retained voltage range from 0.2 to 0.8 pu, the selected sag voltages for detailed analysis were 0.8, 0.5, and 0.2 pu with duration of 80 ms, representing shallow, moderate, and severe conditions, respectively. Based on the laboratory evaluation data, the critical sag thresholds at which the charging processes were interrupted are summarised in Table 6.1.

Table 6.1. Critical sag depths causing EV charging disconnection

EV Models		EV1	EV2	EV3	EV4	EV5	EV6	EV7
Disconnection Voltage – Lv1	80ms	0.2	0.4	0.5	0.2	0.3	0.7	0.6
	120ms	0.2	0.5	0.3	0.3	0.5	0.8	0.6
Disconnection Voltage – Lv2	80ms	0.6	0.7	0.7	0.7	X*	0.7	0.8
	120ms	0.6	0.7	0.6	0.7	X*	0.7	0.8

**Did not disconnect*

5.1.1. Level 1 Charger

Figure 6.1 depicts responses of the EVs, supplied using the level 1 charger, when exposed to voltage sag of 0.8 pu retained voltage for 80 ms. As can be seen, none of the EVs disconnected when subjected to this voltage sag, and all exhibited momentary power surge and cessation when riding through the disturbances.

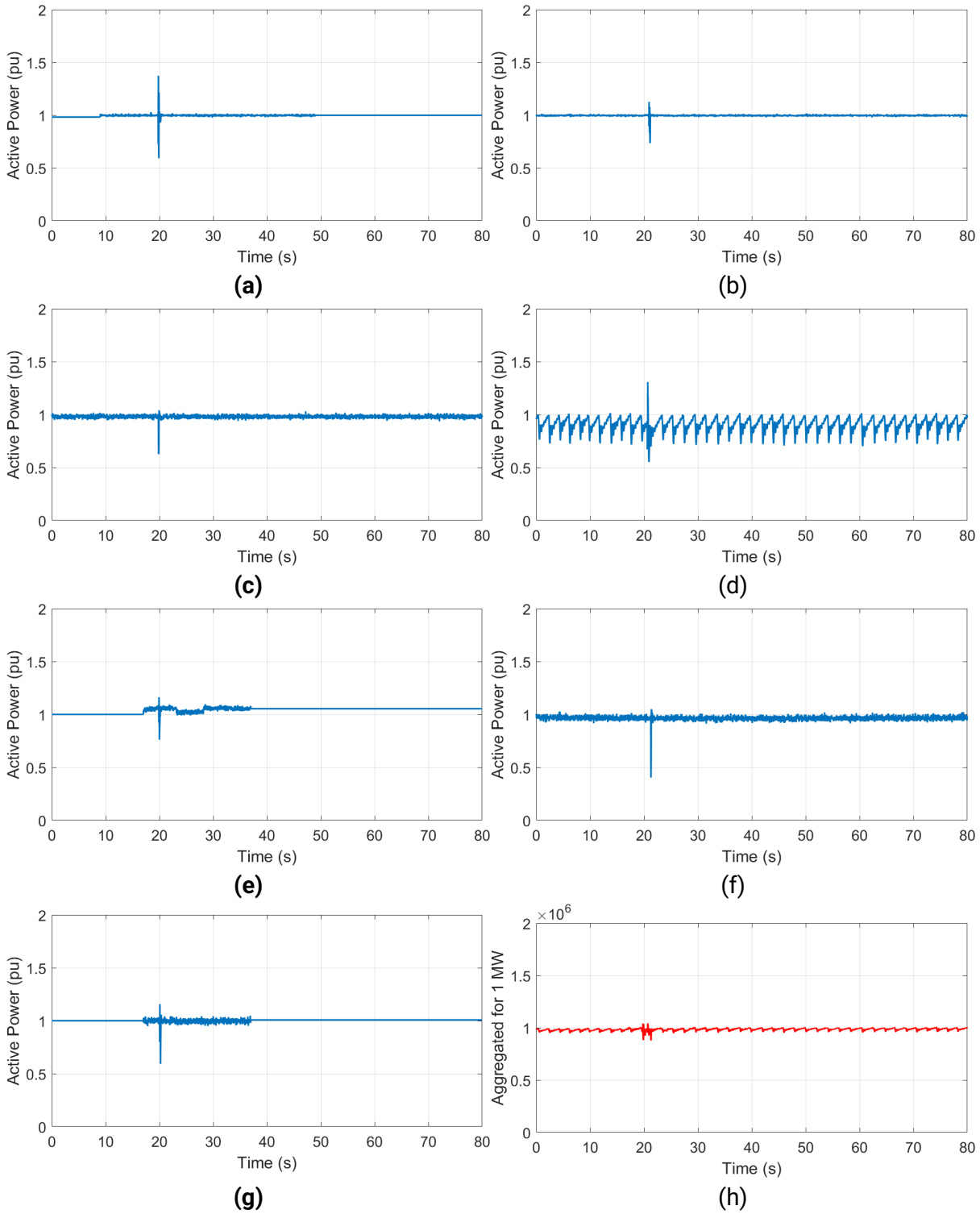

Figure 6.1. Responses of EVs with Level 1 Charger when exposed to voltage sag of 0.8 pu retained voltage and 80 ms duration (a) EV1, (b) EV2, (c) EV3, (d) EV4, (e) EV5, (f) EV6, (g) EV7, (h) Aggregated for 1 MW Load

For a retained voltage of 0.5 pu, as shown in Figure 6.2, three out of seven vehicles experienced charging disconnection. Two main disconnection behaviours were observed; the first involved a short disconnection duration of approximately 3 s followed by a rapid restoration; the second, as seen in the response of EV3 and EV6, featured a longer disconnection of nearly 10 s, with a swift ramp-up to full power within 2 s. The other vehicles all exhibited a transient when riding through the disturbance.

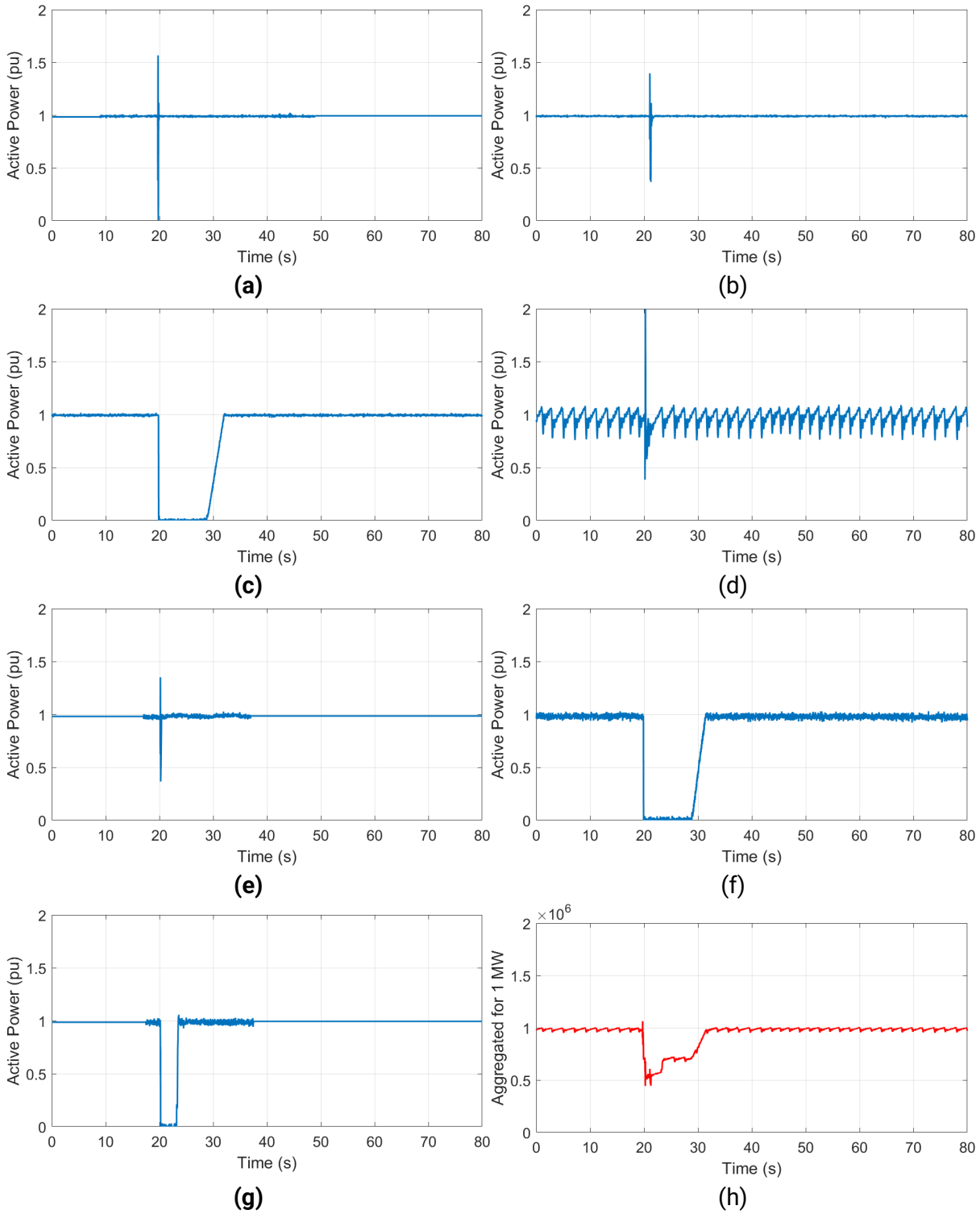

Figure 6.2. Responses of EVs with Level 1 Charger when exposed to voltage sag of 0.5 pu retained voltage and 80 ms duration (a) EV1, (b) EV2, (c) EV3, (d) EV4, (e) EV5, (f) EV6, (g) EV7, (h) Aggregated for 1 MW Load

At a retained voltage of 0.2 pu, all EVs disconnected from charging, as shown Figure 6.3, though their responses varied. These behaviours can be broadly categorised into several groups. EV1 and EV7 experienced short disconnection durations of 3–4 s, followed by immediate reconnection. EV2 also reconnected rapidly; however, its disconnection phase lasted for approximately 10 s. EV3, EV5, and EV6 displayed similar patterns, each disconnecting for 10 s and then ramping up to full power over a period of 2–3 s. EV4, on the other hand, exhibited a distinct response, with a 13-s disconnection followed by an 8-s ramp-up phase. Notably, while overshoot was observed in some disconnection responses, it is not a primary concern at this stage, given its limited impact on system stability analysis.

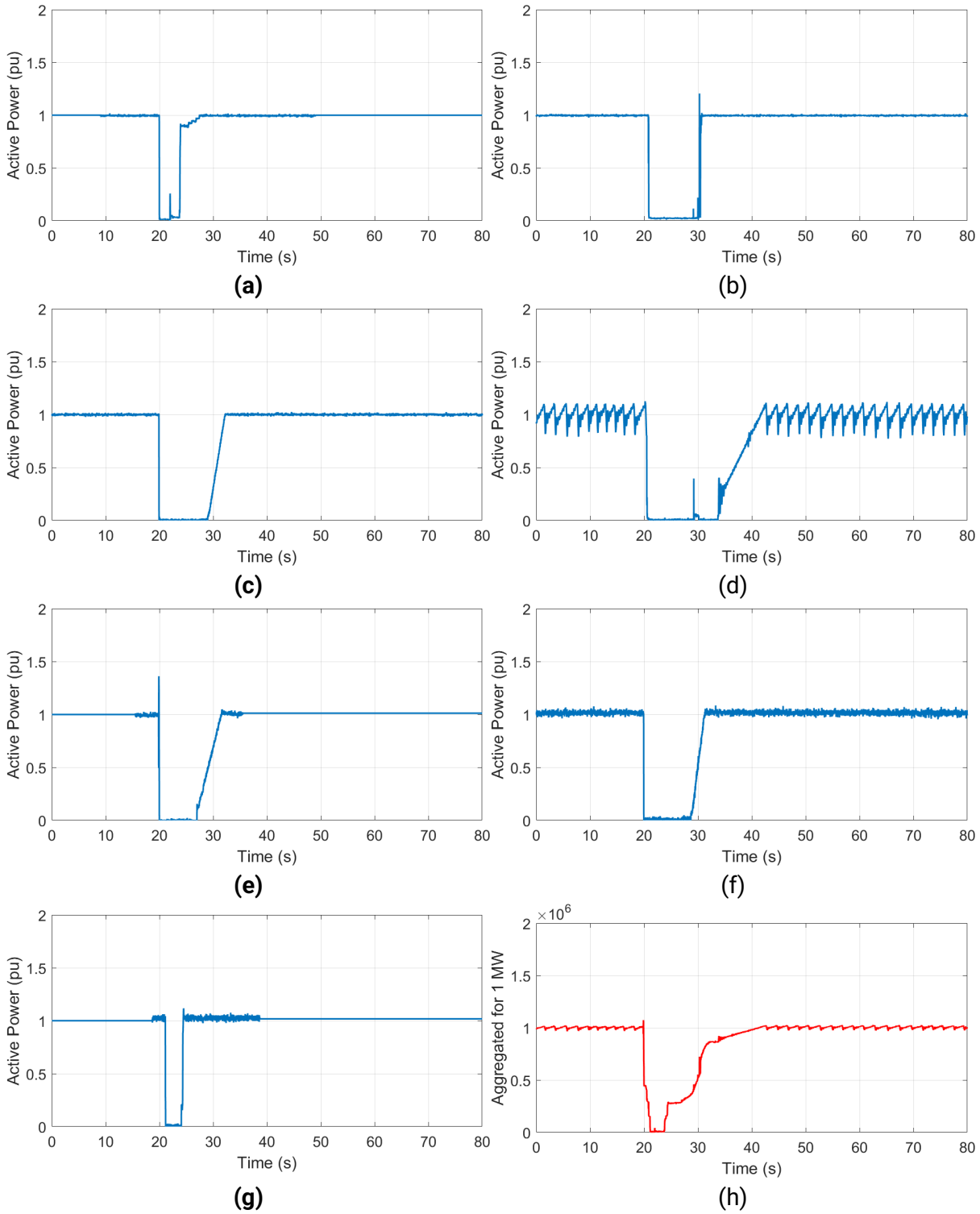

Figure 6.3. Responses of EVs with Level 1 Charger when exposed to voltage sag of 0.2 pu retained voltage and 80 ms duration (a) EV1, (b) EV2, (c) EV3, (d) EV4, (e) EV5, (f) EV6, (g) EV7, (h) Aggregated for 1 MW Load

5.1.2. Level 2 Charger

Figure 6.4 illustrates the responses of the tested EVs to a 0.8 pu voltage sag when supplied using the level 2 charger. All EVs were able to ride through the disturbance, except for EV7, which disconnected for approximately 3 s before quickly resuming charging. EV3 and EV6 experienced a noticeable momentary dip in power consumption, though it did not fully drop to zero.

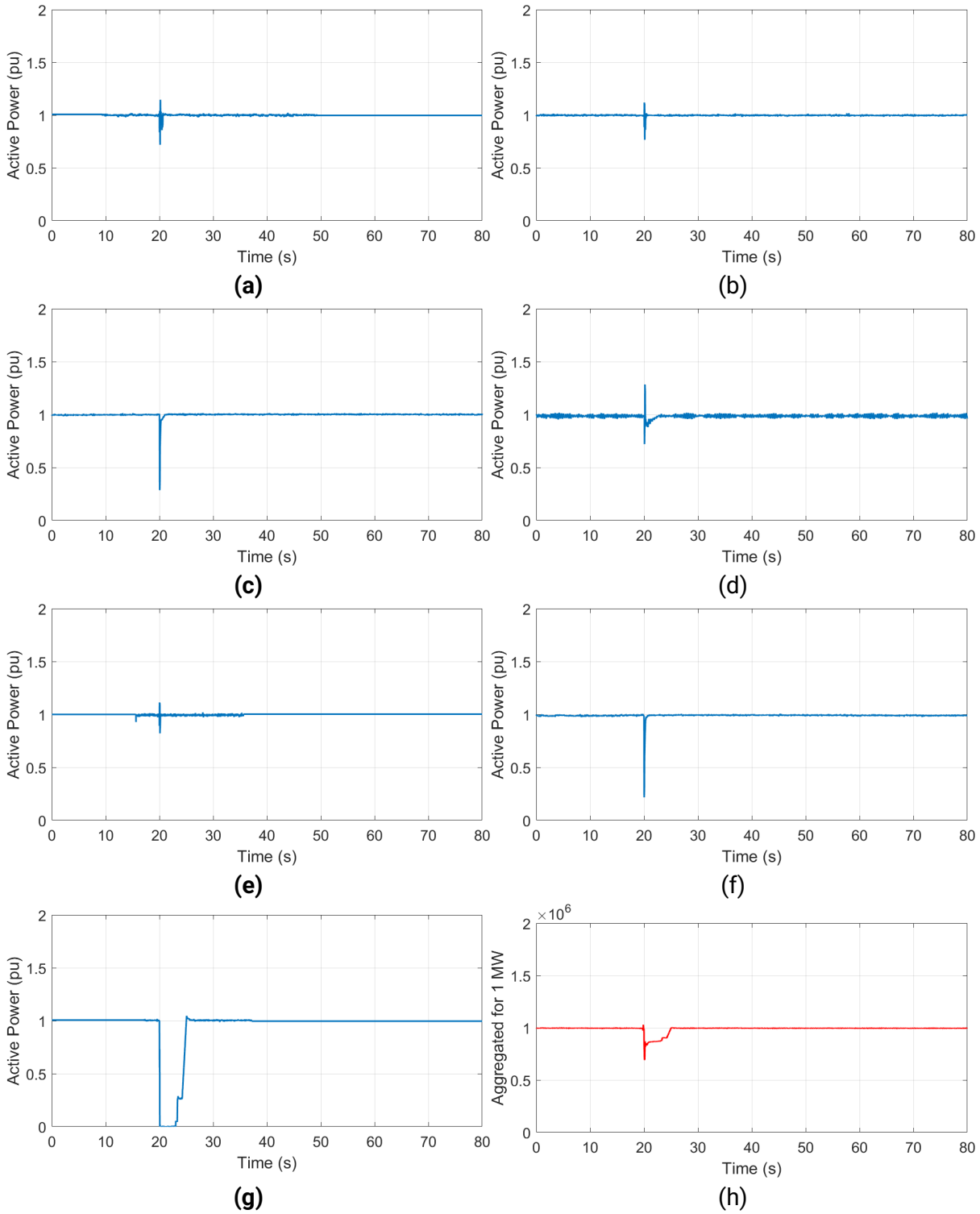

Figure 6.4. Responses of EVs with Level 2 Charger when exposed to voltage sag of 0.8 pu retained voltage and 80 ms duration (a) EV1, (b) EV2, (c) EV3, (d) EV4, (e) EV5, (f) EV6, (g) EV7, (h) Aggregated for 1 MW Load

When subjected to a 0.5 pu retained voltage sag using level 2 charging, most EVs disconnected, apart from EV5, which successfully rode through the event but exhibited a notable power overshoot as described in Figure 6.5. EV1, EV2, and EV7 demonstrated similar responses, characterised by moderate disconnection durations of 3–5 s followed by rapid reconnection. Both EV4 and EV6 experienced longer disconnection phases of around 10 s; however, EV4 took nearly 30 s to fully recover, while EV6 resumed charging in 15 s with a distinct step change in power. EV3 displayed an atypical response, which will be discussed in more detail in the subsequent analysis of the 0.2 pu retained voltage sag condition.

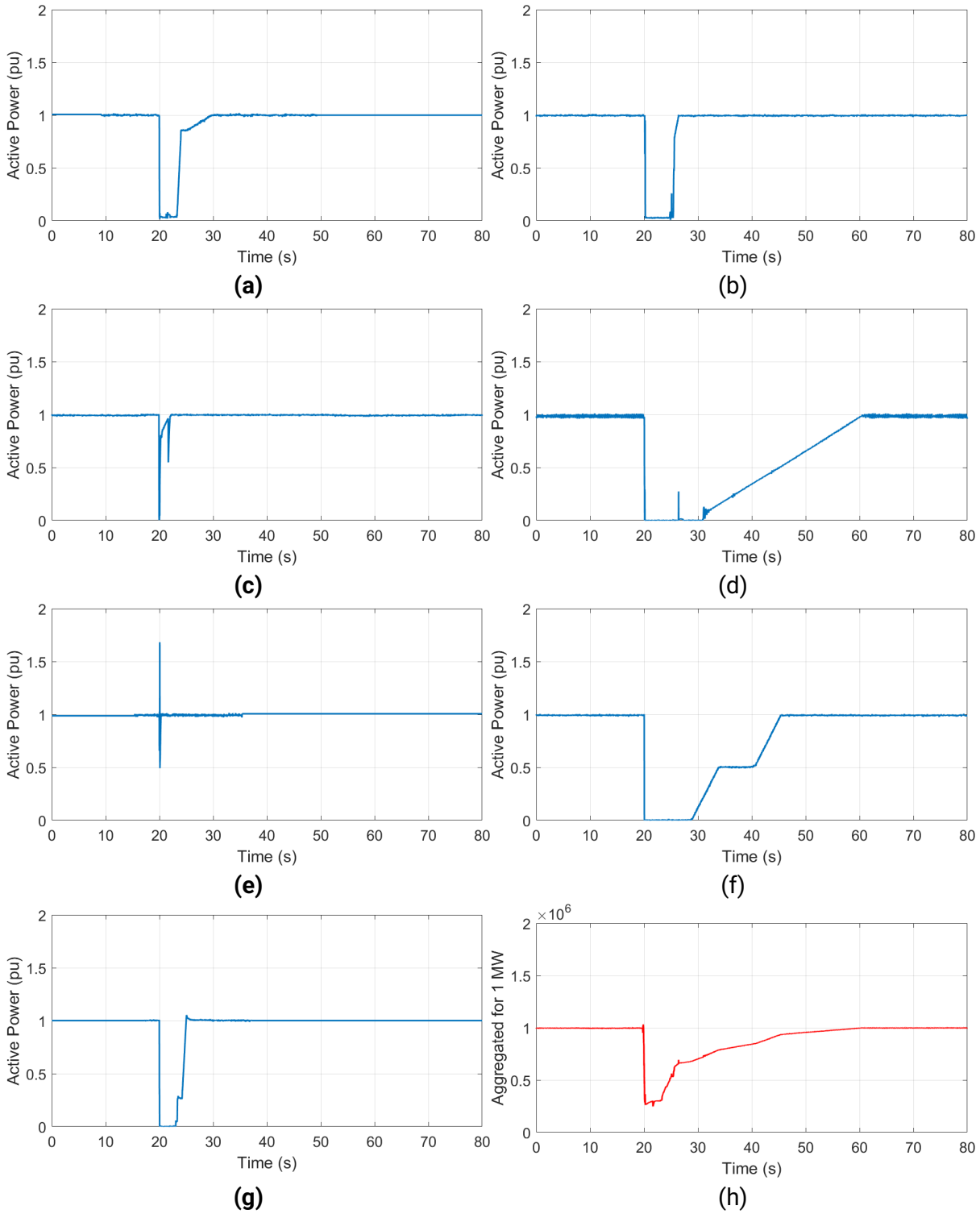

Figure 6.5. Responses of EVs with Level 2 Charger when exposed to voltage sag of 0.5 pu retained voltage and 80 ms duration (a) EV1, (b) EV2, (c) EV3, (d) EV4, (e) EV5, (f) EV6, (g) EV7, (h) Aggregated for 1 MW Load

Consistent with the previous evaluation for a 0.5 pu retained voltage sag, the charging process was interrupted in most EVs when subjected to a 0.2 pu retained voltage sag, with the exception of EV7, which exhibited similar behaviour to its earlier response, as depicted in Figure 6.6. Notably, several inconsistencies were observed. EV2 displayed a significantly prolonged disconnection duration of 40 s, in contrast to the 5 s observed previously. EV1 and EV7 continued to exhibit comparable responses, allowing them to be classified within the same behavioural category. EV3 and EV6 demonstrated identical reconnection patterns, characterised by step changes in power.

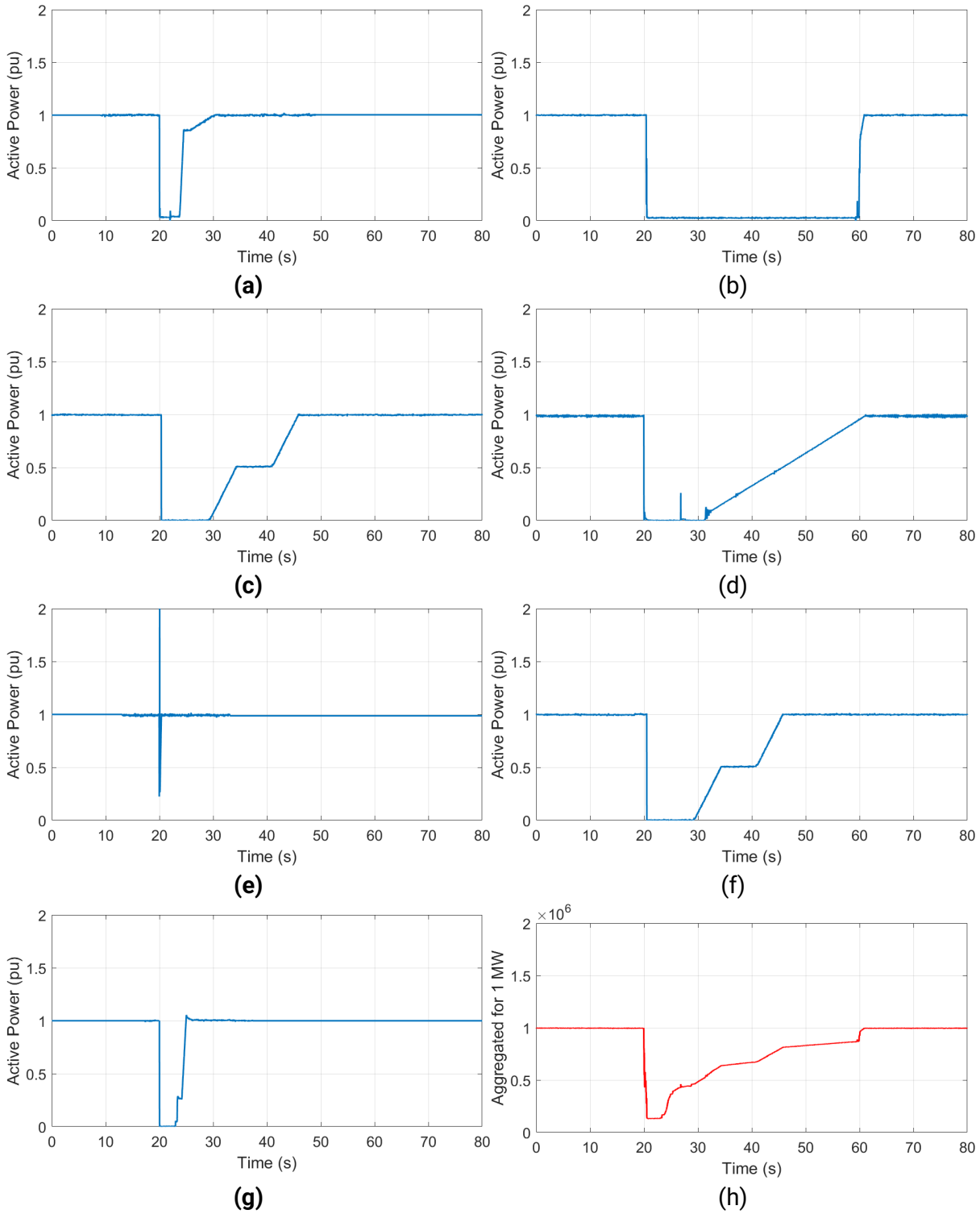

Figure 6.6. Responses of EVs with Level 2 Charger when exposed to voltage sag of 0.2 pu retained voltage and 80 ms duration (a) EV1, (b) EV2, (c) EV3, (d) EV4, (e) EV5, (f) EV6, (g) EV7, (h) Aggregated for 1 MW Load

5.2. Analysis and Proposed EV Model

The individual responses of each EV were presented alongside their aggregated response corresponding to a 1 MW load in Section 6.1. However, the aggregated response was constructed under the assumption of equal contribution from each EV, which does not reflect market reality given the varying levels of vehicle popularity. More critically, incorporating each individual response into the aggregated model is not an efficient approach, as it introduces unnecessary complexity and hampers scalability, particularly when accommodating future test results. Therefore, generalisation of the observed behaviours from the

tested EVs is essential to streamline the modelling process while maintaining representativeness and adaptability. However, at the present stage of the project, the primary focus is placed on disconnection and reconnection behaviour, while the assessment of ride-through characteristics has been deferred to future phases of the study. Hence, the generalisation process for the collected responses is limited to scenarios involving disconnection events only.

Figure 6.7 describes the block diagram used for dynamic EV charging load modelling. This block diagram outputs the generalised responses described in Section 6.2.1 and 6.2.2. The voltage magnitude V_t is measured at each time step and passed through a washout block to make sure only dynamic changes affect the control loop. The second block is a lead lag compensator to adjust the transient response of the model. Current limiters are included to ensure that the current drawn does not exceed a specified value. The control logic is deployed to replicate the disconnection and reconnection behaviour of the EV in response to the voltage sag disturbance, which is described in detail in Figure 6.7. Finally, the last transfer function is to ensure the numerical stability of the model, with T_{num} calculated based on the simulation time step.

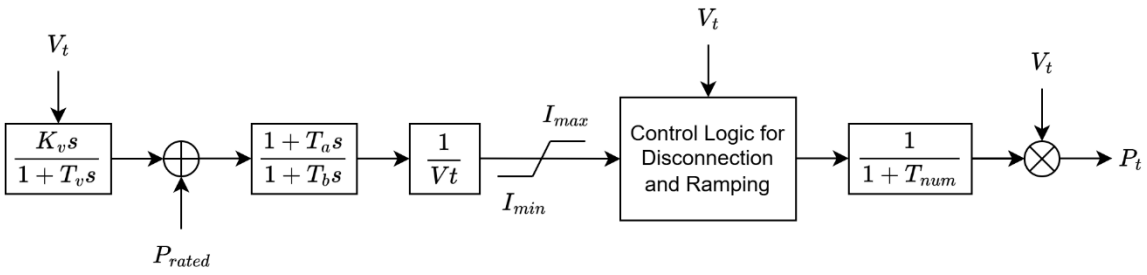

Figure 6.7. Block diagram for dynamic EV modelling

Figure 6.8 illustrates the control logic used in the EV modelling. The control block consists of nine inputs and produces a single output based on the input values. Among these inputs, only two are time series variables: *input_current* and *rms_voltage*, while the remaining inputs are set values that determine the output response. *V_threshold* and *T_threshold* are key parameters that define the critical voltage sag depth and duration at which the EV charging process is interrupted. It is important to note that the proposed control logic effectively models EVs exhibiting multi-stage reconnection behaviour. For EVs that reconnect by transitioning directly from zero power to full rated power, the stable phase can be omitted by setting *stable_time* to zero. In such cases, both *ramp_time1* and *ramp_time2* are defined as half of the total reconnection time, ensuring the model accurately reflects this simplified reconnection process. More importantly, multiple critical sag depth thresholds (*V_threshold, V_threshold1, V_threshold2*) are introduced for groups comprising various EVs that disconnected at different sag depths, particularly under Level 1 charging conditions. For example, the Level 1-Type 1 response was primarily derived from EV3, EV5, and EV6, which disconnected at voltage sag of 0.5, 0.3, and 0.7 pu retained for 80 ms duration, respectively.

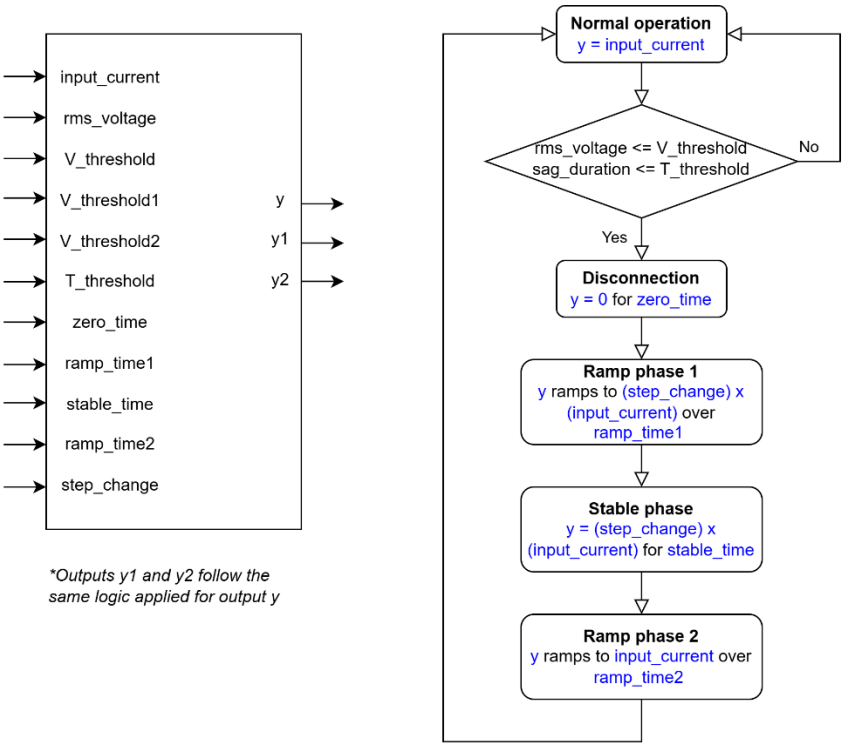

Figure 6.8. Employed control logic state diagram for dynamic EV modelling

5.2.1. Generalised Responses with Level 1 Charger

Figure 6.9 presents the generalised responses of the evaluated EVs for a voltage sag initiated at 20 s. The seven individual responses have been categorised into four representative profiles based on similarity, thereby characterising Level 1 charging behaviour. Response (a) reflects the behaviour of EV3, EV5, and EV6, all of which experienced a moderate disconnection duration of approximately 9 s, followed by a 2.5 s ramp-up to full power. Response (b), representing EV4, is distinguished by the longest disconnection period of 13 s, with a gradual recovery over the subsequent 8 s. Response (c) resembles response (a), but differs in that the power is restored abruptly rather than progressively. Finally, response (d), which characterises EV1 and EV7, exhibits a brief disconnection lasting only 3 s, with immediate reconnection to full power.

In summary, four types of Level 1 EV charging responses have been obtained as follows:

- **Type 1**: Moderate disconnection duration of approximately 10 s, followed by a short reconnection period of 2–3 s.
- **Type 2**: Extended disconnection duration exceeding 10 s, with a long reconnection period of approximately 8 s.
- **Type 3**: Moderate disconnection duration of approximately 10 s, followed by immediate reconnection in less than 1 s.
- **Type 4**: Very short disconnection duration of approximately 3 s, followed by immediate reconnection in less than 1 s.

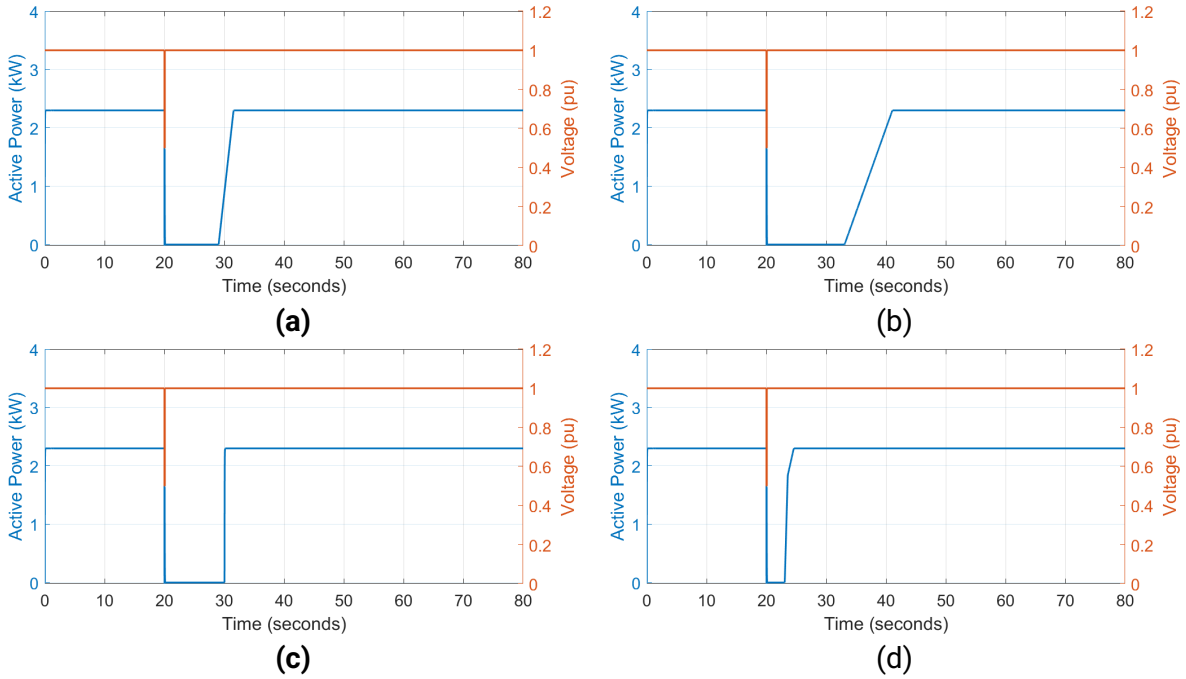

Figure 6.9. Generalised responses with Level 1 Charger for (a) Type 1—EV3, EV5, and EV6, (b) Type 2—EV4, (c) Type 3—EV2, (d) Type 4—EV1 and EV7

5.2.2. Generalised Responses with Level 2 Charger

For Level 2 charging, EV5 did not disconnect under any test condition. Figure 6.10 (a) presents the characteristic response of EV3 and EV6, which is distinguished by a step increase to half-rated power during the reconnection phase. Response (b) resembles that observed during Level 1 charging; however, the reconnection duration exceeds 25 s. Based on statistical patterns, responses (c) and (d) were derived for EV2, which typically experienced a disconnection duration of 6 s under most conditions, extending to 30–40 s in the presence of more severe voltage sags. EV1 and EV7 exhibited behaviour consistent with their Level 1 charging responses, marked by brief disconnections and rapid restoration.

In summary, six types of Level 2 EV charging responses are obtained as follows:

- **Type 1**: Moderate disconnection duration of approximately 10 s, followed by a multi-stage reconnection process with a total reconnection time of around 15 s.
- **Type 2**: Extended disconnection duration exceeding 10 s, with a long reconnection period of approximately 30 s.
- **Type 3.1**: Short disconnection duration of approximately 6 s, with immediate reconnection occurring in less than 1 s.
- **Type 3.2**: Very long disconnection duration exceeding 30 s, followed by immediate reconnection within less than 1 s. *Note: This type is associated with the same EV as Type 3.1 but arises under more severe sag conditions.*
- **Type 4**: Very short disconnection duration of approximately 3 s, with immediate reconnection in less than 1 s.
- **Type 5**: Not disconnected for any assessed sag depth.

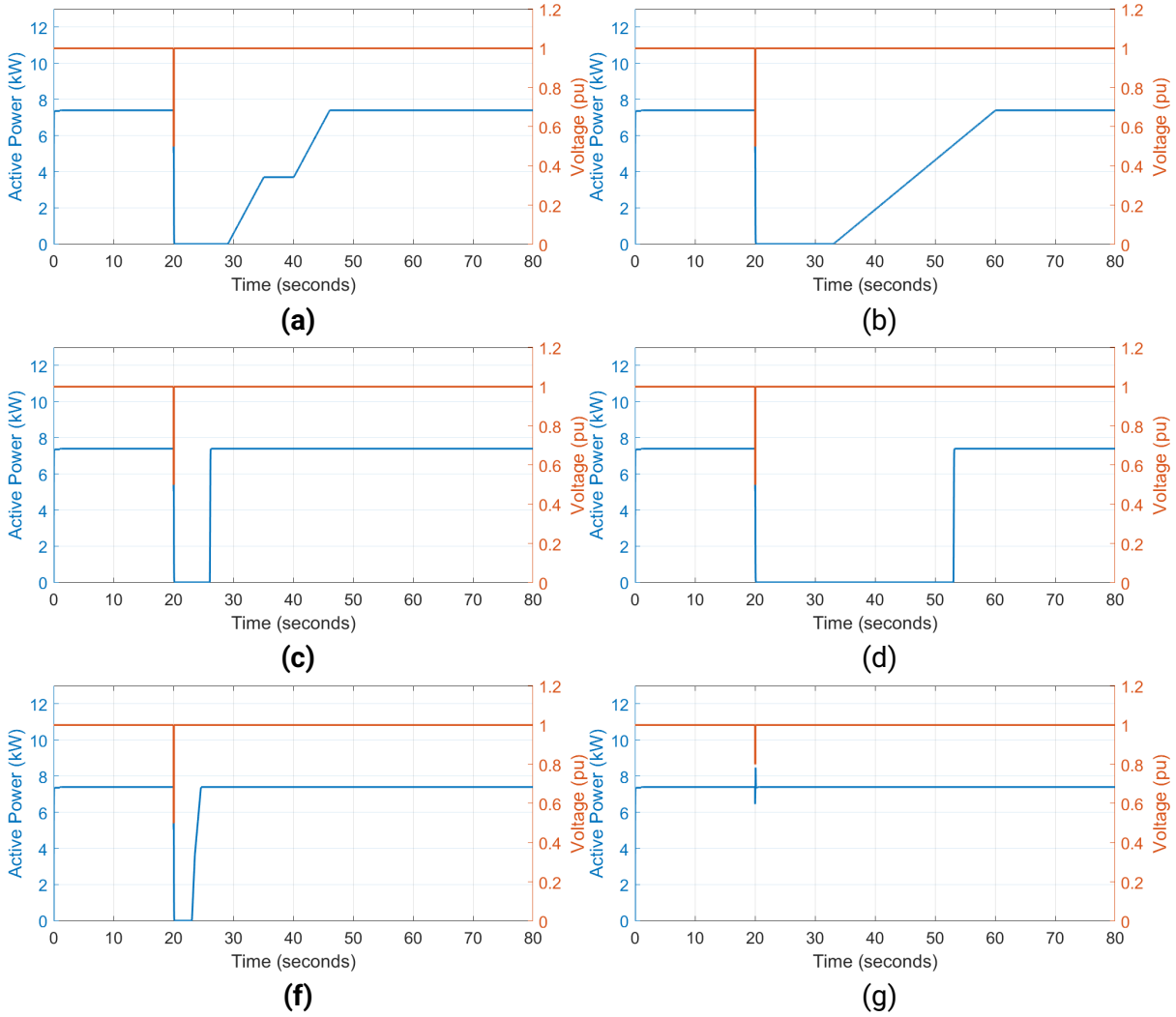

Figure 6.10. Generalised responses with Level 2 Charger for (a) Type 1—EV3 and EV6, (b) Type 2—EV4, (c) Type 3.1—EV2-short disconnection, (d) Type 3.2—EV2-long disconnection, (f) Type 4—EV1 and EV7, (g) Type 5—EV5

5.2.3. Proposed Aggregated EV Model

The EPRI-recommended EV model depicted in Figure 6.11 has been implemented in MATLAB Simulink, with an initial focus on replicating the active power responses of EVs. This model classifies EV behaviour into four main categories based on performance during voltage sag events and subsequent reconnection characteristics. However, the categorisation proposed by EPRI does not fully capture the diverse behaviour observed in this study, particularly the multi-stage ramp-up reconnection patterns identified. Therefore, the generalised responses derived with improved control logic from the EVs tested to date will be utilised for developing an aggregated response. The primary objective of this work is to refine and extend the recommended model by developing a detailed dynamic response framework, enabling its integration into the composite load model for more comprehensive and accurate dynamic load analysis.

Each generalised response corresponds to distinct critical sag depths that trigger disconnection. These values are calculated and summarised in Table 6.2.The fractional distribution of each response type is determined by the proportion of vehicles grouped into each category relative to the total number of vehicles tested.

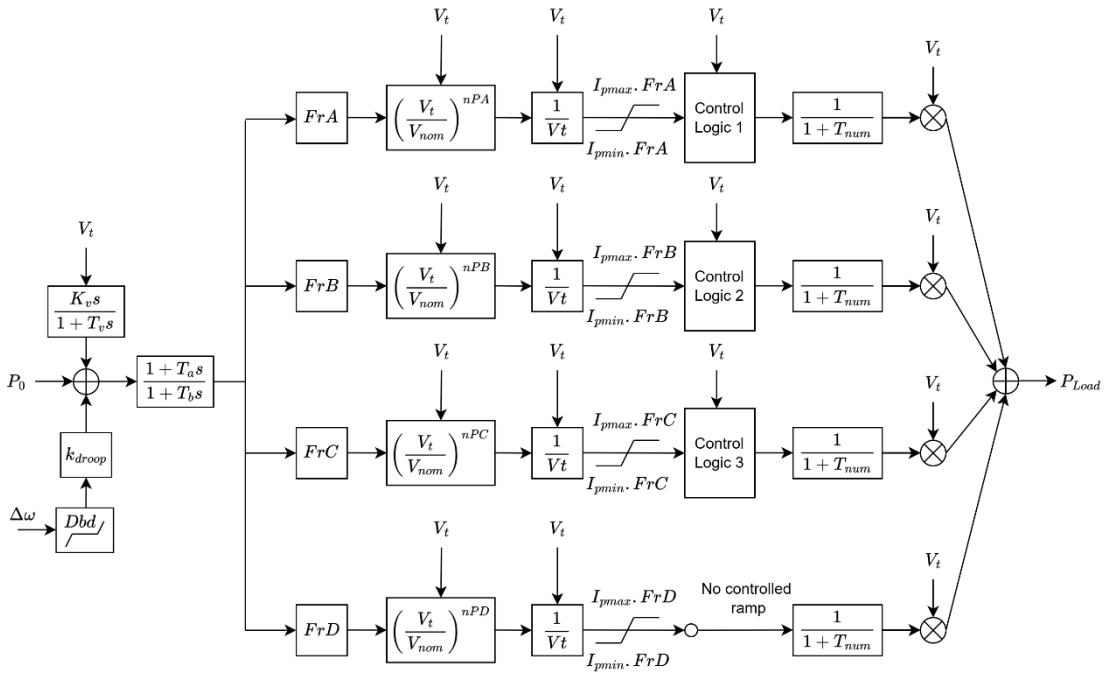

Figure 6.11. EPRI proposed EV model

Table 6.2. Critical sag depths and fraction values for generalised EV responses

Generalised Response		Critical Sag Depth *V_threshold* for 80 ms	Critical Sag Depth *V_threshold* for 120 ms	Fraction in the Aggregated Model
Level 1 Charging	Type 1	0.5/0.3/0.7	0.3/0.5/0.8	3/7
	Type 2	0.2	0.3	1/7
	Type 3	0.4	0.5	1/7
	Type 4	0.2/0.6	0.2/0.6	2/7
Level 2 Charging	Type 1	0.7/0.7	0.6/0.7	2/7
	Type 2	0.7	0.7	1/7
	Type 3.1	0.7	0.7	1/7
	Type 3.2	0.2	0.2	
	Type 4	0.6/0.8	0.6/0.8	2/7
	Type 5	0	0	1/7

Figure 6.12 presents the response of the aggregated EV load model for voltage sag conditions of 80 ms duration and 0.8, 0.2, and 0.5 pu retained voltage. The simulated results were compared with the experimental data, demonstrating good alignment during the disconnection phase. It is also noticeable that the aggregated experimental response showed a certain amount of ripple, which is attributed to one vehicle out of seven (EV4). In the case of the 0.8 pu retained voltage sag, the model showed a significantly higher power overshoot than observed experimentally. This discrepancy highlights the need for further refinement of the overshoot representation in future stages of the project.

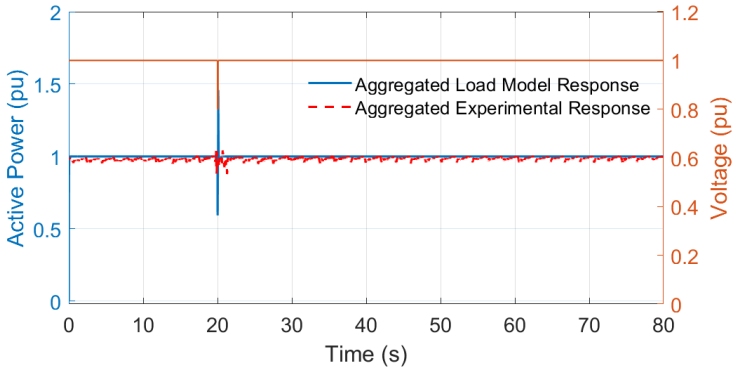

(a)

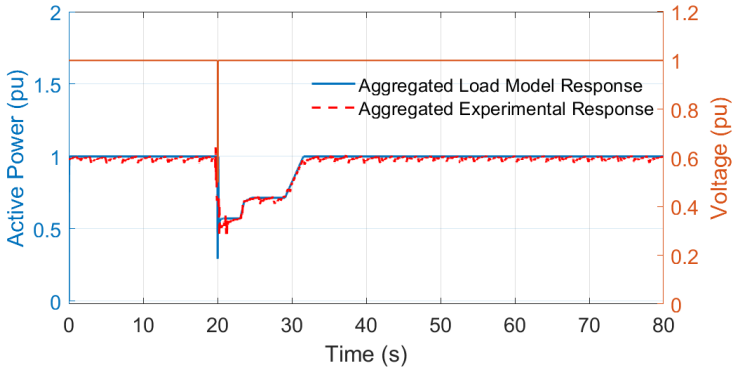

(b)

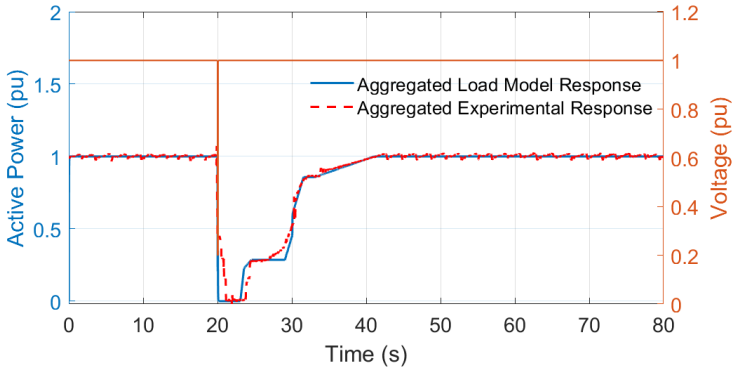

(c)

Figure 6.12 Response of the aggregated model with Level 1 Charger when exposed to 80-ms duration voltage sag for (a) 0.8 pu retained voltage, (b) 0.6 pu retained voltage, (c) 0.4 pu retained voltage and (d) 0.2 pu

The aggregated model was also successfully applied to Level 2 charging scenarios, as illustrated in Figure 6.13. Unlike Level 1 charging, the dynamic modelling for Level 2 was more straightforward due to the consistent disconnection behaviour of most EVs at approximately 0.7 pu retained voltage, which simplified the determination of critical sag thresholds. Compared to Level 1 charging, the reconnection phase for Level 2 charging extended longer, primarily due to the longer disconnection durations observed in certain EVs. Additionally, in this modelling approach, each response type was assigned equal weighting, resulting in a higher influence of longer-duration disconnection behaviours on the aggregated model. As shown in Figure 6.13 (b), slight mismatches between the model and experimental data were identified, primarily attributed to the exclusion of the unusual response of EV6 from the generalisation process. Nevertheless, a general consistency between the modelled and experimental responses remains evident.

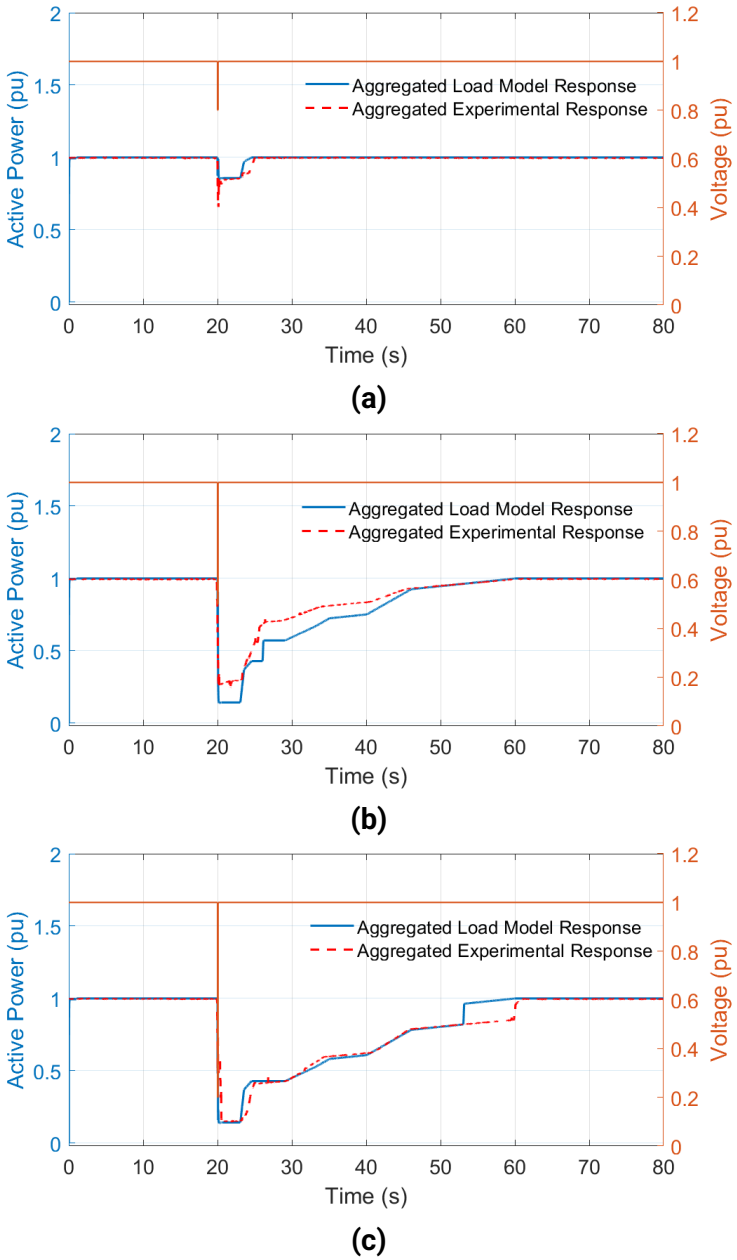

Figure 6.13. Response of the aggregated model with Level 2 Charger when exposed to 80-ms duration voltage sag for (a) 0.8 pu retained voltage, (b) 0.5 pu retained voltage and (c) 0.2 pu retained voltage

5.3. Recommendations and Future Work

The modelling completed so far focusses on the active power behaviour of EVs supplied using Level 1 and Level 2 chargers, without considering reactive power dynamics. Moreover, in the present aggregated model, all EV response types are treated as contributing equally, which does not accurately represent the actual distribution of EVs in the market and may lead to unrealistic load modelling outcomes. To improve the accuracy and applicability of the model, future work could expand in several directions as follows:

- Adding reactive power modelling to allow for a more comprehensive understanding of how EVs affect voltage stability during disturbances.
- Incorporating real-world EV sales or registration data to assign weighted fractions to each response type will make the aggregated model more representative of actual EV fleets.
- Investigating and simulating overshoot phenomena observed during disconnection and reconnection events, which can impact system stability and protection settings.
- Extending the modelling approach to include Level 3 fast chargers, which are increasingly being deployed, especially in commercial and public charging infrastructure, and present different dynamic behaviours compared to Level 1 and 2 chargers.

6. Field Measurements

6.1. Introduction

To support the development of accurate dynamic load models under voltage sag disturbances, three-month field measurements were conducted at three sites. These sites capture a broad range of load types commonly found in power systems. Details of the sites are as follows:

1. Site 1 is an EV DC fast-charging station, offering preliminary results for Level 3 charging behaviour during voltage sags.
2. Site 2 is a commercial site with large refrigeration, walk-in freezers and HVAC (heating, ventilation, and air conditioning) systems, supporting motor load characterisation.
3. Site 3 is an industrial facility dominated by motor drive loads.

Data collected from these sites provide practical validation and complement laboratory-based testing for voltage disturbance analysis.

6.2. Site 1 - Fast EV Charging Station

A power quality monitoring device was deployed at the EV fast-charging station located at the University of Wollongong Innovation Campus. During a three-month data collection period, one notable voltage sag event was captured. Figure 7.1 presents the three-phase voltage and current waveforms recorded during the disturbance. The event involved a decrease in voltage to approximately 0.5 pu in Phases A and B, lasting for over 50 ms. No disconnection of EV charging was detected, as the system promptly returned to normal operation once voltage magnitudes were restored.

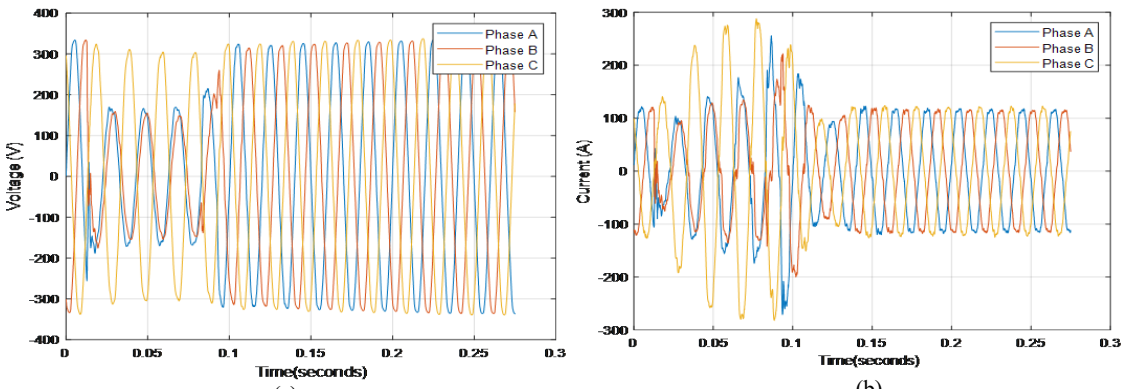

Figure 7.1. Response of DC Fast Charger to voltage sag observed in field measurement, (a) Three-phase supply voltage, (b) Three-phase charging current

6.3. Site 2 - Commercial Load

The second monitoring site was monitored using an ELSPEC power quality analyser. The site is located at the MV/LV transformer supplying a commercial load, primarily consisting of supermarkets and retail facilities. This site was selected due to the high presence of motor-driven equipment such as large-scale air conditioning systems, refrigerators, and freezers. These types of loads are crucial to composite load modelling, particularly in understanding transient behaviour and disconnection tendencies during sag disturbances caused by upstream faults. The monitoring period was December 2024 through the first week of February 2025, during which a total of 14 voltage sag events were captured, as summarised in

Figure 7.2. It is important to note that several brief voltage dips were excluded from the analysis, as they were attributed to system recloser operations rather than genuine sag disturbances.

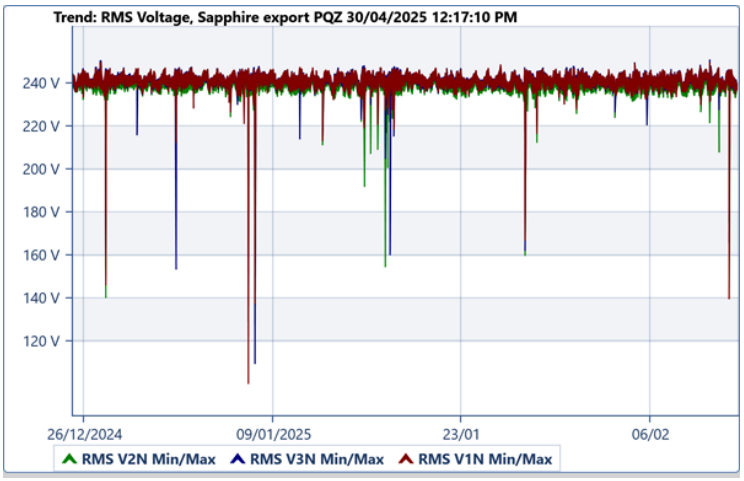

Figure 7.2. Voltage profile at Site 2 throughout the measurement period

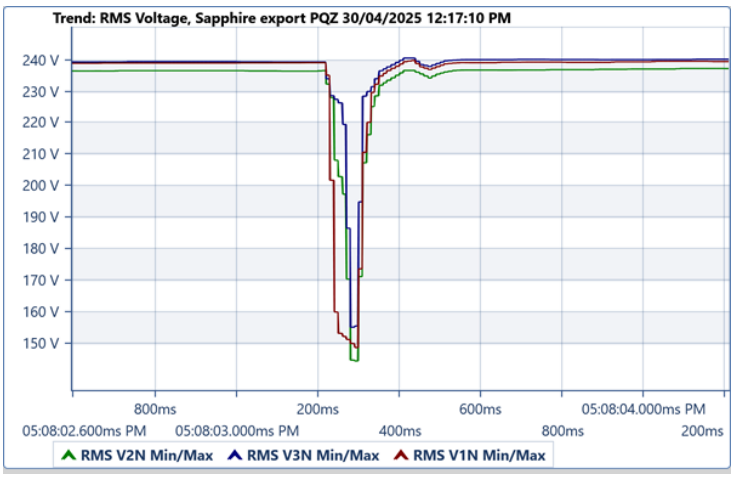

(a)

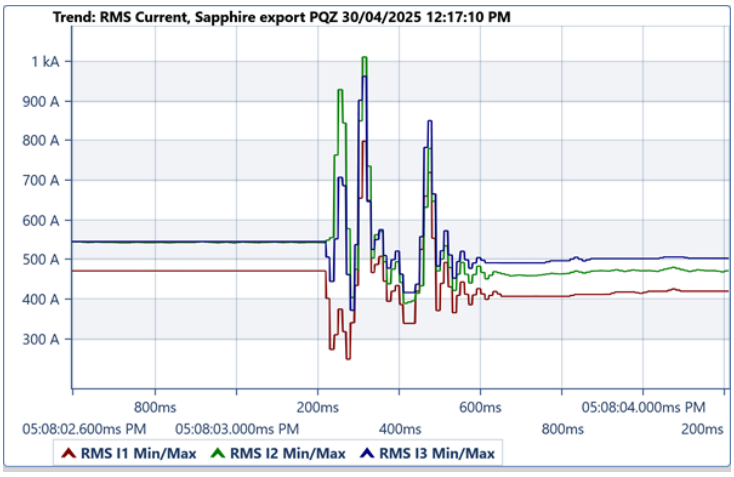

(b)

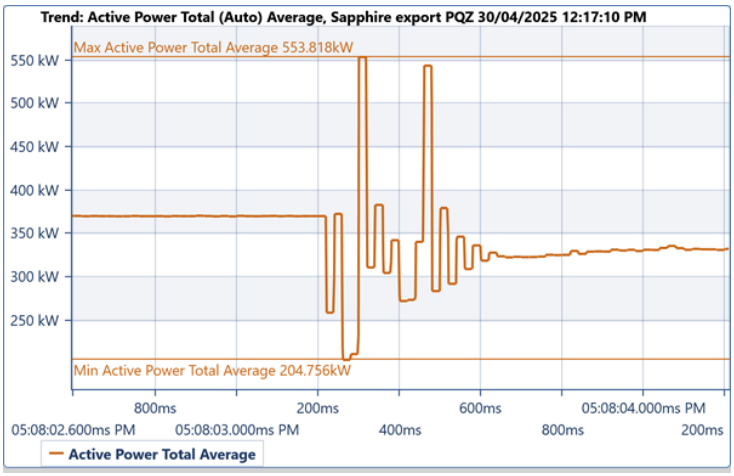

(c)

Figure 7.3. Voltage sag events captured at Site 2, (a) RMS voltage, (b) RMS current, (c) Total average active power

Figure 7.3 presents an example of a voltage sag event recorded at the commercial site. During this event, the voltage on three phases dropped from 240 V to approximately 150 V, corresponding to a retained voltage of approximately 0.63 pu. This disturbance triggered a significant power overshoot, with total demand spiking from 370 kW to 554 kW for a short duration. Once the fault was cleared and the voltage recovered, a reduction in total power consumption was observed, reducing by around 40 kW compared to the pre-sag steady-state level, indicating that some loads were likely disconnected because of the disturbance.

Table 7.1 provides a summary of the voltage sag events recorded at Site 2. The observed sag events varied in depth, with the majority exhibiting retained voltage magnitudes between 0.42 and 0.67 pu. These disturbances were found to trigger noticeable dynamic responses from the connected loads. A key observation is the occurrence of load disconnection following many of the sag events. For example, during sag event number 8, the active power dropped from a pre-fault value of 293 kW to approximately 250 kW post-event, indicating a 43-kW reduction (approximately 15% of the total load), suggesting that several loads likely failed to recover immediately after the voltage returned to normal.

Moreover, nearly all sag events were accompanied by a brief but significant post-sag power overshoot. This phenomenon likely results from the sudden inrush currents as motors attempt to reaccelerate or restart following the disturbance. Striking instances include sag events number 6, 13 and 14, where the active power consumption spiked to more than double the normal operating level, immediately after the sag. Such overshoots can stress electrical infrastructure and contribute to voltage instability if not accurately represented in power system models.

These findings reinforce the importance of capturing both the disconnection and reconnection behaviour of motor loads. They also highlight the necessity of incorporating overshoot dynamics into composite load modelling frameworks to better predict system dynamic behaviour under fault conditions.

Table 7.1. Data on sag events captured at Site 2

Sag Event #	Sag Depth (pu)			Pre-sag Active Power	Post-sag Active Power	Power Reduction		Overshoot	
	Va	Vb	Vc	(kW)	(kW)	(kW)	(%)	(kW)	(%)
1	0.63	0.60	0.65	370	330	40	10.8	554	49.7
2	0.61	0.59	0.62	376	343	33	8.8	580	54.3
3	0.88	0.91	0.64	302	292	10	3.3	384	27.2
4	0.42	0.97	0.54	295	267	28	9.5	483	63.7
5	0.58	0.58	0.60	355	211	44	12.4	0	0
6	0.95	0.53	0.46	213	221	N/A	N/A	447	109.9
7	0.98	0.68	0.65	272	233	29	10.7	300	10.3
8	0.96	0.57	0.48	293	250	43	14.7	400	36.5
9	0.93	0.80	0.95	339	329	10	2.9	368	8.6
10	0.95	0.65	0.85	289	269	20	6.9	454	57.1
11	0.98	0.73	0.67	310	296	14	4.5	510	64.5
12	0.70	0.67	0.68	371	338	23	6.2	749	101.9
13	0.59	0.73	0.69	218	205	13	6.0	472	116.5
14	0.58	0.98	0.69	210	200	10	4.8	397	89.0

Figure 7.4 illustrates the percentage power overshoot and load reduction during voltage sag events at Site 2. Measurements were collected across all three phases, with the understanding that a sag in one phase can induce overshoot or disconnection in another. For each event, the displayed sag voltage reflects the lowest retained voltage across the phases. Likewise, the power overshoot values represent the highest recorded across all phases during the same sag period. As a result, the overshoot and reduction figures may not necessarily correspond to the phase where the sag occurred, but rather the one where the most significant impact was observed. The captured voltage sag events mostly resulted in retained voltage of 0.6-0.7 pu, typically leading to a power overshoot of approximately 60% of pre-sag values occasionally increasing to 100-150%. Regarding the amount of load reduction, most of the recorded values fall in the range of less than 10% of pre-sag values, and there exists only one circumstance where 40% of the load disconnected.

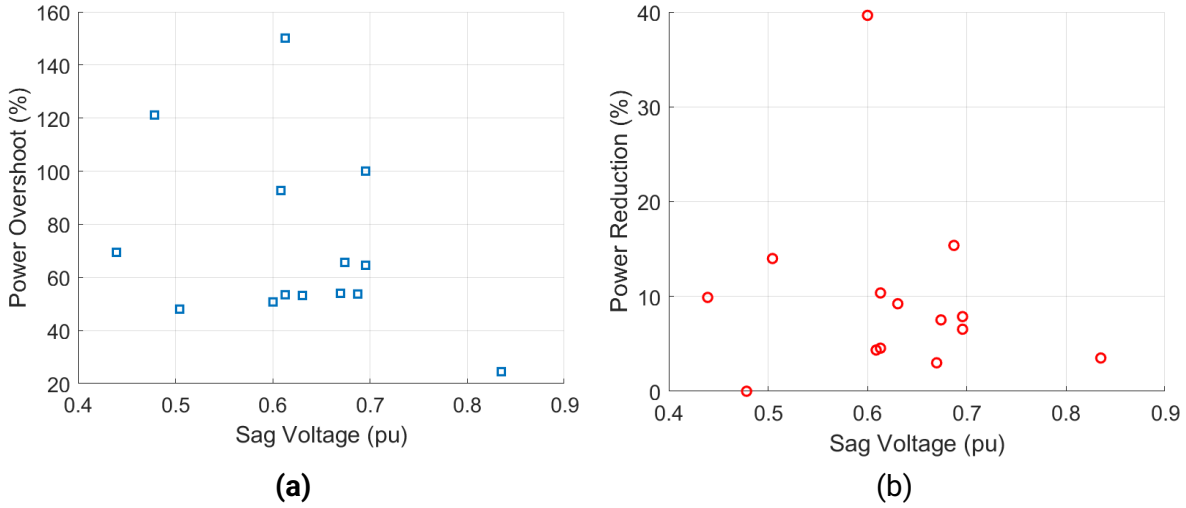

Figure 7.4. Scatter plot of power overshoot and power reduction during voltage sag events

6.4. Site 3 - Industrial Heavy Load

The third site selected for monitoring is located a steel manufacturing facility. An ELSPEC meter is connected to the 33-kV incoming line at this location. The process undertaken at location 3 include cold rolling of steel, metal/paint coating, and finishing facilities. The primary load types at this site are motor systems and general distribution. Similar to Site 2, monitoring was carried out over a period of 3 months. Over the measurement period, a total of five voltage sag events were detected. These events are illustrated in Figure 7.5, showing the characteristic voltage profiles recorded during each disturbance. Details of each sag, including their depth (pu) and duration (ms), are summarised in Table 7.2

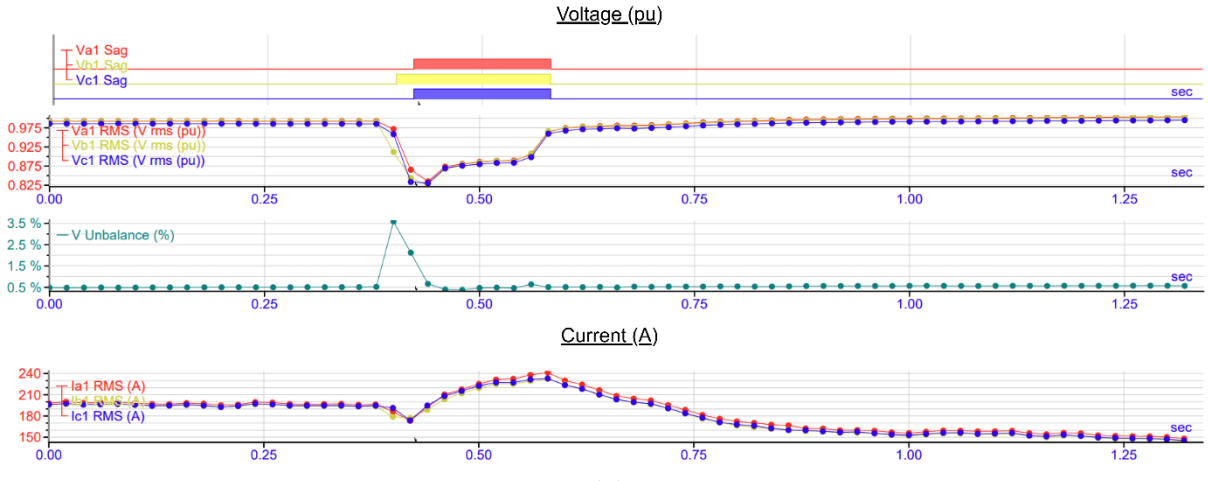

(a)

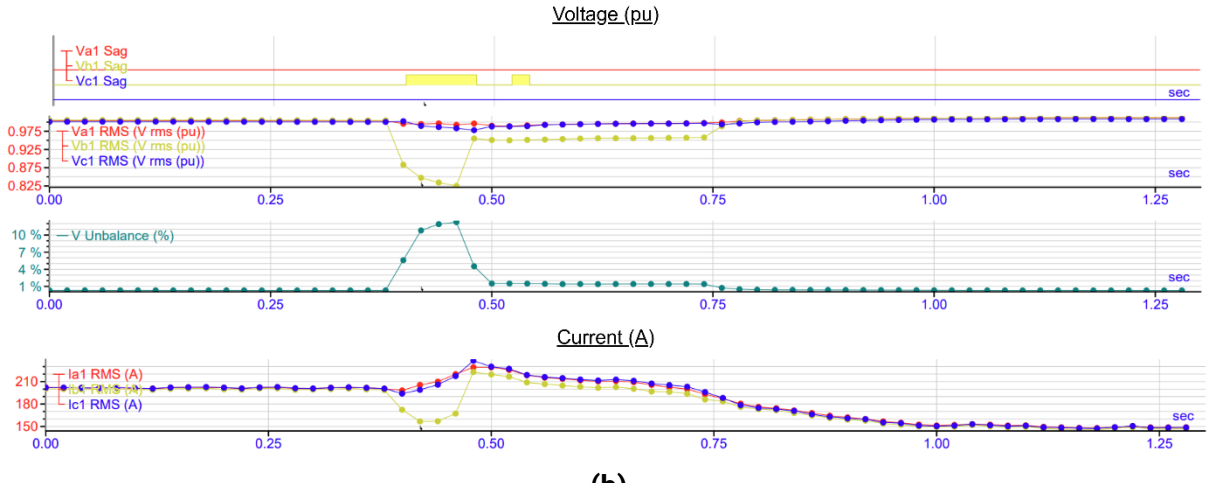

(b)

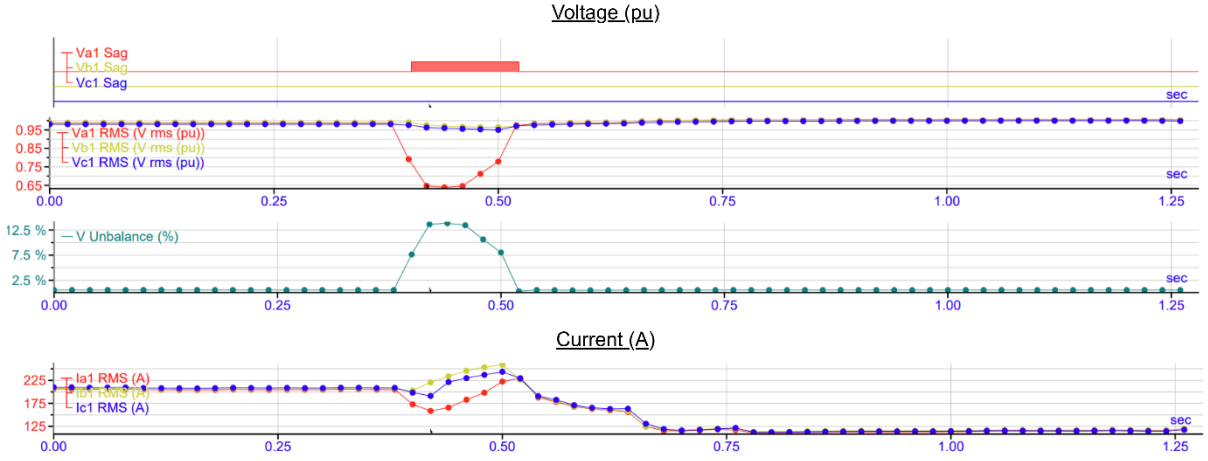

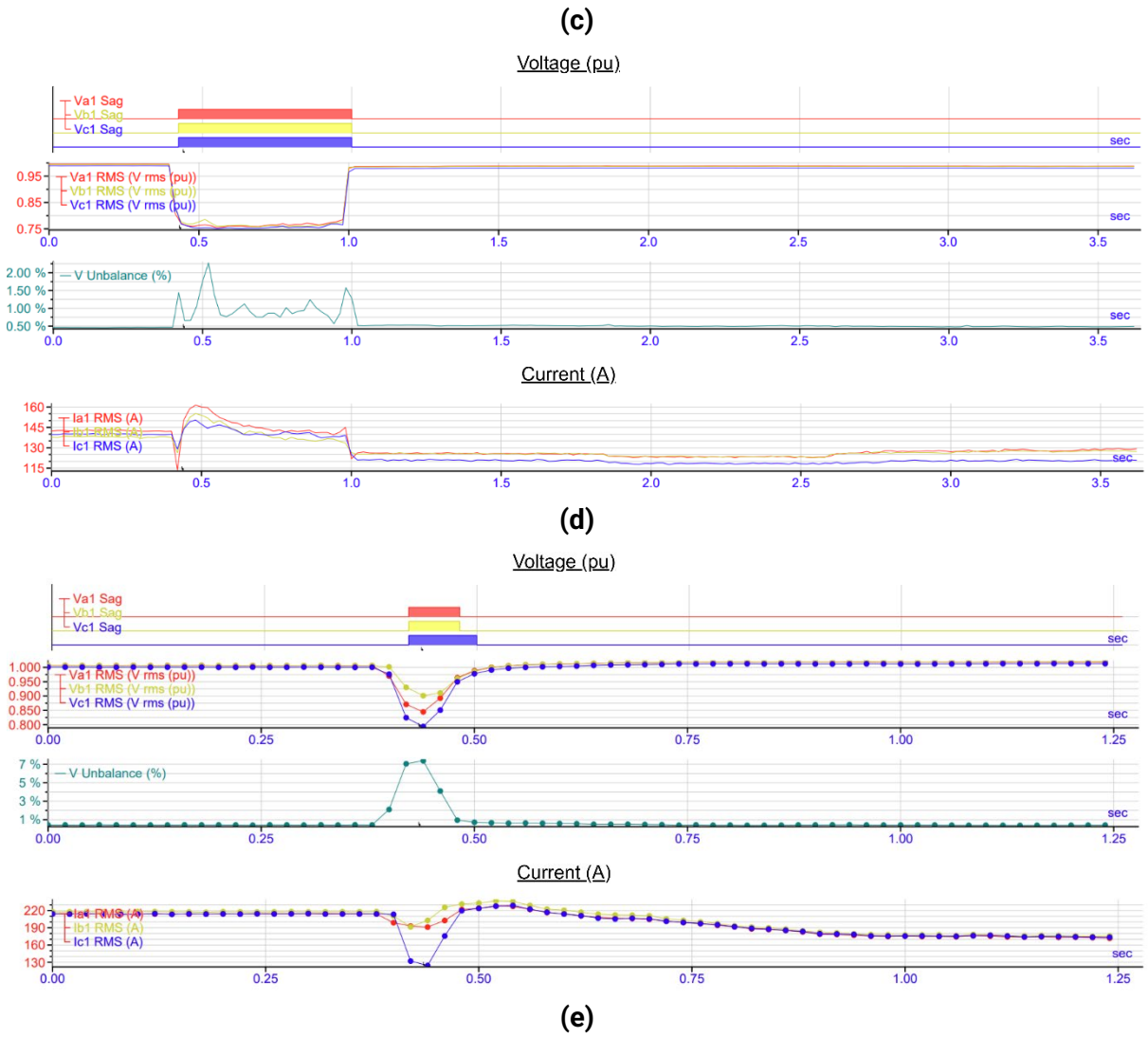

Figure 7.5. Voltage sag events captured at Site 3

The voltage sag events recorded at Site 3 displayed notable variations in both depth and duration. Among the five events captured, sag events 2 and 3 were single-phase sags, while the remaining events involved three-phase disturbances. The measured sag depths ranged from 0.64 to 0.84 pu retained voltage, with durations spanning from 60 ms to 580 ms. Consistent with observations at Site 2, Site 3 also exhibited load disconnections following exposure to voltage sags, regardless of the severity or duration of the event. For instance, for sag event 2, which is a relatively shallow single-phase sag at 0.83 pu retained voltage lasting 100 ms, shedding of approximately 50 A, which corresponds to a 25% reduction in total load demand is observed. Furthermore, power overshoots on return to nominal voltage were evident in all recorded events, with particularly significant spikes observed during events 1 and 3. These findings underscore the sensitivity of industrial motor-driven loads to even moderate voltage disturbances.

Table 7.2. Data on sag events captured at Site 3

Sag Event #	Sag Depth (pu)			Sag Duration (ms)			Pre-sag Condition (A)	Post-sag Condition (A)	Load Reduction		Overshoot	
	Va	Vb	Vc	Va	Vb	Vc			(A)	(%)	(A)	(%)
1	0.84	0.82	0.83	160	180	160	195	160	35	17.9	240	23.1
2	0.99	0.83	0.98	0	100	0	200	150	50	25.0	230	15.0

3	0.64	0.96	0.95	120	0	0	205	110	95	46.3	250	22.0
4	0.75	0.76	0.75	580	580	580	140	120	20	14.3	160	14.3
5	0.84	0.9	0.79	60	60	80	220	170	50	22.7	230	4.5

7. Conclusion for UOW Activities

7.1. EV Testing

The testing of four additional EVs has yielded critical insights into their dynamic behaviour when exposed to voltage sags while supplied to charging infrastructure. Building upon the preliminary findings from Stage 3, this phase reaffirmed the strong dependency of EV response characteristics on the specific vehicle model, primarily due to the unique AC/DC conversion mechanisms embedded within each onboard charger. By testing multiple EVs using the same charging equipment, notable variations in performance were identified. All four EVs disconnected even under moderately severe voltage sags.

Looking ahead, Stage 5 could expand the scope of the project to explore Vehicle-to-Grid (V2G) interactions, providing insight into bidirectional power flow impacts on system dynamics. Additionally, this phase could include a detailed assessment of Level 3 fast chargers, potentially smaller rated examples that could be evaluated using available laboratory infrastructure. The inclusion of tests involving frequency and phase angle jumps, previously only briefly explored in Stage 2 with one vehicle, will also support the refinement of aggregated dynamic models, advancing the robustness of future load modelling frameworks.

7.2. EV Modelling

Utilising the data collected in Stages 2 through 4, the response characteristics of EVs to voltage sag disturbances have been successfully generalised for both Level 1 and Level 2 charging scenarios. This enabled the development of an aggregated EV load model that reflects the real-world charging dynamics of the eight EVs tested to date. The proposed model is conceptually based on the EPRI implementation, but significantly improved through the integration of empirical data, allowing it to more accurately represent practical EV behaviour under disturbance conditions. As a result, the model demonstrates a strong alignment with laboratory measured responses, particularly in capturing disconnection and reconnection patterns.

Though there were advancements, the present model is limited to representing active power only. This restriction poses challenges for fully understanding the dynamic interaction between EV charging and grid performance, especially under fault conditions. Therefore, Stage 5 of the project could focus on expanding the modelling framework to include reactive power behaviour, which is critical for voltage stability analysis. Additionally, statistical investigation on EV sales will be applied to assign appropriate fractional weights to each generalised response type, replacing the current equal-weight assumption to better reflect the actual EV fleet composition. Another key area for future investigation is the accurate modelling of power overshoots observed during ride-through and reconnection phases. This enhancement would provide DNSPs with more reliable tools for assessing system stability margins and improving grid resilience.

7.3. Field Measurements

The three-month field measurements conducted across three distinct sites have provided valuable insights into the impact of voltage sag disturbances on various types of electrical loads. At the EV fast-charging station, only one sag event was captured, which did not result in EV disconnection but revealed current distortion during the disturbance. In contrast, multiple sags were observed at the commercial site dominated by HVAC and refrigeration systems, many of which triggered momentary power overshoots followed by load disconnection. Similarly, the industrial site experienced multiple sags, with

both single- and three-phase disturbances causing noticeable power fluctuations and load shedding, even for sags of relatively short duration and shallow depth.

These observations underscore the critical role of voltage sags in influencing load behaviour and highlight the need for accurate dynamic modelling of load performance during such disturbances, especially in motor-dominated and sensitive load environments. The data collected will contribute to tunning the composite load model, enabling better prediction of system responses during fault conditions and supporting more resilient power system planning.

Looking ahead, the next phase of the project could expand beyond EVs to include extended bench testing of other emerging technologies such as distributed energy resources (DER), battery energy storage systems (BESS), and larger power electronic devices increasingly present in modern distribution networks. Conducting controlled testing on these systems and making the resulting data openly available would address existing knowledge gaps around their dynamic responses to voltage disturbances. This would ultimately assist network operators in anticipating power reductions and potential stability issues, thereby supporting more informed and resilient network planning and operation.

Appendix A: Bench Testing Results

A.1: Parallel Inverter Testing Waveforms (Two Inverters)

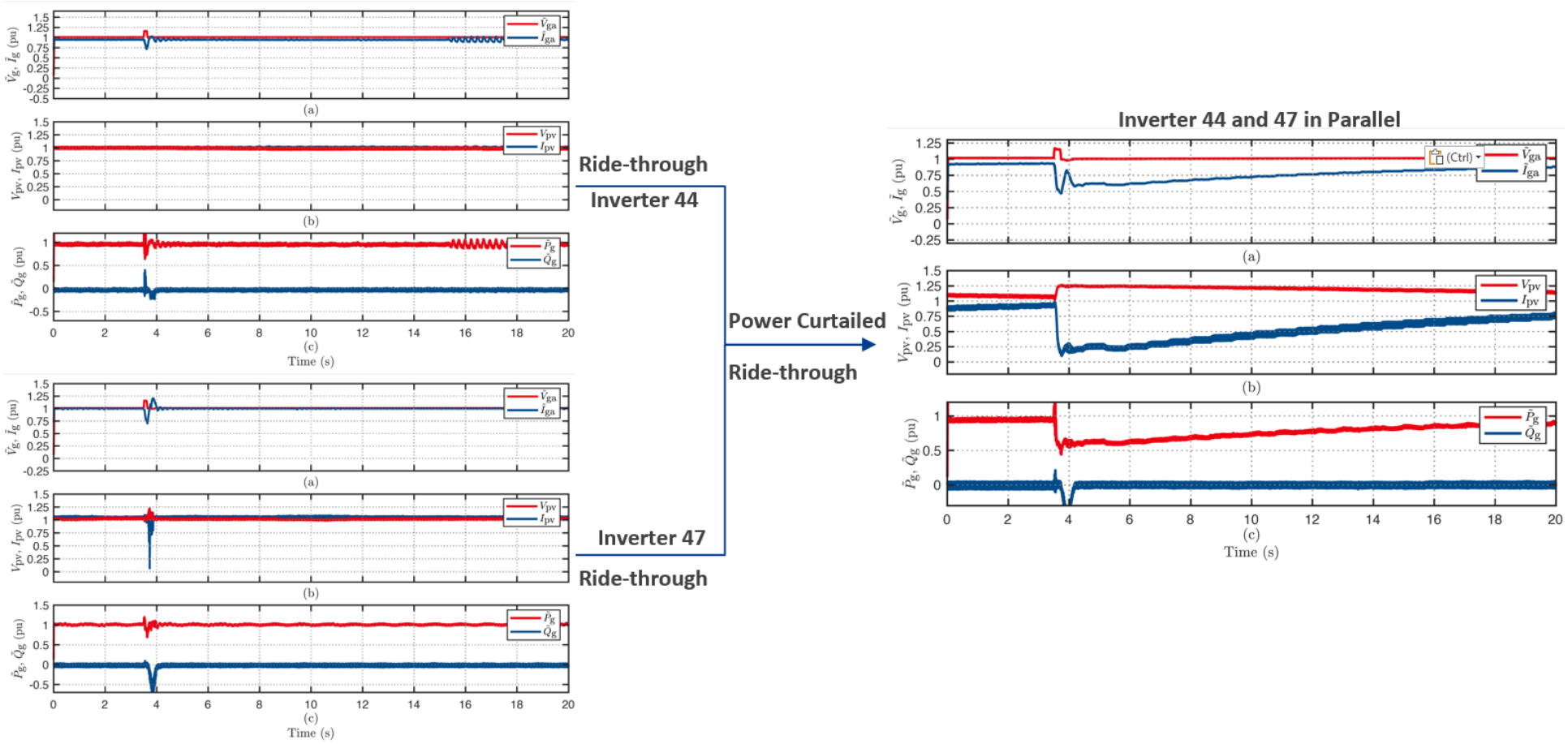

Figure A1.1: Response of inverters 44 and 47 to swell of 1.2 p.u for 120 grid disturbance: individual vs parallel configuration.

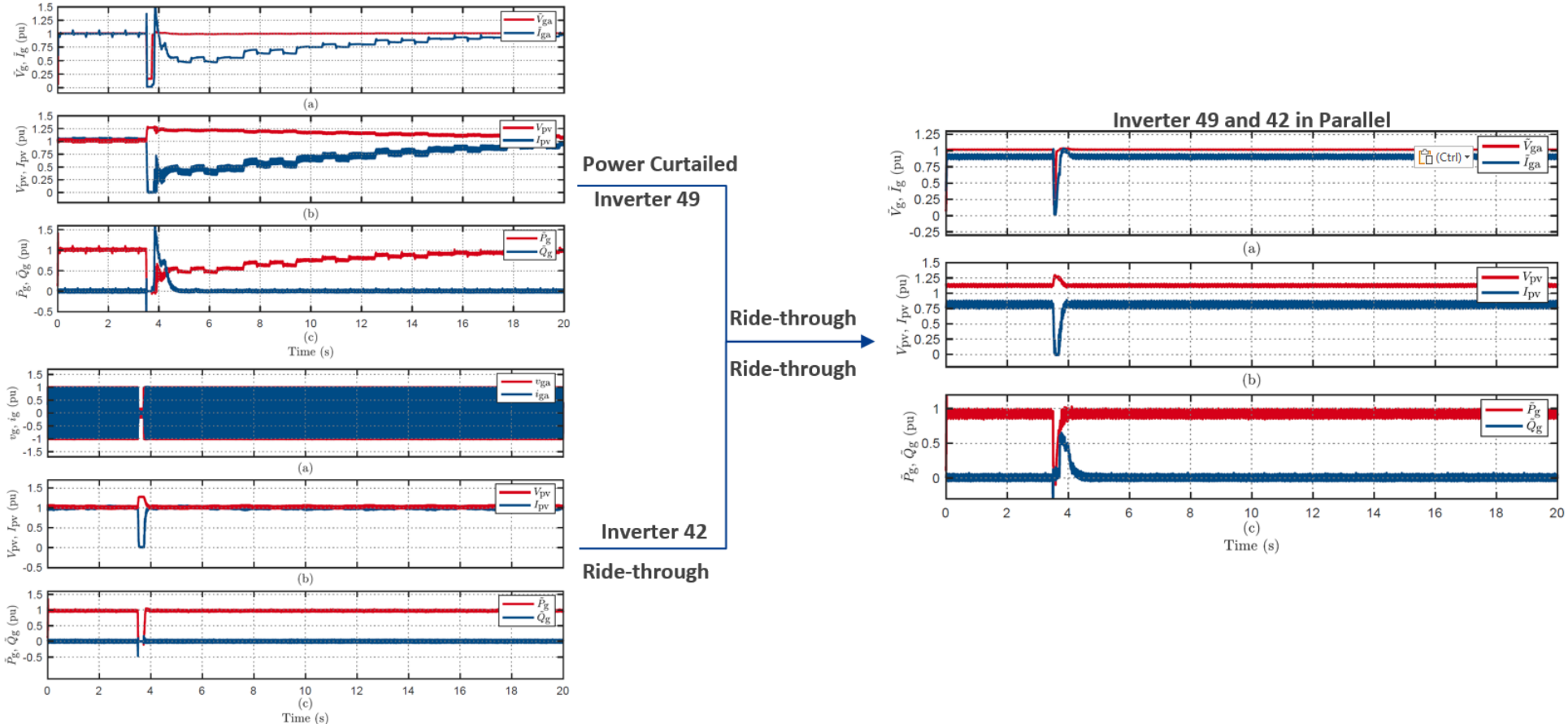

Figure A1.2: Response of inverters 49 and 42 to voltage sag of 0.8p.u for 80ms grid disturbance: individual vs parallel configuration.

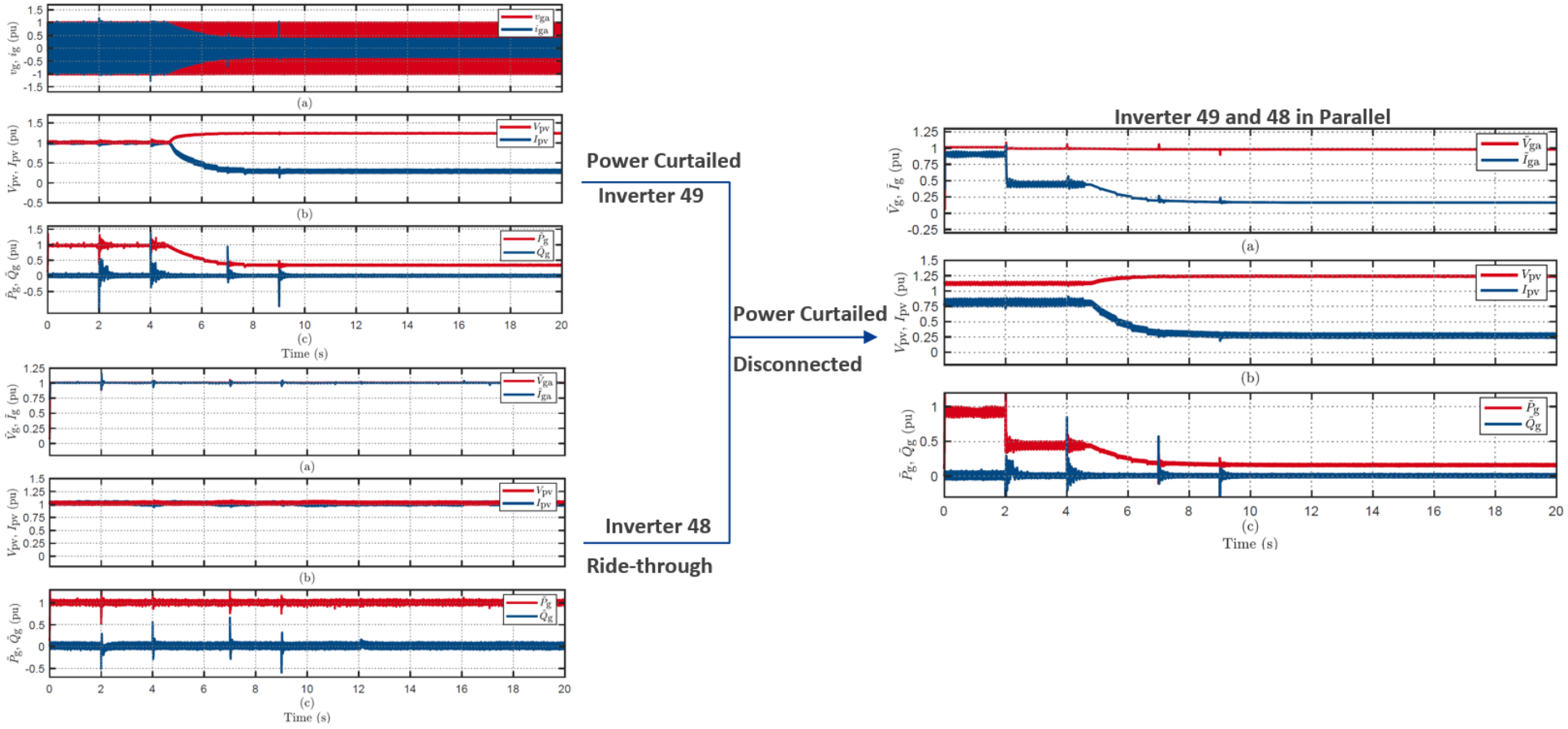

Figure A1.3: Response of inverters 49 and 48 to 30° VPAJ grid disturbance: individual vs parallel configuration.

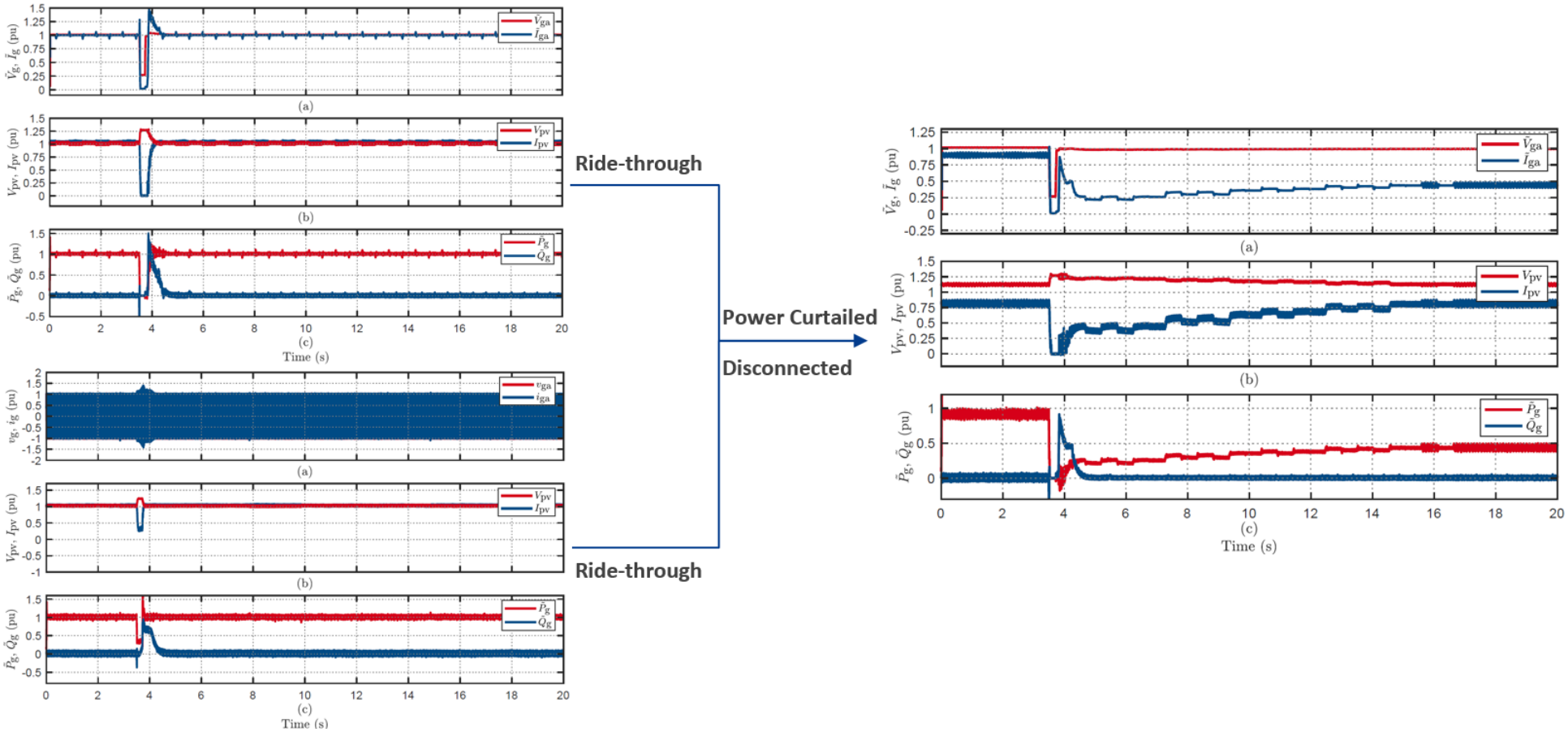

Figure A1.4: Response of inverters 49 and 48 to voltage sag of 0.7p.u for 220ms grid disturbance: individual vs parallel configuration.

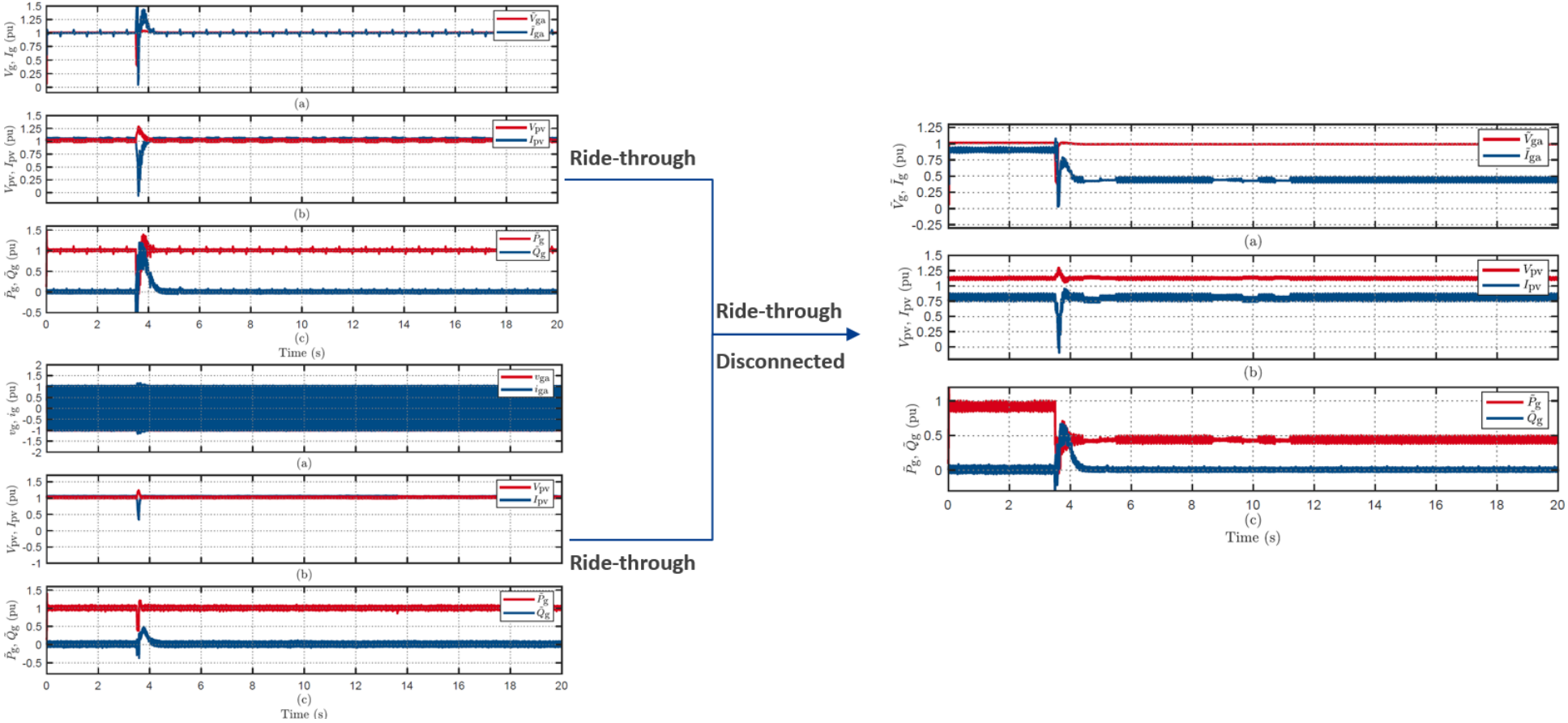

Figure A1.5: Response of inverters 49 and 48 to voltage sag of 0.6p.u for 80ms grid disturbance: individual vs parallel configuration.

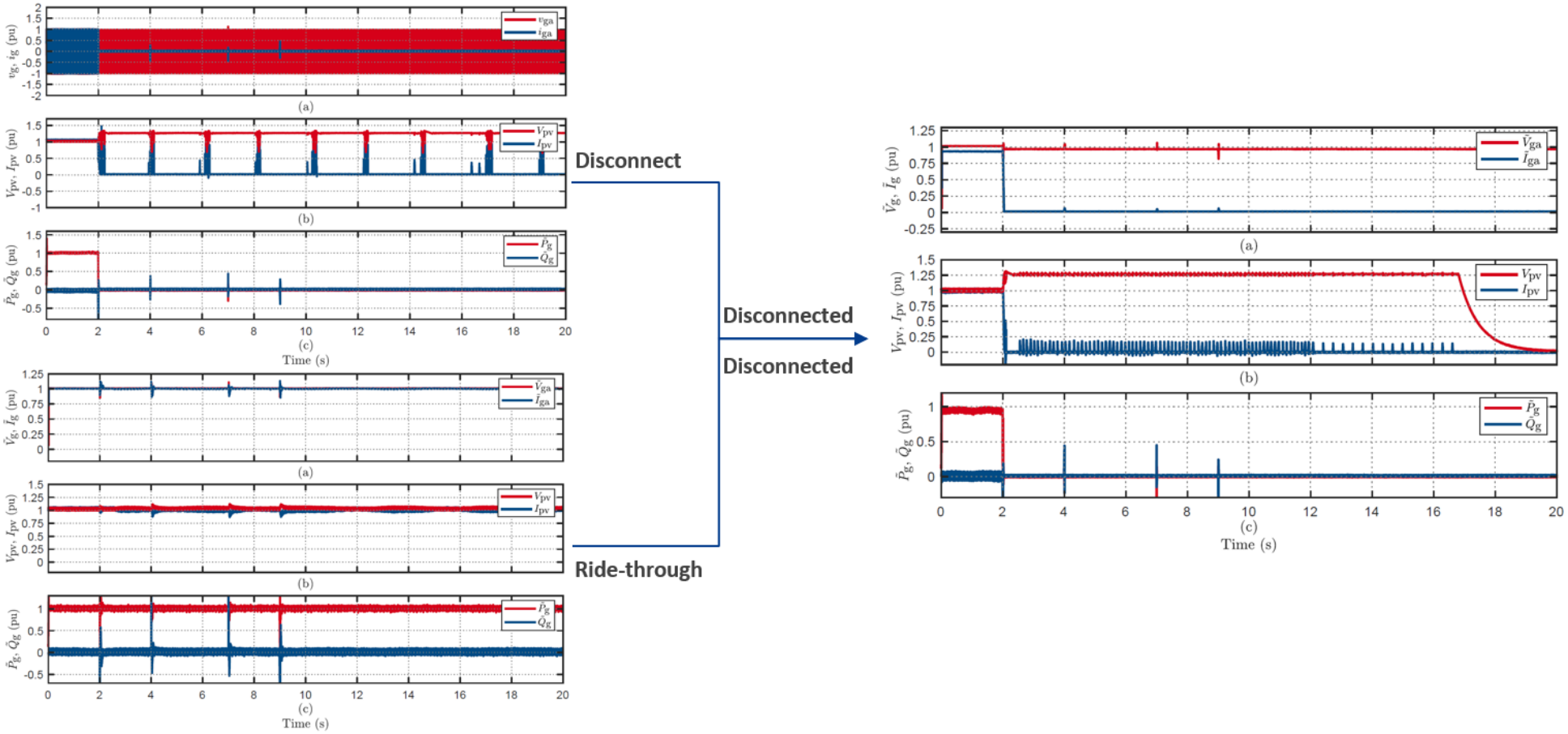

Figure A1.6: Response of inverters 47 and 48 to 30° VPAJ grid disturbance: individual vs parallel configuration.

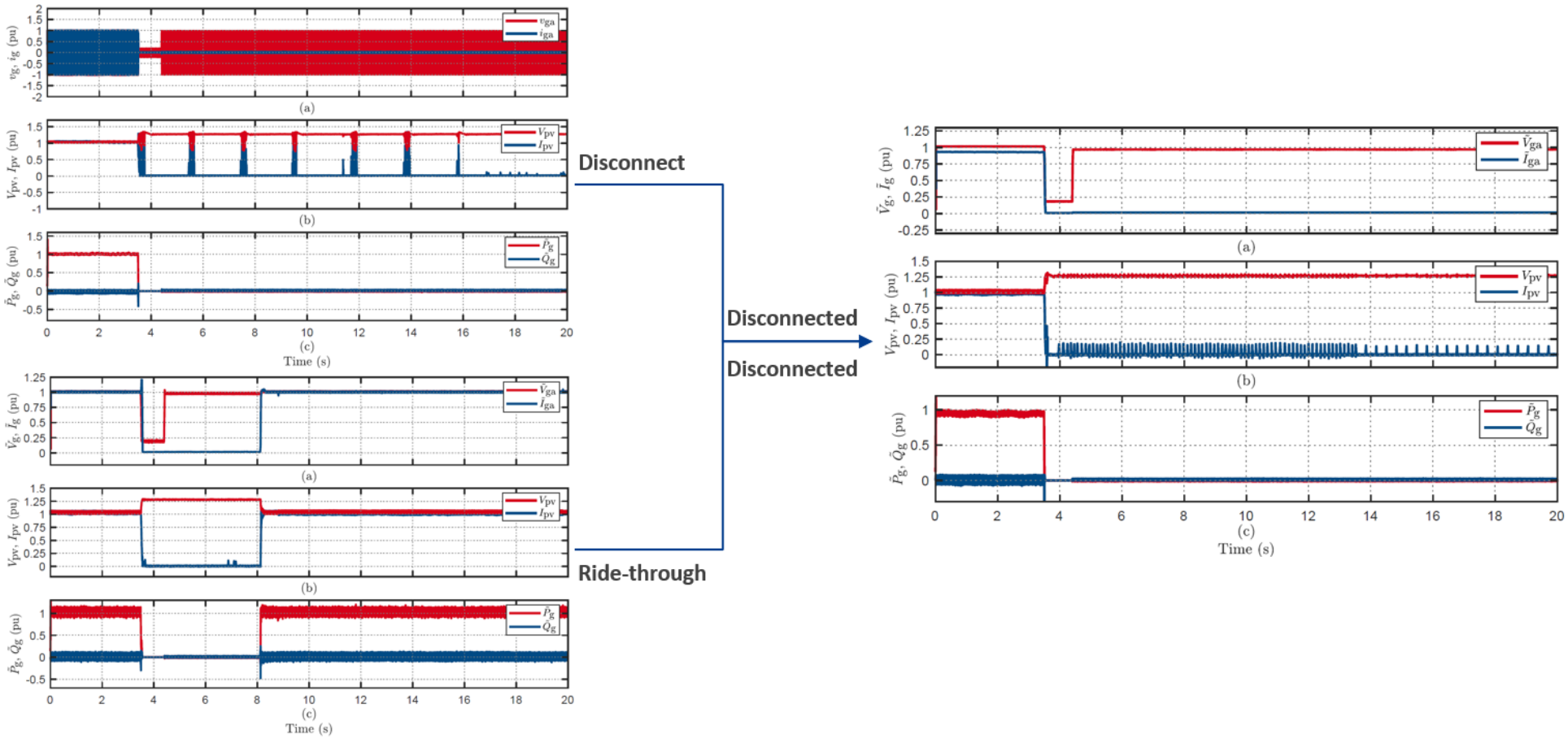

Figure A1.7: Response of inverters 47 and 48 to voltage sag to 50V for 0.9s grid disturbance: individual vs parallel configuration.

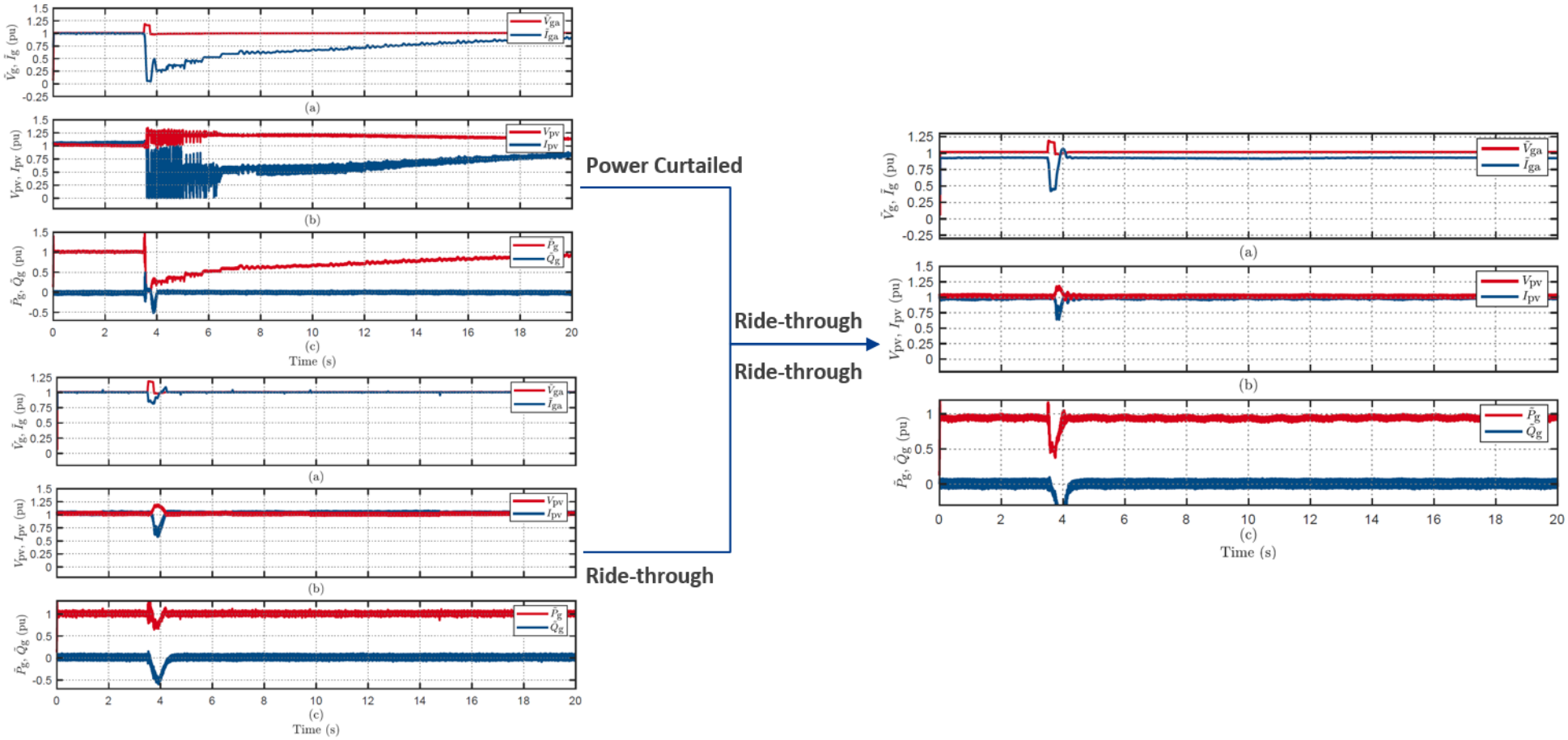

Figure A1.8: Response of inverters 47 and 48 to voltage swell of 1.15p.u for 220ms grid disturbance: individual vs parallel configuration.

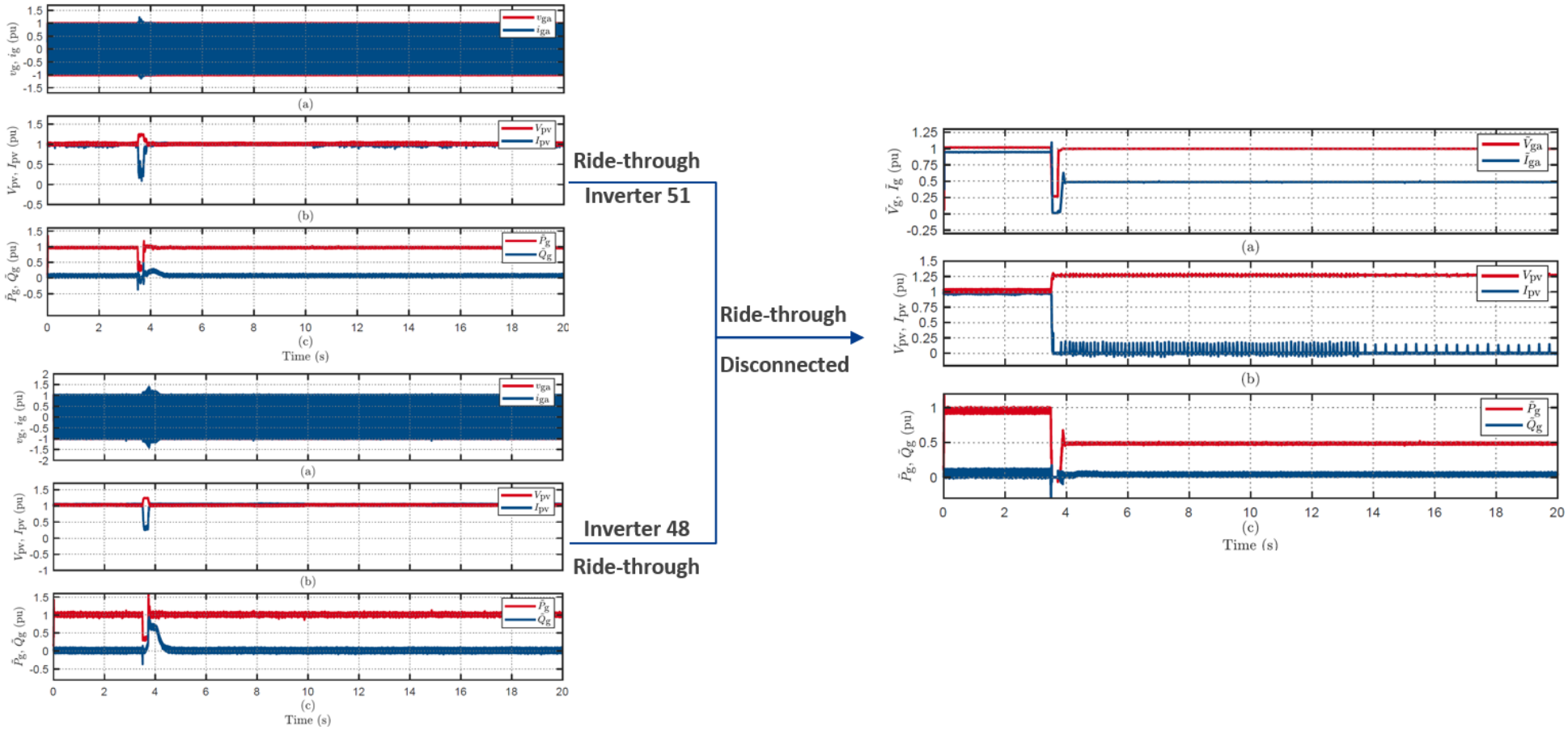

Figure A1.9: Response of inverters 51 and 48 to voltage sag of 0.7p.u for 220ms grid disturbance: individual vs parallel configuration.

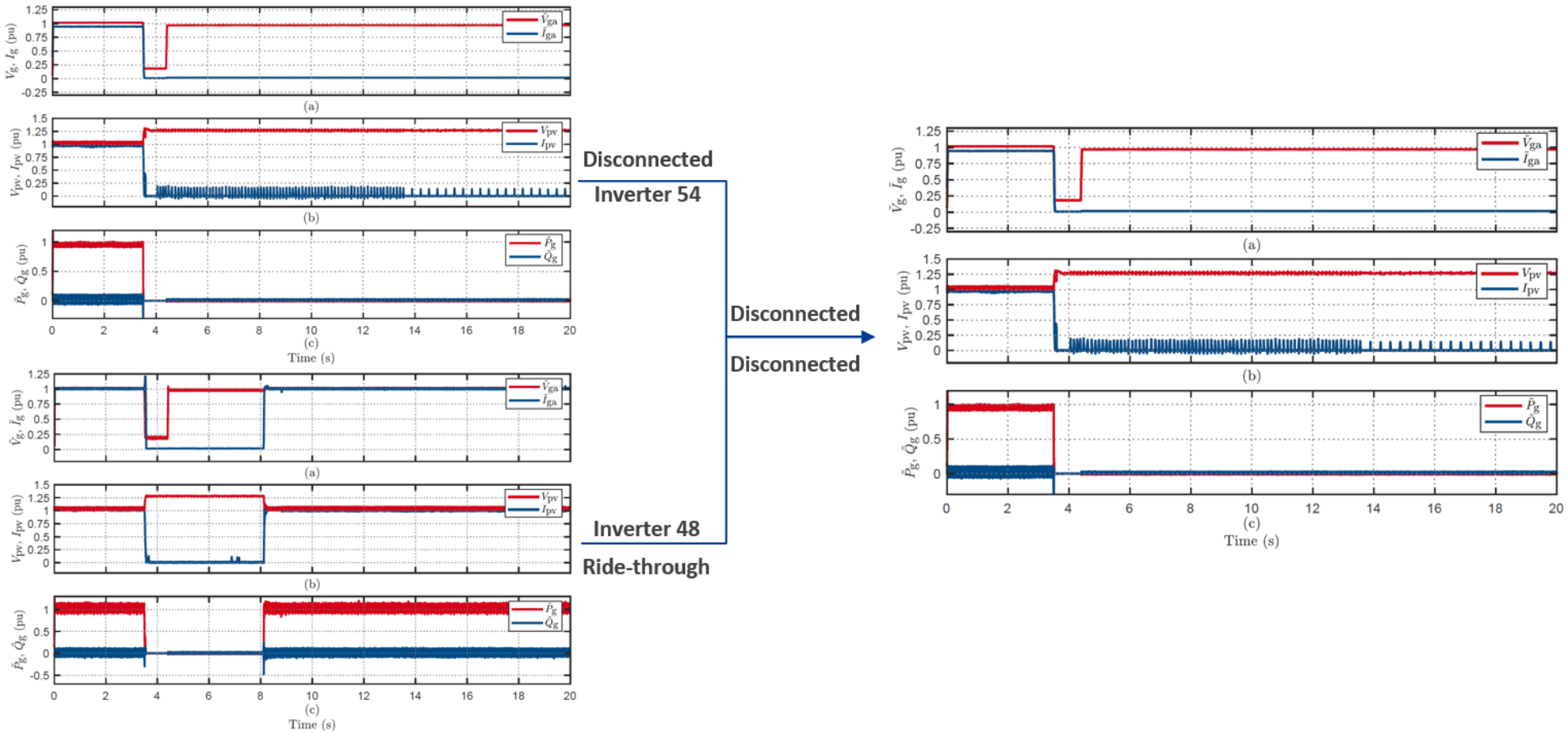

Figure A1.10: Response of inverters 54 and 48 to voltage sag of 180V for 0.9s grid disturbance: individual vs parallel configuration.

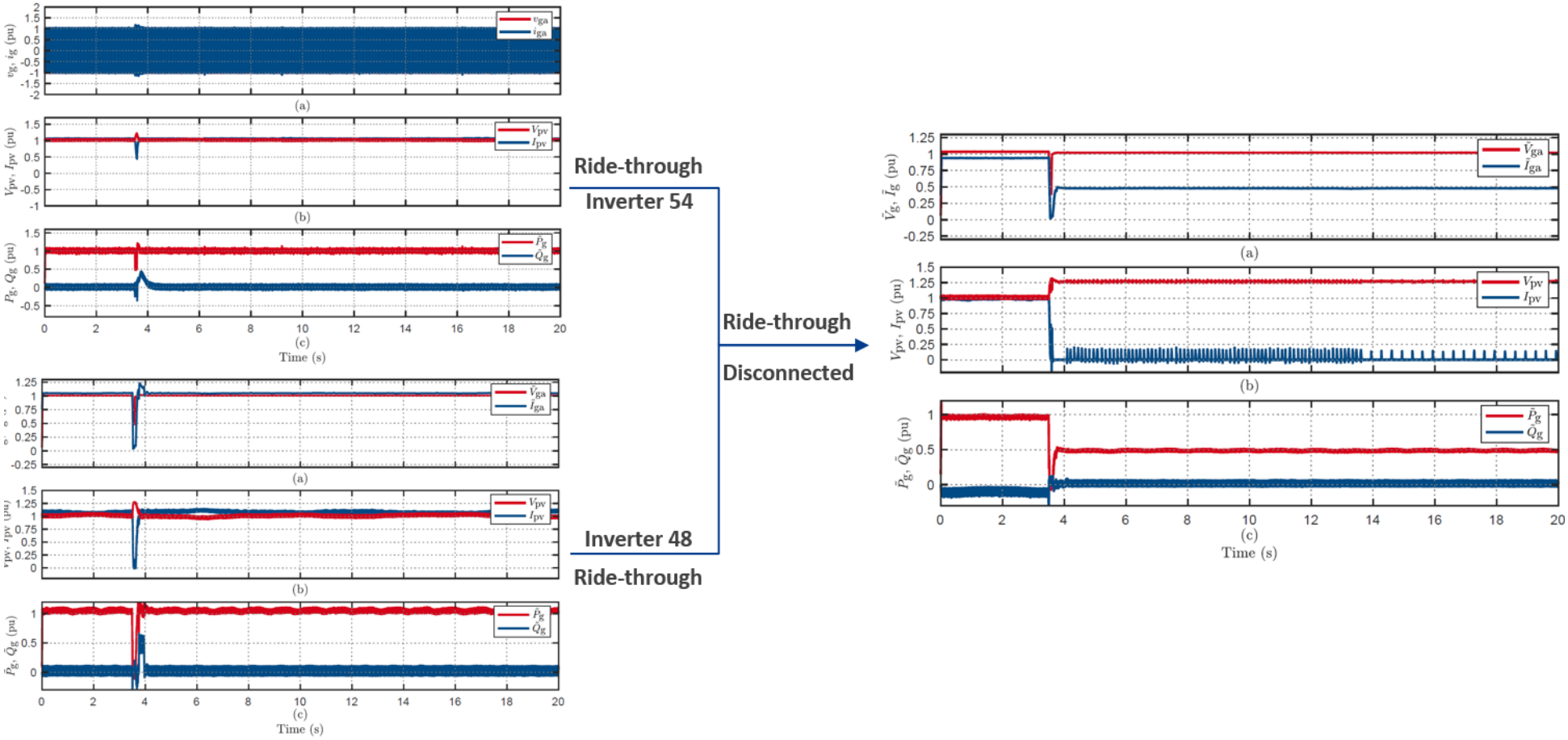

Figure A1.11: Response of inverters 54 and 48 to voltage sag of 0.5p.u for 80ms grid disturbance: individual vs parallel configuration.

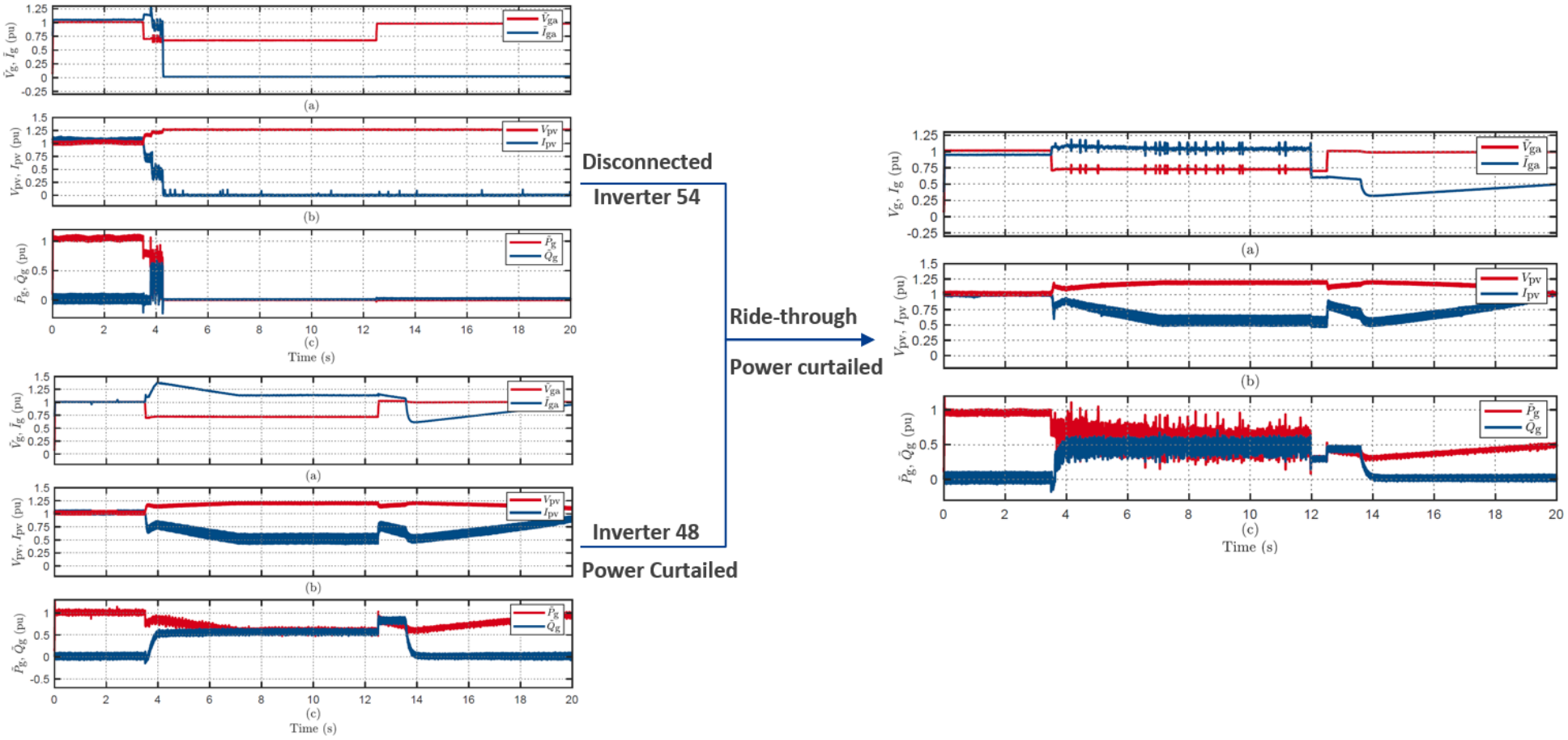

Figure A1.12: Response of inverters 54 and 48 to voltage sag of 50V for 9s grid disturbance: individual vs parallel configuration.

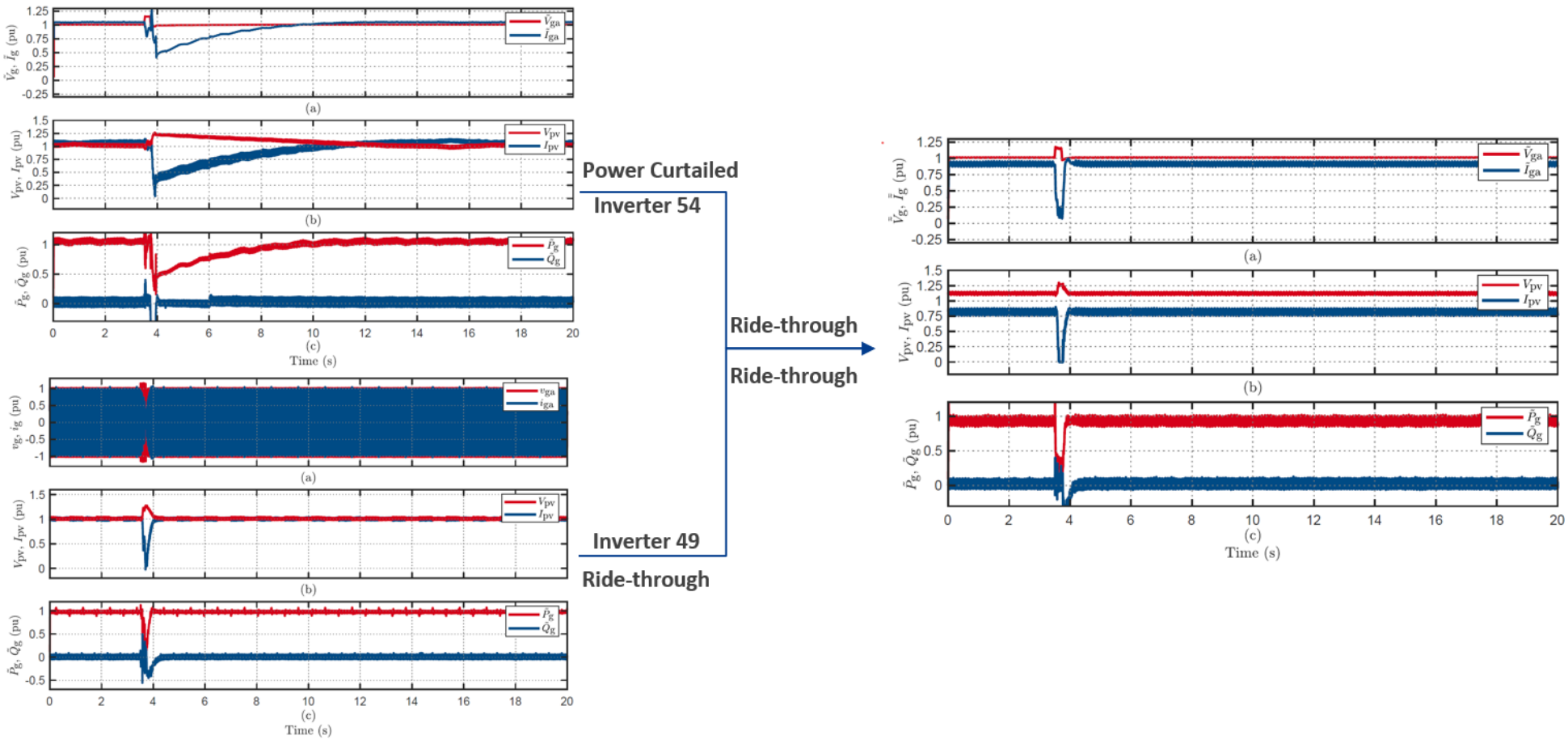

Figure A1.13: Response of inverters 54 and 49 to voltage swell of 1.15p.u for 220ms grid disturbance: individual vs parallel configuration.

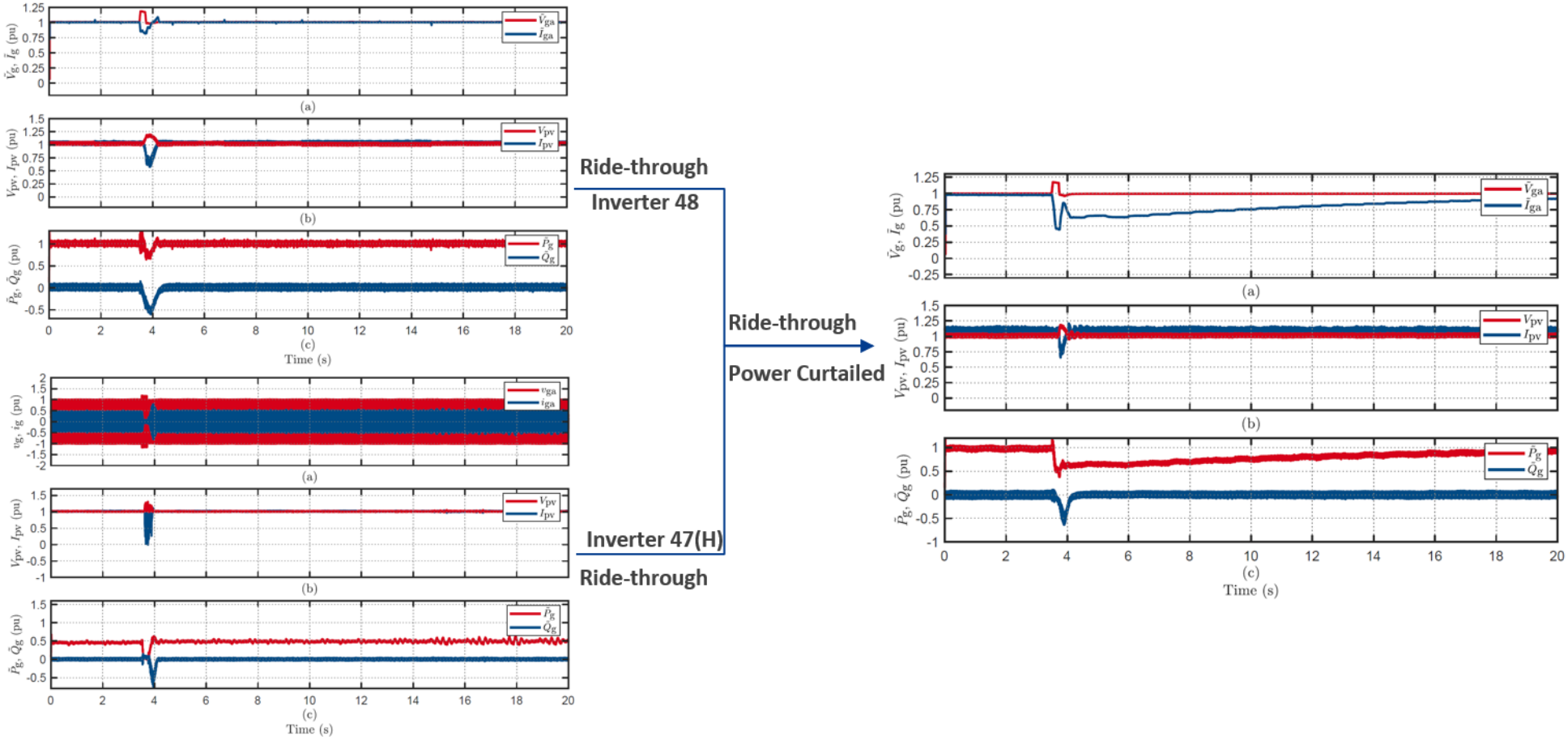

Figure A1.14: Response of inverters 48 and 47 to voltage swell of 1.175p.u for 220ms grid disturbance: individual vs parallel configuration.

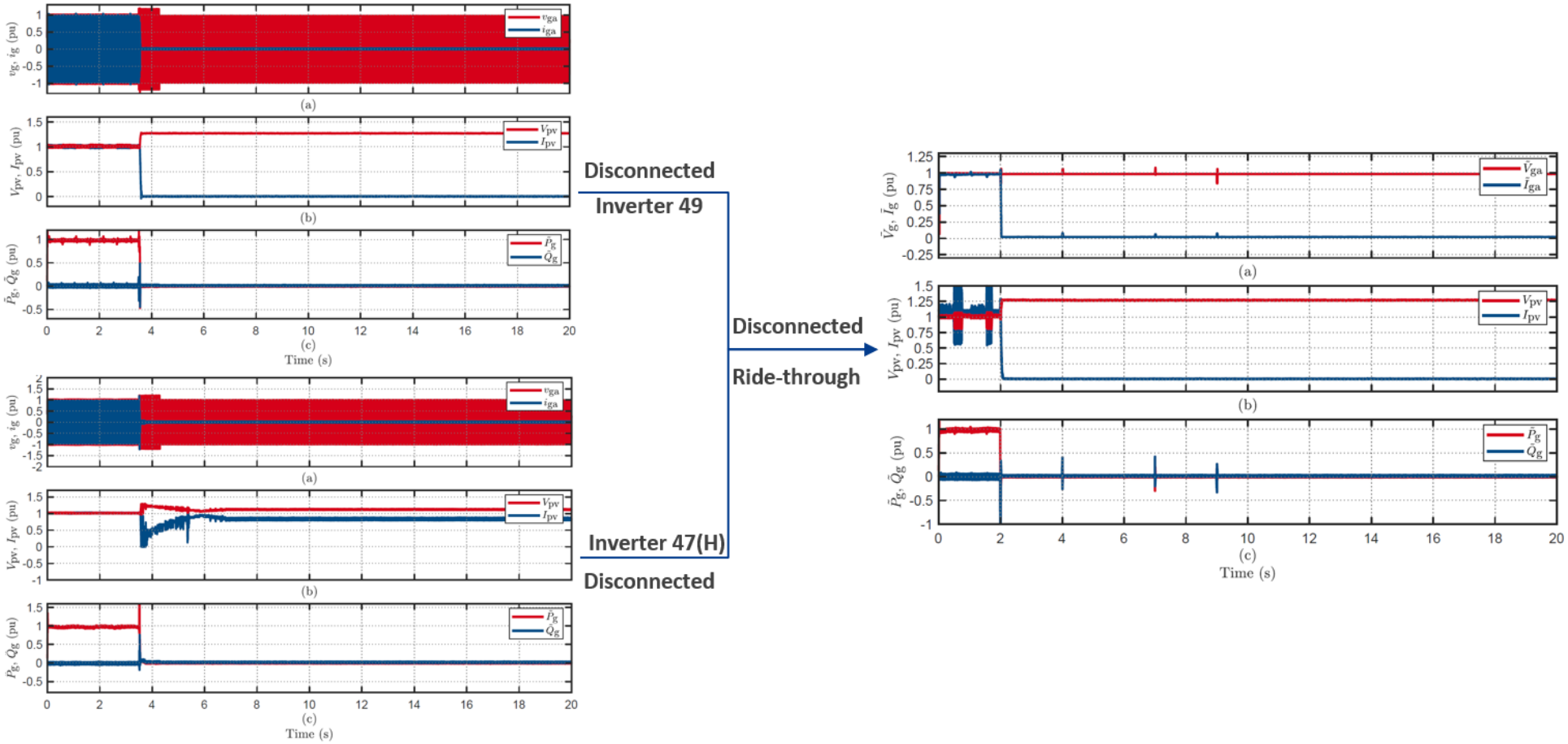

Figure A1.15: Response of inverters 49 and 47 to voltage swell of 1.2p.u for 800ms grid disturbance: individual vs parallel configuration.

A.2: Parallel Inverter Testing Waveforms (Three Inverters)

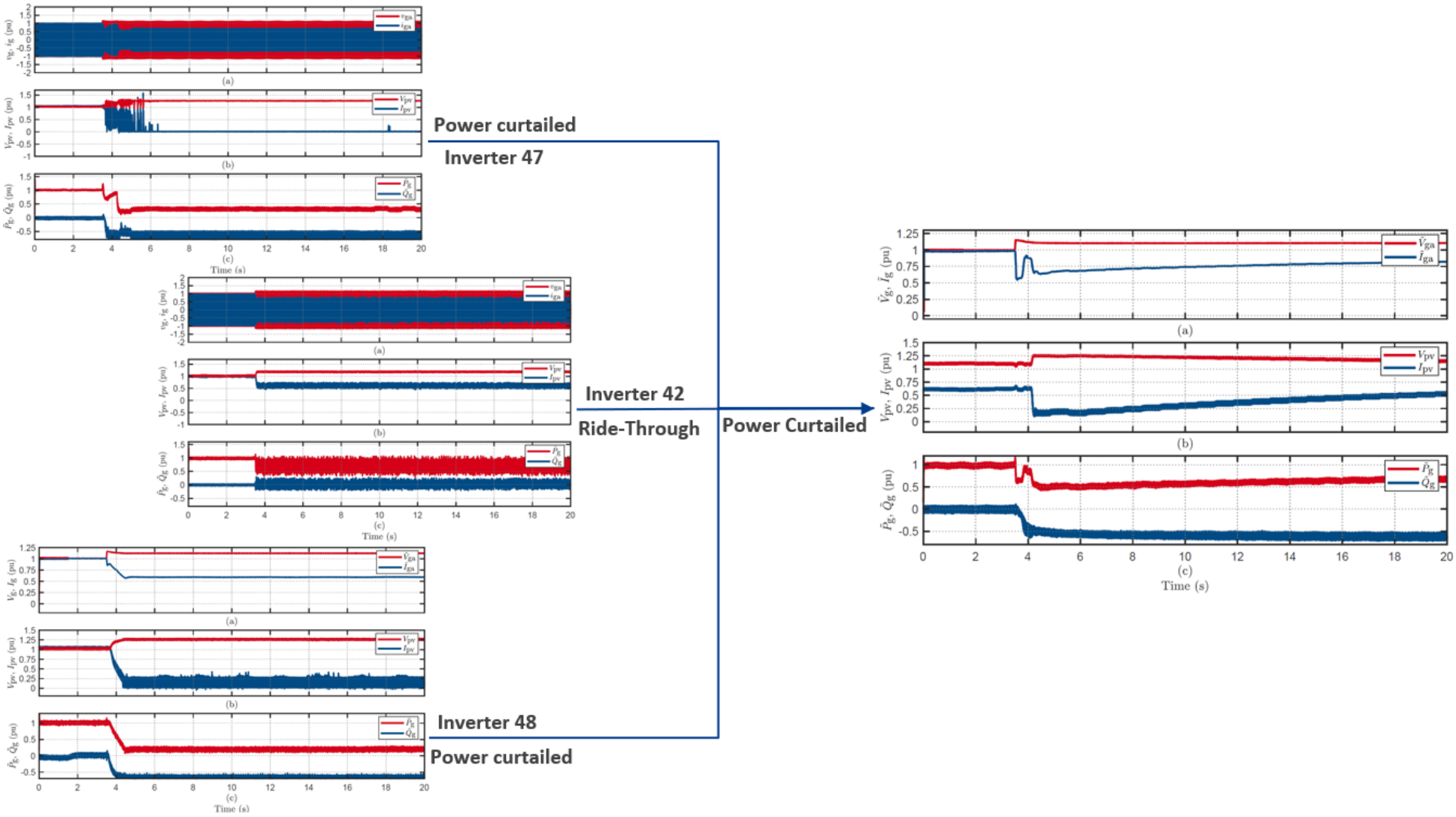

Figure A2.1: Response of inverters 54, 42 and 48 to voltage swell of 30V grid disturbance: individual vs parallel configuration.

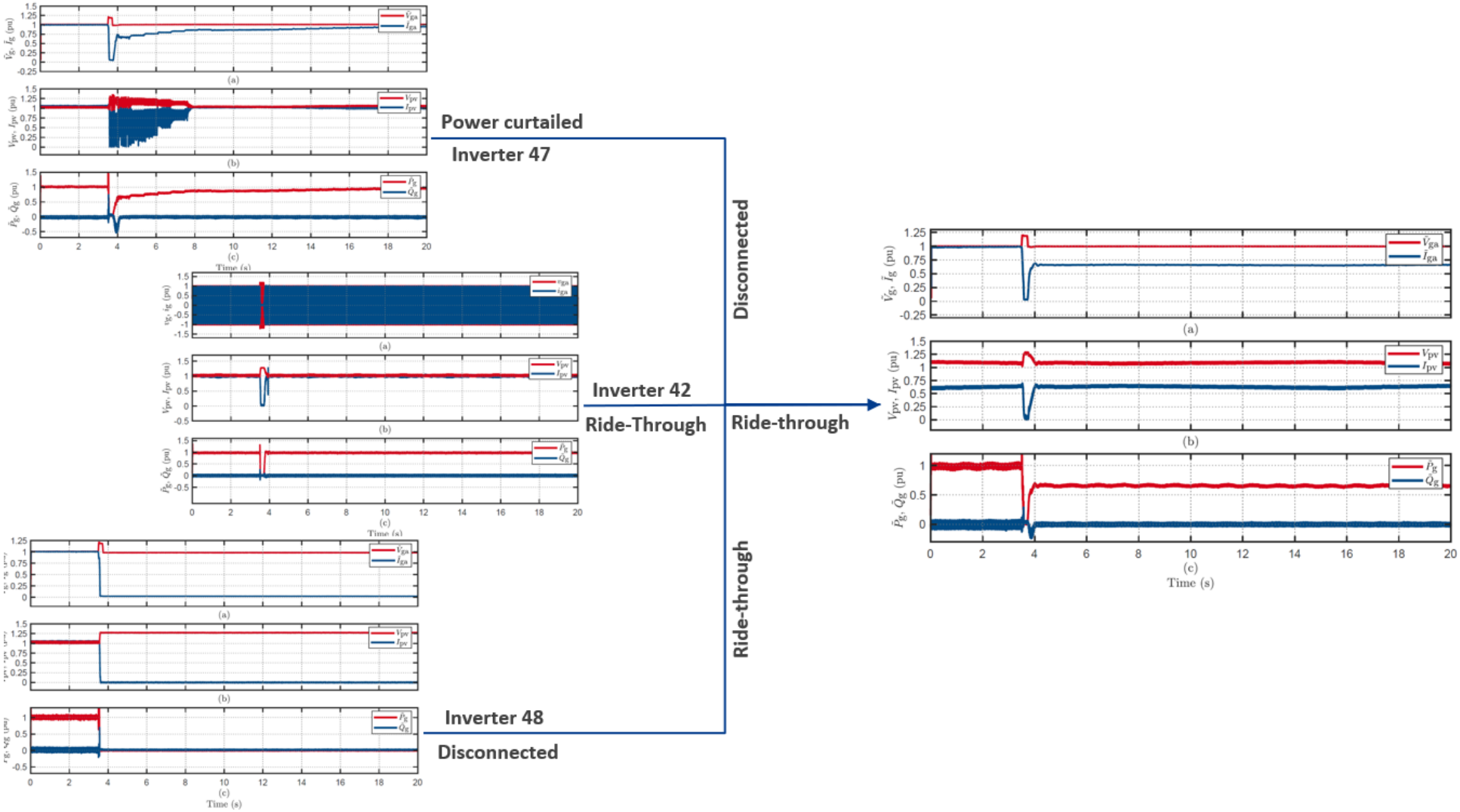

Figure A2.2: Response of inverters 54, 42 and 48 to voltage swell of 1.2p.u for 220ms grid disturbance: individual vs parallel configuration.

A.3: Weak Grid Testing Waveforms

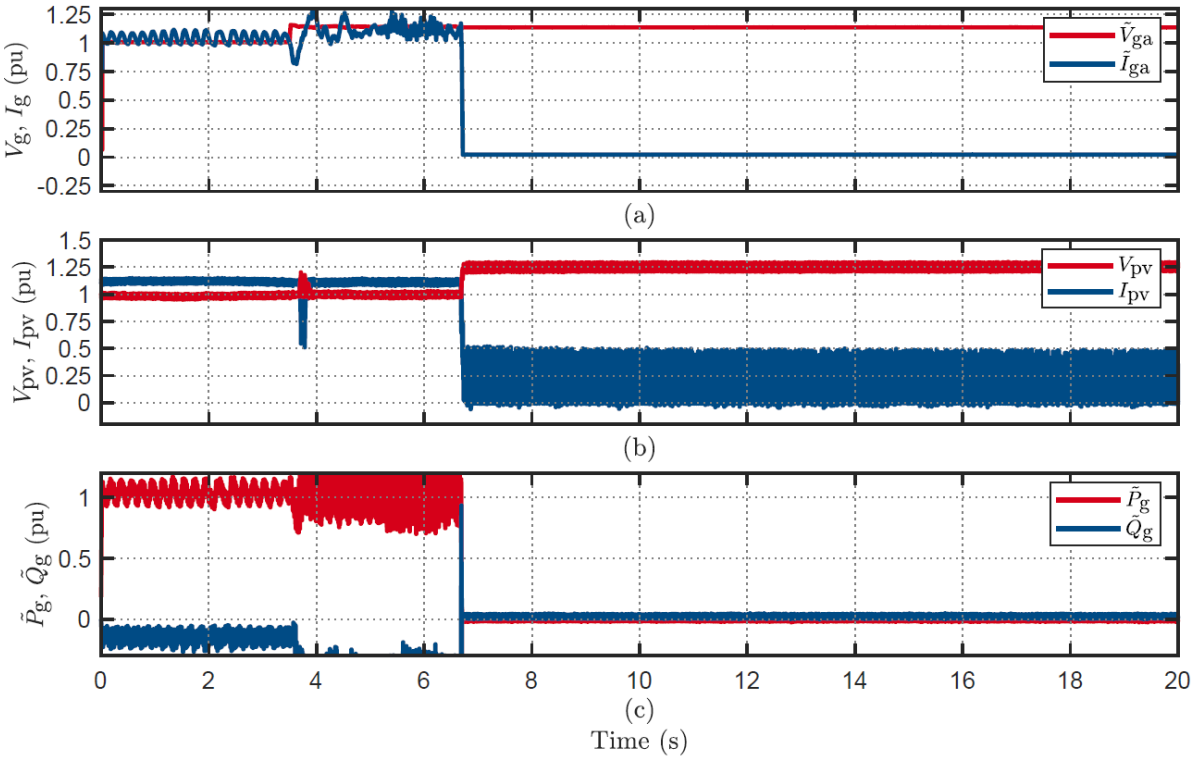

Figure A3.1: Inverter disconnection behaviour to a voltage swell of 30V with 3mH line inductance (SCR 11.2).

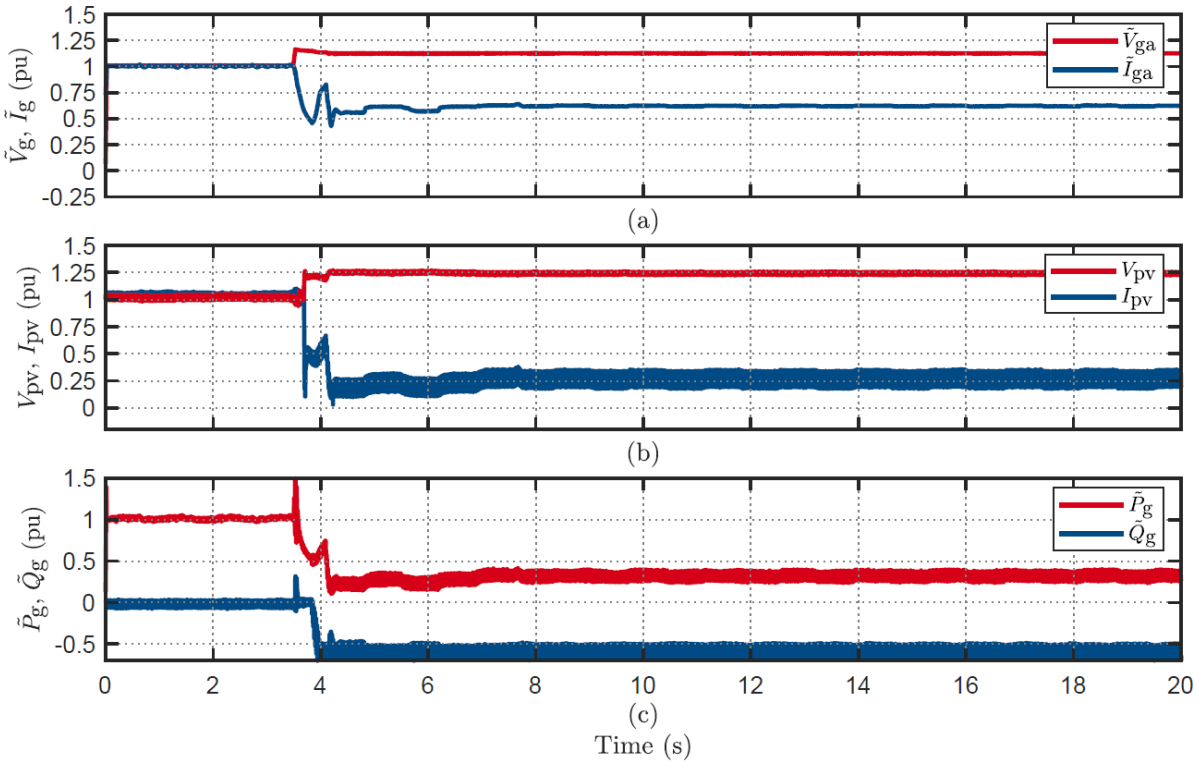

Figure A3.2: Inverter ride-through behaviour to a voltage swell of 30V without line inductance.

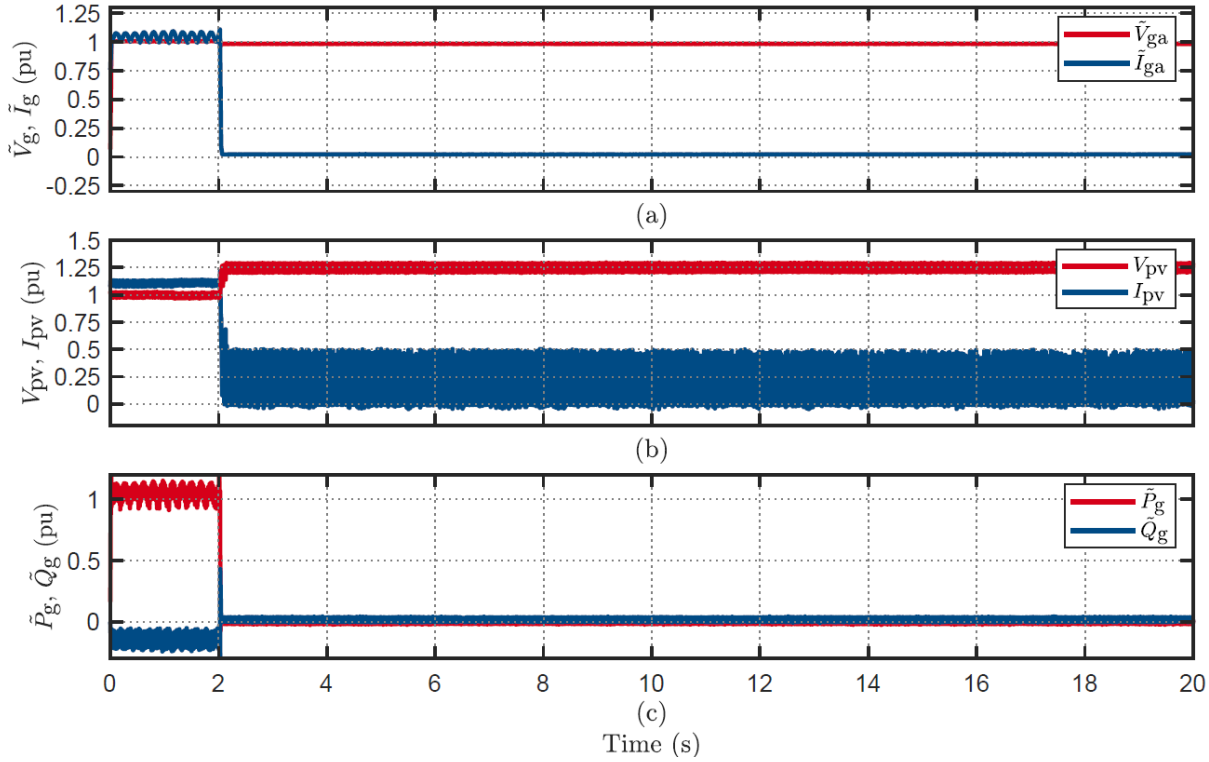

Figure A3.3: Inverter disconnection behaviour to step frequency of 1.95Hz with 3mH line inductance (SCR 11.2).

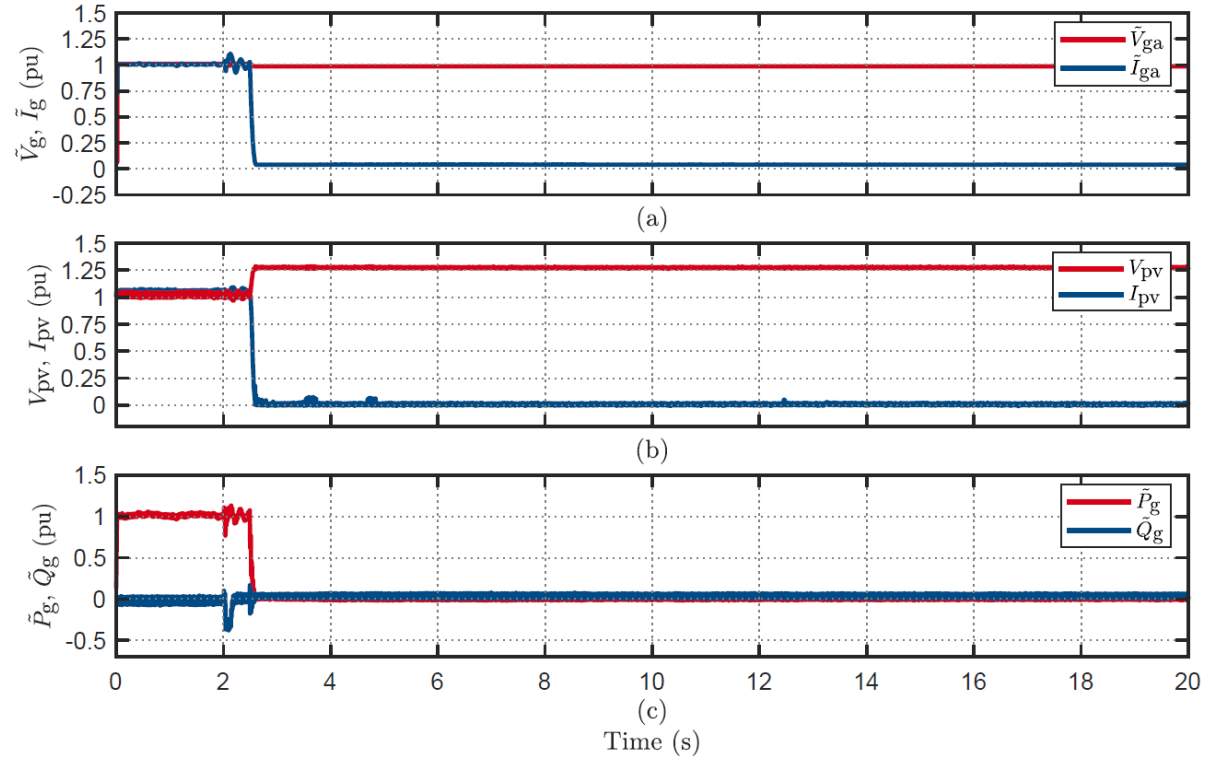

Figure A3.4: Inverter power curtailment behaviour to step frequency disturbance of 1.95Hz without line inductance.

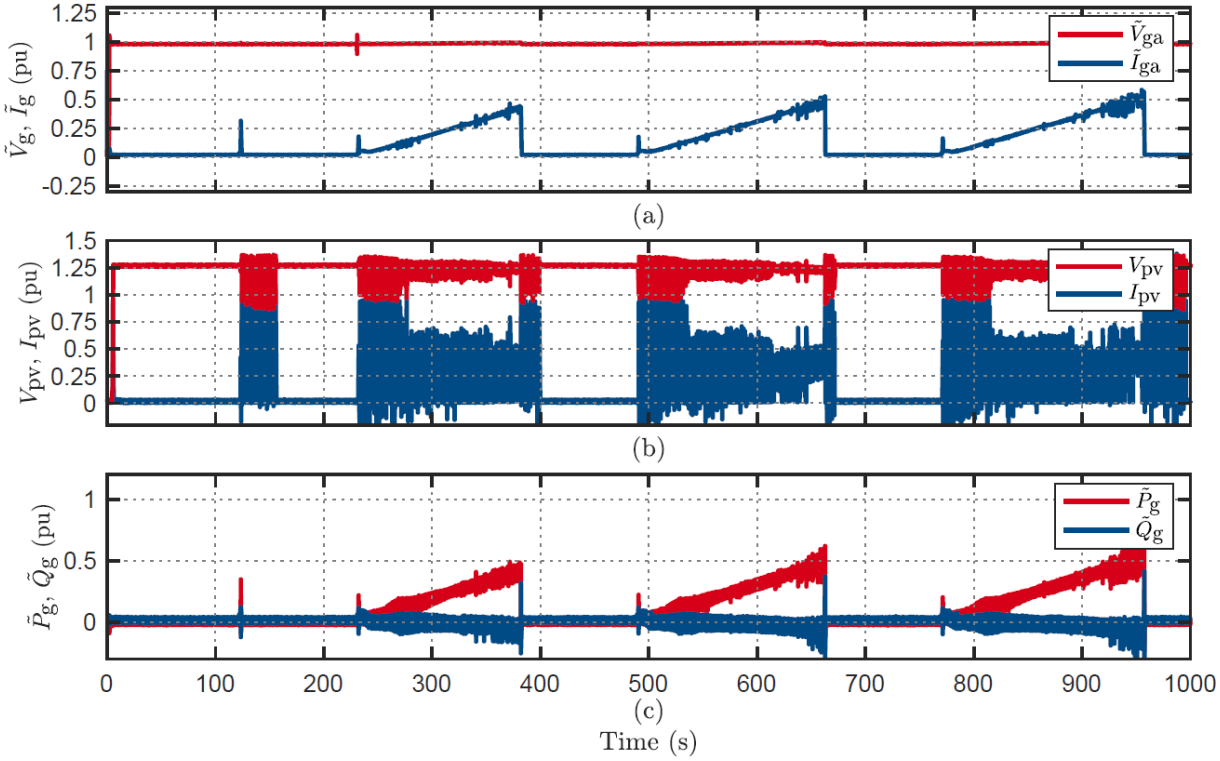

Figure A3.5: Inverter startup steady state response with 4mH (SCR 8.4) line inductance shows disconnection.

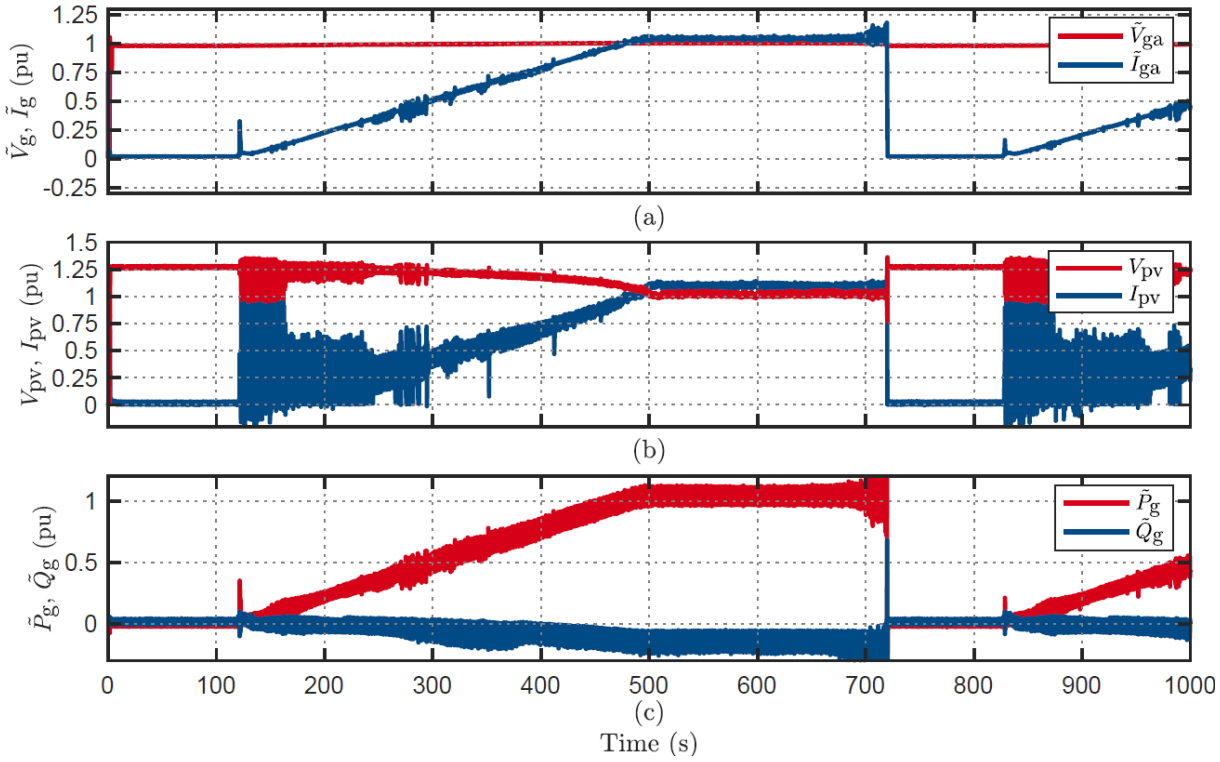

Figure A3.6: Inverter startup steady state response with 3mH (SCR 11.2) line inductance shows disconnection.

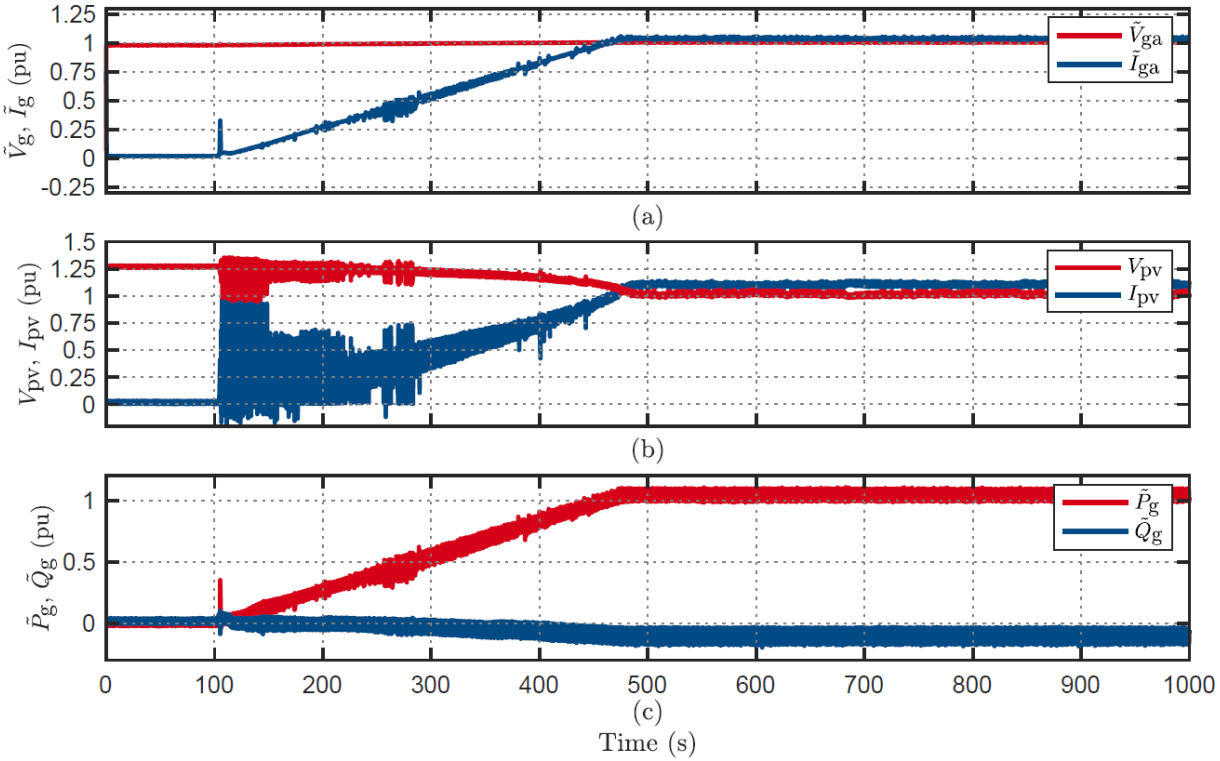

Figure A3.7: Inverter startup steady state response without line inductance shows ride-through.

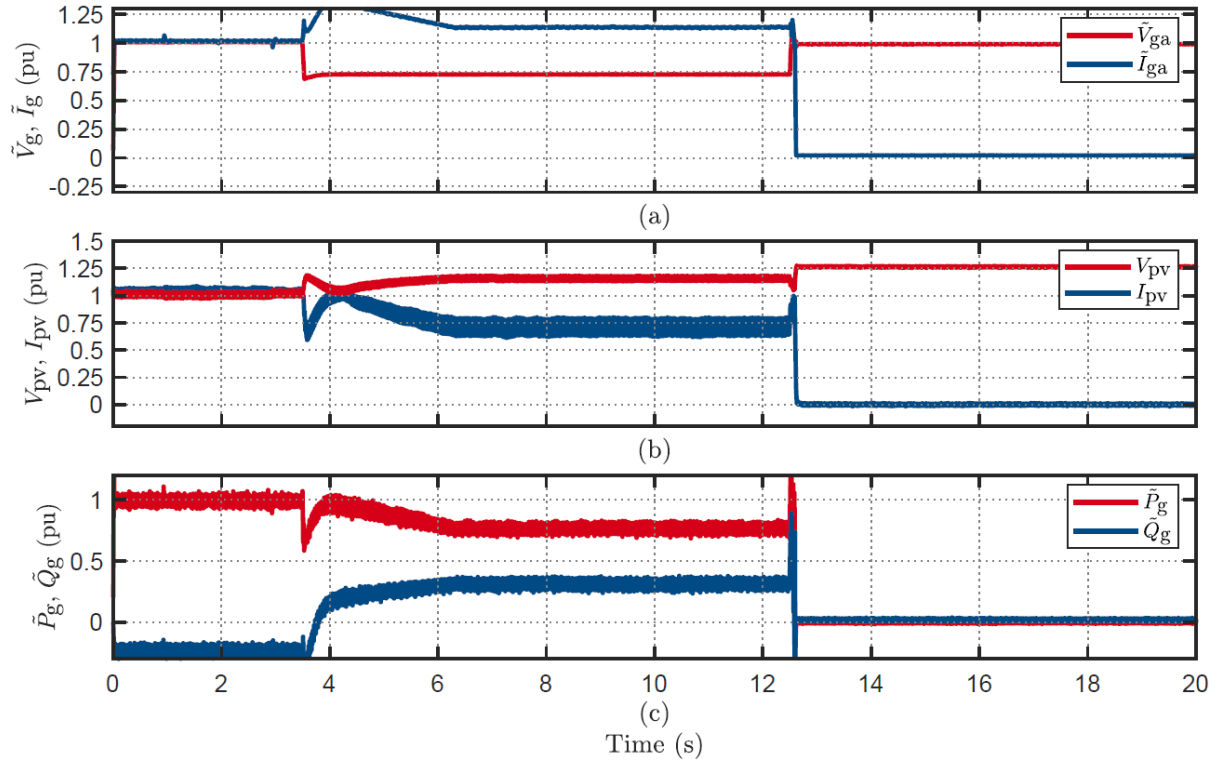

Figure A3.8: Inverter disconnection behaviour to voltage sag disturbance of 70V for 9s with 7mH (SCR 4.8) line inductance.

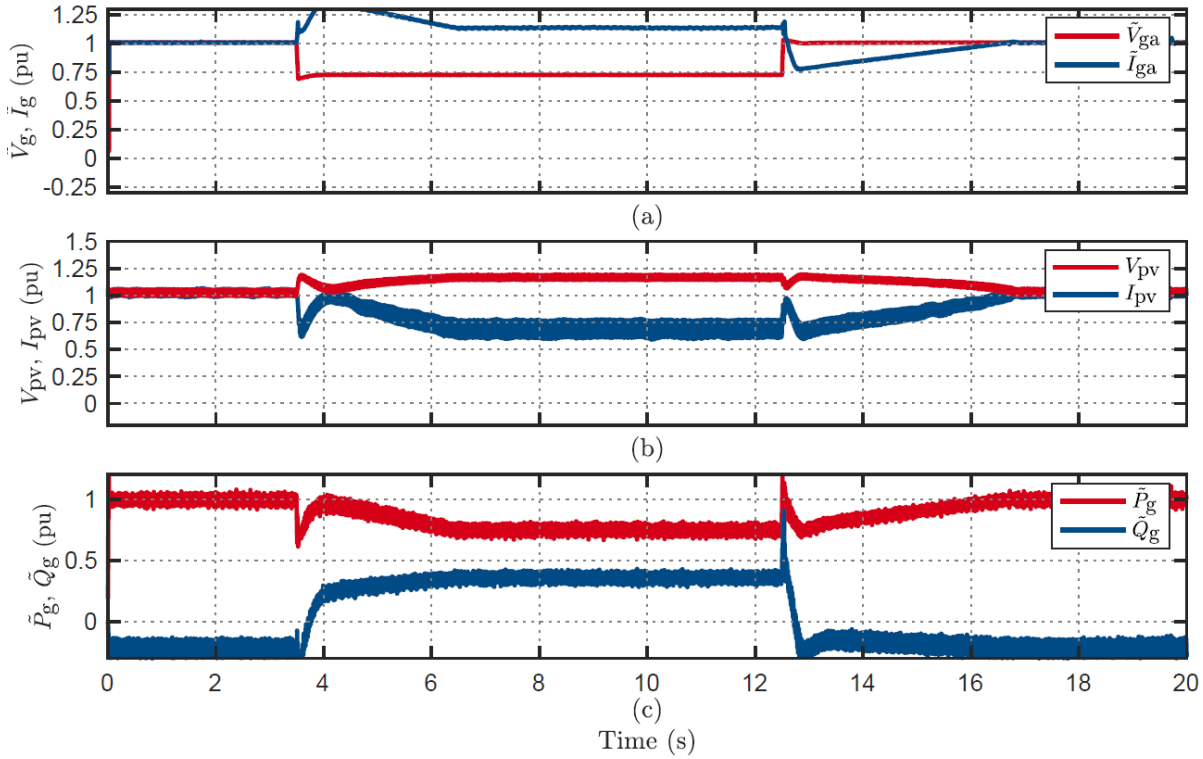

Figure A3.9: Inverter disconnection behaviour to voltage sag disturbance of 70V for 9s with 6mH (SCR 5.6) line inductance.

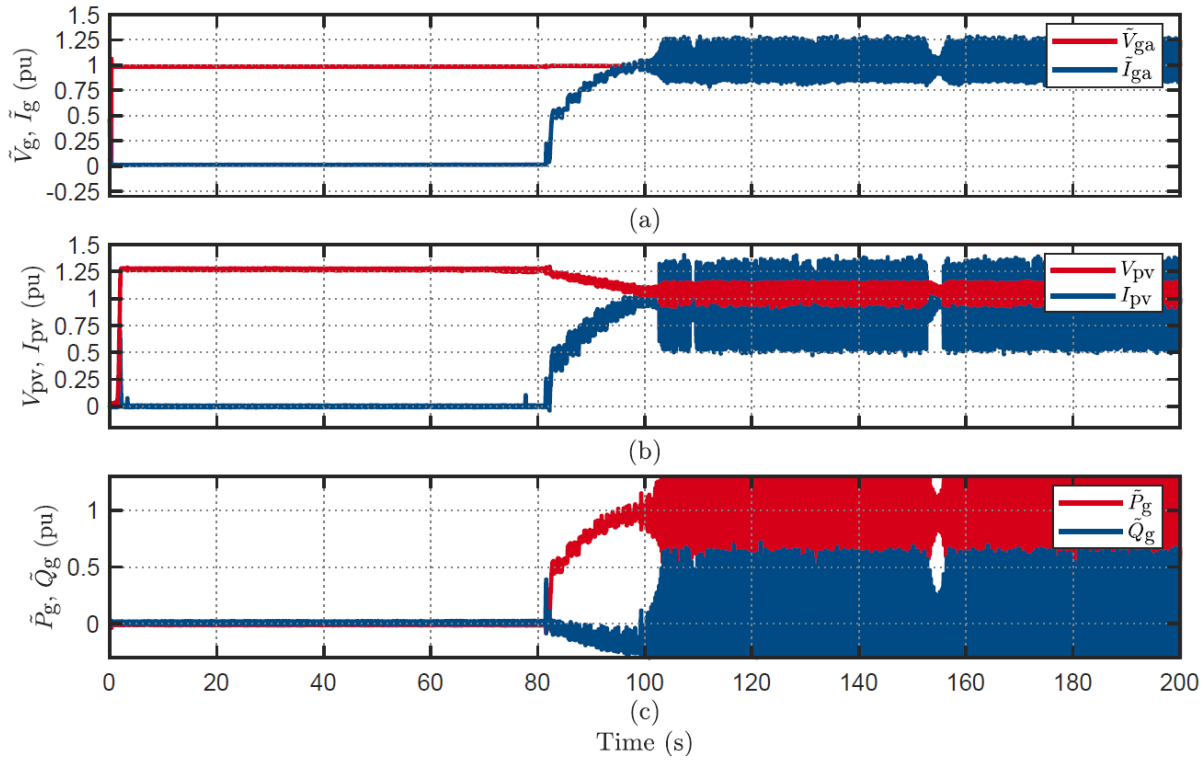

Figure A3.10: Inverter startup steady state response with 3mH (SCR 7.4) line inductance shows power oscillations.

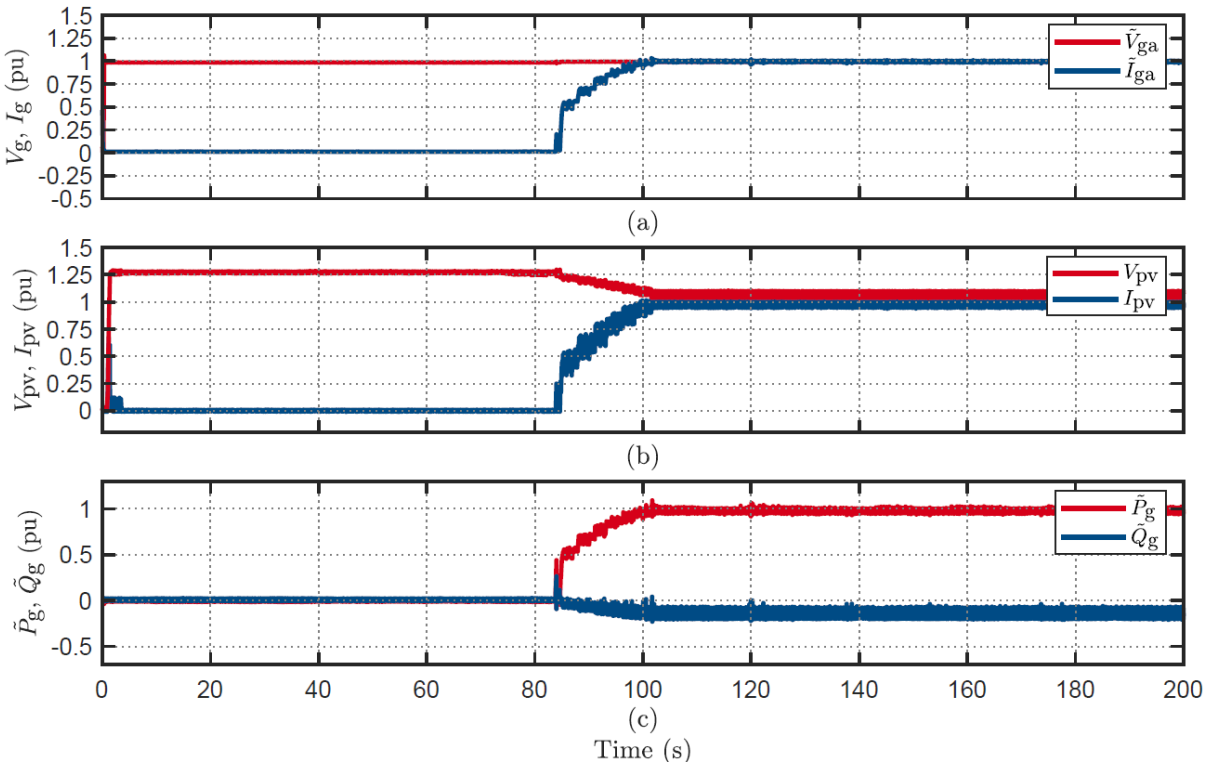

Figure A3.11: Inverter startup steady state response with 2mH (SCR 11.2) line inductance shows stable operation.

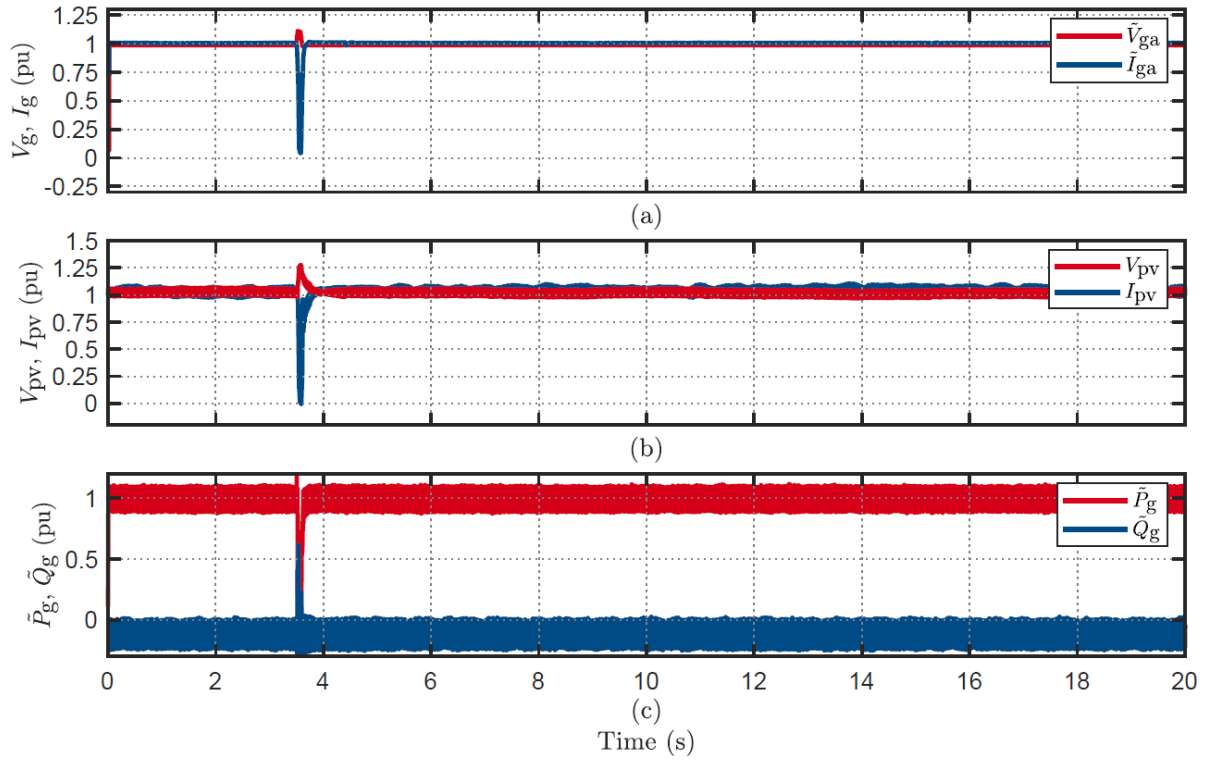

Figure A3.12: Inverter ride-through response to a voltage swell of 1.125 for 80ms with 4mH (SCR 8.4) line inductance (full power).

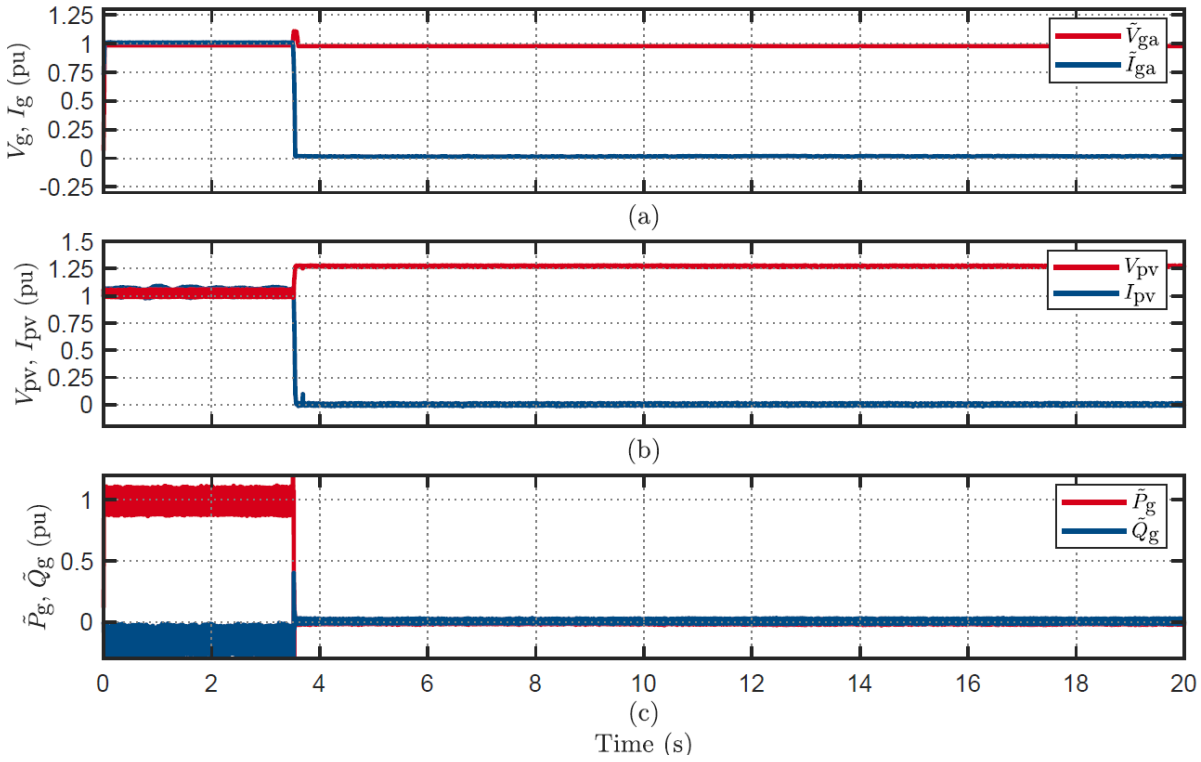

Figure A3.13: Inverter ride-through response to a voltage swell of 1.125 for 80ms with 5mH (SCR 6.7) line inductance (full power).

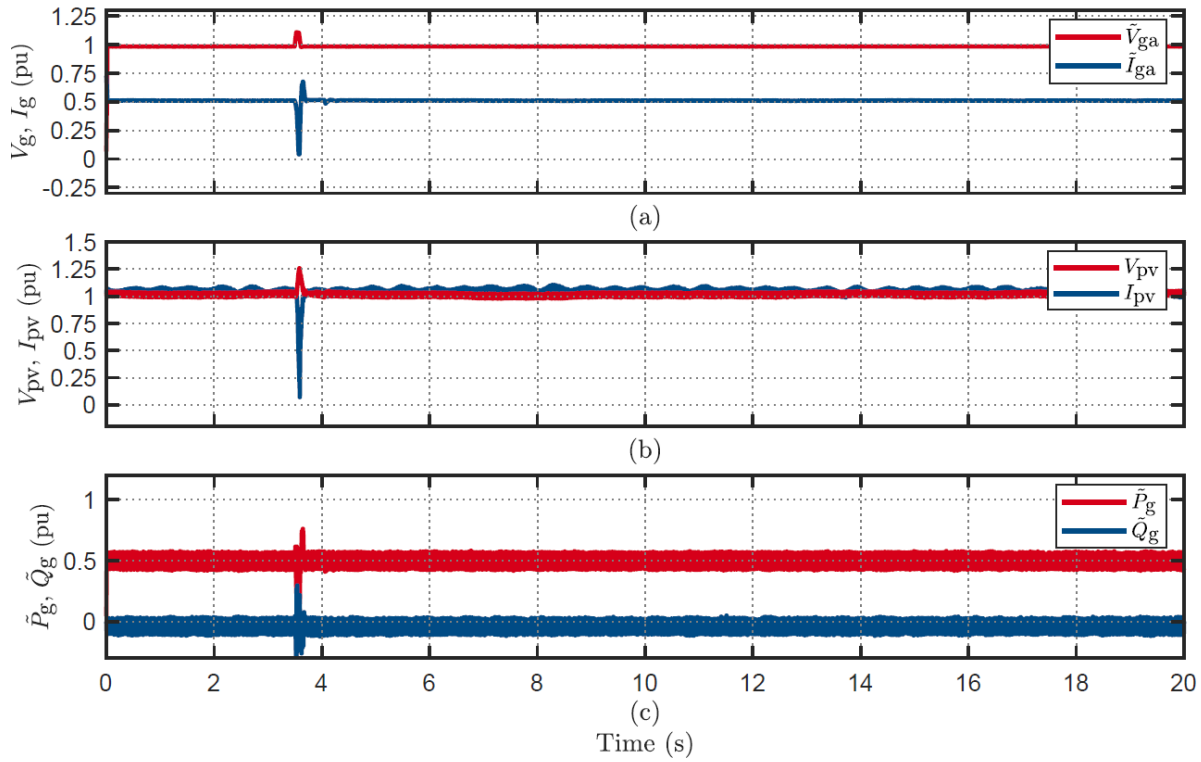

Figure A3.14: Inverter ride-through response to a voltage swell of 1.125 for 80ms with 5mH (SCR 6.7) line inductance (half power).

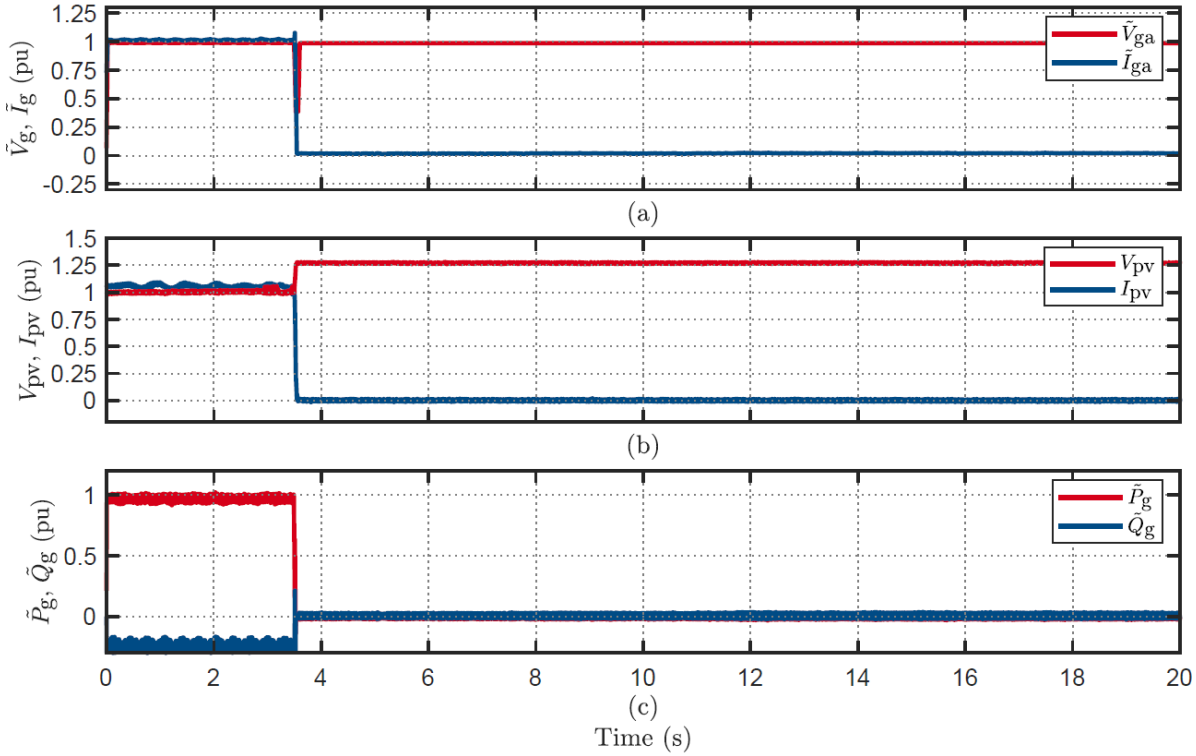

Figure A3.15: Inverter disconnection response to a voltage sag of 0.6p.u for 80ms with 8mH (SCR 4.2) line inductance (full power).

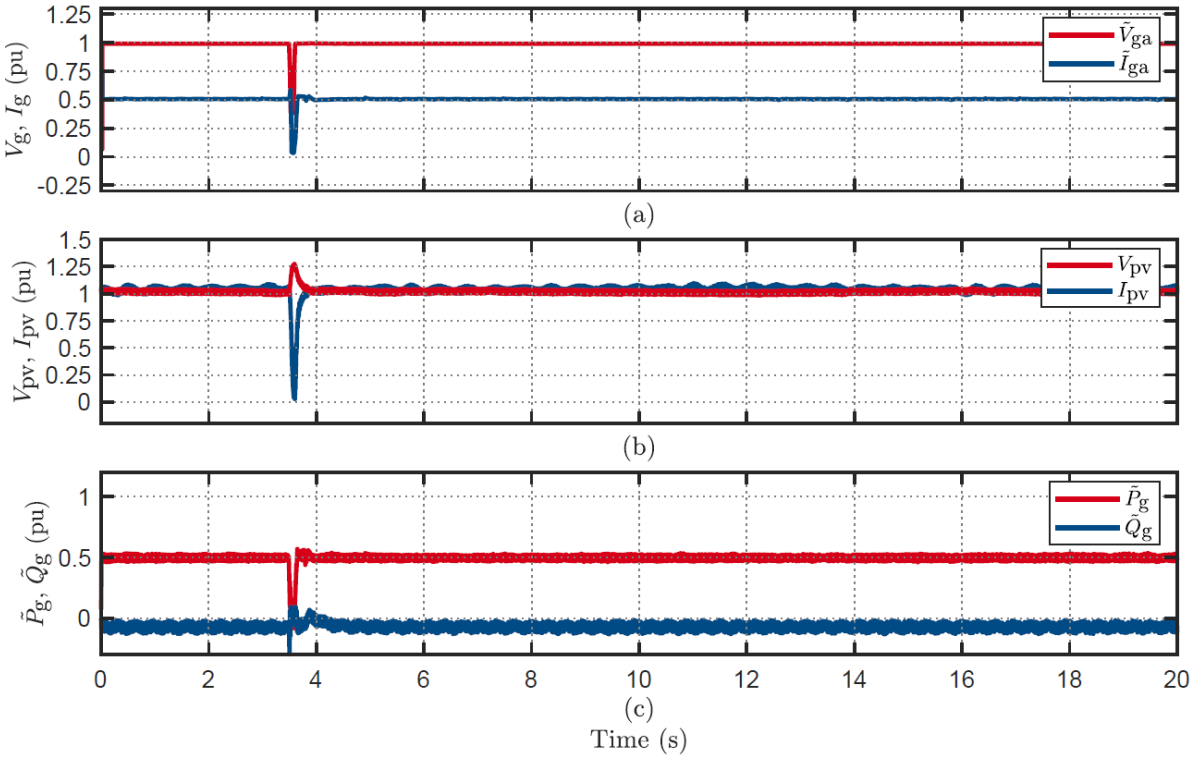

Figure A3.16: Inverter ride-through response to a voltage sag of 0.6p.u for 80ms with 8mH (SCR 4.2) line inductance (half power).

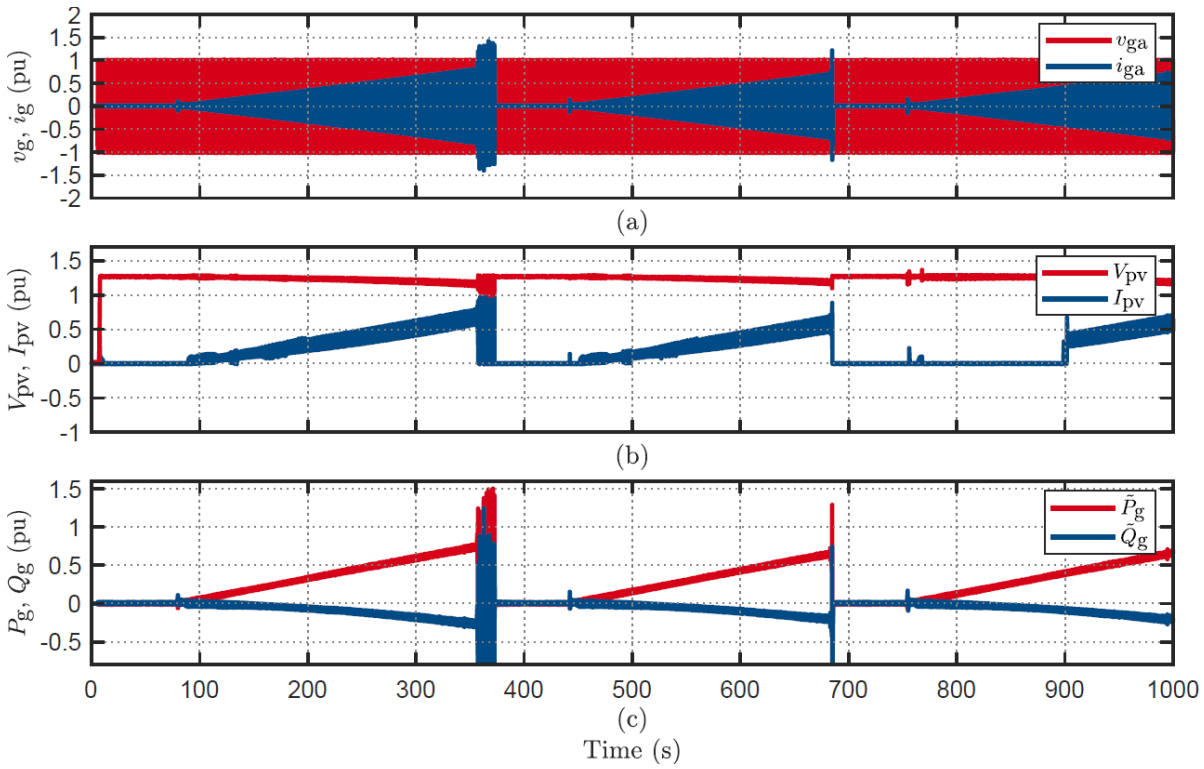

Figure A3.17: Inverter startup steady state response with 7mH (SCR 3.0) line inductance shows cyclic disconnection operation.

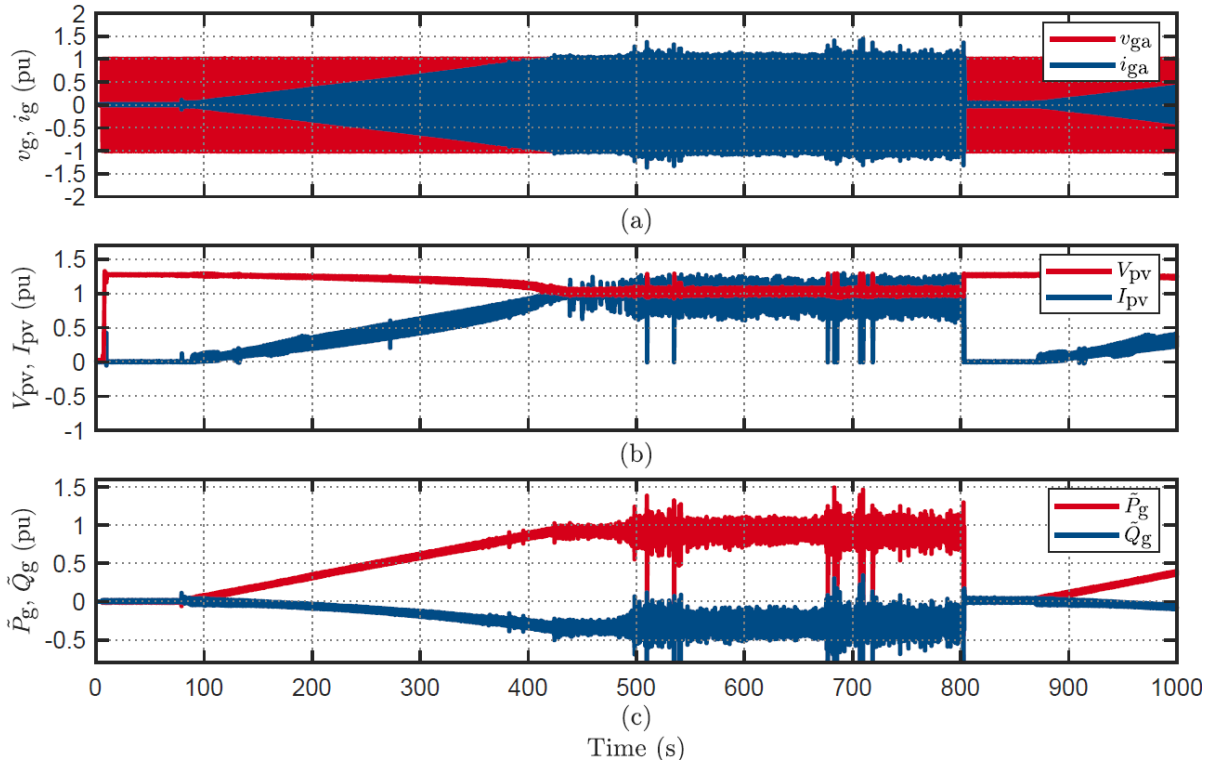

Figure A3.18: Inverter startup steady state response with 5mH (SCR 4.2) line inductance shows ride-through operation.

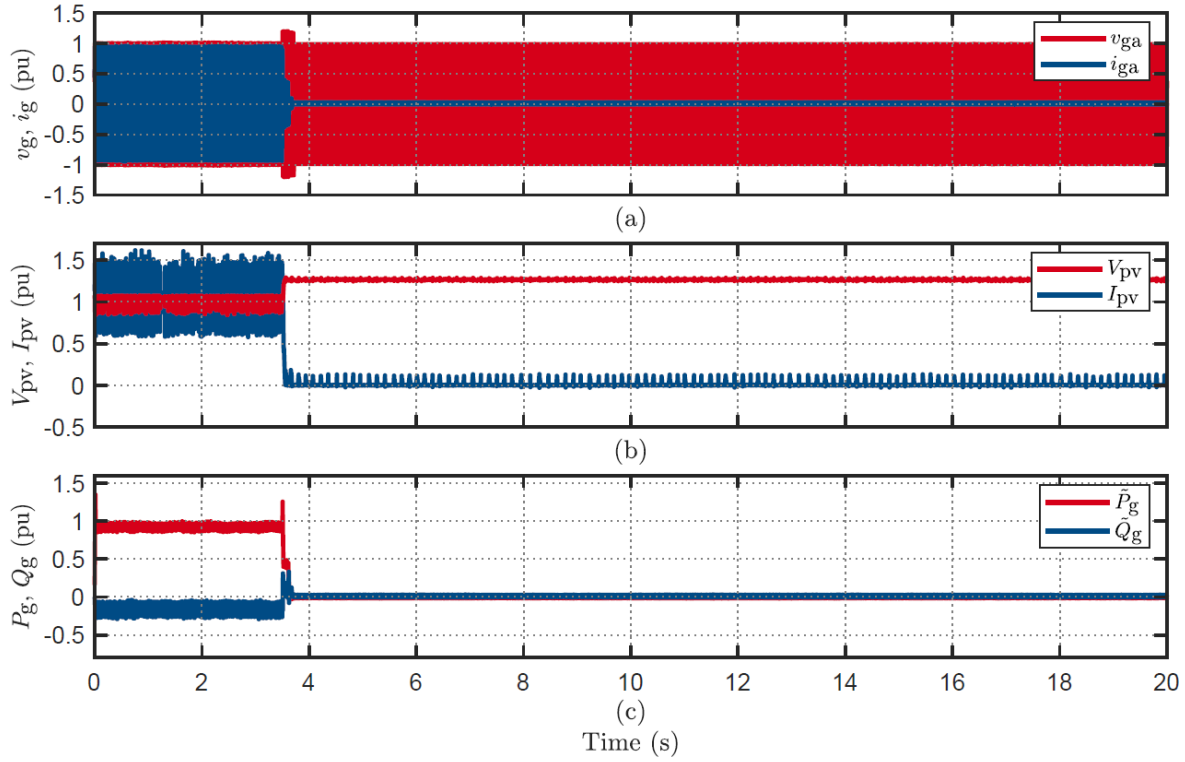

Figure A3.19: Parallel inverters (54: disconnected, 38: disconnected) response to a voltage swell of 1.2p.u for 220ms with 3mH (SCR 5.8) line inductance.

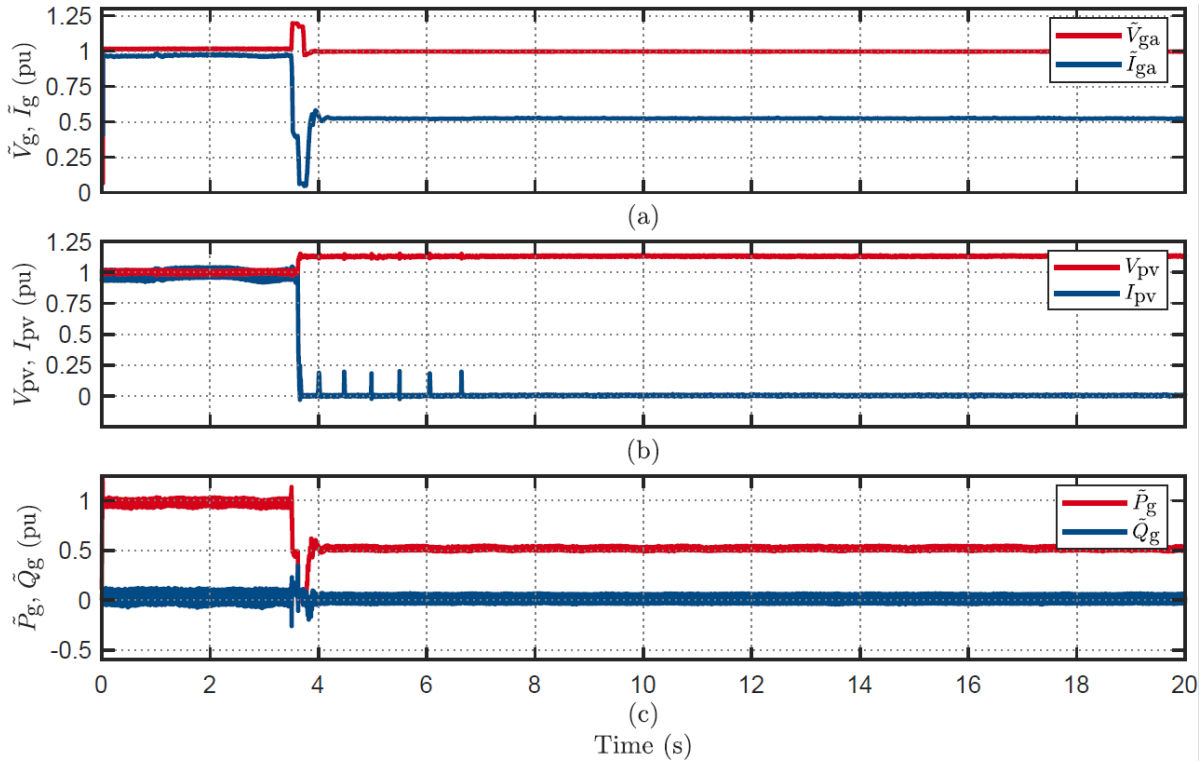

Figure A3.20: Parallel inverters (54: ride-through, 38: power curtailed) response to a voltage swell of 1.2p.u for 220ms without line inductance.

8. References

[1] "A Positive Sequence Model for Aggregated Representation Electric Vehicle Chargers," EPRI, EPRI Project 1-116982, 2022. [Online]. Available: https://certs.lbl.gov/publications/EVCharger_Model_Specifications_2023-Dana_Robson.pdf

[2] AEMO (May 2021) Behaviour of distributed resources during power system disturbances, at https://aemo.com.au/-/media/files/initiatives/der/2021/capstone-report.pdf

[3] AEMO (February 2024) Preliminary Report – Trip of Moorabool – Sydenham 500 kV No. 1 and No. 2 lines https://aemo.com.au/-/media/files/electricity/nem/market_notices_and_events/power_system_incident_reports/2024/preliminary-report---loss-of-moorabool---sydenham-500-kv-lines-on-13-feb-2024.pdf?la=en

[4] Australian Energy Market Operator (AEMO 2022) "Connections in Low System Strength Zones"

[5] F. Arraño-Vargas, S. Jiang, B. Bennett, and G. Konstantinou, "Mitigation of power system oscillations in weak grids with battery ESS: A real-world case study," Energy, 283, Nov.23.

[6] F. Milano, F. Dörfler, G. Hug, D.J. Hill, and G. Verbič, Foundations and challenges of low-inertia systems. In 2018 power systems computation conference (PSCC) (pp. 1-25). IEEE .

[7] M. Ghazavi Dozein, B. C. Pal and P. Mancarella, "Dynamics of Inverter-Based Resources in Weak Distribution Grids," in IEEE Transactions on Power Systems, vol. 37, no. 5, pp. 3682-3692, Sept. 2022,

[8] C. V. Thierry Cutsem *Voltage Stability of Electric Power Systems*. 1998.

[9] W. Mauricio and A. Semlyen, "Effect of Load characteristic on the Dynamic Stability of Power Systems," *IEEE Transactions on Power Apparatus and Systems,* vol. PAS-91, no. 6, pp. 2295-2304, 1972, doi: 10.1109/TPAS.1972.293385.

[10] "Behaviour of distributed resources during power system disturbances," Australian Energy Market Operator (AEMO), 2021. [Online]. Available: https://aemo.com.au/-/media/files/initiatives/der/2021/capstone-report.pdf?la=en&hash=BF184AC51804652E268B3117EC12327A

[11] X. Chang *et al.*, "Research on Dynamic Behavior of Electric Vehicle Converter in power network fault," in *2019 14th IEEE Conference on Industrial Electronics and Applications (ICIEA)*, 19-21 June 2019 2019, pp. 2333-2337, doi: 10.1109/ICIEA.2019.8834031.

[12] D. Kosterev *et al.*, "Load modeling in power system studies: WECC progress update," in *2008 IEEE Power and Energy Society General Meeting - Conversion and Delivery of Electrical Energy in the 21st Century*, 20-24 July 2008 2008, pp. 1-8, doi: 10.1109/PES.2008.4596557.

[13] "Technical Reference Document- Dynamic Load Modeling," North Americal Electric Reliability Coorporation (NERC), 2016. [Online]. Available: https://www.nerc.com/comm/PC/LoadModelingTaskForceDL/Dynamic%20Load%20Modeling%20Tech%20Ref%202016-11-14%20-%20FINAL.PDF

[14] A. Ghosh, D. Poddar, and R. R. Singh, "Impact Analysis of Onboard EV Charger under Power Quality Perturbations," in *2023 9th International Conference on Electrical Energy Systems (ICEES)*, 23-25 March 2023 2023, pp. 69-74, doi: 10.1109/ICEES57979.2023.10110110.

[15] N. Watson, R. Watson, T. Paterson, G. Russell, M. Ellerington, and R. Langella, "Power Quality of a bidirectional Electric Vehicle charger," in *2020 19th International Conference on Harmonics and Quality of Power (ICHQP)*, 6-7 July 2020 2020, pp. 1-5, doi: 10.1109/ICHQP46026.2020.9177892.

[16] M. M. Haque, L. Jones, and B. C. P. Sturmberg, "Response of a Bidirectional EV Charger to Selected Grid Disturbances," in *2021 IEEE Industrial Electronics and Applications Conference (IEACon)*, 22-23 Nov. 2021 2021, pp. 157-162, doi: 10.1109/IEACon51066.2021.9654779.

[17] I. Ziyat, A. Gola, P. R. Palmer, S. Makonin, and F. Popowich, "EV Charging Profiles and Waveforms Dataset (EV-CPW) and Associated Power Quality Analysis," *IEEE Access,* vol. 11, pp. 138445-138456, 2023, doi: 10.1109/ACCESS.2023.3340131.

[18] L. Callegaro, G. Konstantinou, C.A. Rojas, N. Avila, J. Fletcher, (2020). Testing evidence and analysis of rooftop PV inverters response to grid disturbances. IEEE Journal of Photovoltaics, 10(6), 1882-1891.

[19] Zhang, Y., Wiese, N., Liu, Z., & Braun, M. (2023). On the control interaction of synchronous machine and inverter-based resources during system-split situations. International Journal of Electrical Power & Energy Systems, 152, 109227

[20] N. Mckillop E. Franklin , J. Lord , C. Wembridge,, "Assessing the response of eletric vehicles during network fault conditions", CIGRE International Symposium, Cairns, 2023.

[21] J. Undrill F. Tuffner , D. Scoffield , J. Eto , D. Kosterev ,R. Quint, "Distribution-Level Impact of Plug-in Eectric Vehicle Charging on the Transmission System During Fault Conditions", Report prepared for 2021.

[22] H. Satoh M. Masuda "Root-Mean-Square Model of EV Charging Inverter for Balanced Fault", Report prepared for 2023.

[23] L. Sundaresh, P. Mitra, "A Positive Sequence Model for Aggregated Representation Electric Vehicle Chargers", Report prepared for EPRI, 2022.

[24] AS 4777.2:2020, AU/NZ Standard, Grid connection of energy systems via inverters part 2: Inverter requirements, Standards Australia/New Zealand Std. AS 4777.2: 2020

[25] "Electric Vehicle Dynamic Charging Performance Characteristics during Bulk Power System Disturbances," North American Electric Reliability Corporation (NERC), 2023. [Online]. Available: https://www.nerc.com/comm/RSTC/Documents/Grid_Friendly_EV_Charging_Recommendations.pdf

[26] J. U. Tuffner F.K., D. Scoffield, J.H. Eto, D. Kosterev, and R.D. Quint, "Distribution-Level Impacts of Plug-in Electric Vehicle Charging on the Transmission System during Fault Conditions," Pacific Northwest National Laboratory, Richland, WA 2021.

[27] J. L. N. M. E. Franklin , C. Wembridge, "Assessing the response of electric vehicles during network fault conditions," CIGRE International Symposium, Cairns, 2023.

[28] H. S. M. Masuda, "Root-Mean-Square Model of EV Charging Inverter for Balanced Fault," CIGRE International Symposium," Cairns, 2023.